

Copyright  
by  
Thekla Boutsika  
2013

The Dissertation Committee for Thekla Boutsika  
certifies that this is the approved version of the following dissertation:

**Intra-hour Wind Power Variability Assessment using  
the Conditional Range Metric:  
Quantification, Forecasting and Applications**

Committee:

---

Surya Santoso, Supervisor

---

Aristotle Arapostathis

---

Mircea Driga

---

William Grady

---

David Morton

**Intra-hour Wind Power Variability Assessment using  
the Conditional Range Metric:  
Quantification, Forecasting and Applications**

**by**

**Thekla Boutsika, Diploma, M.S.E.**

**DISSERTATION**

Presented to the Faculty of the Graduate School of  
The University of Texas at Austin  
in Partial Fulfillment  
of the Requirements  
for the Degree of

**DOCTOR OF PHILOSOPHY**

THE UNIVERSITY OF TEXAS AT AUSTIN

August 2013

To my mother Eleni Masoura and my father Nikolaos Boutsikas for their  
unconditional love, endless support and unquestionable faith in me.

## Acknowledgments

The work presented in this dissertation is supported in part by National Science Foundation, Grant Number 1162328, a support appreciatively acknowledged.

First of all, I would like to heartily thank Dr. Surya Santoso, my supervisor, for trusting in my capabilities to complete the work presented herein. Since Fall 2010, when I joined his research group, Dr. Santoso managed to guide me through this work by providing useful feedback and constructive criticism, while at the same time respecting my need for independence and giving me enough room to take the research topic to my own desired direction. I'd like to thank him for his academic, moral, and financial support throughout these years, and of course for putting up with me as a student and as a person.

I would also like to thank my committee members, Dr. Aristotle Apostathis, Dr. Mircea Driga, Dr. William Grady and Dr. David Morton for agreeing to serve on my committee and for their valuable input towards this work. At this point, I need to express my deepest gratitude to Dr. Apostathis and Dr. Morton who, at a difficult personal time where I was on the verge of giving everything up, provided financial alternatives and moral assistance and convinced me to go on with my studies.

I am also grateful to all the staff members at the Electrical and Computer Engineering Department and people from the International Student and Scholar Services and the Institute of International Education at Rocky Mountain whom I got to know throughout my stay at UT. Special thanks to Melanie

Gulick, the person possibly most acknowledged by Electrical and Computer Engineering graduate students, for her positive attitude and support, and for always giving solutions to problems in a timely and efficient manner.

Many thanks go out to my lab mates and the other graduate students I got to interact with during my years at UT. I am especially thankful to Swagata Das, for many sleepless nights at the lab trying to encourage each other drinking hot chai and eating chocolate cookies, and Duehee Lee for many fruitful conversations. I am also grateful to Yohan Sutjandra and Yin Wu with whom we shared ideas on homework assignments in the first two years of my graduate studies and parenting concerns in the years to follow.

Doing research towards a graduate degree is a very stressful and demanding task for which a large net of supporting friends and family is considered a prerequisite. I would like to thank all my Greek friends in Austin, and especially Ioannis Rouselakis, Dimitris Prountzos, Vasilis Liaskovotis, Chris Argyropoulos, Emmanouil Kalaitzakis and Nikos Benteinitis, for many relaxing nights at home or at Rio Rita sipping Tito's. Special thanks also to my longtime friend Stamatia Karagianni for listening to my concerns and for always being there despite the eight hour time zone difference.

I am forever grateful to my parents Eleni Masoura and Nikolaos Boutikas, to whom this dissertation is dedicated to, and my brother Stelios Boutikas for always encouraging me to follow my dreams and for always being the safe haven I could return to if things went wrong. I am really indebted to my dad for babysitting his grandson for a whole year so that I could stay in the lab until the small hours.

Last, but certainly not least, my deepest gratitude of all goes out to my husband Dimitris Dimitropoulos and our children Nikos and Melina. I

can't thank Dimitri enough for being such a supportive and understanding husband, for persuading me to finish my degree after our children were born, even when that meant that he would have to spend months apart from them, and foremost for putting up with my unconventional personality over the past ten years.

# **Intra-hour Wind Power Variability Assessment using the Conditional Range Metric: Quantification, Forecasting and Applications**

Publication No. \_\_\_\_\_

Thekla Boutsika, Ph.D.

The University of Texas at Austin, 2013

Supervisor: Surya Santoso

The research presented herein concentrates on the quantification, assessment and forecasting of intra-hour wind power variability. Wind power is intrinsically variable and, due to the increase in wind power penetration levels, the level of intra-hour wind power variability is expected to increase as well. Existing metrics used in wind integration studies fail to efficiently capture intra-hour wind power variation. As a result, this can lead to an underestimation of intra-hour wind power variability with adverse effects on power systems, especially their reliability and economics.

One major research focus in this dissertation is to develop a novel variability metric which can effectively quantify intra-hour wind power variability. The proposed metric, termed conditional range metric (CRM), quantifies wind power variability using the range of wind power output over a time period. The metric is termed conditional because the range of wind power output is conditioned on the time interval length  $k$  and on the wind power average production



$l_j$  over the given time interval. Using statistical analysis and optimization approaches, a computational algorithm to obtain a unique  $p^{th}$  quantile of the conditional range metric is given, turning the proposed conditional range metric into a probabilistic intra-hour wind power variability metric. The probabilistic conditional range metric  $CRM_{k,l_j,p}$  assists power system operators and wind farm owners in decision making under uncertainty, since decisions involving wind power variability can be made based on the willingness to accept a certain level of risk  $\alpha = 1 - p$ .

An extensive performance analysis of the conditional range metric on real-world wind power and wind speed data reveals how certain variables affect intra-hour wind power variability. Wind power variability over a time frame is found to increase with increasing time frame size and decreasing wind farm size, and is highest at mid production wind power levels. Moreover, wind turbines connected through converters to the grid exhibit lower wind power variability compared to same size simple induction generators, while wind power variability is also found to decrease slightly with increasing wind turbine size. These results can lead to improvements in existing or definitions of new wind power management techniques. Moreover, the comparison of the conditional range metric to the commonly used step-changes statistics reveals that, on average, the conditional range metric can accommodate intra-hour wind power variations for an additional 15% of hours within a given year, significantly benefiting power system reliability.

The other major research focus in this dissertation is on providing intra-hour wind power variability forecasts. Wind power variability forecasts use  $p^{th}$  CRM quantiles estimates to construct probabilistic intervals within which future wind power output will lie, conditioned on the forecasted average wind power production. One static and two time-adaptive methods are used to ob-

tain  $p^{th}$  CRM quantiles estimates. All methods produce quantile estimates of acceptable reliability, with average expected deviations from nominal proportions close to 1%. Wind power variability forecasts can serve as joint-chance constraints in stochastic optimization problems, which opens the door to numerous applications of the conditional range metric.

A practical example application uses the conditional range metric to estimate the size of an energy storage system (ESS). Using a probabilistic forecast of wind power hourly averages and historical data on intra-hour wind power variability, the proposed methodology estimates the size of an ESS which minimizes deviations from the forecasted hourly average. The methodology is evaluated using real-world wind power data. When the estimated ESS capacities are compared to the ESS capacities obtained from the actual data, they exhibit coverage rates which are very close to the nominal ones, with an average absolute deviation less than 1.5%.

# Table of Contents

<b>Acknowledgments</b>	<b>v</b>
<b>Abstract</b>	<b>viii</b>
<b>List of Tables</b>	<b>xv</b>
<b>List of Figures</b>	<b>xvii</b>
<b>Chapter 1. Introduction</b>	<b>1</b>
1.1 Background and Motivation . . . . .	1
1.2 Research Objectives . . . . .	6
1.3 Research Approach . . . . .	7
1.3.1 To Develop a Metric to Quantify Intra-hour Wind Power Variability . . . . .	7
1.3.2 To Assess Intra-hour Wind Power Variability . . . . .	8
1.3.3 To Evaluate the Proposed Metric against Existing Metrics	9
1.3.4 To Develop Methods to Forecast Wind Power Variability	9
1.3.5 To Demonstrate the Utility of the Proposed Metric . . .	10
1.4 Original Research Contributions . . . . .	10
1.4.1 Major Contributions . . . . .	10
1.4.2 Supporting Contributions . . . . .	13
1.5 Dissertation Outline . . . . .	14
<b>Chapter 2. Prior Work in Wind Power Variability</b>	<b>15</b>
2.1 Common Measures of Dispersion . . . . .	16
2.2 Measures of Wind Power Dispersion . . . . .	19
2.2.1 Step-Changes . . . . .	20
2.2.1.1 Definition of Step-changes . . . . .	20

2.2.1.2	Applications of Step-changes in Wind Integration Studies . . . . .	21
2.2.1.3	Shortcomings of the Step-changes Approach . . . . .	23
2.2.2	Other Wind Power Variability Metrics . . . . .	27
2.3	Summary . . . . .	30
<b>Chapter 3.</b>	<b>Proposed Conditional Range Metric (CRM) to Quantify Intra-hour Wind Power Variability</b>	<b>32</b>
3.1	Fundamental Concept of the Proposed Metric . . . . .	34
3.2	Definition of the Conditional Range Metric . . . . .	36
3.3	Probabilistic Conditional Range Metric . . . . .	38
3.3.1	Motivation and Approach . . . . .	39
3.3.2	Computation of the Probabilistic CRM . . . . .	44
3.4	Using the Conditional Range Metric to Distinguish between Variable Sources . . . . .	49
3.5	Summary . . . . .	53
<b>Chapter 4.</b>	<b>Evaluation of the Conditional Range Metric</b>	<b>54</b>
4.1	Wind Power Variability Assessment Using the Conditional Range Metric . . . . .	56
4.1.1	Wind Power Variability as a Function of the Wind Power Production . . . . .	56
4.1.2	Wind Power Accommodation for Different Coverage Probabilities . . . . .	59
4.1.3	Wind Power Variability over Various Time Frames . . . . .	61
4.1.4	The Effect of the Wind Farm Nameplate Capacity . . . . .	64
4.1.5	Concluding Remarks . . . . .	66
4.2	Quantifying the Effect of Wind Turbine Size and Technology on Wind Power Variability . . . . .	66
4.2.1	Generating the Wind Power Series . . . . .	67
4.2.2	Quantifying Wind Power and Wind Speed Variability . . . . .	70
4.2.3	The Effect of Wind Turbine Technology . . . . .	71
4.2.4	The Effect of Wind Turbine Size . . . . .	75
4.2.5	The Effect of Wind Power Aggregation . . . . .	76
4.2.6	Concluding Remarks . . . . .	81

4.3	Comparison of the Conditional Range Metric to the Step-changes and Forward Differences Statistics . . . . .	81
4.3.1	Comparison Pairs . . . . .	82
4.3.2	Comparison Schemes . . . . .	85
4.3.3	Comparison Outcomes . . . . .	89
4.3.4	Comparison Results . . . . .	96
4.3.4.1	The Effect of the Wind Farm Size on Wind Power Variability across Different Time Scales . . . . .	96
4.3.4.2	Wind Power Variability as a Function of the Wind Power Production Level . . . . .	99
4.3.4.3	Comparison Results as a Function of the Coverage Rate . . . . .	109
4.3.4.4	Average Comparison Results under all Comparison Schemes . . . . .	117
4.3.5	Concluding Remarks . . . . .	122
4.4	Summary . . . . .	124
<b>Chapter 5.</b>	<b>Forecasting the Conditional Range Metric</b>	<b>125</b>
5.1	Prior Work in Wind Power Forecasting . . . . .	127
5.2	Forecasting Intra-hour Wind Power Variability . . . . .	132
5.2.1	Approach . . . . .	132
5.2.2	Problem Description . . . . .	135
5.3	Estimating CRM Quantiles . . . . .	138
5.3.1	Prior Work in Quantile Estimation . . . . .	139
5.3.2	Evaluation of Quantile Estimates . . . . .	145
5.3.3	Sample Quantile . . . . .	146
5.3.4	Exponentially Weighted Moving Average . . . . .	161
5.3.5	Exponentially Weighted Stochastic Approximation . . . . .	167
5.3.6	Method Evaluation and Comparison . . . . .	177
5.4	CRM Sample Quantiles with Seasonal Considerations . . . . .	187
5.5	Wind Power Variability Incremental Forecast Error . . . . .	193
5.5.1	Wind Power Forecast Series Formation . . . . .	194
5.5.2	Evaluation of the CRM Quantile Estimates from the Forecast on the Actual Wind Power Data . . . . .	199

5.5.3	Comparison of the CRM Sample Quantiles between a Perfect and an Actual Wind Power Forecast . . . . .	204
5.6	Concluding Remarks . . . . .	209
<b>Chapter 6.</b>	<b>Example Application of the Conditional Range Metric: Energy Storage System Size Estimation</b>	<b>212</b>
6.1	Generation of Hour-long Wind Power Production Scenarios . .	216
6.2	Statistical Calculation of the ESS Capacities . . . . .	224
6.3	Application of the ESS Size Estimation Methodology to Real-world Wind Power Data . . . . .	228
6.3.1	Evaluation of the Generated Scenarios . . . . .	228
6.3.2	Statistics of the ESS Characteristics . . . . .	232
6.3.3	Evaluation of ESS Characteristics Coverage Rates . . .	237
6.4	Concluding Remarks . . . . .	246
<b>Chapter 7.</b>	<b>Conclusion and Future Work</b>	<b>248</b>
	<b>Appendices</b>	<b>254</b>
	<b>Appendix A. Wind Power Data</b>	<b>255</b>
A.1	Data Description . . . . .	255
A.2	Data Pre-processing . . . . .	258
	<b>Appendix B. Wind Speed Data and Wind Power Curves</b>	<b>259</b>
B.1	Wind Speed Data . . . . .	259
B.2	Wind Power Curves . . . . .	259
	<b>Bibliography</b>	<b>262</b>
	<b>Vita</b>	<b>276</b>

## List of Tables

4.1	Wind Power Curves . . . . .	67
4.2	Effect of Wind Power Aggregation on $CR_k$ ( $k=15$ minutes) . .	80
4.3	Comparison Pairs . . . . .	86
4.4	Time Interval Lengths under the three Comparison Schemes .	90
4.5	Coverage Rate Difference $dp$ for Wind Power and Net Demand	96
4.6	Ramp Rate Intervals with Coverage Probability 90% for 5-minute Time Intervals . . . . .	107
4.7	Ramp Rate Intervals with Coverage Probability 90% for 60-minute Time Intervals . . . . .	108
4.8	Mean Absolute Deviations from the Nominal Coverage Rate ( $ dp $ [%]) for Comparison Pair 1 (Conditional Range - Step-changes) . . . . .	121
4.9	Mean Absolute Deviations from the Nominal Coverage Rate ( $ dp $ [%]) for Comparison Pair 2 (Conditional Range - Forward Differences) . . . . .	122
5.1	Nominal and Actual Probabilities in percent for a 160.5 MW Wind Farm (WF6, Wind Power Level $l_j = 0.1$ p.u.) . . . . .	150
5.2	Nominal and Actual Probabilities in percent for a 160.5 MW Wind Farm (WF6, Wind Power Level $l_j = 0.5$ p.u.) . . . . .	151
5.3	Nominal and Actual Probabilities in percent for a 160.5 MW Wind Farm (WF6, Wind Power Level $l_j = 0.9$ p.u.) . . . . .	152
5.4	Nominal and Actual Total Probabilities in percent for all Wind Farms (Forecast Time Resolution $k = 5$ minutes) . . . . .	158
5.5	Nominal and Actual Total Probabilities in percent for all Wind Farms (Forecast Time Resolution $k = 60$ minutes) . . . . .	159
5.6	Buffer Size $N_{b,k}$ in Weeks and Weights $w_{b,k}$ for all Wind Farms and Forecast Time Resolutions $k$ (Exponentially Weighted Moving Average) . . . . .	163
5.7	Weights $w_{b,k}$ for all Wind Farms and Forecast Time Resolutions $k$ (Stochastic Approximation) . . . . .	172

5.8	RMSE of Reliability ( $RMSE(r_k)$ ) in percent for all Wind Farms using three Quantile Estimate Approaches (Sample, EWMA, EWSA) . . . . .	179
5.9	Sharpness of $M_{up}$ ( $s_{k,up}$ ) in percent for all Wind Farms using three Quantile Estimate Approaches (Sample, EWMA, EWSA)	180
5.10	Sharpness of $M_{low}$ ( $s_{k,low}$ ) in percent for all Wind Farms using three Quantile Estimate Approaches (Sample, EWMA, EWSA)	181
5.11	Resolution of $M_{up}$ ( $RES_{k,up}$ ) in percent for all Wind Farms using three Quantile Estimate Approaches (Sample, EWMA, EWSA) . . . . .	182
5.12	Resolution of $M_{low}$ ( $RES_{k,low}$ ) in percent for all Wind Farms using three Quantile Estimate Approaches (Sample, EWMA, EWSA) . . . . .	183
5.13	RMSE of Reliability in percent for all Wind Farms using three Sample Quantiles (Year, Season, Month) . . . . .	191
5.14	NMAE <sub>k</sub> for various Forecast Resolutions $k$ . . . . .	196
5.15	RMSE of Reliability in percent for all Wind Farms using Sample Quantiles on Actual and Perfect Wind Power Forecasts . . . .	203
6.1	95 <sup>th</sup> Percentile of the ESS Characteristics . . . . .	238
6.2	95 <sup>th</sup> Percentile of the ESS Characteristics Using the Generated Scenarios and the Actual Data . . . . .	243
A.1	Wind Farm Data . . . . .	256
A.2	Timespan of Wind Power Data . . . . .	257
B.1	Wind Turbine Data . . . . .	261



## List of Figures

1.1	Variability versus predictability for various common renewable energy sources. . . . .	3
1.2	Examples of outputs from sources of energy with different notions of variability. . . . .	5
2.1	Frequency of appearance of the 10-minute step-changes for two test sources. . . . .	25
2.2	Output of two test sources with equal 10-minute step-changes distribution over a four-hour period. . . . .	25
3.1	Characterizing the variability of wind power using two intervals' sizes ( $M_1$ and $M_2$ ) of different magnitudes over two time frames ( $k_1$ and $k_2$ , respectively). . . . .	35
3.2	Definition of the conditional range metric. . . . .	37
3.3	Graphical representation of the conditional range metric quantile. . . . .	47
4.1	The 95 <sup>th</sup> percentile of the conditional range metric of a 91.5 MW wind farm's power production. . . . .	57
4.2	Typical wind power versus wind speed curve for a variable speed wind turbine. . . . .	59
4.3	The conditional range metric of a 91.5 MW wind farm for $k = 60$ -minute time intervals and various percentiles $p$ , as a function of the hourly average production level $l_j$ . . . . .	60
4.4	The 95 <sup>th</sup> percentile of the conditional range metric of a 91.5 MW wind farm for various time intervals as a function of the interval average production level. . . . .	62
4.5	The effect of the time interval length $k$ on the mid-level production ( $l_j = 0.5$ p.u.) expected wind power conditional range. . . . .	63
4.6	The effect of the wind farm nameplate capacity on the conditional range taken over all production levels for $p = 0.9$ and for various time frames $k$ . . . . .	65
4.7	Six different wind power curves representing wind turbines of different technologies and sizes. . . . .	68

4.8	The first wind speed series and the respective wind power series for a time period of 30 minutes. . . . .	69
4.9	The conditional range $CR_{k,l_j}$ for $k = 15$ minutes as a function of wind power production level $l_j$ for all wind turbine types. .	72
4.10	The conditional range $CR_k$ as a function of time interval length $k$ for all wind turbine types. . . . .	73
4.11	The 95 <sup>th</sup> percentile of the conditional range metric $CRM_{\{W,S\}k,s_j,p}$ for $k = 15$ minutes as a function of wind speed level $s_j$ for wind turbine Type I. . . . .	74
4.12	The 95 <sup>th</sup> percentile of the conditional range metric $CRM_{\{W,S\}k,s_j,p}$ for $k = 15$ minutes as a function of wind speed level $s_j$ for wind turbine Type IV. . . . .	74
4.13	The conditional range $CR_{k,p}$ as a function of the percentile $p$ for two time interval lengths ( $k = 5$ and $k = 60$ minutes). . . .	75
4.14	The 95 <sup>th</sup> percentile of the conditional range metric $CRM_{\{W\}k,l_j,p}$ for $k = 60$ minutes using the wind power series from the first and second wind speed series, as well as the sum of the two wind power series. . . . .	77
4.15	The conditional range $CR_{k,l_j}$ for $k = 15$ for wind power series from the first wind speed series as well as the sum of both respective wind power series. . . . .	78
4.16	The 95 <sup>th</sup> percentile of (a) the conditional range $M_k$ , (b) the step-changes $y_k$ , and (c) the forward differences $z_k$ in p.u. values as a function of the wind farm nameplate capacity $P_N$ for various time intervals lengths $k$ . . . . .	98
4.17	The 95 <sup>th</sup> percentile of (a) the conditional range ramp rate $r_{M_k}$ , (b) the step-changes ramp rate $r_{y_k}$ , and (c) the forward differences ramp rate $r_{z_k}$ in p.u./min values as a function of the wind farm nameplate capacity $P_N$ for various time intervals lengths $k$ . 100	
4.18	The 5 <sup>th</sup> percentile of (a) the conditional range ramp rate $r_{M_k}$ , (b) the step-changes ramp rate $r_{y_k}$ , and (c) the forward differences ramp rate $r_{z_k}$ in p.u./min values as a function of the wind farm nameplate capacity $P_N$ for various time intervals lengths $k$ . 101	
4.19	The 95 <sup>th</sup> percentile of (a) the conditional range $M_k$ , (b) the step-changes $y_k$ , and (c) the forward differences $z_k$ in p.u. values taken over time intervals of length 30 minutes and three different average interval production levels (low=0.2 p.u., medium=0.5 p.u., high=0.8 p.u.), as a function of the wind farm nameplate capacity $P_N$ . . . . .	103

4.20	The 95 <sup>th</sup> percentile of (a) the conditional range ramp rate $r_{M_k}$ , (b) the step-changes ramp rate $r_{y_k}$ , and (c) the forward differences ramp rate $r_{z_k}$ in p.u./min values taken over time intervals of length 30 minutes and three different average interval production levels (low=0.2 p.u., medium=0.5 p.u., high=0.8 p.u.), as a function of the wind farm nameplate capacity $P_N$ . . . . .	104
4.21	The 5 <sup>th</sup> percentile of (a) the conditional range ramp rate $r_{M_k}$ , (b) the step-changes ramp rate $r_{y_k}$ , and (c) the forward differences ramp rate $r_{z_k}$ in p.u./min values taken over time intervals of length 30 minutes and three different average interval production levels (low=0.2 p.u., medium=0.5 p.u., high=0.8 p.u.), as a function of the wind farm nameplate capacity $P_N$ . . . . .	105
4.22	Comparison results for (a) ramp size difference $dx$ , (b) ramp rate difference $dr$ , and (c) coverage rate difference $dp$ between the conditional range $M$ and the step-changes $y$ for the 5-minute time frame under the three comparison schemes as a function of the coverage rate $p$ . . . . .	110
4.23	Comparison results for (a) ramp size difference $dx$ , (b) ramp rate difference $dr$ , and (c) coverage rate difference $dp$ between the conditional range $M$ and the forward differences $z$ for the 5-minute time frame under the three comparison schemes as a function of the coverage rate $p$ . . . . .	111
4.24	Comparison results for (a) ramp size difference $dx$ , (b) ramp rate difference $dr$ , and (c) coverage rate difference $dp$ between the conditional range $M$ and the step-changes $y$ for the 60-minute time frame under the three comparison schemes as a function of the coverage rate $p$ . . . . .	115
4.25	Comparison results for (a) ramp size difference $dx$ , (b) ramp rate difference $dr$ , and (c) coverage rate difference $dp$ between the conditional range $M$ and the forward differences $z$ for the 60-minute time frame under the three comparison schemes as a function of the coverage rate $p$ . . . . .	116
4.26	Mean ramp size difference $dx$ as a function of the time interval length $K$ for five wind farms of different nameplate capacities under the three comparison schemes. . . . .	119
4.27	Mean coverage rate difference $dp$ as a function of the time interval length $K$ for five wind farms of different nameplate capacities under the three comparison schemes. . . . .	120
5.1	Hourly wind power forecast and intra-hour variability intervals for a 160 MW wind farm under no uncertainty. . . . .	133

5.2	Probabilistic forecast of intra-hour variability intervals for a 160 MW wind farm. . . . .	135
5.3	Reliability of various CRM percentile estimates as a function of the 5-minute average wind power forecast level for a 114 MW wind farm under the sample quantile estimate approach. . . .	148
5.4	Reliability of various CRM percentile estimates as a function of the hourly wind power forecast level for a 91.5 MW wind farm under the sample estimate approach. . . . .	149
5.5	Actual proportions of the CRM quantile estimates of a 120.6 MW wind farm for various wind power forecast resolutions $k$ under the sample quantile estimate approach. . . . .	154
5.6	Reliability diagram of the CRM quantile estimates of a 120.6 MW wind farm for various wind power forecast resolutions $k$ under the sample quantile estimate approach. . . . .	155
5.7	Reliability of CRM percentile estimates for various forecast resolutions as a function of the nominal quantile for a 120.6 MW wind farm under the sample estimate approach. . . . .	157
5.8	RMSE of CRM quantiles' reliability for various forecast resolutions as a function of wind farm nameplate capacity under the sample quantile estimate approach. . . . .	160
5.9	Reliability diagram of the CRM quantile estimates of a 210 MW wind farm for various wind power forecast resolutions $k$ under the exponentially weighted moving average quantile estimate approach. . . . .	165
5.10	RMSE of CRM quantiles' reliability for various forecast resolutions as a function of wind farm nameplate capacity under the exponentially weighted moving average quantile estimate approach. . . . .	166
5.11	CRM quantile reliability RMSE difference between the exponentially weighted moving average and the sample quantile estimate approach as a function of wind farm nameplate capacity for various wind power forecast resolutions. . . . .	167
5.12	Reliability diagram of the CRM quantile estimates of a 210 MW wind farm for various wind power forecast resolutions $k$ under the exponentially weighted stochastic approximation quantile estimate approach. . . . .	174
5.13	RMSE of CRM quantiles' reliability for various forecast resolutions as a function of wind farm nameplate capacity under the exponentially weighted stochastic approximation quantile estimate approach. . . . .	175

5.14	CRM quantile reliability RMSE difference between the exponentially weighted stochastic approximation and the sample quantile estimate approach as a function of wind farm nameplate capacity for various wind power forecast resolutions. . .	176
5.15	Sharpness of $M_{up}$ as a function of the wind farm nameplate capacity under the three quantile estimation methods. . . . .	184
5.16	Sharpness of $M_{low}$ as a function of the wind farm nameplate capacity under the three quantile estimation methods. . . . .	185
5.17	Resolution of $M_{up}$ as a function of the wind farm nameplate capacity under the three quantile estimation methods. . . . .	186
5.18	Resolution of $M_{low}$ as a function of the wind farm nameplate capacity under the three quantile estimation methods. . . . .	187
5.19	Reliability diagrams of the CRM quantile estimates of a 160.5 MW wind farm for various wind power forecast resolutions $k$ using yearly, seasonal and monthly sample quantiles. . . . .	190
5.20	RMSE of CRM quantiles' reliability for various forecast resolutions as a function of wind farm nameplate capacity under the sample quantile estimate approach with seasonal considerations.	193
5.21	Density of normalized forecast errors under a normal and a truncated normal distribution. . . . .	197
5.22	Reliability diagram of the CRM quantile estimates of a 120.6 MW wind farm for various wind power forecast resolutions $k$ under the sample quantile estimate approach using an artificial wind power forecast. . . . .	202
5.23	CRM quantile reliability RMSE increment when an actual instead of a perfect wind power forecast is used as a function of wind farm nameplate capacity for various wind power forecast time resolutions. . . . .	204
5.24	CRM expected size difference when an actual instead of a perfect wind power forecast is used as a function of wind farm nameplate capacity for various wind power forecast time resolutions. . . . .	206
5.25	CRM quantile estimate reliability RMSE as a function of the wind power forecast NMAE for $k=5$ minutes. . . . .	207
5.26	CRM quantile estimate reliability RMSE as a function of the wind power forecast NMAE for $k=60$ minutes. . . . .	208
5.27	CRM expected size difference when an actual instead of a perfect wind power forecast is used as a function of the wind power forecast NMAE for $k=5$ minutes. . . . .	208

5.28	CRM expected size difference when an actual instead of a perfect wind power forecast is used as a function of the wind power forecast NMAE for $k=60$ minutes. . . . .	209
6.1	Probability mass function of the hourly averages over a year for a 160.5 MW wind farm. . . . .	217
6.2	Cumulative probability mass function of the hourly averages over a year for a 160.5 MW wind farm. . . . .	218
6.3	Quantile function of the minimum $a$ and maximum $b$ deviations from the hourly average $l_j$ over a year for a 160.5 MW wind farm.	219
6.4	Five 60-minute wind production scenarios having the same hourly average, maximum and minimum production. . . . .	223
6.5	The probability mass functions of the hourly average wind power production using the actual data and the data from the generated scenarios for a 160.5 MW wind farm. . . . .	230
6.6	The difference between the joint probability mass functions of the maximum and minimum deviations from the hourly average wind power production using the actual data and the data from the generated scenarios for a 160.5 MW wind farm. . . . .	231
6.7	The probability mass functions of the wind power production using the actual data and the data from the generated scenarios for a 160.5 MW wind farm. . . . .	232
6.8	The probability mass functions of the ESS characteristics for a 160.5 MW wind farm. . . . .	233
6.9	The quantiles $Q(p)$ of the power and energy sizes of the ESS as a function of the quantile rank $p$ for a 160.5 MW wind farm. . . . .	235
6.10	The 85 <sup>th</sup> to 100 <sup>th</sup> percentiles $Q(p)$ of the power and energy sizes of the ESS as a function of the percentile rank $p$ for a 160.5 MW wind farm. . . . .	236
6.11	The 95 <sup>th</sup> percentile of the a) power size $P_{size}$ and b) energy size $E_{size}$ of the ESS for a 160.5 MW wind farm as a function of the hourly average wind power production. . . . .	237
6.12	The 95 <sup>th</sup> percentile of the power energy size of the ESS as a function of the wind farm nameplate capacity. . . . .	240
6.13	Actual coverage rate of the estimated 95 <sup>th</sup> percentile of the ESS characteristics as a function of the wind farm nameplate capacity.	245
B.1	Probability mass function of the wind speed series. . . . .	260
B.2	Wind power curves. . . . .	261

# Chapter 1

## Introduction

This chapter sets the scene for research on the assessment of intra-hour wind power variability. The notions of wind power variability and uncertainty are distinguished and the various perceptions of variability are explained in Section 1.1. Moreover, the need for developing a novel wind power variability metric is justified, and desired features of this metric are presented. The main research objectives are clearly stated in Section 1.2 and the approach taken to meet each of these objectives is summarized in Section 1.3. Finally, major and supporting research contributions are identified and a list of publications is provided in Section 1.4, while an outline of the dissertation is given in Section 1.5.

### 1.1 Background and Motivation

Wind farm installed capacity surpassed 60 GW in the United States, 93 GW in Europe and 282 GW worldwide at the end of 2012 [1]. Despite wind's stochastic nature and the risks associated with it, large scale wind power integration in utility systems has seen distinct increasing trends worldwide in the past years. Wind power is very variable and unpredictable and these characteristics of wind power pose significant risk to both system planners and operators. Within the past decade numerous wind integration studies have been performed with the goal to investigate the effect of wind power variabil-

ity and unpredictability on system reliability, as well as system operations and their cost. Regarding wind power variability, wind integration studies also attempt to estimate its effect on system flexibility, which appears in the form of increased ramp rates, increased time periods with minimum generation, and increased operating reserve requirements.

The risks associated with the integration of wind in utility systems are attributed to its stochastic nature and specific characteristics. Wind is often characterized as a very variable, highly unpredictable and non-dispatchable source of energy. While wind power variability and unpredictability are often used interchangeably, a distinction between these terms is important. Figure 1.1 shows the variability and predictability content of various renewable energy sources. From this graph it is evident that some sources can have a very volatile but known output, such as tidal power, while others, like wind power, have both a volatile and a very uncertain output. In the past years wind power forecasting has undergone extensive research and significant improvements have been made in reducing wind power forecasting uncertainty. However, it is crucial to realize that wind power variability will be present and will have to be dealt with even when all uncertainty is removed under perfect forecasts, making the analysis and quantification of wind power variability a significant research topic.

Regarding wind's characterization as being a non-dispatchable source, a necessary distinction to be made is between intermittent, variable, and non-dispatchable sources of energy. An intermittent source of energy is characterized by unintentional pauses which make the output of the source completely unavailable, while a variable source is any source with undesired or uncontrolled changes in output. On the other hand, a non-dispatchable source is characterized by the inability to control its output on demand. These charac-



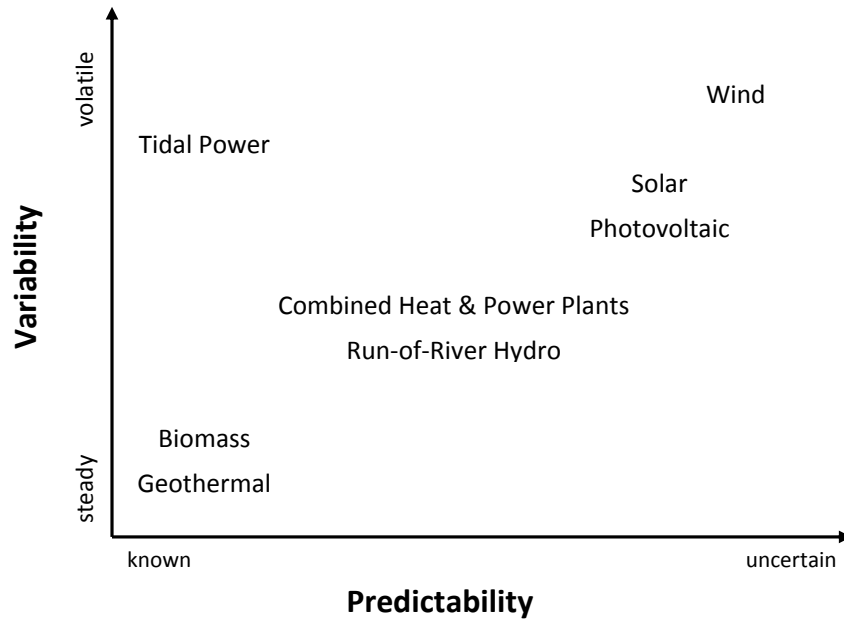


Figure 1.1: Variability versus predictability for various common renewable energy sources. Some sources can have a very volatile but known output, such as tidal power, while others, like wind power, have both a volatile and a very uncertain output.

teristics have to do more with the control over the source’s output and less with the knowledge of it. As with variability and predictability, a source’s output can have only one or all of the above characteristics. Figure 1.2 depicts some examples of various sources and their outputs regarding variability. The output in MW from three sources, denoted wind, sinewave and direct geothermal, is depicted over a time period of 10 hours. Though the three sources produce similar amounts of energy over the 10-hour period the variability content in their power output varies significantly. The sinewave is considered a variable yet not intermittent source. The direct geothermal power is a fictitious source, which would correspond to a thermal power station using geothermal steam

in a steam turbine without any other controls. Since geothermal steam has a constant flow, this source represents a steady and not intermittent output, yet it is a non-dispatchable source. Using the above definitions wind power is an intermittent source of energy, since wind speeds below cut-in and above cut-off make it completely unavailable. (Notice the total unavailability of the wind power in Fig. 1.2 close to minute 60 and after minute 590). Moreover, wind power is variable since it changes uncontrollably with time. Furthermore, wind power is a non-dispatchable source of energy, since its output cannot be dictated. Various ways have been shown to reduce wind power variability, however it is important to understand that the only way wind power intermittency and non-dispatchability can be overcome is by coupling wind with dispatchable and fully controllable generators, such as gas turbines, or with energy storage units.

Acknowledging that wind power variability will be present even under perfect forecasts makes its analysis of critical importance, since underestimating wind power variability can have adverse effects on power systems, especially their reliability and economics. Therefore, a metric which can efficiently quantify the short-term variability of wind power is of big significance, not only for power system planners and operators, but also for wind farm owners and investors. However, the prevalent wind power variability metric used in wind integration studies, which is based on the step-changes of wind power taken over various time frames, fails to effectively capture wind power variation within an interval, since it is calculated from the differences between average wind power values. On the other hand, other recently proposed metrics lack a clear connection to power system operations. Thus, a novel intra-hour wind power variability metric is deemed necessary, especially with the current rate at which wind power penetration levels increase, since for large penetrations

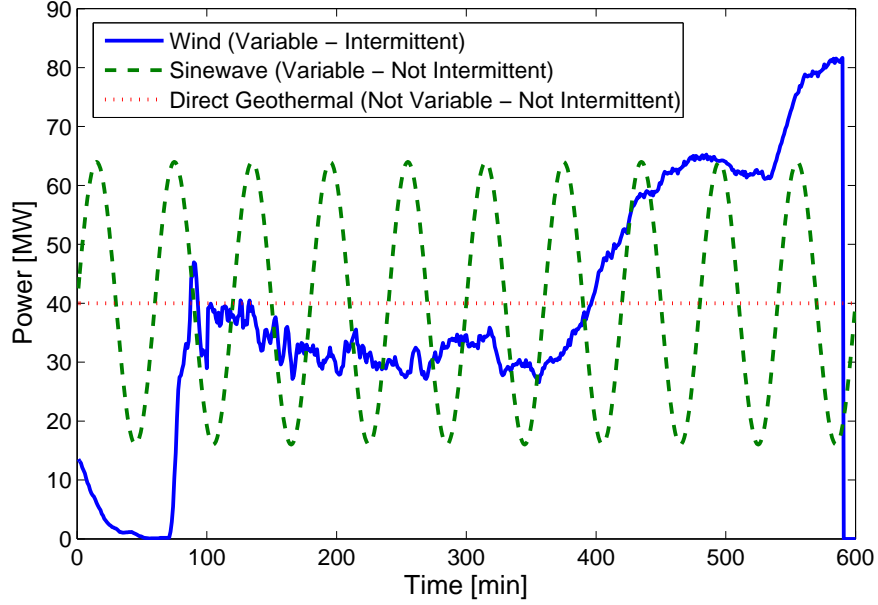


Figure 1.2: Examples of outputs from sources of energy (wind, sinewave, direct geothermal) with different notions of variability. Wind is a variable, intermittent and non-dispatchable source of energy. Notice the total unavailability of the wind power close to minute 60 and after minute 590.

the intra-hour variation of wind power becomes comparable in size to the intra-hour demand variation.

The novel metric should not only efficiently characterize wind power variability and effectively overcome the shortcomings of current metrics, but it should also be of practical value to power system operators and wind farm owners. Quantifying wind power variability, regardless of its uncertainty, can provide important characteristics a generator must have so as to accommodate wind power fluctuations, essentially improving wind power management techniques. At the planning time scale, ramping requirements of controllable units and an adequately flexible system generation portfolio can be specified

to accommodate wind power. At the operational time scale, generation output and reserve allocation can be tuned to achieve desired short-term (hours to minutes) variability. In addition, analysis of wind power variability and especially the factors which affect it can lead to ways of reducing wind power variability to more acceptable risk levels for power systems, however keeping in mind that wind power variability cannot be eliminated without the use of some dispatchable source of energy.

## 1.2 Research Objectives

The main objective of the work presented herein is to assess intra-hour wind power variability. For this purpose a novel intra-hour wind power variability metric is proposed. The new metric is expected to assist power system operators and wind farm owners in quantifying and hence more efficiently managing wind power variability over various time frames. Moreover, the new metric can be used to obtain wind power variability forecasts, which can assist in decision making under uncertainty, when the uncertainty comes from wind power variability.

Specific research objectives towards assessing intra-hour wind power variability are listed below:

- *Objective 1: To develop a metric to quantify intra-hour wind power variability*

This objective involves developing a formal definition and a detailed computational algorithm for the proposed intra-hour wind power variability metric.

- *Objective 2: To assess intra-hour wind power variability*

This objective requires an extensive performance analysis of the proposed intra-hour wind power variability metric using a large set of real-world wind power data.

- *Objective 3: To evaluate the proposed metric against existing metrics*

This objective entails the identification of shortcomings of currently used wind power variability metrics and the demonstration of how they can be overcome by the proposed metric.

- *Objective 4: To develop methods to forecast wind power variability*

This objective links the proposed intra-hour wind power variability metric to the definition of a wind power variability forecast and explains how the forecast can be obtained.

- *Objective 5: To demonstrate the utility of the proposed metric*

This objective demonstrates the practical value of the proposed intra-hour wind power variability metric to power system operators and wind farm owners through an example application.

## 1.3 Research Approach

The approach taken towards meeting each of the previously defined research objectives is summarized in this section.

### 1.3.1 To Develop a Metric to Quantify Intra-hour Wind Power Variability

The approach taken towards defining a wind power variability metric involves the use of the range as a measure of dispersion. Thus, the general idea

of the proposed intra-hour wind power variability metric lies in quantifying the variability of a source using its range of outputs over a given period. The proposed conditional range metric (CRM) defines the endpoints of an interval  $[M_{low}, M_{up}]$  within which the wind power output lies over a given length intra-hour time frame. The size of this interval provides a measure of wind power variability, which corresponds to the largest change the wind power output can undergo within the given time frame. The metric is termed conditional since the range of wind power output is conditioned on the time frame length  $k$  and on the wind power average production  $l_j$  over the given time frame.

A single value of the conditional range metric provides information on an instance of wind power variability. The quantiles of the CRM are used to obtain a measure of intra-hour wind power variability over the course of a longer period. Using statistical analysis and optimization approaches a computational algorithm to obtain a unique  $p^{th}$  quantile of the conditional range metric is given. In this manner the proposed conditional range metric  $CRM_{k,l_j,p} = [M_{low_{k,l_j,p}}, M_{up_{k,l_j,p}}]$  is turned into a probabilistic intra-hour wind power variability metric. The provision of  $p^{th}$  CRM quantiles is of significance, because it gives power system operators and wind farm owners a measure of intra-hour wind power variability in the long term and allows them to make decisions involving wind power variability based on their willingness to accept a certain level of risk  $\alpha = 1 - p$ .

### 1.3.2 To Assess Intra-hour Wind Power Variability

To assess intra-hour wind power variability the proposed conditional range metric is applied on a large set of real-world wind power and wind speed data. The purpose of this analysis is to identify how certain variables

affect intra-hour wind power variability, which in turn can lead to diagnosing time periods and conditions with increased wind power variability, as well as providing characteristics of means used to reduce wind power variability to more acceptable risk levels. The sensitivity analysis quantifies wind power variability due to intrinsic variables, such as changes in the average wind power output directed by changes in wind speed, as well as wind power variations due to extrinsic factors, such as the wind turbine size and technology.

### **1.3.3 To Evaluate the Proposed Metric against Existing Metrics**

The evaluation of the proposed metric against existing metrics is done by comparing the performance of the conditional range metric against the step-changes statistics. Wind power step-changes are differences of wind power averages taken over different length time intervals and their standard deviation is the prevalent wind power variability metric used in numerous wind integration studies. The purpose of the comparison between the conditional range metric and the step-changes is to evaluate the ability of both metrics to assess intra-hour wind power variability, and more specifically their ability to estimate the size of the largest change in wind power output over a given length time frame, and the rate at which this change occurs.

### **1.3.4 To Develop Methods to Forecast Wind Power Variability**

Towards meeting this objective, first a wind power variability forecast is defined as the interval  $[P_{w,min}, P_{w,max}]$  within which the wind power output  $P_w$  over an intra-hour time frame will lie, given the forecast for the average wind power production over this time frame. Hence, a wind power variability forecast is essentially a future value of the conditional range metric. To obtain

a probabilistic wind power variability forecast, i.e. a forecast which provides several interval estimates  $[P_{w,min}, P_{w,max}]$  associated with different probabilities  $p$ , conditional range metric quantiles are estimated employing static and time adaptive quantile estimation methodologies.

### **1.3.5 To Demonstrate the Utility of the Proposed Metric**

The utility of the proposed metric is demonstrated by providing an example practical application of the conditional range metric. The application considered involves the coupling of wind power with an energy storage system so as to reduce wind power variability. The methodology provided estimates the size, in terms of power and capacity, of an energy storage system with the goal of minimizing wind power imbalances from the hourly average, essentially 'firming' the wind power output.

The validation of the studies performed towards meeting Objectives 2-5 is done using real-world wind power and wind speed data. All algorithms and computations have been implemented in MATLAB.

## **1.4 Original Research Contributions**

In this section the major and supporting research contributions towards meeting the previously defined objectives, along with the relevant publications are listed.

### **1.4.1 Major Contributions**

The major research contributions are:



- To meet Objective 1 a novel probabilistic intra-hour wind power variability metric, termed conditional range metric is defined. The proposed metric quantifies wind power variability by measuring the size of an interval within which the wind power output lies. The metric is based on the range of the wind power output over a given time frame, conditioned on the average wind power production over that time frame. The formal definition and a detailed computational methodology to obtain a unique  $p^{th}$  quantile of the conditional range metric are given in Chapter 3. The work has been published in [2]:
  - T. Boutsika and S. Santoso, “Quantifying short-term wind power variability using the conditional range metric,” *Sustainable Energy, IEEE Transactions on*, vol. 3, no. 3, pp. 369-378, July 2012.
- As part of Objective 2 the conditional range metric has been applied on real-world wind power data from 18 wind farms spanning a period of 1 up to 4 years, and on two 30-week long wind speed series. Among others, the effects of wind power production, wind farm size, wind turbine size and wind turbine technology on wind power variability have been examined. The effects of these variables are not only described in a qualitative manner, but are also quantified using the conditional range metric. The results from this analysis are presented in Sections 4.1 and 4.2 and have been published in [2, 3]:
  - T. Boutsika and S. Santoso, “Quantifying short-term wind power variability using the conditional range metric,” *Sustainable Energy, IEEE Transactions on*, vol. 3, no. 3, pp. 369-378, July 2012.

- T. Boutsika and S. Santoso, “Quantifying the effect of wind turbine size and technology on wind power variability,” in *Power and Energy Society General Meeting, 2013 IEEE*, July 2013, pp. 1-5.
- To achieve Objective 4, probabilistic wind power variability forecasts are proposed which can be used in conjunction with state-of-the-art wind power forecasts. The wind power variability forecasts are defined as intervals within which the wind power output will lie, conditioned on the forecasted average wind power production. The  $p^{th}$  CRM quantiles are used to construct such intervals, essentially wind power inequalities of the form  $\{M_{low_k, l_j, p} \leq x_n \leq M_{up_k, l_j, p} \text{ with probability } p\}$ , which bound the wind power output  $x_n$  over a time interval of length  $k$  and average wind power production  $l_j$ . The importance of these inequalities stems from the fact that they can serve as so-called joint chance constraints in several stochastic optimization problems. Thus, wind power variability forecasts open the door to numerous applications of the conditional range metric which can reduce the risk in decision making due to uncertainty from wind power variability, starting at the wind turbine or farm level and ranging up to the balance authority aggregated level. One static and two time adaptive methodologies to obtain CRM quantile estimates for wind power variability forecasts are provided. These are based on sample quantiles, from historical wind power variability data, and their adaptations, using an exponentially weighted moving average and a stochastic approximation approach. The definition of wind power variability forecasts and the methodologies to obtain them are given in Chapter 5.

### 1.4.2 Supporting Contributions

Supporting research contributions are

- Working towards meeting Objective 3, the wind power conditional range is compared under three different schemes to the wind power step-changes and forward differences statistics, which are the prevalent wind power variability metric applied in wind integration studies. The results of this comparison reveal the shortcomings of the currently used step-changes approach, and quantify their inability to reliably assess the size and rate of change in wind power output over intra-hour time intervals. Part of the comparative analysis presented in Section 4.3 has been published in [4]:
  - T. Boutsika and S. Santoso, “Quantifying short-term wind power variability,” in *Power and Energy Society General Meeting, 2011 IEEE*, July 2011, pp. 1-7.
- To meet Objective 5 a practical example application of the conditional range metric is given. In this application, a detailed algorithm to estimate the size of an energy storage system is presented. The storage system is coupled with a wind farm, with the goal of firming its output, by minimizing the deviations of the wind power output from the wind power hourly average. Its size is estimated using a forecast of hourly wind power averages and historical wind power variability values, and is evaluated using real-world wind power data. The energy storage system sizing algorithm is described in Chapter 6 and has been published in [5]:
  - T. Boutsika and S. Santoso, “Sizing an energy storage system to minimize wind power imbalances from the hourly average,” in *Power*

*and Energy Society General Meeting, 2012 IEEE*, July 2012, pp. 1-8.

## **1.5 Dissertation Outline**

This document is outlined as follows. Common measures of variability and a summary of wind power variability metrics used in wind integrations studies are given in Chapter 2, followed by the definition and computational algorithm of the proposed conditional range metric, which is presented in detail in Chapter 3. The conditional range metric is evaluated in Chapter 4 using real-world wind power and wind speed data. The evaluation involves an extensive performance analysis of the conditional range and its comparison to the commonly used step-changes. Then, wind power variability forecasts and methods to obtain them are elaborated in Chapter 5, whereas the practical example application of the conditional range metric is reported in Chapter 6. Finally, Chapter 7 provides the conclusion and future research directions.

## Chapter 2

### Prior Work in Wind Power Variability

In statistics, statistical dispersion or variability refers to the spread of values of a random variable. On the other hand, location or central tendency refers to the mean or expected value of the random variable. Dispersion and location are the most important properties of a probability distribution. In physical sciences, sources of statistical dispersion of a measured quantity can be extrinsic, such as systematic or random measurement errors, or the observed variability might be intrinsic to the phenomenon.

Wind power can be considered as a random variable with intrinsic variability, since it is determined by a number of variables that are seldom unchanging and hardly stable. These variables include wind speed and direction, temperature and atmospheric pressure. But even if these variables are considered static, other parameters such as the wind turbine size and technology may affect the variability of the wind power output. Though much effort has been placed in mitigating the adverse effects of wind power uncertainty in recent years, by providing ever improving methods to estimate the central tendency of wind power, little focus has been given on wind power variability.

This chapter provides a review of common measures of statistical dispersion (Section 2.1) along with their applications in wind power (Section 2.2). The most widely used wind power variability metric in wind integration studies is presented in Section 2.2.1, while other approaches to characterize wind

power variability are given in Section 2.2.2.

- **Publications:** Part of the work presented in this chapter has been published in [2, 4]:
  - T. Boutsika and S. Santoso, “Quantifying short-term wind power variability,” in *Power and Energy Society General Meeting, 2011 IEEE*, July 2011, pp. 1-7.
  - T. Boutsika and S. Santoso, “Quantifying short-term wind power variability using the conditional range metric,” *Sustainable Energy, IEEE Transactions on*, vol. 3, no. 3, pp. 369-378, July 2012.

## 2.1 Common Measures of Dispersion

Measures of dispersion (or measures of spread) are used to characterize the spread of values of a random variable  $X$ . Common measures of dispersion include the following [6]:

- Variance,  $Var$
- Standard deviation,  $\sigma$
- Coefficient of variation,  $c_v$
- Mean (or median) absolute deviation,  $MAD$
- Interquartile range,  $IQR$
- Range,  $R$

Let  $X$  be a continuous random variable with probability density function  $f_X$  and cumulative density function  $F_X$ . The variance of  $X$  is its second order central moment, given by:

$$Var(X) = \int_{-\infty}^{\infty} (x - \mu)^2 f_X(x) dx = E[(X - \mu)^2] = E[X^2] - E[X]^2 \quad (2.1)$$

where  $\mu = \int_{-\infty}^{\infty} x f_X(x) dx = E[X]$  is the mean of  $X$ . The variance describes how far the values of  $X$  lie from its mean.

The standard deviation of  $X$  is the positive square root of the variance:

$$\sigma(X) = \sqrt{Var(X)} \quad (2.2)$$

The standard deviation is easier to manipulate since it has the same units as the random variable  $X$ , while the variance has the units of  $X^2$ . Moreover, though both measures are location invariant, only the standard deviation is linear in scale.

Variance and standard deviation are suitable measures of dispersion when  $X$  is normally distributed. One of the most frequent uses of standard deviation is to construct confidence intervals of a random variable's mean, using the Central Limit Theorem. The most known example is the  $3\sigma$ -rule or empirical rule, which states that under the assumption of a normal distribution 99.7% of all values lie within three standard deviations of the mean.

The coefficient of variation is a dimensionless measure of dispersion, given by:

$$c_v = \frac{\sqrt{E[(X - E[X])^2]}}{E[X]} = \frac{\sigma}{\mu} \quad (2.3)$$

Essentially, the coefficient of variation is the standard deviation normalized by the value of the mean. Thus, it gives a measure of dispersion of the random variable relative to its location. This measure is suitable for comparison between two variables with very different means, however it cannot be applied

to variables having zero (or near-zero) mean. The inverse of the coefficient of variation is the signal to noise ratio, used in signal processing to quantify how much a signal has been corrupted by noise.

The mean absolute deviation of  $X$  is given by:

$$MAD(X) = E[|X - E[X]|] \quad (2.4)$$

For the median absolute deviation, mean  $E[\cdot]$  is replaced by the median in the above equation. The mean absolute deviation is a more robust estimator of scale than standard deviation or variance, because it is more resilient to outliers. It has been used widely in the concept of forecasting under the name of mean absolute error  $MAE = \sum_{i=1}^n |e_i|/n$  with  $e_i = y_i - f_i$ , where for each observation  $e_i$  is the error,  $f_i$  is the forecast and  $y_i$  is the true value.

The interquartile range of  $X$  is given by the difference between the 75<sup>th</sup> and the 25<sup>th</sup> percentile of  $X$ :

$$IQR(X) = Q_X(0.75) - Q_X(0.25) \quad (2.5)$$

In (2.5)  $Q_X(i)$  denotes the  $i^{th}$  percentile of  $X$ ,  $i = 1, 2, \dots, 99\%$ , given by:

$$Q_X(i) = F_X^{-1}(i) = \inf\{x : P[X \leq x] \geq i\} \quad (2.6)$$

where  $F_X^{-1}$  is the inverse of the cumulative distribution function of  $X$ . The interquartile range is mostly used to build box plots, which are graphical representations of probability distributions. The IQR of data from a sample of  $X$  can be estimated using order statistics or optimization techniques.

Finally, the range of  $X$  is the length of the smallest interval which contains all the values from the support of  $X$ , i.e. all values of  $X$  for which  $f_X(x) \neq 0$ . It should be noted that only random variables supported on a



bounded interval have a finite range, such as the beta, the continuous uniform or the truncated normal. However, the sample range from a sample of the random variable  $X$  is always finite. It is calculated by subtracting the smallest (sample minimum) from the greatest (sample maximum) observation:

$$R(X) = \max(X) - \min(X) \quad (2.7)$$

The above measures of dispersion can be applied to discrete random variables by replacing integrations with summations and the probability density function with the probability mass function. Care should be taken when the above measures of dispersion are estimated from a data sample, since they are all prone to outliers. This means that an outlier in the data, i.e. a value that is separate from the body of the data, can skew the measure significantly.

The median absolute deviation does not move quite as much as the standard deviation or variance in response to data with outliers. This is because in the standard deviation, the distances from the mean are squared, so large deviations are weighted more heavily, and thus outliers can heavily influence it. On the other hand, unless used with a large sample size the range can be a poor and weak measure of dispersion, since it only depends on two of the observations. However, since only the middle 50% of the data affects the interquartile range, this measure is the most robust to outliers.

## 2.2 Measures of Wind Power Dispersion

Wind power is intrinsically very variable and attempts have been made to characterize wind power variability. The most widely used variability metric in wind integration studies is the standard deviation of the wind power or net demand step-changes taken over various time frames, as described in

Section 2.2.1. A short overview of wind power variability metrics proposed in other reports and research papers is given in Section 2.2.2.

### 2.2.1 Step-Changes

Time series models have been extensively used for short-term wind power forecasting, however, one of the purposes of analyzing wind speed and wind power time series and performing statistical analysis on historical data has also been to obtain a measure of wind power variability. Indeed, the most widely used measure of dispersion to characterize the variability of wind power is the standard deviation of the wind power step-changes taken over various time frames, which can be obtained from the analysis of the wind power time series.

#### 2.2.1.1 Definition of Step-changes

To estimate the variability of wind power using step-changes, first the continuous wind power output  $x(t)$ , with  $t$  being the time, is measured at successive points in time spaced at uniform time intervals of length  $T_s$  so as to generate a discretized wind power time series  $x_n$ ,  $n = 1, 2, \dots, N$ . The step-changes time series  $y_{k,i}$  for the desired time frame  $k$ , where  $k \geq T_s$ , is then defined from the difference between two successive average wind power outputs  $\bar{x}_{k,i}$  taken over  $k$ -long time intervals:

$$y_{k,i} = \bar{x}_{k,i+1} - \bar{x}_{k,i}, \quad i = 1, 2, \dots, q-1 \quad (2.8)$$

where  $q = \lfloor N/k \rfloor = \max\{m \in \mathbb{Z} | m \leq N/k\}$ . In (2.8)  $\bar{x}_{k,i}$  refers to the sample mean of the wind power over the desired time frame  $k$ :

$$\bar{x}_{k,i} = \frac{1}{k} \sum_{m=1}^k x_{k(i-1)+m}, \quad i = 1, 2, \dots, q \quad (2.9)$$

To estimate the standard deviation of the time series  $y_{k,i}$  the unbiased sample standard deviation,  $s_{y_{k,i}}$ , can be used:

$$s_{y_{k,i}} = \sqrt{\frac{1}{q-2} \sum_{i=1}^{q-1} (y_{k,i} - \bar{y}_{k,i})^2} \quad (2.10)$$

where  $\bar{y}_{k,i}$  is the sample mean of the entire wind power step-changes series  $y_{k,i}$ :

$$\bar{y}_{k,i} = \frac{1}{q-1} \sum_{i=1}^{q-1} y_{k,i} \quad (2.11)$$

### 2.2.1.2 Applications of Step-changes in Wind Integration Studies

A summary of findings of wind integration studies from several utilities in the United States on the grid impacts of wind power variability can be found in [7], whereas a description of how wind integration studies have evolved in the past years in terms of determining the operating reserves requirements is given in [8]. The operating reserves are spinning and non-spinning reserves used to balance load and generation at all times, and are chosen in ways so as to comply with the resource and demand balancing reliability standards imposed by North American Electric Reliability Corporation [9].

The effect wind variability has on operating reserves, such as the increase in regulation (seconds up to 5 minutes) and load following (intra-hourly effects) or the changes in unit commitment (hourly impacts), is estimated by applying statistical methods on wind power and demand time series, either specifically generated for the study or taken from historical data. When the sample standard deviation  $s_{y_{k,i}}$  of the step-changes from (2.10), calculated over various time frames  $k$  using data from the whole time series or some subset of it, is used as a variability metric, the operating reserves requirements are

estimated to be equal to  $3s_{y_{k,i}}$  so as to accommodate variability at 99.7% of all instances under the assumption that the step-changes are normally distributed.

The standard deviation of the step-changes has been used as a metric for variability in numerous older [10–13], as well as more recent wind integration studies [14–18]. The Minnesota Wind Integration Study [10] is one of the first wind integration studies in the U.S. and estimates the impact of 1500 MW of wind power on the system’s projected 2010 peak load of 10,000 MW, corresponding to a 15% penetration level (ratio of nameplate wind generation to peak system load). An additional 8 MW for regulation and 30 MW for load following reserves are determined by taking three times the standard deviation of the 1-minute and 10-minute net demand (load minus wind) step-changes, respectively. The New York ISO Wind Integration Study [12] looks at the impact of 3,300 MW wind power on the system’s 33,000 MW peak load. Using the same approach this study estimates that a 10% penetration level would result in a need for 36 MW more regulation and in a 3% increase in the standard deviation of net demand 5-minute step-changes. The Electric Reliability Council of Texas Wind Integration Study[13] also uses the standard deviation of the step-changes over various time frames, ranging from 1 minute to 1 hour, as a measure to characterize net demand variability. This study estimated the impact of various wind power penetration levels, ranging from 7.67% to 23% based on the 2008 estimated peak load, on the ERCOT system and resulted in an increase in the standard deviation of 1-minute, 5-minutes and 15-minutes step-changes by 14%, 18% and 19% respectively for the highest wind power penetration level.

Increased needs in load following reserves due to wind power variability are estimated based on the standard deviation of the 10-minute net demand

step-changes in the Montana [15] and Nebraska [16] Wind Integration Studies, as well as the Western Wind and Solar Integration Study (WWSIS) [17]. The Montana Wind Integration Study estimates the impact of an additional 10-150 MW wind power, while the Nebraska Wind Integration Study evaluates the effects of wind energy penetration levels, based on wind energy to total energy sales, ranging between 10% and 40%. The focus of the Western Wind and Solar Integration Study (WWSIS) is to investigate the operational impact of up to 35% energy penetration of wind, photovoltaics (PVs), and concentrating solar power (CSP) on the power system operated by the WestConnect group of utilities in Arizona, Colorado, Nevada, New Mexico, and Wyoming. Finally, the Southwest Power Pool (SPP) Wind Integration Study [18] evaluates the impact of integrating high levels of wind penetration on the SPP transmission system, by examining wind energy penetration levels of 10%, 20% and 40%. In this study the 5<sup>th</sup> and 95<sup>th</sup> percentiles of the the 10-minute step-changes are used as a metric to estimate increased needs in up and down regulation, respectively.

### **2.2.1.3 Shortcomings of the Step-changes Approach**

Although the standard deviation of step-changes has been widely used to characterize wind power and net demand variability, this approach suffers from the following shortcomings:

1. Step-changes are calculated between average values over two time intervals and thus they do not convey any information about the variability within the intervals, which can lead to an underestimation of variability.
2. The knowledge conveyed by step-changes is partial, since they provide information on ramp rates, but not on their duration, information which

can benefit power system operators in planning their reserves needs.

3. Three standard deviations of the step-changes (variability instances) capture 99.7% of all variability instances only under the assumption that the step-changes are normally distributed, which means that three standard deviations of the step-changes might be insufficient reserves.

Generation providing regulation reserves has to be able to follow the variability of net demand within the 5-minute time frame, while load following reserves account for the variability of demand within the 1-hour time frame. In wind integration studies where the step-changes approach is used, regulation and load-following reserves are estimated using three standard deviations of the 1-minute and 10-minute step-changes, respectively. However, as the simple case study in [4] reveals, using the step-changes over smaller time frames as a measure to characterize variability within longer time frames can lead in an underestimation of the variability. The case study deals with the variability exhibited from two test sources, sources 1 and 2, within the 1-hour time frame. Figure 2.1 shows the 10-minute step-changes histograms of the two sources over a 24-hour period, which are identical. When three standard deviations of the 10-minute step-changes are used as a metric to characterize variability within the 1-hour time frame, the two sources have equal variability with  $3\sigma_{10min_{S1}} = 3\sigma_{10min_{S2}} = 45.5$  MW.

Yet, the two test sources exhibit a completely different intra-hour behavior, as is depicted in Fig. 2.2. Thus, determining the intra-hour variability of a source using the 10-minute step-changes can lead to an underestimation of the source's variability. Moreover, from the step-changes histogram a highest ramp rate of 25 MW/10 min is perceived, but without any information on the duration of this ramp rate, no safe conclusion about the largest ramp

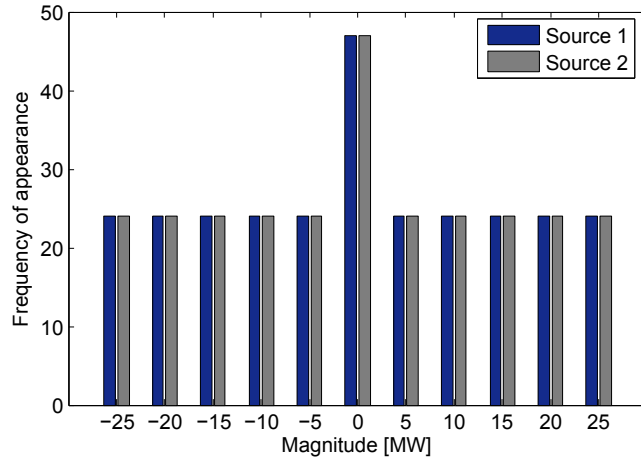


Figure 2.1: Frequency of appearance of the 10-minute step-changes for two test sources (Source 1, Source 2). The two sources have equal variability with  $3\sigma_{10min}(S1) = 3\sigma_{10min}(S2) = 45.5$  MW.

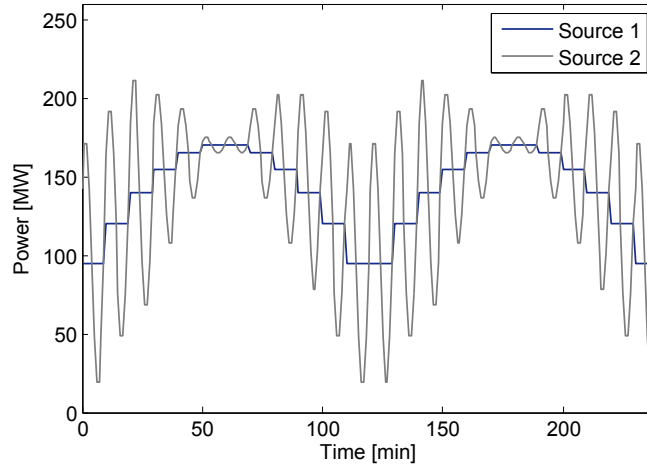


Figure 2.2: Output of two test sources with equal 10-minute step-changes distribution over a four-hour period. The second source exhibits a larger intra-hour variability.

rate in the 1-hour time frame can be drawn. The proposed metric overcomes these shortcomings, since the two sources have different variability under the proposed metric as is shown in Section 3.4. In addition, the first two shortcomings of using wind power step-changes to characterize wind power variability are exposed with the comparative analysis presented in Section 4.3 using real-world wind power data.

Regarding the third shortcoming, the misconception about step-changes arises from the fact that in most wind integration studies where wind power step-changes have been used, the metric for wind power variability is taken to be three standard deviations of the step-changes. The  $3\sigma$  rule is widely adopted because, under the assumption of a normal distribution, it captures 99.7% of all instances. If wind speeds are considered independent the addition of the output from a large number of wind farms will result in a normal distribution per the central limit theorem. However, recent studies have exhibited results which reject the assumption that the wind power step-changes are normally distributed for variation times of one up to four hours [19, 20]. In [19] a beta distribution is used to describe the wind power output, while the distribution of the wind power step-changes is found to follow an exponential decay. In [20]  $\chi^2$ -goodness-of-fit tests are performed to evaluate the suitability of a Laplace, a general extreme value, and a normal distribution for describing wind power variability, with the Laplace distribution outperforming the other distributions. In all cases, however, the step-changes distributions remain leptokurtic, indicating larger tails than the normal distribution. Hence, the use of the  $3\sigma$  rule for quantifying wind power variability may provide insufficient results if the underlying normality assumption is not satisfied.



### 2.2.2 Other Wind Power Variability Metrics

Other than the step-changes, in a few wind integration studies reserves are determined using a multiple of the standard deviation of the differences  $z_i$  of the net demand  $x_i$ ,  $i = 1, 2, \dots, N$  from a rolling moving average:

$$z_i = x_i - \bar{x}_{i-k, i+k} \quad (2.12)$$

where

$$\bar{x}_{i-k, i+k} = \frac{1}{2k+1} \sum_{i=1}^{2k+1} x_i \quad (2.13)$$

denotes the net demand rolling moving average. This approach has been adopted in [21–23]. The Arizona Public Service Wind Integration Study [21] examines the operating impacts and costs of integrating various wind energy penetration levels ranging from 1% to 10%, whereas the New England [22] and Portland [23] Wind Integration Studies examine the impact from an additional 400 MW and 10 GW to the respective systems. Under this approach regulation reserves are determined using the differences of the 1-minute net demand from a 20-minute moving average, whereas for the load-following reserves the differences of 10-minute average values from an hourly trend are used. A similar approach is used in Avista Corporation Wind Integration Study [24], which examines the impact of wind power penetration levels ranging from 5% to 30%. In this study the load-following reserve requirements are specifically tied to the system’s reliability performance using the Power Balancing Control Performance CPS2 compliance, which requires the 10-minute average Area Control Error to be less than a specified bound for more than 90% of all available 10-minute time intervals.

In a few wind integration studies wind power variability is not estimated by applying only measures of dispersion on the wind power time series,

but it is also combined with wind power uncertainty [25, 26]. This approach is adopted despite the fact that wind power variability will be present and pose risks to system operations even when all uncertainty is removed with perfect wind power forecasts. Eastern Wind Integration and Transmission Study [25] combines wind variability with wind forecast errors. In this study the standard deviation of 1-minute step-changes is estimated to be 1 MW per 100 MW wind plant for the wind step-changes and 0.33% of the total hourly load for the load step-changes. Assuming that for the 1-minute time frame load and wind variability are independent the standard deviations of load and all wind farms are geometrically added. The result showed that the variability of adding 60 GW of wind power on a 100 GW load was estimated not to have an effect on the regulation reserves requirements. However, the wind uncertainty is determined to have a more significant effect on regulation reserves than the wind variability, an effect which is incorporated by using the standard deviation of the wind hourly forecast error in the regulation requirements ( $RR$ ) equation:

$$RR = 3\sqrt{(0.33\%l_{1h})^2 + (\sigma_{wind_{\Delta 1h}})^2} \quad (2.14)$$

where  $l_{1h}$  is the hourly total load and  $\sigma_{wind_{\Delta 1h}}$  is the standard deviation of the wind power hour ahead ( $\Delta 1h$ ) forecast error.

The California Independent System Operator (CAISO) Wind Integration Study [26] is another study to estimate operating reserves by combining variability and uncertainty of wind and load. In this study a completely different approach is performed and the increase in operating reserves is calculated based on a detailed mathematical model of the CAISO's actual scheduling, real time dispatch and regulation processes and their timelines, using appropriate forecasted load and wind data series. Though this methodology provides a robust and accurate assessment of the additional capacity, ramping and ramp

duration requirements that the CAISO regulation and load following systems will be facing when the 20% Renewable Portfolio Standard is achieved, the proposed methodology is not only very complicated but also very system specific.

Finally, some recently proposed metrics to characterize wind power variability involve analysis in the frequency domain and make use of the power spectral density of the wind power output. In [27] the measured wind power data with sampling resolutions of 1 second up to 1 hour are found to follow the Kolmogorov spectrum of energy between frequencies of 30 seconds to 2.6 days. The Kolmogorov's energy spectrum  $E$  is proportional to the wave number  $k$  and the rate  $\psi$  of energy dissipation per unit volume:

$$E(\psi, k) = C\psi^{2/3}k^{-5/3} \quad (2.15)$$

In [28] the power spectral density is used to show the reduction of wind variability due to geographic disparity. The wind power variability reduction is measured by providing a methodology to quantify the deviation ( $\Delta\beta$ ) from the Kolmogorov spectrum when multiple wind farms are aggregated:

$$E = C\psi^{2/3}k^{-5/3+\Delta\beta} \quad (2.16)$$

where  $\log(\Delta\beta)$  is a function of the correlation coefficient and the nameplate capacity ratio between the wind farm to be interconnected and the already interconnected wind farms.

Another attempt to use the power spectral density in [29] results in an ultra-diurnal variation metric to quantify intra-day wind power variability. The proposed ultra-diurnal variation metric (UDVM) compares variations with infra-diurnal frequencies to the mean wind power output. A derating

factor  $\alpha$  is calculated by summing the power density values at all frequencies higher than the diurnal frequency and dividing by the total power. The UDVM is then given by the multiplication of the derating factor  $\alpha$  with the coefficient of variation  $(\sigma/\mu)$ . Thus, the ultra-diurnal variation metric measures the magnitude of the variance resulting from deviations with cycle less than once per day.

However, the power spectral density loses all temporal information, since it provides information only about the amplitudes and not the phases of the associated sine waves, making it extremely difficult to derive useful conclusions in the time domain. Instead, Fourier transforms can be used to incorporate both the magnitude and the phase information of the signal. Still, when the signal is described using a partial sum Fourier series, two significant shortcomings remain. The first is the computational complexity which arises from manipulating trigonometric functions. The second, and more significant, is that it is extremely hard to derive useful conclusions about the signal in the time domain from the frequency domain analysis, because the partial sum Fourier series expansion of a function converges to the function in  $L^2$ , but pointwise convergence is not guaranteed. In fact, the Gibbs phenomenon describes that the partial sum Fourier series oscillates near the jumping points of the function, resulting in larger maximum values than the actual maxima of the function [30]. Most importantly, variability metrics relying on analysis in the frequency domain lack a clear connection to power system operations.

## 2.3 Summary

This chapter provides definitions and applications of most common measures of dispersion of random variables in Section 2.1. A summary of how

wind power variability is estimated in various wind power integration studies is given in Section 2.2. The step-changes approach, which is most widely used as a measure of wind power variability, along with its shortcomings is presented in Section 2.2.1. Other wind power variability metrics from wind integration studies and papers are summarized in Section 2.2.2.

## Chapter 3

### Proposed Conditional Range Metric (CRM) to Quantify Intra-hour Wind Power Variability

Wind power variability is an inherent characteristic of wind power and will be present in all wind conditions. Even in the case of a perfect hourly wind power forecast, the effects of intra-hour wind power variability cannot be ignored. Hence, the ability to measure variability is of critical importance because it allows engineers to quantify and therefore manage wind power variability at the desired time scale. The importance of measuring wind power variability is highly recognized by the North American Electric Reliability Corporation. Therefore, characteristics of potential metrics for variable generation and system flexibility requirements to accommodate high levels of wind power are described in [31].

The need for a metric to quantify intra-hour wind power variability increases with increasing wind power penetration levels, because the intra-hour variation of wind power (in MW) becomes comparable to that of load variation. For example, for a given year in the ERCOT service area, the maximum wind power production was 4777.06 MW compared to a system peak load of 62258.15 MW. For this modest 7.7% wind penetration level, the largest change in wind power within a 5-minute interval was 781.42 MW versus a respective load variation of 892.52 MW [4]. Moreover, the inability of current variability metrics presented in Section 2.2 to effectively capture intra-hour variations in

wind power deem a novel intra-hour wind power variability metric necessary.

Desired features of a novel intra-hour wind power variability metric are listed below:

1. The proposed metric should efficiently quantify intra-hour wind power variability.
2. The proposed metric should be straightforward to compute and of practical value to power system operators as well as wind farm owners and investors.
3. The proposed metric should characterize wind power variability regardless of its uncertainty error level.

This chapter presents the proposed metric to quantify intra-hour wind power variability in detail. The fundamental concept of the metric is laid out in Section 3.1, while the formal definition of the metric is given in Section 3.2. The methodology to extend the proposed metric into a probabilistic metric is outlined in Section 3.3. The chapter concludes with examples which compare the values of the proposed metric on various sources and explain how the proposed metric encompasses the aforementioned desired features.

- **Publications:** Part of the work presented in this chapter has been published in [2, 4]:

- T. Boutsika and S. Santoso, “Quantifying short-term wind power variability,” in *Power and Energy Society General Meeting, 2011 IEEE*, July 2011, pp. 1-7.

- T. Boutsika and S. Santoso, “Quantifying short-term wind power variability using the conditional range metric,” *Sustainable Energy, IEEE Transactions on*, vol. 3, no. 3, pp. 369-378, July 2012.

### 3.1 Fundamental Concept of the Proposed Metric

Contrary to the step-changes approach where average values are used, the proposed metric should be defined in a way which entails information about all the data within the desired variability time frame, so as to be able to distinguish the variability of the two sources from the case study presented in Section 2.2.1.3. A measure of dispersion which envelopes all the data in a random sample is the range, which is defined as the difference between the maximum and the minimum observations of the set. Thus, the proposed metric uses the range as a measure of dispersion for the varying wind power output.

Since wind power output  $X$  is bounded below by zero (or some small negative number due to ancillary loads) and above by the wind farm nameplate capacity  $P_N$ , the range of the wind power is  $R = \max(X) - \min(X) = P_N$ . However, over a smaller time frame wind power is expected to vary by much smaller amounts. The proposed conditional range is the size  $M_k$  of the interval within which wind power output  $X$  lies over a given time frame  $k$ . The conditional range  $M_k$  provides a measure of wind power variability, which corresponds to the largest change the wind power output can undergo within the given time frame  $k$ . It is termed conditional, because the range’s value is conditioned on the length of the time frame  $k$ .

In Fig. 3.1 wind power values for a time period of one hour are depicted, normalized based on the wind farm nameplate capacity. For two time intervals having different lengths,  $k_1$  and  $k_2$ , wind power values lie in two inter-



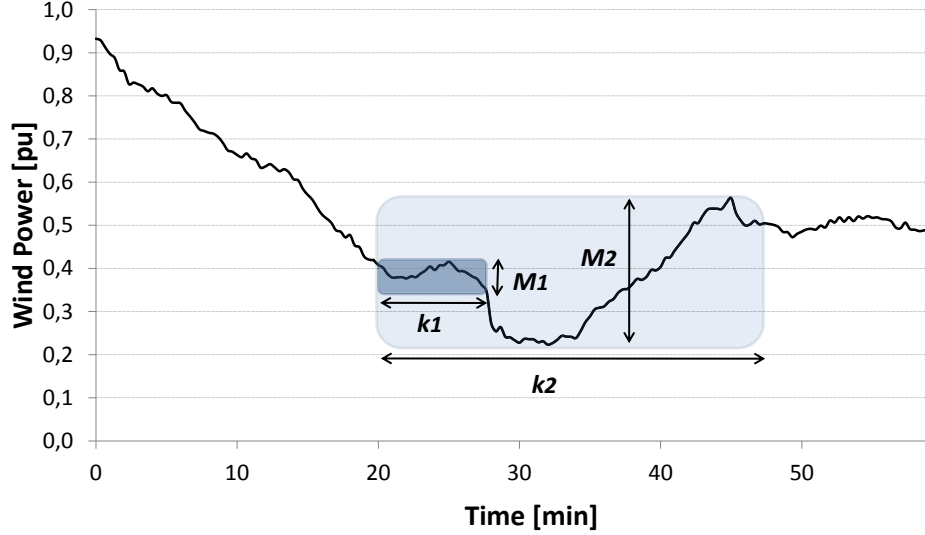


Figure 3.1: Characterizing the variability of wind power using two intervals' sizes ( $M_1$  and  $M_2$ ) of different magnitudes over two time frames ( $k_1$  and  $k_2$ , respectively). The shaded rectangle's width  $M$  depends on its length  $k$  and corresponds to the largest change the wind power can undergo within it.

vals of different sizes,  $M_1$  and  $M_2$ , respectively. The length of the first shaded rectangle is chosen to be  $k_1 = 7$  minutes and the resulting width is  $M_1 = 0.04$  p.u. This means that within the specific 7-minute interval the largest change in wind power is 4% of the wind farm's nameplate capacity. For the first rectangle this is a ramp down starting at minute 25 up to minute 27. The length of the second shaded rectangle is  $k_2 = 28$  minutes and the resulting width is  $M_2 = 0.335$  p.u. Thus, for the specific 28-minute interval, the largest change in wind power is a ramp up starting at minute 30 up to minute 45 and having a magnitude of 33.5% of the wind farm's nameplate capacity.

### 3.2 Definition of the Conditional Range Metric

Let  $M_k$  be the conditional range of the wind power output  $x(t)$  in an interval  $[t_i, t_i + k]$ ,

$$M_k = M_{up_k} - M_{low_k} \quad (3.1)$$

where

$$M_{low_k} \leq x(t) \leq M_{up_k}, \quad \forall t \in [t_o, t_o + k] \quad (3.2)$$

Given a discretized wind power output time series  $x_n$ ,  $n = 1, 2 \dots N$ , for each initial time  $i$  and time interval length  $k$ , the endpoints  $M_{low_{i,k}}$  and  $M_{up_{i,k}}$  of the conditional range  $M_{i,k}$  are uniquely defined by:

$$M_{i,k} = M_{up_{i,k}} - M_{low_{i,k}} = \max_{n \in K_i} x_n - \min_{n \in K_i} x_n \quad (3.3)$$

where  $K_i$  is the interval  $[i, i + k - 1]$ .

The conditional range series  $M_{i,k}$  is generated by calculating the interval's size  $M_k$  over all available  $k$ -long time intervals  $K_i$ ,  $i = 1, 2 \dots N - k + 1$ , using (3.3) over the entire wind power series. The series consists of pairs of values  $(M_{low_{i,k}}, M_{up_{i,k}})$ . However, the conditional range endpoint values  $M_{low_{i,k}}$  and  $M_{up_{i,k}}$  have a large span. For example,  $M_{low_{i,k}}$  can range from zero, when the wind power production is low, up to approximately the nameplate capacity, when the production is at the highest. Conditioning the range not only on the length of the time interval  $k$ , but also on the interval average wind production level  $l_j$ , limits the span of  $M_{low_{i,k,l_j}}$  and  $M_{up_{i,k,l_j}}$ , forcing them to take values closer to  $l_j$ , as is illustrated in Fig. 3.2.

Based on the above discussion, the proposed conditional range metric  $CRM$  is defined as the interval:

$$CRM_{i,k,l_j} = [M_{low_{i,k,l_j}}, M_{up_{i,k,l_j}}] \quad (3.4)$$

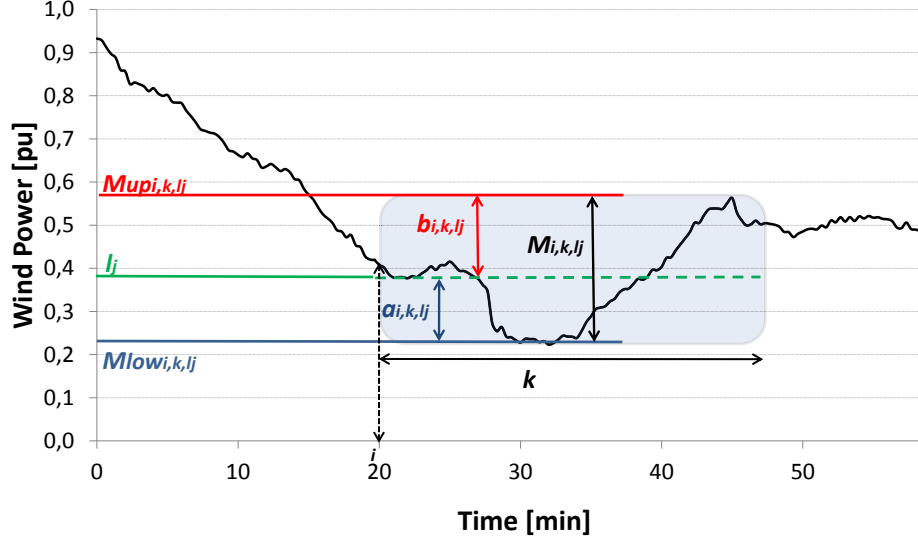


Figure 3.2: Definition of the conditional range metric. For each initial time  $i$ , time interval length  $k$  and wind power interval average production level  $l_j$  the endpoints  $M_{low_{i,k,l_j}}$  and  $M_{up_{i,k,l_j}}$  uniquely define the conditional range  $M_{i,k,l_j}$  and the wind power output lies in the interval  $[M_{low_{i,k,l_j}}, M_{up_{i,k,l_j}}]$  with probability  $p = 1$ .

and the conditional range  $CR$  is the size of this interval:

$$CR_{i,k,l_j} = M_{up_{i,k,l_j}} - M_{low_{i,k,l_j}} \quad (3.5)$$

which serves as a measure of wind power variability over a time interval starting at point  $i$ , having length  $k$  and average wind power production  $l_j$ . For the shaded rectangle given in Fig. 3.2 the initial minute in time is  $i = 20$ , the time interval length is  $k = 28$  minutes and the interval average wind power production is  $l_j = 0.376$  p.u., normalized based on the wind farm nameplate capacity. For this specific time interval the conditional range metric is  $CRM_{28,0.376,20} =$

$[0.228, 0.563]$  p.u., which means that the minimum and maximum wind power output in this interval is 0.228 and 0.563 p.u., respectively. The resulting conditional range is  $CR_{28,0.376,20} = M_{up_{28,0.376,20}} - M_{low_{28,0.376,20}} = 0.335$  p.u. and it equals the size of the largest wind power ramp in this interval.

### 3.3 Probabilistic Conditional Range Metric

Just like the step-changes are used to characterize variations in wind power, the conditional range metric (CRM), as defined in (3.4), also constitutes a wind power variability metric. This metric, which corresponds to the largest change the wind power output can undergo within an interval, can be considered as a random variable. However, a single sample from the CRM random variable provides little general information on wind power variability. Indeed, to obtain a measure of how much the conditional range values vary over the course of a longer period, for example to get a feeling of the 15-minute CRM interval size variation over the course of a year, some statistic of the CRM random variable needs to be estimated. In wind integration studies three standard deviations of the step-changes are used to estimate the biggest variations in wind power output, but for the conditional range metric the chosen statistic is its quantile. In this section, the approach taken towards extending the CRM to a probabilistic wind power variability metric is described in Section 3.3.1, while a detailed algorithm to obtain a unique  $p^{th}$  CRM quantile, denoted  $CRM_{k,l_j,p}$ , is given in Section 3.3.2.

### 3.3.1 Motivation and Approach

For a specific  $k$ -long time interval with initial point  $i$  and interval average wind power production  $l_j$  the wind power output lies in the interval  $[M_{low_{i,k,l_j}}, M_{up_{i,k,l_j}}]$  with probability  $p = 1$ . However, this information is of little use to power system operators, since for another  $k$ -long time interval with initial point  $m$  and interval average wind power production  $l_j$  the size or endpoints of the respective interval  $[M_{low_{m,k,l_j}}, M_{up_{m,k,l_j}}]$  may be completely different. On the other hand, using a time series of conditional range metric values, the proposed metric can be extended into a probabilistic intra-hour wind power variability metric, i.e. a metric of the form:

Metric has value at most  $A$  with probability at least  $B$

When a metric  $X$  follows a normal distribution, then taking  $A = 3\sigma_X$  leads to  $B = 99.7\%$ . But, to avoid possible violations of any normality assumptions instead of using the standard deviation as a measure of dispersion for the CRM values, quantiles are used to extend the proposed metric into a probabilistic metric. In this sense, the CRM has value at most equal to its  $p^{th}$  quantile ( $A$ ) with probability at least  $p$  ( $B$ ). An empirical probability distribution of the proposed metric can be obtained by calculating several quantiles  $p$  of the CRM. The provision of  $p^{th}$  CRM quantiles is of significance, because it gives power system operators and wind farm owners a measure of wind power variability and allows them to make decisions involving wind power variability based on their willingness to accept a certain level of risk  $\alpha = 1 - p$ . Next, the approach to obtain a unique  $p^{th}$  CRM quantile is described.

The  $p^{th}$  quantile  $Q_X(p)$  of a random variable  $X$  is defined in (2.6) using the inverse of the cumulative distribution function  $F_X^{-1}$ , thus  $Q_X(p) =$

$F_X^{-1}(p) = \inf\{x | P(X \leq x) \geq p\}$ . When the underlying distribution and hence the cumulative distribution function is unknown, the  $p^{th}$  sample quantile  $Q_X(p)$  from an  $N$ -long sample of  $X$  can be estimated using order statistics. For this, the  $N$  values of  $X$  are sorted and the desired quantile resolution  $1/q$  is selected, with  $p = r/q$  ( $r$  is the quantile rank,  $r = 1, 2, \dots, q$ ). To compute  $Q_X(p)$ , the estimate for the  $r^{th}$   $q$ -quantile of  $X$ , a real valued index  $h$  is computed. When  $h$  is an integer, the  $h^{th}$  smallest of the ordered values,  $X_{(h)}$ , is the quantile estimate. Otherwise an interpolation scheme is used to compute the quantile estimate from the ceiling function  $X_{(\lceil h \rceil)}$  and the floor function  $X_{(\lfloor h \rfloor)}$ . Throughout this work the sample quantiles are calculated from:

$$Q_X(p) = \begin{cases} X_{(h)} & \text{if } h \in \mathbb{Z} \\ \frac{X_{(\lceil h-1/2 \rceil)} + X_{(\lfloor h+1/2 \rfloor)}}{2} & \text{if } h \notin \mathbb{Z} \end{cases} \quad (3.6)$$

where  $h = Np + 1/2$ . Equation (3.6) represents the inverse of the empirical cumulative distribution function, but with averaging at the discontinuities.

The ordering of values in a one-dimension sample is straightforward. However, when it comes to multiple variables, such as the conditional range metric, there is no unique definition for a multivariate quantile analogous to (2.6). Several attempts have been made to extend the concept of the quantile to a multivariate setting and to obtain quantile definitions with certain desired attributes. The two most common methods involve analytical approaches through inverse distribution functions and  $L_1$  optimization [32], or geometrical considerations such as halfspace depth and projections [33]. The advantages of using analytical approaches to define vector-valued quantile functions include efficient algorithms and tractable asymptotics, whereas geometric approaches benefit from equivariance properties and intuitive contents.

Thus, conditional range values  $CR_{i,k,l_j}$  of a wind power series  $x_n$  computed using (3.5) can be easily ordered and a sample quantile can be obtained

from (3.6). However, the estimation of a  $p^{th}$  sample quantile of CRM, denoted  $[M_{low_{k,l_j,p}}, M_{up_{k,l_j,p}}]$ , involves a more sophisticated approach. The proposed probabilistic wind power variability metric has to be given in a form suitable for direct use by power system operators and wind farm owners, thus it is necessary to provide a methodology to calculate a scalar-valued instead of a vector-valued quantile function. The procedure towards this methodology is described below.

The first quality a  $p^{th}$  CRM sample quantile  $[M_{low_{k,l_j,p}}, M_{up_{k,l_j,p}}]$  should have, follows from the  $\{P(X \leq x) \geq p\}$  part of (2.6). That is, the  $M_{low_{k,l_j,p}}$  and  $M_{up_{k,l_j,p}}$  values should be such, that over all available  $k$ -long time intervals with average wind power production  $l_j$  the probability that the interval  $[M_{low_{k,l_j,p}}, M_{up_{k,l_j,p}}]$  envelopes the wind power should be at least  $p$ . Two obvious such values valid for any time frame  $k$ , average production  $l_j$  and quantile  $p$  are  $M_{low_{k,l_j,p}} = 0$  and  $M_{up_{k,l_j,p}} = P_N$ , the range of the wind power. To narrow this range, the condition that the resulting interval  $(M_{up_{k,l_j,p}} - M_{low_{k,l_j,p}})$  is minimized is requested, in analogy to the infimum imposed in (2.6). Hence, the initial problem of calculating a  $p^{th}$  conditional range metric sample quantile  $[M_{low_{k,l_j,p}}, M_{up_{k,l_j,p}}]$  from an  $N$ -long wind power series  $x_n$  can be mathematically formulated as follows:

Given  $k, l_j$ , and  $p$   
Find  $M_{low_{k,l_j,p}}$  and  $M_{up_{k,l_j,p}}$

such that  $(M_{upk,l_j,p} - M_{lowk,l_j,p})$  is minimized and such that over all  $k$ -long time intervals  $K_i$ :

$$P \left( \left\{ \inf_{n \in K_i} x_n \geq M_{lowk,l_j,p} \right\} \cap \left\{ \sup_{n \in K_i} x_n \leq M_{upk,l_j,p} \right\} \middle| \bar{x}_n = l_j \right) \geq p, \quad i = 1, 2, \dots, N - k + 1, \quad (3.7)$$

where:

$k$	is the desired time interval length,
$l_j$	is the desired production level,
$p$	is the desired quantile (or coverage probability),
$K_i$	is the interval $[i, i + k - 1]$ , and
$\bar{x}_n$	is the interval average wind production, $\bar{x}_n = \frac{1}{k} \sum_{n \in K_i} x_n$ .

Thus, given the length of the time interval  $k$  and the interval average wind power production level  $l_j$ , we search for values  $M_{lowk,l_j,p}$  and  $M_{upk,l_j,p}$  that have the desired coverage probability  $p$ , i.e. that envelope (or cover) the wind power with at least probability  $p$ , and form a range with minimum width. For example, given a wind power time series from a 100 MW wind farm over a year period, we want to find the lower  $M_{lowk,l_j,p}$  and upper  $M_{upk,l_j,p}$  endpoints of the wind power range, taken over 15-minute ( $k$ ) intervals with 30 MW ( $l_j$ ) average production and coverage probability at least 90% ( $p$ ). The points  $M_{lowk,l_j,p}$  and  $M_{upk,l_j,p}$  should be such, that within the specific year in 90% of the 15-minute intervals with 30 MW average production, the wind power output falls within  $[M_{lowk,l_j,p}, M_{upk,l_j,p}]$ . Moreover, the interval  $[M_{lowk,l_j,p}, M_{upk,l_j,p}]$  should be the smallest possible.

However, it is possible for multiple pairs  $(M_{lowk,l_j,p}, M_{upk,l_j,p})$  to minimize  $(M_{upk,l_j,p} - M_{lowk,l_j,p})$  and satisfy (3.7). Indeed, consider an interval



$[M_{low_{k,l_j,p}}, M_{up_{k,l_j,p}}]$  which satisfies (3.7) and has width  $M_{up_{k,l_j,p}} - M_{low_{k,l_j,p}} = \alpha$ . Then it is possible for other pairs  $(M_{low_{k,l_j,p}}, M_{up_{k,l_j,p}})$ , which are on the line  $y = \alpha + x$ , to define intervals which provide the same coverage probability  $p$ . Therefore, another condition is added to ensure that a unique pair of values and hence a scalar-valued quantile function is defined. For this purpose the deviation time series are introduced. The minimum  $a_{i,k}$  and maximum  $b_{i,k}$  deviation series are generated by calculating the minimum and maximum deviation from the interval average production over all available time intervals  $K_i$  of length  $k$ :

$$a_{i,k} = \frac{1}{k} \sum_{n \in K_i} x_n - \min_{n \in K_i} x_n \quad (3.8)$$

$$b_{i,k} = \max_{n \in K_i} x_n - \frac{1}{k} \sum_{n \in K_i} x_n \quad (3.9)$$

where  $K_i = [i, i + k - 1]$ ,  $i = 1, 2, \dots, N - k + 1$ . The deviation series  $a_{i,k}$  and  $b_{i,k}$  are then filtered by the interval average wind power production level  $\bar{x}_n = \frac{1}{k} \sum_{n \in K_i} x_n = l_j$  resulting in separate deviation series for each production level,  $a_{i,k,l_j}$  and  $b_{i,k,l_j}$ ,  $i = 1, 2, \dots, N_{k,l_j}$ .

Given a wind power output over a time interval, the deviation series essentially measure the largest excursions of the wind power output (in both directions) from the interval average production. For example, in Fig. 3.2 the shaded rectangle depicts the wind power output from a wind farm over a  $k = 28$  minutes time interval starting at minute  $i = 20$ . The interval average production is  $l_j = 0.376$  p.u., normalized on the wind farm nameplate capacity. For this specific interval, the minimum deviation is  $a_{28,0.376,20} = 0.148$  p.u. and it provides the largest excursion of the wind power output from the interval average in the negative direction. Similarly, the maximum deviation shows that the furthest the wind power output can deviate from the interval average

production in the positive direction is  $b_{28,0.376,20} = 0.187$  p.u.

Here it should be noted that the deviation series are actually filtered not using production levels but production level intervals. Let  $1/m$  denote the production level resolution, i.e.  $l_j = j/m$  p.u. with  $j = 1, 2, \dots, m$ , then throughout this dissertation  $\{\bar{x}_n = l_j\}$  refers to the normalized average wind power production interval  $\bar{x}_n$  lying in  $((2j-1)/2m, (2j+1)/2m]$ .

Using the deviation series the following constraint is added to (3.7):

$$\begin{aligned} P(\sup_{n \in K_i} \{x_n - \bar{x}_n\} \leq M_{up_{k,l_j,p}} - l_j) = \\ P(\sup_{n \in K_i} \{\bar{x}_n - x_n\} \leq l_j - M_{low_{k,l_j,p}}) \end{aligned} \quad (3.10)$$

which essentially imposes the condition that over all  $K_i$  intervals the probabilities that  $a_{i,k,l_j} \leq l_j - M_{low_{k,l_j,p}}$  and  $b_{i,k,l_j} \leq M_{up_{k,l_j,p}} - l_j$  be equal. Thus, the solution of the system of equations (3.7) and (3.10) that minimizes  $(M_{up_{k,l_j,p}} - M_{low_{k,l_j,p}})$  provides a unique pair of values  $(M_{low_{k,l_j,p}}, M_{up_{k,l_j,p}})$ .

### 3.3.2 Computation of the Probabilistic CRM

Starting with an  $N$ -long wind power time series  $x_n$ ,  $n = 1, 2, \dots, N$ , the desired time interval length  $k$ , desired production level  $l_j$ , and desired coverage rate  $p$  are specified. The algorithm described next provides the endpoints of the  $p^{th}$  quantile of the CRM,  $CRM_{k,l_j,p} = [M_{low_{k,l_j,p}}, M_{up_{k,l_j,p}}]$ .

First, the minimum  $a_{i,k}$  and maximum  $b_{i,k}$ ,  $i = 1, 2, \dots, N - k + 1$ , deviation series are calculated from (3.8) and (3.9), respectively. Next, the deviation series are filtered by the desired interval average wind power production level  $\bar{x}_n = \frac{1}{k} \sum_{n \in K_i} x_n = l_j$  resulting in the production specific deviation series  $a_{i,k,l_j}$  and  $b_{i,k,l_j}$ ,  $i = 1, 2, \dots, N_{k,l_j}$ . The additional constraint in (3.10) requires the values  $l_j - M_{low_{k,l_j,p}}$  and  $M_{up_{k,l_j,p}} - l_j$  to be same rank quantiles of the

deviation series  $a_{i,k,l_j}$  and  $b_{i,k,l_j}$ , respectively. Since no assumption about the underlying distribution of the deviation series is made, a quantile estimate can be calculated from the sample data series. For this, the  $N_{k,l_j}$  values of the deviation series  $a_{i,k,l_j}$  and  $b_{i,k,l_j}$  are sorted and the desired quantile resolution  $1/q$  is selected, with  $\tau = r/q$  ( $r = 1, 2, \dots, q$ ). To compute  $Q_{A_{k,l_j}}(\tau)$  and  $Q_{B_{k,l_j}}(\tau)$ , the estimates for the  $r^{th}$   $q$ -quantile of  $a_{i,k,l_j}$  and  $b_{i,k,l_j}$  (3.6) is used:

$$Q_{A_{k,l_j}}(\tau) = \begin{cases} a_{(h)} & \text{if } h \in \mathbb{Z} \\ \frac{a_{(\lceil h-1/2 \rceil)} + a_{(\lfloor h+1/2 \rfloor)}}{2} & \text{if } h \notin \mathbb{Z} \end{cases} \quad (3.11)$$

$$Q_{B_{k,l_j}}(\tau) = \begin{cases} b_{(h)} & \text{if } h \in \mathbb{Z} \\ \frac{b_{(\lceil h-1/2 \rceil)} + b_{(\lfloor h+1/2 \rfloor)}}{2} & \text{if } h \notin \mathbb{Z} \end{cases} \quad (3.12)$$

where  $h = N_{k,l_j}\tau + 1/2$ .

The sample quantiles calculated from (3.11) and (3.12) partition the  $N_{k,l_j}$  ordered samples from the deviation series  $a_{i,k,l_j}$  and  $b_{i,k,l_j}$  in  $q$  disjoint sets  $SA_{k,l_j}$  and  $SB_{k,l_j}$ . The  $r^{th}$  set contains  $(N_{k,l_j})/q$  values from an interval with quantile endpoints  $(Q_{A_{k,l_j}}(r/q - 1/q), Q_{A_{k,l_j}}(r/q)]$  and  $(Q_{B_{k,l_j}}(r/q - 1/q), Q_{B_{k,l_j}}(r/q)]$ , where  $r = 1, 2, \dots, q$ . Using all available pairs  $(a, b)$  sampled jointly from the deviation series  $a_{i,k,l_j}$  and  $b_{i,k,l_j}$  the joint probability density matrix  $V_{k,l_j}(i, j)$  can be calculated from:

$$V_{k,l_j}(i, j) = P(\{a \in SA_{k,l_j,i}\} \cap \{b \in SB_{k,l_j,j}\}) \quad (3.13)$$

Thus, the value of  $V(i, j)$  gives the probability that a sample  $(a, b)$  from the deviation series has  $a$  in the  $i^{th}$  of the  $SA_{k,l_j}$  sets (i.e.  $a \in (Q_{A_{k,l_j}}(i/q - 1/q), Q_{A_{k,l_j}}(i/q)]$ ) and  $b$  in the  $j^{th}$  of the  $SB_{k,l_j}$  sets (i.e.  $b \in (Q_{B_{k,l_j}}(j/q - 1/q), Q_{B_{k,l_j}}(j/q)]$ ).

The  $p^{th}$   $q$ -quantile of the conditional range  $M_{k,l_j}$  can then be estimated from:

$$Q_{M_{k,l_j}}(p) = (Q_{A_{k,l_j}}(\tau_p) + Q_{B_{k,l_j}}(\tau_p)) \quad (3.14)$$

where

$$\tau_p = \inf\left\{\tau : \sum_{i=1}^{\tau} \sum_{j=1}^{\tau} V_{k,l_j}(i, j) \geq p\right\} \quad (3.15)$$

Hence, instead of choosing an arbitrary sample pair  $(a, b)$  from the deviation series as the  $p^{th}$  quantile for the conditional range, values  $Q_{A_{k,l_j}}(\tau_p)$  and  $Q_{B_{k,l_j}}(\tau_p)$  are restricted to be same rank  $(\tau_p)$  quantiles of the deviation series  $a_{i,k,l_j}$  and  $b_{i,k,l_j}$ . Thus, the pairs  $(a, b)$  from which the  $p^{th}$  quantile for the conditional range is chosen are forced to lie on a line in the Euclidean space. The rank  $\tau_p$  of the deviation series quantiles is a function of the desired conditional range quantile rank  $p$ , and in general  $\tau_p \neq p$ .

The pair  $(Q_{A_{k,l_j}}(\tau_p), Q_{B_{k,l_j}}(\tau_p))$  indicates deviations from the interval average wind power production level, accordingly the corresponding endpoints of the wind power interval  $x \in [M_{low_{k,l_j,p}}, M_{up_{k,l_j,p}}]$  would be  $M_{low_{k,l_j,p}} = l_j - Q_{A_{k,l_j}}(\tau_p)$  and  $M_{up_{k,l_j,p}} = Q_{B_{k,l_j}}(\tau_p) + l_j$ . Thus, the endpoints of the  $p^{th}$  CRM quantile, denoted  $CRM_{k,l_j,p}$ , are given by  $[M_{low_{k,l_j,p}}, M_{up_{k,l_j,p}}] = [l_j - Q_{A_{k,l_j}}(\tau_p), l_j + Q_{B_{k,l_j}}(\tau_p)]$ , with  $\tau_p$  from (3.15). It should be noted that because the range is not centered around the interval average production, the quantiles of the two deviation series  $a_{i,k,l_j}$  and  $b_{i,k,l_j}$  are in general not the same,  $Q_{A_{k,l_j}}(\tau_p) \neq Q_{B_{k,l_j}}(\tau_p)$ .

Figure 3.3 illustrates graphically the concept of choosing a unique pair from the minimum  $a$  and maximum  $b$  deviation pair values. In this figure, the dots represent deviation pairs  $(a, b)$  from the deviation series  $a_{i,k,l_j}$  and  $b_{i,k,l_j}$ . The pairs  $(a, b)$  from which the  $p^{th}$  quantile for the conditional range is chosen, are forced to lie on the blue curve, for which  $a = Q_{A_{k,l_j}}(\tau_p)$  and  $b = Q_{B_{k,l_j}}(\tau_p)$  are same rank quantiles. The blue curve is obtained by connecting the points  $(Q_{A_{k,l_j}}(\tau_p), Q_{B_{k,l_j}}(\tau_p))$  for successive values of  $p$ . The dotted line represents the line  $a = b$ , and since the solid blue and the dotted black line do not coin-

cide, it becomes evident that  $Q_{A_{k,l_j}}(\tau_p) \neq Q_{B_{k,l_j}}(\tau_p)$ . For a specific coverage probability  $p = 75\%$ , the unique pair  $(a_p^*, b_p^*)$  from the solid blue line is chosen in such a way, that the box formed by the red lines and the  $x$  and  $y$  axes, i.e the rectangle with corners the points  $(0,0)$ ,  $(0, b_p^*)$ ,  $(a_p^*, b_p^*)$  and  $(a_p^*, 0)$ , is the smallest perimeter box to contain at least  $p = 75\%$  of the total number of  $(a, b)$  pairs. In this case,  $a_p^* = Q_{A_{k,l_j}}(\tau_p)$  and  $b_p^* = Q_{A_{k,l_j}}(\tau_p)$ .

Moreover, in Fig. 3.3 the dashed green line is the line  $b = Q_{A_{k,l_j}}(\tau_p) + Q_{B_{k,l_j}}(\tau_p) - a$  for  $p = 75\%$ . Any rectangle with corners the points  $(0,0)$ ,  $(0, d)$ ,

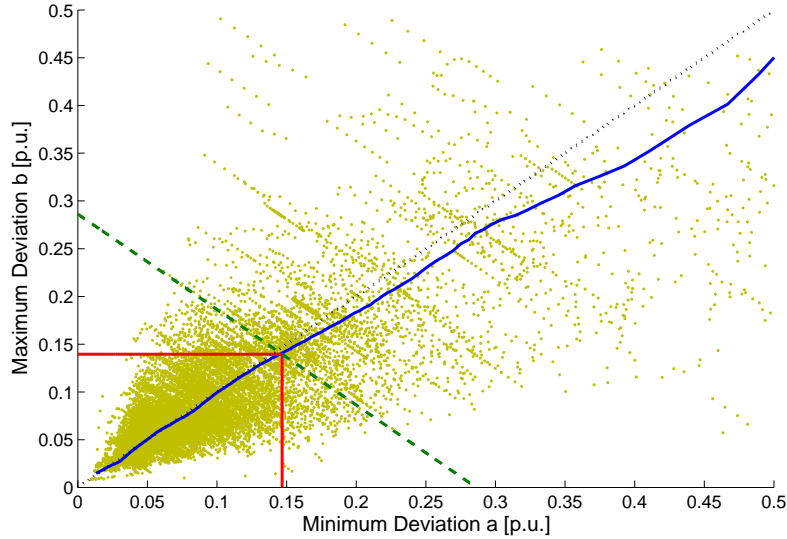


Figure 3.3: Graphical representation of the conditional range metric quantile using the minimum  $a$  and maximum  $b$  deviation pairs (dots). The pairs  $(a, b)$  from which the  $p^{th}$  quantile for the conditional range is chosen are forced to lie on the blue line, for which  $a = Q_{A_{k,l_j}}(\tau_p)$  and  $b = Q_{B_{k,l_j}}(\tau_p)$  are same rank quantiles. The number of  $(a, b)$  pairs enclosed by the box formed from the red lines and the  $x$  and  $y$  axes equals  $p\%$  of the total number of  $(a, b)$  pairs. The dotted line is the  $a = b$  line. The dashed line is the line  $b = Q_{A_{k,l_j}}(\tau_p) + Q_{B_{k,l_j}}(\tau_p) - a$  for  $p = 75\%$ .

$(c, d)$ ,  $(c, 0)$ , for which the upper right corner  $(c, d)$  lies on the dashed green line has the same perimeter with the depicted rectangle (red lines). Thus, for any such rectangle the CRM interval has the same width  $M_{up_{k,l_j,p}} - M_{low_{k,l_j,p}} = Q_{B_{k,l_j}}(\tau_p) + Q_{A_{k,l_j}}(\tau_p)$ . From this it becomes evident, that there may be more than one pair of values  $(c, d)$  for which the respective rectangle contains  $p\%$  of the total number of  $(a, b)$  pairs. This is why (3.7) by itself is not sufficient to obtain a unique  $(M_{low_{k,l_j,p}}, M_{up_{k,l_j,p}})$  pair, and an additional constraint is needed.

The data presented in Fig. 3.3 come from real-world wind power data of a 160 MW wind farm spanning a period of one year. The dots  $(a, b)$  come from the deviation series  $a_{i,k,l_j}$  and  $b_{i,k,l_j}$  calculated for  $k = 60$  minutes and  $l_j = 0.5$  p.u. The desired probability for the conditional range is  $p = 0.75$  and the deviation series quantile rank is  $\tau_p = 0.815$ , for which  $Q_{A_{60,0.5}}(0.815) = 0.1468$  p.u. and  $Q_{B_{60,0.5}}(0.815) = 0.1395$  p.u. The conditional range endpoints are  $M_{low_{60,0.5,0.75}} = 0.5 - Q_{A_{60,0.5}}(0.815) = 0.3532$  p.u. and  $M_{up_{60,0.5,0.75}} = 0.5 + Q_{B_{60,0.5}}(0.815) = 0.6395$  p.u. Thus, for the specific 160 MW wind farm, over all hour-long time intervals in the given year with average wind power 80 MW the wind power falls within  $[56.5, 102.3]$  MW at least 75% of the time.

Consequently, using a wind power production series  $x_n$  the  $p^{th}$  quantile of the conditional range can be calculated from (3.8)-(3.9) and (3.11)-(3.15) for any interval average wind power production level  $l_j$  and any desired time interval length  $k$ :

$$CR_{k,l_j,p} = Q_{A_{k,l_j}}(\tau_p) + Q_{B_{k,l_j}}(\tau_p) \quad (3.16)$$

while, the  $p^{th}$  quantile of the conditional range metric is:

$$\begin{aligned} CRM_{k,l_j,p} &= [M_{low_{k,l_j,p}}, M_{up_{k,l_j,p}}] \\ &= [l_j - Q_{A_{k,l_j}}(\tau_p), l_j + Q_{B_{k,l_j}}(\tau_p)] \end{aligned} \quad (3.17)$$

Since the probability of realization of any  $p^{th}$  quantile ( $p = r/q$ ,  $r = 1, 2, \dots, q$ ) is  $1/q$ , averaging the  $CR$  and  $CRM$  values over all  $q$ -quantiles provides expected values for the conditional range and the conditional range metric:

$$CR_{k,l_j} = \frac{\sum_p CR_{k,l_j,p}}{q} \quad (3.18)$$

$$CRM_{k,l_j} = \left[ l_j - \frac{\sum_p Q_{A_{k,l_j}}(\tau_p)}{q}, l_j + \frac{\sum_p Q_{B_{k,l_j}}(\tau_p)}{q} \right] \quad (3.19)$$

A weighted sum of the  $CR_{k,l_j,p}$  values, with weights  $w_j$  equal to the probability of the interval average production  $\bar{x}_n$  being  $l_j$ , gives the  $p^{th}$  quantile of the conditional range  $CR_{k,p}$ . This is the average size of the largest possible wind power ramp within a time interval length  $k$ :

$$CR_{k,p} = \sum_j CR_{k,l_j,p} \cdot w_j = \sum_j CR_{k,l_j,p} \cdot P(\bar{x}_n = l_j) \quad (3.20)$$

and its expected value can be calculated from:

$$CR_k = \frac{\sum_p CR_{k,p}}{q} \quad (3.21)$$

In summary, the variability of the wind power is characterized by the size of the interval within which the wind power output lies over a given time frame (the larger the size of this interval the higher the wind power variability). The interval endpoints (CRM) can be calculated from (3.17) or (3.19), while the size of this interval (CR) can be calculated from (3.16) or (3.18), as percentiles or expected values respectively.

### 3.4 Using the Conditional Range Metric to Distinguish between Variable Sources

This section illustrates how effective the conditional range metric is at distinguishing between variable sources and attempts a preliminary evaluation

of the conditional range metric against the desired features of an intra-hour wind power variability metric presented in the beginning of this chapter. A more detailed evaluation using real-world wind power and wind speed data is presented in Chapter 4.

First, the conditional range metric values of the sources presented in Section 1.1 are compared. The three sources depicted in Fig. 1.2 correspond to the wind power output of a 82.5 MW wind farm (Source A - Wind), a sinewave output with period one hour (Source B - Sinewave) and a constant output (Source C - Direct Geothermal). Sources B and C have hourly averages of  $l_j = 40$  MW, thus their conditional range will be compared to the conditional range of the wind farm under  $k = 60$  minutes and  $l_j = 40$  MW. For Source C the conditional range is  $CR_{60min,40MW,p(SC)} = 0$  MW for all probabilities  $p$ , which is expected since Source C is a constant output source and thus exhibits no variability. The conditional range of Source B is  $CR_{60min,40MW,p(SB)} = 48$  MW, which is double the amplitude of the sinewave. The conditional range is constant over all probabilities  $p$ , which is attributed to the fact that the variation in Source B is of a systematic fashion. Finally, for Source A over the period of a year the conditional range varies between  $CR_{60min,40MW,0.05(SA)} = 6.5$  MW for  $p = 0.05$  and  $CR_{60min,40MW,0.95(SA)} = 49$  MW for  $p = 0.95$ , which means that the conditional range effectively recognizes that wind power varies in a random manner. Thus, the largest change the wind power undergoes within an hour is less than 6.5 MW for 5% of the hours in a year and exceeds 49 MW for another 5% of the hours in a year.

Comparing the conditional range to the step-changes the two variable sources (Source 1 and Source 2) of the case study presented in Section 2.2.1.3 are examined. The two sources have the same standard deviation of 10-minute step-changes. Thus, in the context of load-following reserves, using



three standard deviations of the 10-minute step-changes as a metric to characterize variability within the 1-hour time frame, the two sources have equal variability with  $3\sigma_{10min(S1)} = 3\sigma_{10min(S2)} = 45.5$  MW. However the 99.7<sup>th</sup> percentile ( $p = 0.997$ ) of the conditional range from (3.16) for  $k = 60$  minutes and average hourly production equal to  $l_j = 145$  MW (which is constant over the entire period), yields  $CR_{60min,145MW,0.997(S1)} = 75$  MW for the first and  $CR_{60min,145MW,0.997(S2)} = 192.4$  MW for the second source, respectively. Thus the proposed metric can more efficiently capture the intra-hour variability of the two sources, effectively revealing the higher variability of the second source. It should be noted that the use of quantiles for the conditional range satisfies that the desired coverage probability is always achieved, whereas the use of three standard deviations guarantees a coverage probability of 0.997 only under normality assumptions.

Since the conditional range corresponds to the biggest change the source output can undergo within a given time frame, the conditional range value reveals that 99.7% of all intra-hour ramps (here ramp denotes the largest change within an hour) are less than 75 MW and 192.4 MW for the first and second source, respectively. However the metric fails to assign a rate to these ramps. But even without a rate the wind power (or net demand) ramping information is valuable to power system operators, since they can assign the total ramping requirement to multiple generators and thus achieve any ramp rate. On the other hand, the currently used step-changes metric recognizes that the biggest ramp from one 10-minute interval to the next is close to 25 MW, but it also fails to provide a rate and a duration for this ramp. Assuming the ramp rate to be 25 MW/10 minutes and using the worst case scenario with a ramp rate duration of 60 minutes results in an hourly ramp of 150 MW, which is an overestimate of the ramping capabilities of the first source and an underes-

timate of the ramping capabilities of the second source. A more thorough comparison between the step-changes and the conditional range capabilities in assessing wind power ramps is presented in Section 4.3 using real-world wind power data.

These simple evaluations show that the proposed metric satisfies the first desired feature, since it efficiently quantifies intra-hour wind power variability and overcomes the shortcomings of current metrics. Moreover, the conditional range is conditioned on the time interval average wind power and assumes it to be known, but its calculation does not depend on the uncertainty level of this production or how a forecast of this production is obtained, as will be further explained in Section 5.5.

Finally, regarding the utility of the proposed metric, the methodology to calculate the probabilistic CRM  $CRM_{k,l_j,p} = [M_{low_{k,l_j,p}}, M_{up_{k,l_j,p}}]$  presented in Section 3.3 is straightforward. This methodology essentially estimates wind power variability intervals  $[M_{low_{k,l_j,p}}, M_{up_{k,l_j,p}}]$ , which bound wind power  $x_n$  with average wind power production  $l_j$  over a  $k$ -long time frame. These intervals are probabilistic, since they are associated with a coverage rate  $p$ , and they define inequalities of the form

$$M_{low_{k,l_j,p}} \leq x_n \leq M_{up_{k,l_j,p}} \quad \text{with probability } p \quad (3.22)$$

These inequalities can serve as so-called joint chance constraints in several stochastic optimization problems where the uncertainty comes from the wind power output  $x_n$ . Hence, these inequalities open the door to numerous applications of the proposed metric useful for power system operators as well as wind farm owners and investors, as will be outlined in Chapter 6.

### 3.5 Summary

This chapter provides the fundamental concept of the proposed intra-hour wind power variability metric in Section 3.1 and a formal definition of the proposed conditional range metric (CRM) in Section 3.2. With the conditional range metric the variability of the wind power is characterized by the size of the interval  $[M_{low}, M_{up}]$  within which the wind power output lies over a given time frame (the larger the size of this interval the higher the wind power variability). The methodology to obtain uniquely defined  $p^{th}$  CRM quantile estimates  $CRM_{k,l_j,p}$  for average wind power production level  $l_j$  over a time interval  $k$  is presented in Section 3.3. The example computations of the CRM given in Section 3.4 provide a preliminary positive evaluation of the proposed variability metric.

## Chapter 4

### Evaluation of the Conditional Range Metric

The importance of measuring intra-hour wind power variability and the inability of current metrics to adequately capture intra-hour variations in wind power has lead to the proposed conditional range metric (CRM), defined in the previous chapter. One of the desired features a novel intra-hour wind power variability metric should possess, is its ability to efficiently quantify intra-hour wind power variability and effectively overcome the shortcomings of current metrics. The efficacy of the conditional range metric in distinguishing between different variable sources is briefly outlined in Section 3.4, in which a preliminary evaluation of the proposed against current variability metrics is attempted.

In this chapter a more detailed evaluation of the conditional range metric as an intra-hour wind power variability metric is presented, by applying it on real-world wind power and wind speed data. Using the conditional range metric on real-world wind power and wind speed data can help determine the factors which aggravate the adverse effects of wind power variability, and at the same time define circumstances which alleviate these effects. In this way, conditions or time periods with increased variation in wind power, as well as remedies to reduce wind power variability, can be identified. Quantification of wind power variability can also be used to determine requirements and characteristics of other dispatchable generators and energy storage units, which can

be used to accommodate wind power fluctuations across different operating time scales.

Section 4.1 illustrates the efficacy of the conditional range metric in quantifying intra-hour wind power variability by presenting the results of an extensive performance analysis of the proposed metric in wind power variability assessment. In Section 4.2 the conditional range metric is used to quantify the effect of wind turbine technology and size on wind power variability. Moreover, Section 4.3 compares the performance of the conditional range metric to the step-changes statistics in assessing the size of intra-hour wind power ramps. The comparison reveals the shortcomings of the prevalent step-changes approach, while at the same time points out why they are overcome when the conditional range metric is used.

- **Publications:** Part of the work presented in this chapter has been published in [2–4]:

- T. Boutsika and S. Santoso, “Quantifying short-term wind power variability using the conditional range metric,” *Sustainable Energy, IEEE Transactions on*, vol. 3, no. 3, pp. 369-378, July 2012.
- T. Boutsika and S. Santoso, “Quantifying the effect of wind turbine size and technology on wind power variability,” in *Power and Energy Society General Meeting, 2013 IEEE*, July 2013, pp. 1-5.
- T. Boutsika and S. Santoso, “Quantifying short-term wind power variability,” in *Power and Energy Society General Meeting, 2011 IEEE*, July 2011, pp. 1-7.

## 4.1 Wind Power Variability Assessment Using the Conditional Range Metric

The purpose of the sensitivity analysis presented in this section is to evaluate qualitative and quantitative effects certain influential variables have on the conditional range metric. The variables investigated include the conditions, which are the production level  $l_j$ , the quantile  $p$  and the time interval length  $k$ , as well as the wind farm nameplate capacity  $P_N$ . The real-world wind power data used in this Section come from 17 wind farms in the ERCOT system, with nameplate capacities ranging from 28.5 MW to 226.5 MW, and include wind power production data with a 1-minute resolution spanning a period of one year (WF2 - WF18, year 4 – see Appendix A.1).

### 4.1.1 Wind Power Variability as a Function of the Wind Power Production

The 95<sup>th</sup> percentile of the conditional range metric of one wind farm taken over a one-year period and for a time interval length of  $k = 15$  minutes is depicted in Fig. 4.1, as a function of the interval average wind power production level  $l_j$ . It is reminded that, the depicted range values are actually conditioned on the average wind power production level intervals, where  $\bar{x}_n \in l_j = j/m$  if  $(2j - 1)/2m < \bar{x}_n \leq (2j + 1)/2m$ . Here the average production levels are set to  $l_j = 0.01, 0.02, \dots, 1$  p.u., normalized on the wind farm nameplate capacity  $P_N = 91.5$  MW (WF15). To obtain this graph the system of equations (3.7) and (3.10) is solved repeatedly for average production level values  $l_j = 0.01, 0.02, \dots, 1$  p.u., keeping the parameters  $k = 15$  minutes and coverage probability  $p = 0.95$  constant, using the methodology given in Section 3.3.2 .

For each interval average production level  $l_j$  shown on the  $x$ -axis, the

respective circle and plus-sign have  $y$ -values  $M_{up15,l_j,0.95} = l_j + Q_{B15,l_j}(\tau_{0.95})$  and  $M_{low15,l_j,0.95} = l_j - Q_{A15,l_j}(\tau_{0.95})$  such that over all the 15-minute long intervals in the given year  $P(M_{low15,l_j,0.95} \leq x(t) \leq M_{up15,l_j,0.95}) \geq 0.95$ . The dashed line is the line  $y = l_j$ , representing the  $CRM$  values of a source that exhibits no variation within a 15-minute interval.

As an example, for an interval average production level  $l_j = 0.8$  p.u., the conditional range metric (CRM) is determined from Fig. 4.1 by the  $y$ -values of the plus-sign ( $M_{low} = 0.7166$  p.u.) and the circle ( $M_{up} = 0.8747$  p.u.),

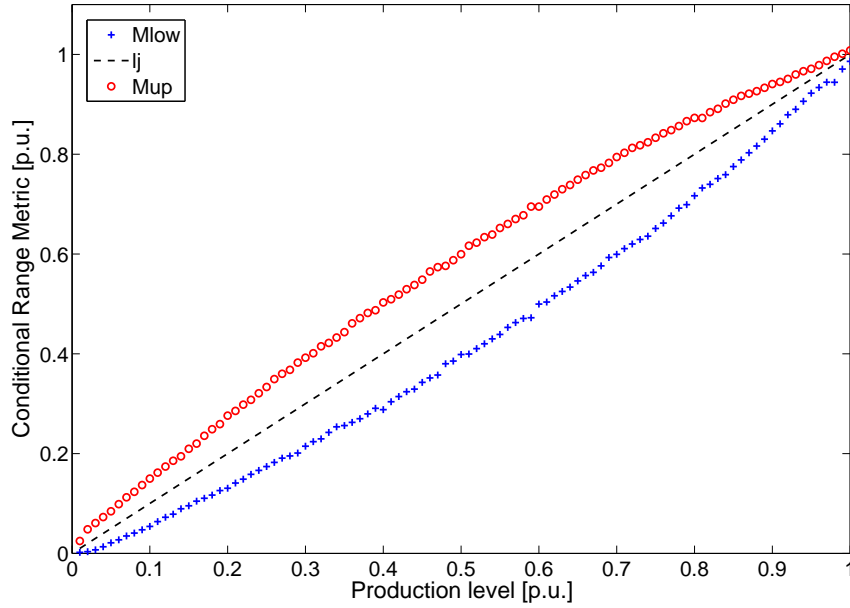


Figure 4.1: The 95<sup>th</sup> percentile of the conditional range metric( $CRM = [M_{low}, M_{up}]$ ) of a 91.5 MW wind farm's (WF15) power production. The conditional range is conditioned on the time interval of interest  $k = 15$  minutes and the interval average production level  $l_j$ . For each production level  $l_j$  the  $y$ -values of the circle and the plus-sign are the points  $M_{up}$  and  $M_{low}$ , respectively.

respectively. Thus, if the 15-minute interval average wind power production is  $l_j = 0.8$  p.u. the wind power production lies within  $[0.7166, 0.8747]$  p.u. with probability  $p = 0.95$ . For this production level, the largest variation in wind power output is less than conditional range  $CR_{15,0.8,0.95} = M_{up} - M_{low} = 0.1581$  p.u. or approximately 14.5 MW for 95% of the 15-minute intervals in a year. The respective deviations would be  $Q_B = M_{up} - l_j = 0.0747$  p.u. and  $Q_A = l_j - M_{low} = 0.0834$  p.u., from which it can be seen that the deviations are not centered around the interval average production level.

From Fig. 4.1 it is evident that wind power variability is higher at mid-level production ( $0.3 \leq l_j \leq 0.7$  p.u.), since the conditional range assumes much smaller values at very low or very high production levels. Based on Fig. 4.1, for the specific 91.5 MW wind farm a production level of  $l_j = 0.59$  p.u. exhibits the highest 15-minute variability with a conditional range of  $CR_{15,0.59,0.95} = 0.225$  p.u. In fact, mid-level wind power production is most variable for all wind farms considered, regardless of the percentile  $p$  and time interval length  $k$ .

To explain the high variability of mid-level wind power production a typical wind power curve, such as the one depicted in Fig. 4.2 corresponding to a variable speed wind turbine, is examined. This curve relates input wind speed at the turbine hub height to wind power output from the turbine. Wind power output is negligible for wind speeds lower than the cut-in wind speed (4 m/sec) and rises between the cut-in and the rated wind speed (15 m/sec). The higher variability at mid-level production depicted in Fig. 4.1 is attributed exactly to this large slope of the wind power versus wind speed curve at mid-level production, which causes even a small change in the input wind speed to have a large effect on the wind power output.



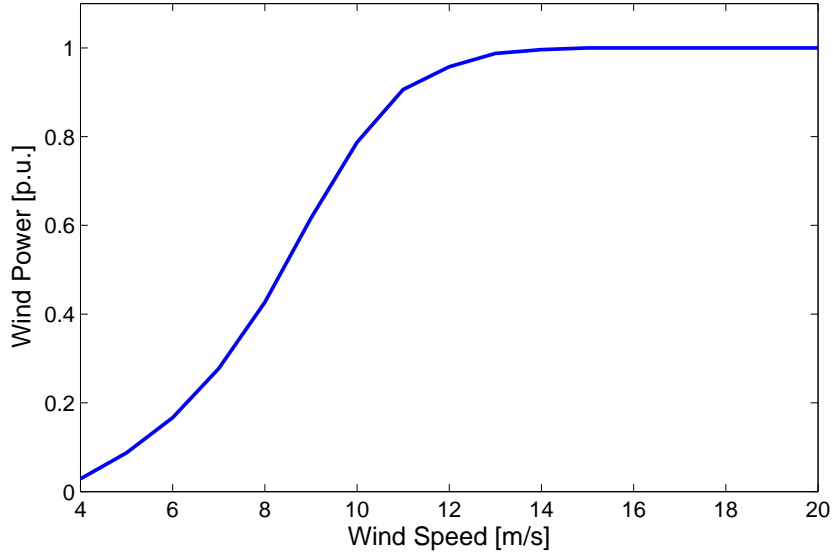


Figure 4.2: Typical wind power versus wind speed curve for a variable speed wind turbine. The large slope of the wind power curve for mid-level wind power production causes wind power variability to be higher at mid-level than low or high-level productions.

#### 4.1.2 Wind Power Accommodation for Different Coverage Probabilities

The effect of the quantile  $p$  for the same 91.5 MW wind farm (WF15) used in Section 4.1.1 but for a time interval length of  $k = 60$  minutes is depicted in Fig. 4.3. As expected, the CRM interval increases with increasing percentiles  $p$ , meaning larger intervals for higher coverage rates. For example, for a production level of  $l_j = 0.5$  p.u. the conditional range metric takes values  $CRM_{60,0.5,p=0.9} = [0.299, 0.699]$  p.u. and  $CRM_{60,0.5,p=0.3} = [0.428, 0.577]$  p.u. for coverage rates 90% and 30%, respectively. Thus, wind power variations over certain length time intervals do not have a constant size but vary over time, and small size variations are more frequent than large ones. For this spe-

cific example the magnitude of the respective conditional range reveals that in 30% over all hours in the given year (with  $l_j = 0.5$  p.u.), the largest intra-hour change in wind power output has size less than 13.6 MW ( $\approx 0.577 - 0.428$  p.u.). On the other hand, in 90% of all hours with average production  $l_j = 0.5$  p.u. the largest intra-hour change in wind power output has size less than 36.6 MW ( $= 0.699 - 0.299$  p.u.). This means that only 10% of the hours exhibit a largest intra-hour change in wind power output greater than 36.6 MW .

The provision of an empirical probability distribution for the conditional range metric, by solving the system of equations (3.7) and (3.10) with the methodology given in Section 3.3.2 for various coverage probabilities  $p$ ,

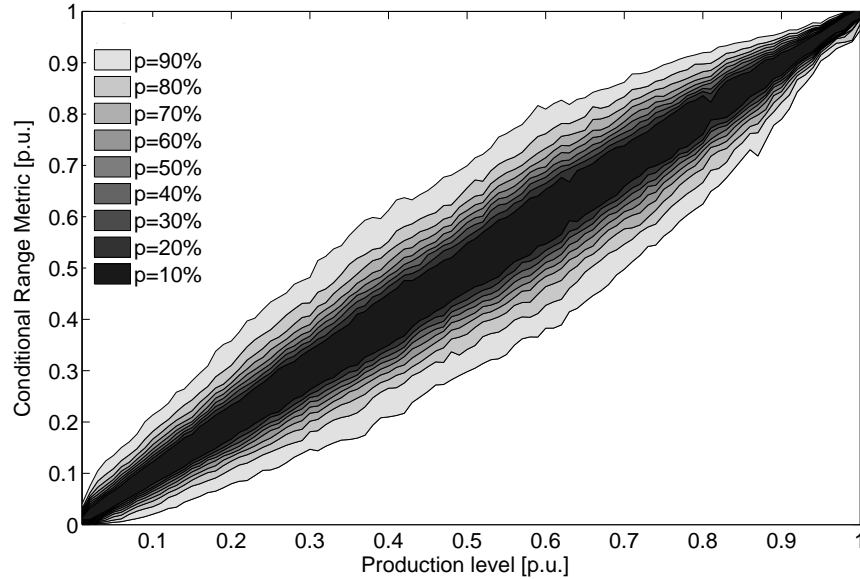


Figure 4.3: The conditional range metric ( $CRM = [M_{low}, M_{up}]$ ) of a 91.5 MW wind farm (WF15) for  $k = 60$ -minute time intervals and various percentiles  $p$ , as a function of the hourly average production level  $l_j$ . The interval around the average wind power production preserves the same shape for all percentiles, but increases in size with increasing coverage rate.

allows power system operators and wind farm owners to make decisions based on their willingness to accept a certain level of risk. Thus, a power system operator may choose the size of generation to be used for accommodating wind power variability according to a desired coverage rate, which should be linked to a minimum acceptable level of power system reliability. Similarly, a wind farm owner may choose the appropriate size for an energy storage system to integrate a certain level of wind power variability, by evaluating the cost against the benefit of the storage system for various probabilities  $p$ .

#### 4.1.3 Wind Power Variability over Various Time Frames

Figure 4.4 depicts the 95<sup>th</sup> percentile of the conditional range for the same 91.5 MW wind farm as a function of interval average wind power production for time intervals of length  $k$  equal to 5, 10, 15, 30 and 60 minutes. The time interval length  $k$  chosen represents critical time frames for power system operations (economic dispatch, hour-ahead scheduling), ancillary services (regulation, load following) and forecast updates (demand and wind). The figure reveals that the larger the time interval  $k$  is, the larger the CRM interval is, indicating larger variations in wind power over longer time frames. This effect is more pronounced at mid-level wind power productions. For example, for an interval average wind power production of  $l_j=0.4$  p.u. the conditional range varies from  $CR_{5,0.4,0.95}=0.075$  p.u. for  $k=5$  minutes up to  $CR_{60,0.4,0.95}=0.52$  p.u. for  $k=60$  minutes.

Figure 4.5 gives the expected conditional range  $CR_{k,l_j}$  value, calculated from (3.18) with  $l_j=0.5$  p.u., as a function of the time interval length  $k$  for five wind farms of different sizes, ranging from 37.5 to 210 MW (WF14, WF12, WF4, WF2, WF7). From this figure it is also evident that the con-

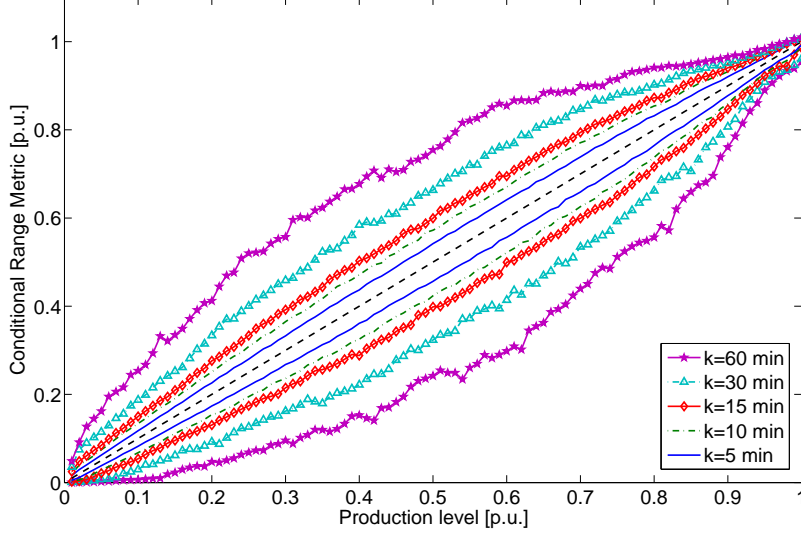


Figure 4.4: The 95<sup>th</sup> percentile of the conditional range metric  $CRM_{k,l_j,p=0.95}$  of a 91.5 MW wind farm for various time intervals ( $k = 5, 10, 15, 30, 60$  minutes) as a function of the interval average production level. The variability increases with increasing time intervals  $k$  and this effect is more pronounced at mid-level wind power productions.

ditional range value increases with increasing time interval length  $k$ , however this relationship is not linear but rather follows a cubic polynomial function (i.e.  $CR \approx \sum_{i=0}^3 a_i \cdot k^i$ ).

To explain the effect of the time interval length, the power output of a large wind farm can be viewed as the aggregated output of its many wind turbines. At smaller time scales the fluctuations in the output of these turbines are uncorrelated, and the addition of their uncorrelated variabilities is expected to result in a lower aggregated variability. However, over longer time frames the change in the wind power output of all turbines follows the same trend, increasing or decreasing, which is dictated by weather related changes in the wind speed. Quantifying wind power variability over different length

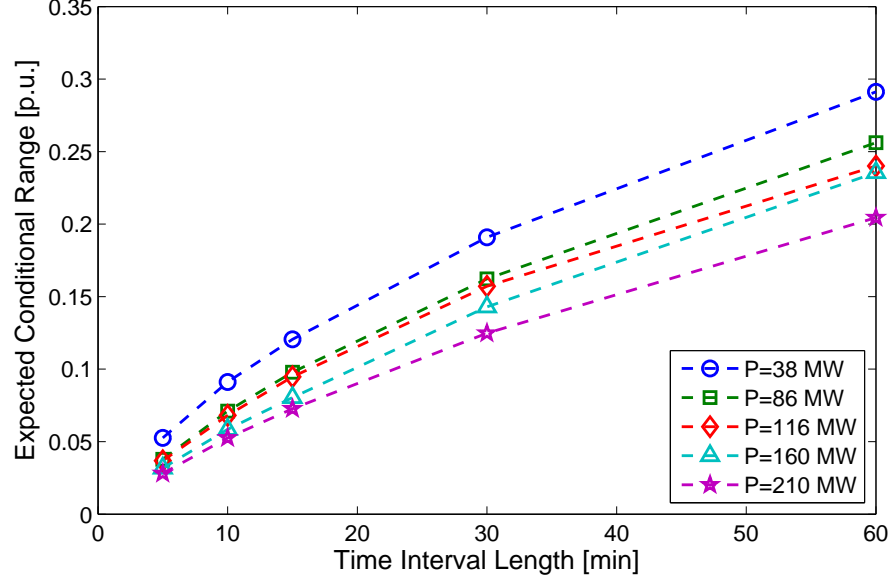


Figure 4.5: The effect of the time interval length  $k$  on the mid-level production ( $l_j = 0.5$  p.u.) expected wind power conditional range  $CR_{k,l_j}$ . Variability increases with increasing time interval length  $k$  and decreases as the wind farm nameplate capacity increases.

time frames is useful for determining the optimal ampere-hours (Ah) of an energy storage unit coupled with a wind farm with the purpose of reducing the variability and intermittency of wind power.

Observing Fig. 4.1, Fig. 4.3, and Fig. 4.4 it is noted that the curves of the upper  $M_{up_{k,l_j,p}}$  and lower  $M_{low_{k,l_j,p}}$  CRM endpoints as a function of the average wind power production level  $l_j$  always exhibit a similar shape, resembling some polynomial function. The preservation of this shape for varying time interval lengths  $k$  and coverage probabilities  $p$  suggests that the upper  $M_{up_{k,l_j,p}}$  and lower  $M_{low_{k,l_j,p}}$  CRM endpoints can be represented as functions of the average wind power production level  $l_j$  using some regression analysis technique.

Moreover, the effects of the time interval length, average wind power production and coverage rate, i.e. the conditions  $k$ ,  $l_j$ ,  $p$ , on the conditional range metric values for all wind farms considered are qualitatively similar to the ones presented here for a 91.5 MW wind farm. Next, the wind power variability difference between the considered wind farms due to their different sizes is quantified.

#### 4.1.4 The Effect of the Wind Farm Nameplate Capacity

From Fig. 4.5 it is evident that wind power variability, normalized on the wind farm size, decreases with increasing wind farm nameplate capacity. The effect of the wind farm's size on the conditional range is also depicted in Fig. 4.6 which gives the conditional range  $CR_{k,p}$ , calculated from (3.20) over all production levels for  $p = 0.9$  and for various time interval lengths  $k$ , as a function of the wind farm nameplate capacity  $P_N$ . The 17 wind farms considered have nameplate capacities ranging from 28.5 to 226.5 MW. This figure reveals that the higher the wind farm capacity is, the lower the conditional range value is, and thus the smaller the size of wind power output changes (in p.u. values).

The effect of the wind farm nameplate capacity on the conditional range values can again be attributed to the power output of a large wind farm being the aggregated output of its many wind turbines. Thus, a positive change from one minute to the next in one wind turbine's output can be canceled out by a negative change in another turbine's output, resulting in a smaller change in the wind farm's total wind power output. A higher number of wind turbines with a wider geographical spread in a large wind farm has a more pronounced effect on this averaging, especially over shorter time frames.

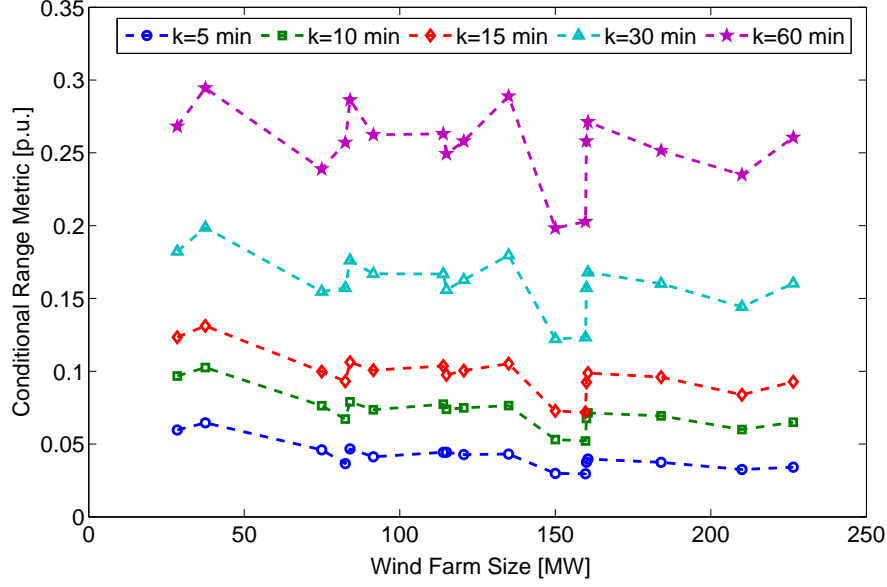


Figure 4.6: The effect of the wind farm nameplate capacity on the conditional range  $CR_{k,p}$  taken over all production levels for  $p = 0.9$  and for various time frames ( $k = 5, 10, 15, 30, 60$  minutes). Wind power variability is inversely proportional to the wind farm nameplate capacity, but this effect is more pronounced for smaller time intervals.

Indeed, from Fig. 4.6 a trend in reduced variability with increasing wind farm nameplate capacity  $P_N$  can be seen, especially for smaller time intervals  $k$ . However, for larger time intervals this trend is not so distinct and using only the wind farm size no robust conclusion can be drawn regarding the effect it has on the wind power conditional range. This is because there are multiple factors affecting wind power variability, such as the individual type and number of wind turbine generators in each wind farm as well as their location. The effect of wind turbine size and technology on wind power variability is presented in the next section.

#### 4.1.5 Concluding Remarks

In this section the effect certain influential variables have on wind power variability is examined. The variables include the conditions of the proposed metric, i.e the time interval length  $k$ , the average wind power production level  $l_j$ , and the coverage probability  $p$ , as well as the wind farm size  $P_N$ . Using the proposed conditional range metric  $CRM_{k,l_j,p}$  the wind power variability is found to be larger at mid-level wind power production  $l_j$  and increase with increasing time interval length  $k$  and increasing coverage probability  $p$ . The higher variability at mid-level wind power productions is attributed to the large slope of the wind power curve at mid-level productions. Moreover, for varying values of the conditions  $\{k, l_j, p\}$ , the upper  $M_{up_{k,l_j,p}}$  and lower  $M_{low_{k,l_j,p}}$  CRM endpoints can always be represented as polynomial functions of the average wind power production level  $l_j$ . Regarding the effect of wind farm size, wind power variability appears to decrease with increasing wind farm nameplate capacity  $P_N$ , since a large number of wind turbines allows for more averaging in the variability of their outputs. However, other factors influencing wind power variability, such as the location of the wind farm and the turbine size and technology, cause wind farms of similar sizes to exhibit different conditional range metric values.

## 4.2 Quantifying the Effect of Wind Turbine Size and Technology on Wind Power Variability

This section examines the effect of wind turbine size and technology on wind power variability. For this, two wind speed series (WS1 and WS2 - see Appendix B.1) comprising of real-world wind speed data with a 1-minute resolution spanning a period of 30 weeks are used. The wind speed series are



passed through six different wind power curves, corresponding to wind turbines of different technologies and sizes (Type I-IV, Size A-B - see Appendix B.2).

#### 4.2.1 Generating the Wind Power Series

To quantify wind power variability the wind speed series need to be converted to wind power series by passing them through wind power curves, which relate wind speed at the turbine hub height to wind power output from the turbine. To study the effect of wind turbine technology four wind power curves are used (Type I-IV), and two additional curves are used to study the effect of wind turbine size (Size A-B). Table 4.1 presents the wind power curves names and respective turbine generator description, along with the wind turbine size. Figure 4.7 depicts the wind power curves with wind power given in p.u. values. The wind turbine classification is according to [34] and the wind power curves have been taken from the manufacturers' technical specifications. More information on the wind turbines is given in Appendix B.2.

The wind power curve relates wind speed at the turbine hub height to wind power output from the turbine. Only two wind turbines (Type I and

Table 4.1: Wind Power Curves

Curve Name	Generator Description	Power [kW]
Type I	Fixed speed induction	1500
Type II	Variable slip induction	1500
Type III	Double-fed induction (DFIG)	1500
Type IV	Full converter (synchronous with IGBT)	1500
Size A	Variable slip induction	660
Size B	Variable slip induction	1650

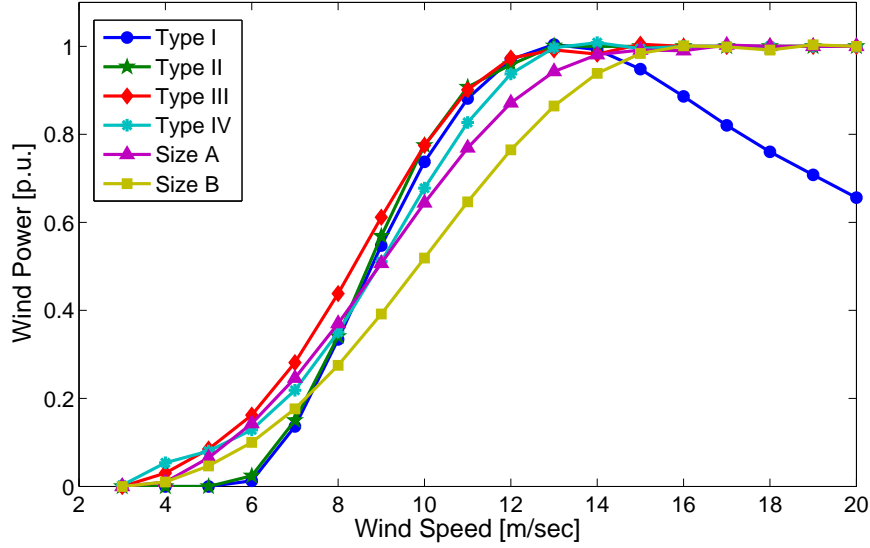


Figure 4.7: Six different wind power curves representing wind turbines of the same size (1500 kW) but different technologies (Type I-fixed speed, Type II-variable slip, Type III-DFIG, Type IV-full converter), as well as units of the same technology (Type II) but different sizes (Size A-660 kW, Size B-1650 kW).

Type II) have hub heights which are not equal to the measurement height. For these turbines the measured wind speed needs to be converted to a wind speed at the turbine hub height, by applying a wind power logarithmic or power law profile [35]. A power law profile is of the form:

$$\frac{u}{u_r} = \left(\frac{z}{z_r}\right)^a \quad (4.1)$$

where  $u$  is the estimated wind speed at height  $z$  and  $u_r$  is the measured wind speed at the measurement height  $z_r$ . In (4.1)  $a$  is an empirically obtained exponent, with typical value  $1/7$ . However, since the deviation of the hub height from the measurement height is very small, and decreases even more with the power law, no adjustment is made to the measured wind speed series. Thus, each wind speed series (WS1, WS2) is passed directly through each

wind power curve (Type I-IV, Size A-B) and twelve wind power series with a 1-minute resolution and a 30 week span are calculated. Six more wind power series are produced by summing the wind power series calculated from WS1 and WS2 for each wind power curve. The first wind speed series WS1 and the four respective wind power series (Type I-IV) are depicted in Fig. 4.8.

From Fig. 4.8 it is evident that the generated wind power series have similar profiles. The rated wind speed, i.e. the input wind speed which produces the rated output of the wind turbine, is close to 13-14 m/sec for all wind turbines. For wind speeds below the rated wind speed, the full converter wind turbine (Type IV) has a lower output than the other wind turbine types. For

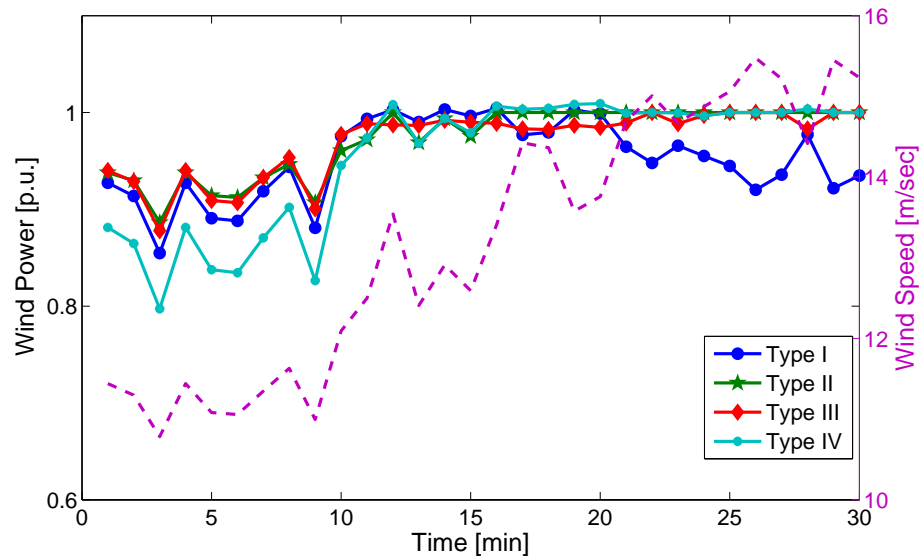


Figure 4.8: The first wind speed series (dashed line, right hand y-axis) and the respective wind power series (TypeI, II, III and IV, left hand y-axis) for a time period of 30 minutes. For wind speeds below the rated (13-14 m/sec) the wind power output of the TypeIV-full converter is lower than the other types. For wind speeds beyond rated all wind turbines generate their maximum power with the exception of TypeI-fixed speed (stall effect).

wind speeds beyond the rated wind speed, all wind turbines generate their rated output, except for the fixed speed wind turbine (Type I). This is attributed to the fact, that the fixed speed wind turbine has no power control on the blades. When the wind speed exceeds the rated value, wakes are formed above the top surface of the airfoils, causing the blades to stall and the wind power output to decrease [35].

#### 4.2.2 Quantifying Wind Power and Wind Speed Variability

The conditional range metric (CRM) is used on the generated wind power series to quantify wind power variability. All CRM values are calculated for time lengths  $k = 5, 10, 15, 30, 60$  minutes and for 200 quantiles  $p = r/200$ ,  $r = 1, 2, \dots, 200$ , by solving the system of equations (3.7) and (3.10) with the methodology given in Section 3.3.2. For each of the 18 generated wind power series the CRM of the wind power, denoted  $CRM_{\{W\}k,l_j,p}$ :

$$CRM_{\{W\}k,l_j,p} = [M_{\{W\}low_{k,l_j,p}}, M_{\{W\}up_{k,l_j,p}}] \quad (4.2)$$

is calculated for wind power averages  $l_j = 0.01, 0.02, \dots, 1$  p.u., where  $\bar{x}_n \in l_j = j/m$  if  $(2j - 1)/2m < \bar{x}_n \leq (2j + 1)/2m$ ,  $j = 1, 2, \dots, 100$ ,  $m = 100$ . Similarly, for the two wind speed series the CRM of the wind speed series, denoted  $CRM_{\{S\}k,s_j,p}$ , is calculated from:

$$CRM_{\{S\}k,s_j,p} = [N_{\{S\}low_{k,s_j,p}}, N_{\{S\}up_{k,s_j,p}}] \quad (4.3)$$

for wind speed averages  $s_j = 0.25, 0.50, \dots, 25$  m/sec, by using the wind speed series instead of the wind power series as input in the system of equations (3.7) and (3.10). Thus, in (4.3) points  $N_{\{S\}low_{k,s_j,p}}$  and  $N_{\{S\}up_{k,s_j,p}}$  refer to minimum and maximum wind speed in an interval with average wind speed  $s_j$ .

In addition, a new CRM value, denoted  $CRM_{\{W,S\}k,s_j,p}$  is calculated for the wind power series:

$$CRM_{\{W,S\}k,s_j,p} = [M_{\{W\}low_{k,s_j,p}}, M_{\{W\}up_{k,s_j,p}}] \quad (4.4)$$

for wind speed averages  $s_j = 0.25, 0.50, \dots, 25$  m/sec. In (4.4) points  $M_{\{W\}low_{k,s_j,p}}$  and  $M_{\{W\}up_{k,s_j,p}}$  refer to minimum and maximum wind power values in an interval for which the respected wind speed values have average  $s_j$ . The new  $CRM_{\{W,S\}k,s_j,p}$  has the following interpretation: In a  $k$ -long time interval with wind speed average  $s_j$  the wind power output lies in the interval  $[M_{\{W\}low_{k,s_j,p}}, M_{\{W\}up_{k,s_j,p}}]$  with probability  $p$ .

#### 4.2.3 The Effect of Wind Turbine Technology

The effect of wind turbine technology is shown in Fig. 4.9, which depicts the expected conditional range  $CR_{k,l_j}$  as a function of the wind power production level  $l_j$  for the four wind turbine types (Type I-IV). The  $CR_{k,l_j}$  is calculated from (3.18) for  $k = 15$  minutes using the wind power series  $CRM_{\{W\}k,l_j,p}$  calculated by passing the first wind speed series (WS1) through the wind power curves (Types I-IV). For example, Fig. 4.9 reveals that for a 15-minute interval with wind power average production  $l_j = 0.25$  p.u. (375 kW), the expected size of the largest change in wind power output within the interval is 0.37 p.u. (549 kW) for wind turbine Type I, 0.35 p.u. (532 kW) for wind turbine Type II, 0.23 p.u. (341 kW) for wind turbine Type III, and 0.22 p.u. (333 kW) for wind turbine Type IV.

A hypothetical constant power output generator would have  $CR_{k,l_j}$  values equal to zero under all production levels, whereas wind power variability appears to be higher at mid production levels  $l_j$ . This is true for all types,

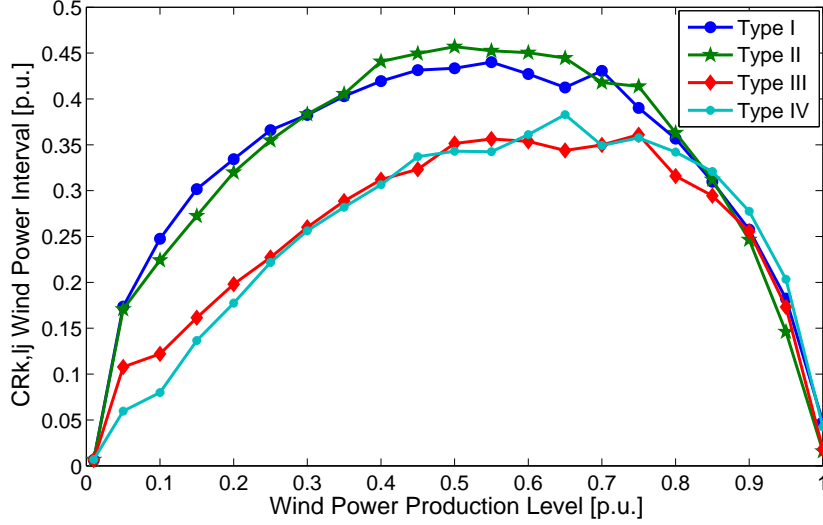


Figure 4.9: The conditional range  $CR_{k,l_j}$  for  $k = 15$  minutes as a function of wind power production level  $l_j$  for all wind turbine types. Wind turbines connected through converters to the grid (Types III-IV) exhibit lower wind power variability compared to simple induction generators (Types I-II)

while Type I (fixed speed) and Type II (variable slip) wind turbines present higher wind power variability than Type III (DFIG) and Type IV (full converter) for all production levels. Wind power variability also increases with increasing time interval length for all wind turbine types, as can be seen in Fig. 4.10, which illustrates the conditional range  $CR_k$  from (3.21) as a function of time interval length  $k$ , using again the wind power  $CRM_{\{W\}k,l_j,p}$  (WS1 and Type I-IV).

Figures 4.11 and 4.12 depict the 95<sup>th</sup> percentile of the conditional range metric  $CRM_{\{W,S\}k,s_j,p} = [M_{\{W\}low_{k,s_j,p}}, M_{\{W\}up_{k,s_j,p}}]$  for wind speed averages  $s_j$  ranging from 3 to 20 m/sec taken over 15-minute long time intervals, for wind turbine Types I and IV, respectively. The CRM values in Fig. 4.11 are ob-

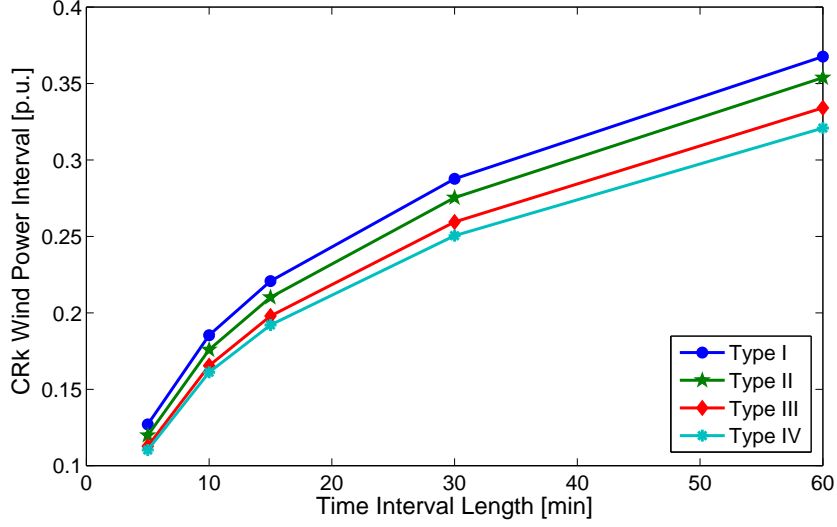


Figure 4.10: The conditional range  $CR_k$  as a function of time interval length  $k$  for all wind turbine types. Wind power variability increases with increasing time interval length.

tained by passing the first wind speed series (WS1) through wind power curve Type I, which corresponds to the output from a fixed speed wind turbine. Similarly, the CRM values in Fig. 4.12 are obtained by passing the first wind speed series (WS1) through wind power curve Type IV, which corresponds to the output from a wind turbine connected to the grid through a converter. In these figures, the solid line refers to upper  $M_{up}$  and the dashed to lower  $M_{low}$  endpoints of the  $CRM$  wind power interval, whereas the dotted line depicts the respective wind power curve.

As expected, the CRM curves resemble shifted versions of the respective wind power curves (dotted lines). Thus, for full converter turbines (Fig. 4.12), wind power variability ( $M_{up} - M_{low}$ ) reduces to zero for wind speeds higher than the rated. However, for fixed speed turbines (Fig. 4.11), the lower CRM interval endpoint  $M_{low}$  (dashed line) is zero at high wind speeds, in-

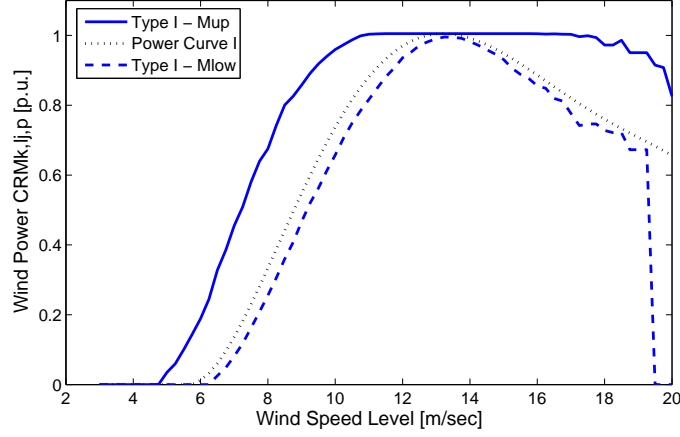


Figure 4.11: The 95<sup>th</sup> percentile of the conditional range metric  $CRM_{\{W,S\}k,s_j,p} = [M_{\{W\}low_{k,s_j,p}}, M_{\{W\}up_{k,s_j,p}}]$  for  $k = 15$  minutes as a function of wind speed level  $s_j$  for wind turbine TypeI (fixed speed). The solid line refers to upper  $M_{up}$  and the dashed to lower  $M_{low}$  endpoints of the  $CRM$  wind power interval, which envelopes the respective wind power curve (dotted line).

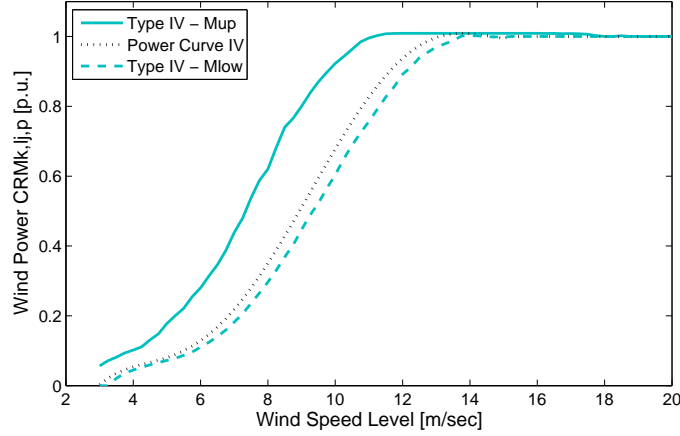


Figure 4.12: The 95<sup>th</sup> percentile of the conditional range metric  $CRM_{\{W,S\}k,s_j,p} = [M_{\{W\}low_{k,s_j,p}}, M_{\{W\}up_{k,s_j,p}}]$  for  $k = 15$  minutes as a function of wind speed level  $s_j$  for wind turbine TypeIV (full converter). For wind speeds higher than the rated wind power variability reduces to zero.



creasing wind power variability to the nameplate capacity. This is due to the fact that the fixed speed turbine's cut-out wind speed, i.e. the wind speed beyond which the turbine stops generating electricity, equals 20 m/sec. Thus, in a 15-minute long time interval with average wind speed equal to 20 m/sec some wind speed values will be higher than the fixed speed turbine cut-out wind speed and the wind turbine will cease to generate electricity.

#### 4.2.4 The Effect of Wind Turbine Size

The effect of the wind turbine size is depicted in Fig. 4.13, which plots the conditional range  $CR_{k,p}$  from (3.20) as a function of the percentile  $p$  for the two different size wind turbines (Size A and B) and for two time intervals

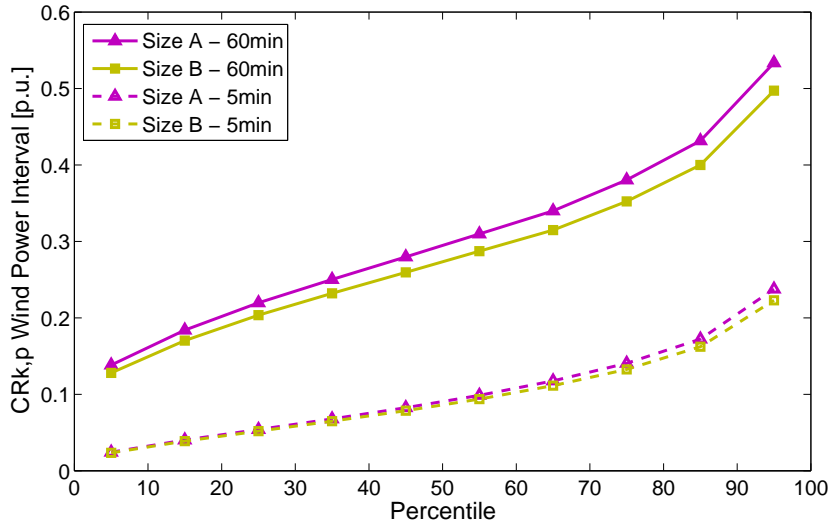


Figure 4.13: The conditional range  $CR_{k,p}$  as a function of the percentile  $p$  for two time interval lengths ( $k = 5$  and  $k = 60$  minutes). The smaller wind turbine (SizeA-660 kW) exhibits slightly higher variability than the larger turbine (SizeB-1650 kW).

( $k = 5$  and  $k = 60$  minutes). Again, the wind power series are calculated using the first wind speed series (WS1). As anticipated, the  $CR_{k,p}$  values increase with increasing percentile  $p$  and time interval length  $k$ . Regarding the turbine size, the output from the smaller wind turbine (Size A) exhibits slightly higher variability in p.u. values than the larger wind turbine (Size B), an effect which is more pronounced at higher percentiles and larger time intervals.

#### 4.2.5 The Effect of Wind Power Aggregation

The effect of wind power aggregation on wind power variability is studied by comparing the conditional range values of one wind power series calculated from either one of the wind speed series (WS1 or WS2) to the sum of both wind power series (denoted WS1+WS2) for each wind power curve. Figure 4.14 illustrates the effect of wind power aggregation for wind turbine Size A (variable slip - 660 kW), by depicting the 95<sup>th</sup> percentile of the conditional range metric  $CRM_{\{W\}k,l_j,p} = [M_{\{W\}low_{k,l_j,p}}, M_{\{W\}up_{k,l_j,p}}]$  for  $k = 60$  minutes. The two wind speed series have similar mean and standard deviation values and thus, the generated wind power series exhibit similar wind power variability levels. However the aggregated wind power output exhibits less variability in p.u. values despite the fact that the two wind speed series are not correlated (correlation coefficient  $r_{WS1,WS2} = -0.0414$ ). The  $y$ -values of the dotted line in Fig. 4.14 represent the conditional range metric for a hypothetical constant power output generator, for which  $CRM = [M_{low}, M_{up}]_{k,l_j,p} = [l_j, l_j]_{k,l_j,p}, \forall k, p$ .

Similarly, Fig. 4.15 compares the conditional range  $CR_{k,l_j}$  from (3.18) for the 15-minute long time interval under all wind turbine types. The comparison between the wind power variability from the wind speed series WS1 to the variability from the sum of both wind power series (from WS1 and WS2)

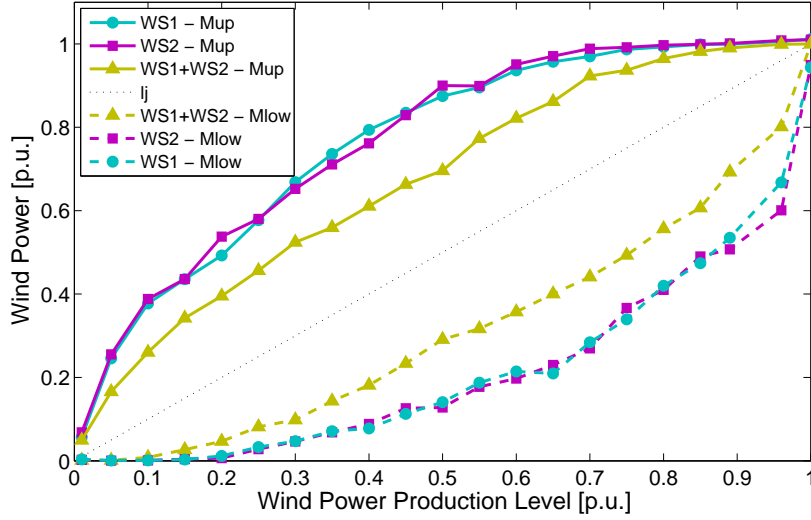


Figure 4.14: The 95<sup>th</sup> percentile of the conditional range metric  $CRM_{\{W\}k,l_j,p} = [M_{\{W\}lowk,l_j,p}, M_{\{W\}upk,l_j,p}]$  for  $k = 60$  minutes as a function of wind power production level  $l_j$  for wind turbine Size A using the wind power series from wind speed series WS1 and WS2, as well as the sum of the two wind power series (denoted WS1+WS2). The aggregated wind power output exhibits lower wind power variability under all production levels.

reveals that the aggregated wind power output is less variable for all wind turbine types.

Two factors contribute to the reduced wind power variability when the wind power output from two wind turbines is summed. The first is that in the aggregated output some positive changes in wind power output of the first turbine are canceled out by negative changes in wind power output of the second turbine. Indeed, in the case where both wind turbines have average wind power output  $l_j$  taken over  $k$ -long time intervals the aggregated average wind power output is also  $l_j$ . Then, for some of these  $k$ -long time intervals with aggregated average wind power production  $l_j$ , the sign of the

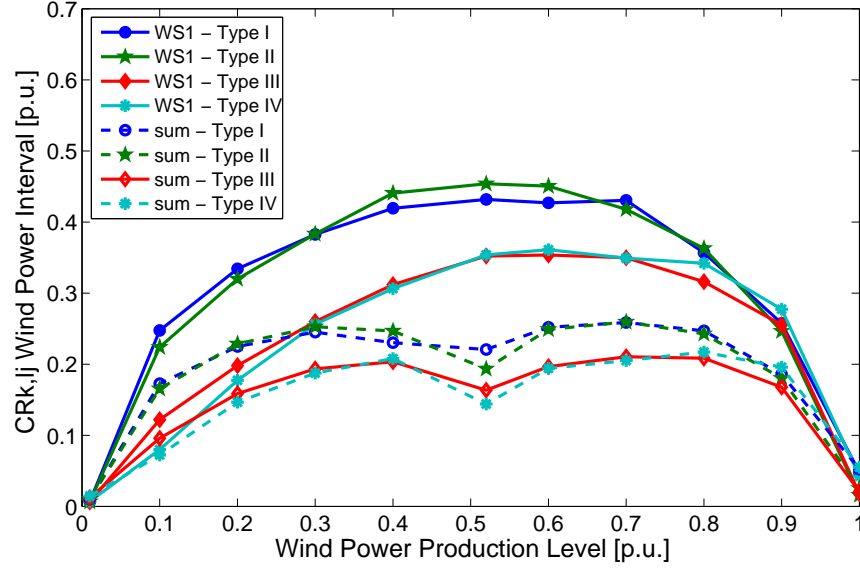


Figure 4.15: The conditional range  $CR_{k,l_j}$  for  $k = 15$  minutes as a function of wind power production level  $l_j$  for all wind turbine types and for wind power series from WS1 as well as the sum of both respective wind power series (WS1+WS2). The aggregated wind power output exhibits lower wind power variability under all turbine types.

conditional range, i.e. the sign of the largest change in wind power output, of each wind turbine may be opposite. In this case, the conditional range value of the summed output will be much smaller than the individual conditional range values of each wind turbine. The existence of such intervals with low conditional range value causes the expected conditional range  $CR_{k,l_j}$  of the summed output to be much lower than the expected conditional range of the individual turbines. Since wind power variability is highest at mid-production wind power levels, the existence of time intervals with small conditional range values over these intervals, results in a higher reduction in the expected conditional range value of the summed output. Thus, wind power variability is

higher at mid-production levels, but reduction in wind power variability due to aggregation is also higher at these levels, as is verified from the dip at 0.5 p.u. for the dashed lines in Fig. 4.15.

The other reason for reduced variability when wind power is aggregated, has to do with the relationship between the average wind power production of each individual turbine. Consider the case where the average wind power production of the individual turbines, taken over a  $k$ -long time interval, is  $l_j + \alpha$  and  $l_j - \alpha$ , respectively. Then for these  $k$ -long time intervals the aggregated average production is  $l_j$ . Averaging the conditional range values, i.e. the largest changes in wind power output, over these  $k$ -long time intervals, it is obvious that the two wind turbines exhibit very different expected conditional range values. For example, for  $l_j = 0.3$  p.u. and  $\alpha = 0.2$  p.u., the wind turbine with average production 0.5 p.u. has higher variability than the wind turbine with average production 0.1 p.u. However, as can be seen in Fig. 4.15, the expected conditional range values do not vary proportionally to the average wind power production level (e.g. for Type I  $CR_{k=15, l_j=0.5 \text{ p.u.}} = 0.43$  p.u. compared to  $CR_{15, 0.1} = 0.25$  p.u.). Hence, for these  $k$ -long time intervals with aggregated average wind power output  $l_j = 0.3$  p.u., the expected conditional range of the aggregated output is lower than the respective conditional range of the individual turbines (e.g. for Type I in Fig. 4.15  $0.38 = CR_{15, 0.3} > (CR_{15, 0.1} + CR_{15, 0.5})/2 = 0.34$  p.u.). For large  $\alpha$  values, for which one or both the individual turbine averages ( $l_j + \alpha$  and  $l_j - \alpha$ ) go to very low or very high values, this effect is even more pronounced. For example, for aggregated average wind power output  $l_j = 0.5$  p.u., in some of the  $k$ -long time intervals the average wind power output of the individual turbines is 0.1 p.u. and 0.9 p.u. Since wind power variability at these production levels is much lower than wind power variability at mid-production levels, the aggregated

wind power variability is significantly reduced. Hence, this is another reason why the expected conditional range  $CR_{k,l_j}$  for the aggregated output depicted in Fig. 4.15 exhibits a dip at 0.5 p.u. production level.

Table 4.2 lists the  $CR_k$  values from (3.21) for 15-minute time intervals. The conditional range values are calculated by passing the first wind speed series through wind power curves Type I - IV (denoted WS1) and by taking the sum of the wind power series obtained by passing both wind speed series through the respective wind power curves (denoted WS1+WS2). Conditional range values are given in p.u. and kW values. The increase in % of the conditional range values between WS1 and WS1+WS2 is also listed as a percentage of the WS1 value. The conditional range values in Table 4.2 reveal that an increase by 100% in wind power installed capacity causes an increase by no more than 75% in wind power variability. This outcome verifies reduction in wind power variability due to wind power aggregation, calling for further study of the factors that influence it, along with inspection of their quantitative effect on this reduction.

Table 4.2: Effect of Wind Power Aggregation on  $CR_k$  (k=15 minutes)

	WS1		WS1+WS2		Increase
	[p.u.]	[kW]	[p.u.]	[kW]	[%]
Type I	0.212	317.26	0.185	553.92	75
Type II	0.205	307.26	0.179	538.07	75
Type III	0.199	297.80	0.163	489.08	64
Type IV	0.188	282.45	0.157	470.58	67

#### 4.2.6 Concluding Remarks

The conditional range metric is applied on two wind speed series passed through six wind power curves, corresponding to wind turbines of different technologies and sizes, in order to quantify the effects wind turbine size and technology have on wind power variability. The results reveal that wind turbines connected through converters to the grid exhibit lower wind power variability compared to same size simple induction generators, and that wind power variability decreases slightly with increasing wind turbine size. Most importantly, wind power aggregation offers a significant reduction in wind power variability for all wind turbine technologies and sizes. For the specific non-correlated wind speed series, an increase by 100% in wind power installed capacity results in an increase in wind power variability intervals by no more than 75%, for all considered wind turbines. This outcome leaves ample room for the study of methodologies to reliably estimate this reduction, under more general conditions.

### 4.3 Comparison of the Conditional Range Metric to the Step-changes and Forward Differences Statistics

In this section, the proposed conditional range is compared to the step-changes and forward differences statistics, which have been used in wind integration studies to characterize wind power variability. Through this comparison possible shortcomings of the step-changes and forward differences, in terms of their ability to estimate wind power ramp sizes and their rates, are identified and it is demonstrated why these shortcomings can be overcome by the proposed metric. The comparison is done using real-world wind power data, which come from 13 wind farms in the ERCOT system, with nameplate

capacities ranging from 28 MW to 210 MW, and include wind power production data with a 1-minute resolution spanning a period of one year (WF1 - WF7, WF11, WF13 - WF15, WF17, WF18, year 3 – see Appendix A.1).

#### 4.3.1 Comparison Pairs

The purpose of comparing the conditional range to the step-changes is to find out whether the information derived from the statistical analysis of the step-changes is sufficient to assess the size and rate of wind power ramps. Here wind power ramps constitute the largest possible changes in wind power output over a certain length time interval. These wind power changes (ramps) can be regarded to have a specific rate (ramp rate) over a specific duration (ramp duration):

$$\text{ramp size [MW]} = \text{ramp rate [MW/min]} \cdot \text{ramp rate duration [min]} \quad (4.5)$$

As has been noted in Section 2.2.1, the prevalent wind power variability metric used in numerous wind integration studies is based on the spread of the wind power step-changes  $y_{k,j}$ , taken over successive time intervals, captured by their standard deviation  $s_{y_{k,j}}$ . It is reminded that, starting from the wind power time series  $x_n$ ,  $n = 1, 2, \dots, N$ , the wind power step-changes time series  $y_{k,j}$  for the desired time frame  $k$  can be created using the following equation:

$$y_{k,j} = \bar{x}_{k,j+1} - \bar{x}_{k,j}, \quad j = 1, 2, \dots, q-1 \quad (4.6)$$

where  $q = \lfloor N/k \rfloor$  and  $\bar{x}_{k,j}$  refers to the sampled mean of the wind power over the desired time frame  $k$ :

$$\bar{x}_{k,j} = \frac{1}{k} \sum_{m=1}^k x_{k(j-1)+m}, \quad j = 1, 2, \dots, q \quad (4.7)$$



Then, the unbiased sample standard deviation,  $s_{y_{k,j}}$ , can be used to estimate the standard deviation of the time series  $y_{k,j}$ :

$$s_{y_{k,j}} = \sqrt{\frac{1}{q-2} \sum_{j=1}^{q-1} (y_{k,j} - \frac{1}{q-1} \sum_{j=1}^{q-1} y_{k,j})^2} \quad (4.8)$$

Step-changes, as they are given in (4.6), are essentially forward differences of wind power averages. Alternatively, wind power variability of a wind power series over a  $k$ -long time interval can be characterized using forward differences of spacing  $k$  of the wind power series itself. Using an  $N$ -long wind power series  $x_n$ , the wind power forward differences time series  $z_{k,i}$  is then defined by:

$$z_{k,i} = x_{i+k} - x_i, \quad i = 1, 2, \dots, N - k \quad (4.9)$$

Thus, each value of the step-changes series  $y_k$  is the average of  $k$  successive forward difference values  $z_k$ . Obviously, for  $k = 1$  the step-changes and forward differences series are identical.

On the other hand, using the basic concept of the conditional range metric described in Chapter 3 the wind power conditional range series  $M_{k,i}$  is generated by calculating the interval's size  $M_k$  over all  $k$ -long time intervals:

$$M_{k,i} = M_{up_{k,i}} - M_{low_{k,i}} = \max_{n \in K_i} x_n - \min_{n \in K_i} x_n \quad i = 1, 2, \dots, N - k \quad (4.10)$$

where  $K_i$  is the interval  $[i, i + k - 1]$ . By definition, the conditional range is the largest change (largest possible ramp) the wind power output can undergo within a given time frame. However, contrary to the step-changes, the conditional range provides the largest change in wind power output in an interval, without specifying the sign of this change. That is, the conditional range provides only the size of the largest wind power ramp in an interval.

To provide a ramp rate (in MW/min) for the ramp of size  $M_{k,i}$  defined by the conditional range in each  $k$ -long time interval  $K_i$ , the following series is defined:

$$r_{M_{k,i}} = \frac{M_{k,i}}{n_{max,i} - n_{min,i}} \quad i = 1, 2, \dots, N - k \quad (4.11)$$

where  $n_{max,i} \in K_i$  is the time-point at which the wind power output attains its maximum in the  $K_i$  interval:

$$n_{max,i} = \arg \max_{n \in K_i} x_n \quad (4.12)$$

and  $n_{min,i} \in K_i$  is the time-point at which the wind power output attains its minimum in the  $K_i$  interval:

$$n_{min,i} = \arg \min_{n \in K_i} x_n \quad (4.13)$$

It should be noted, that the ramp rate defined in (4.11) might not be the largest possible rate of wind power output change within the specific time interval. Rather this rate is the rate associated with the largest possible size of wind power output change within the interval.

Similarly, to relate a ramp rate (in MW/min) to the step-changes  $y_k$  and forward differences  $z_k$  it is observed that they too can be viewed as wind power changes over a  $k$ -long time interval, having units [MW/ $k$  min]. Thus, dividing the step-changes series  $y_k$  and the forward differences  $z_k$  by the length  $k$  of the time interval, the following ramp rate series are defined:

$$r_{y_{k,j}} = \frac{y_{k,j}}{k} \quad j = 1, 2, \dots, \lfloor N/k \rfloor - 1 \quad (4.14)$$

and

$$r_{z_{k,i}} = \frac{z_{k,i}}{k} \quad i = 1, 2, \dots, N - k \quad (4.15)$$

To compare the ability of the conditional range against the step-changes and the forward differences in assessing the size of wind power ramps over  $k$ -long time intervals, the statistics of the conditional range series  $M_{k,i}$  from (4.10) are compared against the statistics of the absolute step-changes  $|y_{k,j}|$  from (4.6) and the absolute forward differences  $|z_{k,i}|$  from (4.9). Step-changes and forward differences distinguish between positive and negative changes in wind power output, however here absolute values are taken since the conditional range specifies only a size and not a sign for the change in wind power output. To compare the information regarding the ramp rates associated with the wind power ramp sizes the statistics of the ramp rate series defined by (4.11), (4.14) and (4.15) are compared.

For the comparison, the conditional range and step-changes or forward differences ramp sizes and rates may be taken over time intervals of different lengths and the conditional range can also be compared against multiples of the step-changes and forward differences. The comparison pairs used in this section are given in Table 4.3. In Table 4.3,  $K$  refers to the time interval length of the conditional range, whereas  $k$  refers to the time interval length of the step-changes or forward differences.  $L$  is the multiple of the step-changes or forward differences against which the conditional range is compared. The same variables are used for both ramp sizes and ramp rates.

### 4.3.2 Comparison Schemes

By comparing the conditional range to the step-changes approach, the two main shortcomings of the step-changes are being exposed. The first is that because step-changes are calculated as differences of average wind power values from one time interval to the next they do not convey information of the

Table 4.3: Comparison Pairs

Pair	Ramp Size [MW]	
1	$M_K$	$L \cdot  y_k $
2	$M_K$	$L \cdot  z_k $
Ramp Rate [MW/min]		
3	$r_{M_K}$	$L \cdot r_{y_k}$
4	$r_{M_K}$	$L \cdot r_{z_k}$

wind power variability within each time interval. The second is that although the step-changes provide some information on ramp rates they do not provide adequate information on their duration, and are thus of little use to power system operators since they cannot fully assess the size of wind power ramps. The comparison of the conditional range to the forward differences statistics, reveals that these shortcomings are apparent in forward differences as well, however at a lesser extent.

The following comparison schemes are used to expose the two shortcomings of the wind power step-changes and forward differences:

- Scheme A:  $k = K, L = 1$

This comparison scheme examines whether by tracking the step-changes or forward differences and their rates over  $k$ -long time intervals a conclusion on the wind power variability within these intervals can be drawn.

- Scheme B:  $k < K, L = 1$

This comparison scheme examines whether step-changes or forward differences and their rates taken over time intervals of length  $k$  can be used to estimate the size and rates of wind power ramps in longer time frames of length  $K$ .

- Scheme C:  $k < K$ ,  $L = K/k$

This comparison scheme examines whether taking exact multipliers  $K/k$  of the step-changes or forward differences and their rates is suitable for estimating wind power variability in longer time frames of length  $K$ .

From their definition in (4.6) and (4.9), step-changes  $y_k$  and forward differences  $z_k$  cannot convey information of the wind power variability within the time interval of length  $k$ . This is due to the fact that a step-change  $y_{k,i}$  is essentially an average of  $k$  wind power output forward differences of the form  $(x_{i+k} - x_i)$ . However, these forward differences are taken from sampled wind power points  $x_{i+k}$  and  $x_i$  belonging to two different  $k$ -long time intervals. On the other hand, the conditional range  $M_k$  is the difference between two sampled wind power points in the same  $k$ -long time interval. The simple case study from [4] given in Section 2.2.1.3 using two fictitious sources with sinusoidal outputs exposes this shortcoming of the step-changes. In this Section, the results from comparison scheme A using real-world wind power data indicate if the information that the step-changes and the forward differences fail to capture is actually essential in assessing the size of wind power ramps. That is, comparison scheme A examines whether it is common for the wind power output changes within an interval to be larger than the changes from one interval to the next.

Because step-changes  $y_k$  are averages of wind power output forward differences  $z_k$  over  $k$ -long time intervals, they can be considered as average ramp rates [MW/ $k \cdot \text{min}$ ], as the definitions of the ramp rate series  $r_{y_k}$  and  $r_{z_k}$  in (4.14) and (4.15) imply. However, by looking at the step-changes  $y_k$  no information about the duration of these ramp rates is revealed in order to estimate the size of a ramp over a larger time interval  $K$ . Nonetheless,

in some wind integration studies it has been assumed that step-changes  $y_k$  taken over intervals of length  $k$  can be used as is to estimate power variability over larger intervals  $K$  [8]. For example, 1-minute net demand step-changes have been used to estimate regulation needs in the 5-minute frame and 10-minute net demand step-changes have been used to estimate intra-hour load variability [10, 15–17]. The wind power output in Fig. 3.1 actually justifies this assumption, since for the larger shaded rectangle ( $k_2 \times M_2$ ) the largest ramp in the time frame of length 28 minutes ( $K$ ) has a duration of 15 minutes ( $k$ ). The results from comparison scheme B evaluate the general validity of this assumption.

Comparison scheme C on the other hand examines whether another simplistic approach, namely to use the exact multiplier  $K/k$  of the step-changes  $y_k$  and forward differences  $z_k$ , yields better results in assessing wind power ramps in the  $K$ -minute frame. Since the duration of the wind power ramp rate is unknown, this comparison scheme evaluates the validity of the assumption about wind power step-changes  $y_k$  having duration  $K/k$  over  $K$ -long time intervals. In other words, under this assumption the largest change in the wind power output ( $\text{MW}_{\text{in } K \text{ min}}$ ) over a  $K$ -long time interval would be equal to  $(\text{MW}/k \cdot \text{min}) \cdot (K/k)$ , which translates to  $M_K = y_k \cdot (K/k)$ . The results from comparison schemes B and C essentially reveal the importance of the knowledge of the ramp rate duration in assessing the size of wind power ramps.

Using the available wind power data (WF1 - WF7, WF11, WF13 - WF15, WF17, WF18, year 3 – see Appendix A.1) wind power step-changes time series  $y_{k,j}$  and wind power forward differences time series  $z_{k,i}$  are generated from (4.6) and (4.9), respectively, over time frames of  $k = 1, 5, 10, 15, 30$  and 60 minutes. The respective ramp rates series  $r_{y_{k,j}}$  and  $r_{z_{k,i}}$  are calculated from (4.14) and (4.15). Similarly, wind power conditional range series  $M_{k,i}$

and ramp rate series  $r_{M_k,i}$  are calculated over time intervals of length  $k = 5, 10, 15, 30$  and  $60$  minutes using (4.10) and (4.11), respectively. As before, the chosen time interval lengths  $k$  represent critical time frames for power system operations (economic dispatch, hour-ahead scheduling), ancillary services (regulation, load following) and forecast updates (load and wind).

For all the comparison pairs listed in Table 4.3 the comparison is made using the time interval lengths  $K$  and  $k$  given in Table 4.4 under the three comparison schemes A, B, and C. It is reminded that under comparison schemes A and B the multiplier of the step-changes or forward differences is  $L = 1$ , whereas under comparison scheme C the multiplier is  $L = K/k$ . For example, for comparison pair 1 (conditional range against absolute step-changes) Table 4.4 shows that, the 5-minute conditional range  $M_5$  is compared to the same time interval length 5-minute step-changes  $|y_5|$  under scheme A. Under scheme B the 5-minute conditional range  $M_5$  is compared to the shorter time interval length 1-minute step-changes  $|y_1|$ , whereas under scheme C it is compared to the exact multiplier (5) of the 1-minute step-changes  $5 \cdot |y_1|$ .

### 4.3.3 Comparison Outcomes

For reasons explained in Section 2.2.1.3 the comparison between the conditional range and the step-changes or forward differences is done not using their standard deviation but rather by comparing their sample quantiles  $Q_{M_K}(p)$  and  $Q_{|y_k|}(p)$  or  $Q_{|z_k|}(p)$ . Sample quantiles are also used when comparing the respective ramp rate series. It is reminded that the  $p^{th}$  quantile  $Q_X(p)$ ,  $p \in [0, 1]$ , of a random variable  $X$  with cumulative distribution function  $F_X(x)$  is given by:

$$Q_X(p) = F_X^{-1}(p) = \inf\{x : P(X \leq x) \geq p\} \quad (4.16)$$

Table 4.4: Time Interval Lengths under the three Comparison Schemes

Comparison	Conditional Range	Step-changes/Forward Differences
Scheme	$K$ [min]	$k$ [min]
A	5	5
	10	10
	15	15
	30	30
	60	60
B	5	1
	10	5
	15	5
	30	10
	30	15
	60	10
	60	15
	60	30
C	5	1
	10	5
	15	5
	30	10
	30	15
	60	10
	60	15
	60	30

Since no assumption about the underlying distribution of the conditional range, the step-changes or the forward differences is made a quantile estimate can be calculated from the sample data series. The sample quantile  $Q_{X_N}(p)$  can be estimated from the order statistics of a sample  $X_1, X_2, \dots, X_N$ ,



where the  $i^{th}$  order statistic  $X_{(i)}$  is such that  $X_{(1)} \leq X_{(2)} \leq \dots \leq X_{(N)}$ . When order statistics are used, the estimate of the  $p^{th}$  sample quantile  $\hat{Q}_{X_N}(p)$  from an  $N$ -long sample can be derived by computing a real-valued index  $h = N \cdot p + 1/2$ . When  $h$  is an integer the sample quantile estimate  $\hat{Q}_{X_N}(p)$  is given by the  $h^{th}$  order statistic:

$$\hat{Q}_{X_N}(p) = X_{(h)} \quad (4.17)$$

Otherwise one can choose from several rounding or interpolation schemes, the most simple being the inverse of the empirical cdf, where  $\hat{Q}_{X_N}(p) = X_{(\lceil h \rceil)}$ .

From the quantile definition in (4.16) it is evident that the percentage of values from the sample  $x_n$  which are less than the sample quantile  $Q_X(p)$  is equal to  $p$ . If the random variable is the conditional range  $M_k$ , then the probability of the largest wind power ramp in a  $k$ -long time interval having size less than the sample quantile  $Q_{M_k}(p)$  is at least  $p$ . If the wind power ramps are undesired, e.g. they appear in time periods of little demand variation or they are negatively correlated with demand ramps, then reserves have to be set aside to counteract the wind power ramps. Setting aside reserve power equal to the conditional range sample quantile  $Q_{M_k}(p)$  would result in an ability to counteract the wind power ramps in  $k$ -long time intervals with a coverage rate of at least  $p$  (thus,  $p$  is the percentage of successfully counteracted wind power ramps). Since the sign of the power ramp is unknown, generators would have to be able to ramp both up and down in order to counteract down and up wind power ramps, respectively. Moreover, the provision of quantiles  $Q_{M_k}(p)$  allows power system operators to choose the amount of reserves according to the desired coverage rate  $p$ .

Similarly, the generators which provide the necessary reserves to counteract wind power ramps must have certain ramp rate capabilities, which can

be determined by the sample quantiles of the conditional range ramp rate series  $r_{M_k}$ . A generator with a ramp rate capability equal to  $Q_{r_{M_k}}(p)$  manages to counteract wind power ramp rates with a coverage rate of at least  $p$ . It should be noted that since ramp rates can be both positive and negative, low rank sample quantiles correspond to high negative ramp rates, while high rank sample quantiles correspond to high positive ramp rates. Thus, for a probability  $p$ , only  $(1 - p)\%$  of the positive wind power ramp rates in  $k$ -long time intervals are larger than the sample quantile  $Q_{r_{M_k}}(p)$ , whereas only  $(1 - p)\%$  of the negative wind power ramp rates in  $k$ -long time intervals are larger than the sample quantile  $Q_{r_{M_k}}(1 - p)$ .

The question that arises is how well the respective step-changes sample quantile  $Q_{|y|}(p)$  ( $Q_{r_y}(p)$ ) or forward differences sample quantile  $Q_{|z|}(p)$  ( $Q_{r_z}(p)$ ) perform with respect to counteracting wind power ramp sizes (or rates). To address this question, for each time interval pair listed in Table 4.4, the following results from the comparison between the step-changes or the forward differences and the conditional range are denoted:

1. Ramp Size Difference  $dx$

This quantity is the answer to the question: For a given coverage rate  $p$  what is the difference in reserve power  $dx$  needed so that  $L \cdot Q_{|y_k|}(p) + dx = Q_{M_K}(p)$  (or  $L \cdot Q_{|z_k|}(p) + dx = Q_{M_K}(p)$ )? In other words, how much more (or less) reserves  $dx$  are needed, in addition to  $L \cdot Q_{|y_k|}(p)$  (or  $L \cdot Q_{|z_k|}(p)$ ), so as to achieve the same coverage rate  $p$  (percentage of successfully counteracted wind power ramps) as the respective conditional range reserves  $Q_{M_K}(p)$ ?

2. Ramp Rate Difference  $dr$

This quantity is the answer to the question: For a given coverage rate

$p$  what is the difference in ramp rate capability  $dr$  needed so that  $L \cdot Q_{r_{y_k}}(p) + dr = Q_{r_{M_K}}(p)$  (or  $L \cdot Q_{r_{z_k}}(p) + dr = Q_{r_{M_K}}(p)$ )? In other words, how much more (or less) ramping capability do the generators providing reserves need to have, in addition to  $L \cdot Q_{r_{y_k}}(p)$  (or  $L \cdot Q_{r_{z_k}}(p)$ ), so as to achieve the same coverage rate  $p$  (percentage of successfully counteracted wind power ramp rates) as the respective conditional range ramp rate  $Q_{r_{M_K}}(p)$ ?

### 3. Coverage Rate Difference $dp$

This quantity is the answer to the question: What is the actual coverage rate  $p + dp$  of a given step-changes quantile  $L \cdot Q_{|y_k|}(p)$  (or forward difference quantile  $L \cdot Q_{|z_k|}(p)$ ) in terms of accommodating the size of wind power ramps? That is,  $dp$  is the solution to the equation  $L \cdot Q_{|y_k|}(p) = Q_{M_K}(p + dp)$  (or  $L \cdot Q_{|z_k|}(p) = Q_{M_K}(p + dp)$ ). When using reserves equal to a step-changes quantile  $L \cdot Q_{|y_k|}(p)$  (or forward difference quantile  $L \cdot Q_{|z_k|}(p)$ ) it is assumed that they can successfully counteract  $p$  percent of the wind power ramps (nominal coverage rate) over a given time period. However, this quantile can in fact counteract  $p + dp$  percent of the wind power ramps, and thus  $dp$  represents the deviation from the nominal coverage rate  $p$ . Stated differently, a negative  $dp$  is the additional percentage of  $K$ -long time-intervals with wind power ramp sizes successfully counteracted by the conditional range quantile  $Q_{M_K}(p)$  which the absolute step-changes quantile  $L \cdot Q_{|y_k|}(p)$  (or forward differences quantile  $L \cdot Q_{|z_k|}(p)$ ) fails to counteract. Since the focus of this comparison is in assessing the size of wind power ramps, the deviation from nominal coverage rate  $dp$  is calculated only for the size and not the rate of wind power ramps. Deviations from nominal coverage rates

are of critical importance since large deviations can severely affect the system reliability.

An estimate of how large these deviations can get can be obtained by the results presented in [4], in which the 99.7<sup>th</sup> conditional range quantile is compared to the 99.7<sup>th</sup> percentile of the absolute step-changes using aggregated wind power and demand data with a 1-minute resolution spanning a period of one year. More specifically in [4], the 5-minute wind power and net demand conditional range 99.7<sup>th</sup> percentile  $Q_{M_5}(0.997)$  is compared to 1-minute absolute wind power and net demand step-changes 99.7<sup>th</sup> percentile  $Q_{|y_1|}(0.997)$ . In addition, the 60-minute wind power and net demand conditional range 99.7<sup>th</sup> percentile  $Q_{M_{60}}(0.997)$  is compared to the sum of the 1-minute and 10-minute wind power and net demand absolute step-changes 99.7<sup>th</sup> percentiles  $Q_{|y_1|}(0.997) + Q_{|y_{10}|}(0.997)$ .

The chosen time length comparison pairs are according to comparison scheme B and stem from the fact that in several wind integration studies, regulation reserves which correspond to the accommodation of net-demand variability in the 5-minute time frame are estimated using three standard deviations of the 1-minute step-changes, while load following reserves which correspond to reserves accommodating intra-hour net demand variations are estimated using three standard deviations of the 10-minute step-changes. Since a system carries both regulation and load-following reserves to account for intra-hour net demand variability, the sum of both absolute step-changes quantiles (current metrics) is compared to the respective conditional range quantile (proposed metric).

The results for the coverage rate differences  $dp_5$ , where  $Q_{|y_1|}(0.997) = Q_{M_5}(0.997 + dp_5)$ , and  $dp_{60}$ , where  $Q_{|y_1|}(0.997) + Q_{|y_{10}|}(0.997) = Q_{M_{60}}(0.997 +$

$dp_{60}$ ), for the two comparison pairs are summarized in Table 4.5. The quantiles are calculated from the respective conditional range and step-changes series, which are formed either using the whole year wind power series or some seasonal subset of it. All coverage rate differences are negative, which reveals the inability of the step-changes to effectively assess the size of wind power and net demand ramps.

From Table 4.5, it becomes evident that for wind power ramps the coverage rate differences  $dp_5$  and  $dp_{60}$  remain relatively low. This is attributed to the high rank of the nominal rate  $p$  and to the fact that the wind power time series is the aggregated output of numerous wind farms which has a diminishing effect on wind power variability. However, the 99.7<sup>th</sup> percentile of the hourly net demand conditional range can counteract net demand ramp sizes in up to 20.87% more hours in a year (or even 41.77% more hours during the summer months). In fact, when the absolute step-changes and the conditional range are compared using three times their standard deviations, as is adopted in wind integration studies, the coverage rate difference can even exceed  $-50\%$ .

A part of the net demand intra-hour ramps, as they are captured by the conditional range  $M_{60}$ , is covered through the economic dispatch operating setpoints of generators providing energy. But the rest has to be covered by generators providing load-following reserves. If these generators don't have enough ramping capabilities to accommodate for the intra-hour net demand variability the system reliability performance is heavily affected. Thus, estimating reserves using quantiles of the proposed conditional range can significantly improve the system reliability performance.

Table 4.5: Coverage Rate Difference  $dp$  for Wind Power and Net Demand

	Wind		Net Demand	
	$dp_5$	$dp_{60}$	$dp_5$	$dp_{60}$
Total	-0.38%	-1.53%	-2.32%	-20.87%
Spring	-0.14%	-1.17%	-1.70%	-15%
Summer	-0.51%	-1.28%	-3.27%	-41.77%
Fall	-0.50%	-1.61%	-2.29%	-21.66%
Winter	-0.58%	-2.15%	-2.29%	-12.38%

#### 4.3.4 Comparison Results

In this section a summary of the most important results from the comparison between the wind power conditional range and the wind power step-changes or forward differences statistics is presented.

##### 4.3.4.1 The Effect of the Wind Farm Size on Wind Power Variability across Different Time Scales

Figure 4.16 depicts the 95<sup>th</sup> percentile of the wind power conditional range  $Q_{M_k}(0.95)$ , the absolute wind power step-changes  $Q_{|y_k|}(0.95)$  and the absolute wind power forward differences  $Q_{|z_k|}(0.95)$  as a function of the wind farm size. The percentiles for each wind farm are given in p.u. values based on the wind farm nameplate capacity  $P_N$  and are depicted for various time interval lengths  $k$ . For all wind farm sizes and time interval lengths depicted the conditional range percentile exhibits a higher value than the respective forward difference percentile, which in turn exhibits a higher value than the respective step-changes percentile. As expected, the wind power forward differences can characterize wind power variability more efficiently than the wind

power step-changes, which are averages of forward differences. However, the performance of the forward differences is still inferior to that of the proposed conditional range.

From this figure it is evident that for each wind farm the values of the wind power conditional range, as well as the wind power step-changes and forward differences increase as the time interval  $k$  increases. This result is in accordance to the results depicted in Fig. 4.5. As has already been denoted, the higher wind power variability over longer time frames is attributed to the fact that over longer time frames the changes in wind power output are weather dictated and the effect of cancellations between positive and negative changes of the wind farm's turbines wind power output subsides.

Regarding the effect of the wind farm nameplate capacity on wind power variability, a higher number of wind turbines with a wider geographical spread in a large wind farm has a more pronounced effect on the variability cancellations in their output, resulting in reduced wind power variability as the wind farm size increases. Indeed, from Fig. 4.16 a trend in reduced variability with increasing wind farm nominal power can be seen. However, the relationship between the conditional range  $M_k$  or the step-changes  $y_k$  or the forward differences  $z_k$  and the wind farm nameplate capacity  $P_N$  is not strictly linear, since wind power variability is affected by numerous factors including the exact number and type of wind turbines and their location.

Nonetheless, using linear fittings ( $Q = a \cdot P_N + b$ ) for the depicted percentiles of  $M_k$ ,  $y_k$  and  $z_k$  for each time length  $k$  the resulting slopes  $a$  are negative, which indicates a reduction in wind power variability for increasing wind farm size over all time frames. In fact the slope  $a$  decreases (in absolute numbers) as the time interval length  $k$  increases, demonstrating that this trend is less pronounced in longer time frames. Moreover, comparing the linear fit-

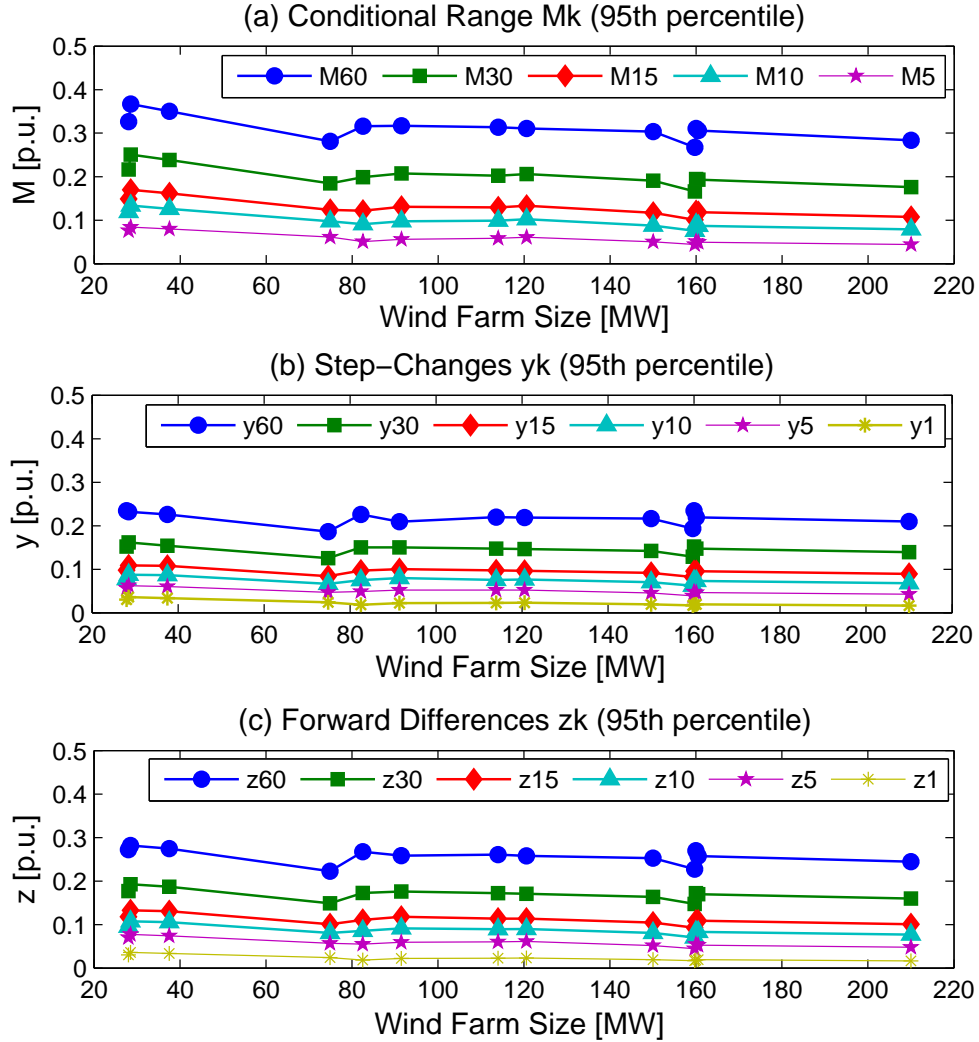


Figure 4.16: The 95<sup>th</sup> percentile of (a) the conditional range  $M_k$ , (b) the step-changes  $y_k$ , and (c) the forward differences  $z_k$  in p.u. values as a function of the wind farm nameplate capacity  $P_N$  for various time intervals lengths  $k$ . The size of the conditional range as well as the step-changes and the forward differences grows with increasing time intervals  $k$  and decreasing nameplate capacities  $P_N$  of the wind farms. The conditional range exhibits higher values than the forward differences and the step-changes for all  $k$  and  $P_N$ .



tings it is found that the slope of the  $M_k$  percentiles fitting has higher values than the slope of the  $y_k$  or  $z_k$  percentiles fitting, revealing that the proposed metric can capture the cancellation effects from geographical wind power averaging in large wind farms more efficiently.

Figure 4.17 and Fig. 4.18 depict the 95<sup>th</sup> and 5<sup>th</sup> percentile of the conditional range ramp rates  $Q_{r_{M_k}}(0.95)$ , the step-changes ramp rates  $Q_{r_{y_k}}(0.95)$ , and the forward differences ramp rates  $Q_{r_{M_k}}(0.95)$  as a function of the wind farm size  $P_N$  for various time interval lengths  $k$ , respectively. Thus, only 5% of the ramp rates in the given year have positive values higher than the rates depicted in Fig. 4.17 and negative values lower than the rates depicted in Fig. 4.18. In both these figures the conditional range ramp rates are higher (in absolute values) than the respective time frame step-changes and forward differences ramp rates, which shows the inability of the latter to effectively capture wind power ramp rates. Moreover, positive and negative ramp rate values appear fairly symmetric around zero. For all wind farm sizes and time interval lengths depicted the ramp rates decrease in absolute values with increasing wind farm size. As has been noted, the size of the wind power ramps increases with increasing time interval length  $k$ , however, the ramp rates decrease in absolute values with increasing  $k$ . This means that high ramp rates which appear in smaller time intervals don't have a large enough duration to produce high ramp rates over longer time intervals.

#### 4.3.4.2 Wind Power Variability as a Function of the Wind Power Production Level

To study the effect of the production level the conditional range series as well as the step-changes and forward differences series are first filtered by the interval average production level  $\bar{x}_{k,i} = l_j$  to create separate series for each

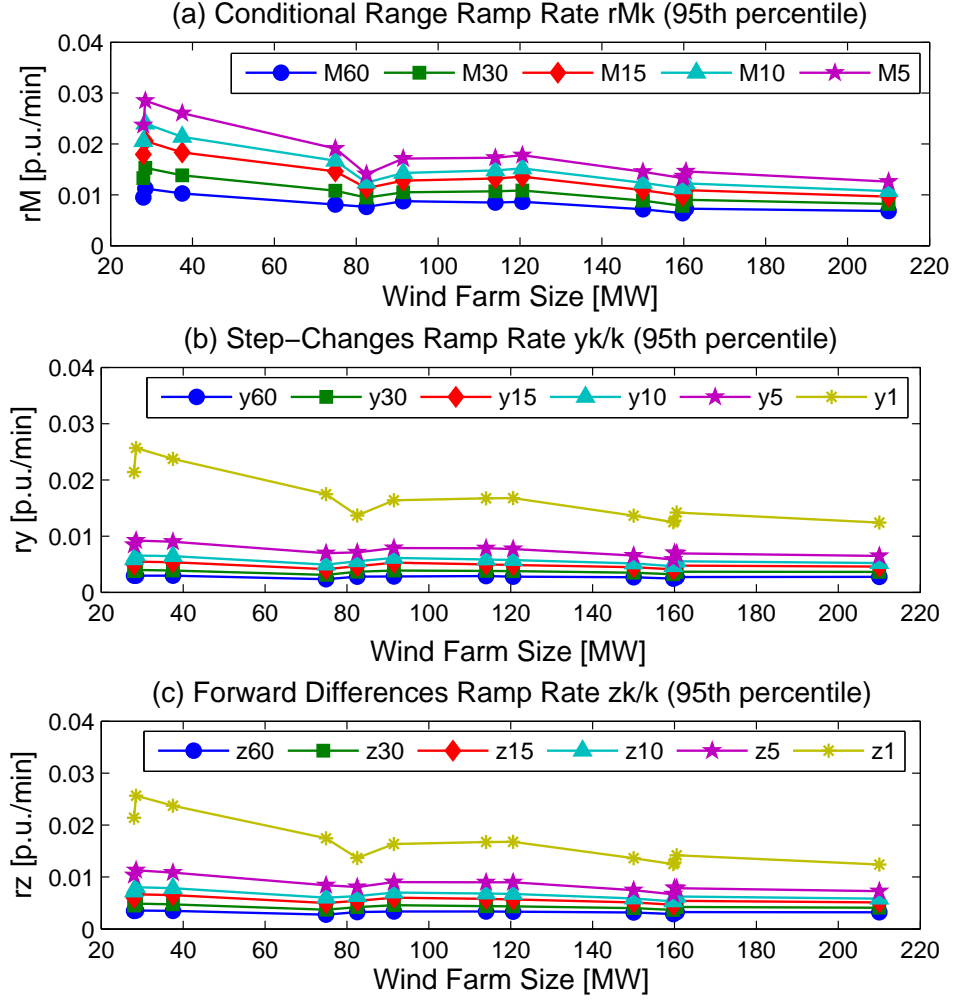


Figure 4.17: The 95<sup>th</sup> percentile of (a) the conditional range ramp rate  $r_{M_k}$ , (b) the step-changes ramp rate  $r_{y_k}$ , and (c) the forward differences ramp rate  $r_{z_k}$  in p.u./min values as a function of the wind farm nameplate capacity  $P_N$  for various time intervals lengths  $k$ . The ramp rates of the conditional range as well as the step-changes and the forward differences grow with decreasing time intervals  $k$  and decreasing nameplate capacities  $P_N$  of the wind farms. The conditional range exhibits higher ramp rates than the forward differences and the step-changes for all  $k$  and  $P_N$ .

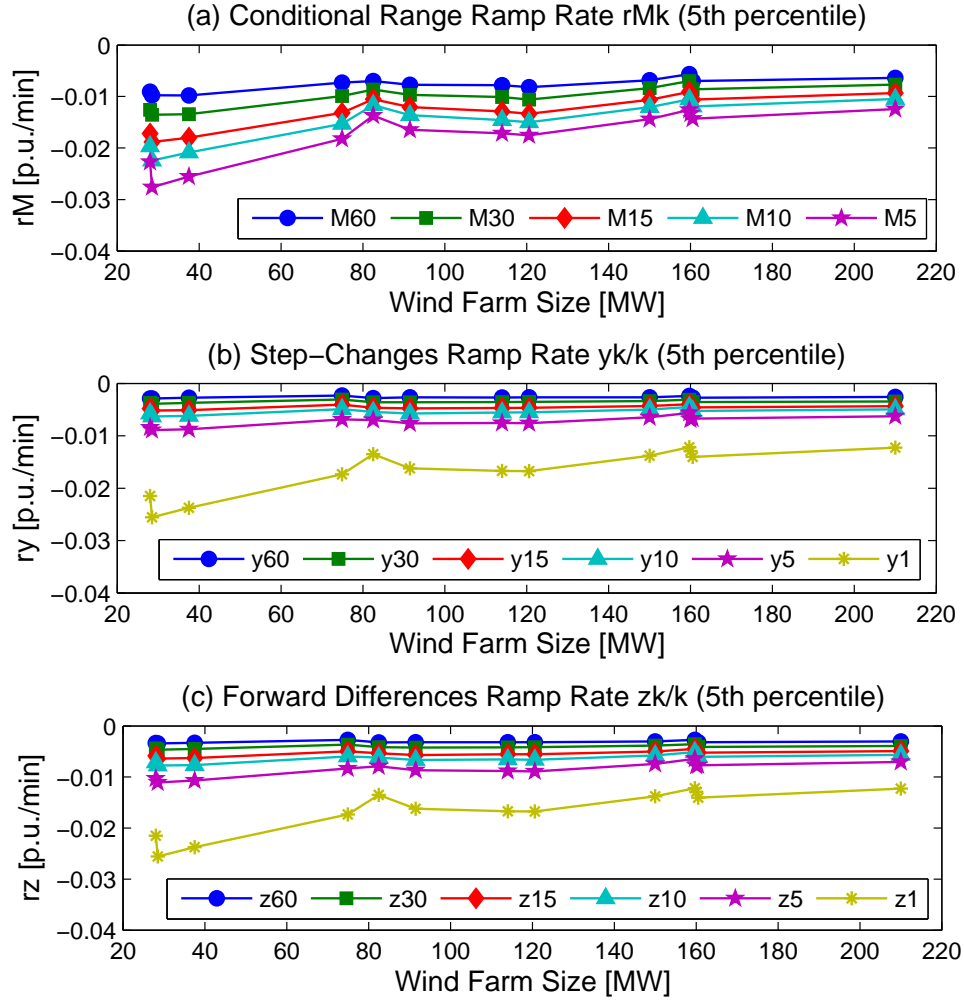


Figure 4.18: The 5<sup>th</sup> percentile of (a) the conditional range ramp rate  $r_{M_k}$ , (b) the step-changes ramp rate  $r_{y_k}$ , and (c) the forward differences ramp rate  $r_{z_k}$  in p.u./min values as a function of the wind farm nameplate capacity  $P_N$  for various time intervals lengths  $k$ . The ramp rates of the conditional range as well as the step-changes and the forward differences grow (in absolute values) with decreasing time intervals  $k$  and decreasing nameplate capacities  $P_N$  of the wind farms. The conditional range exhibits higher ramp rates than the forward differences and the step-changes for all  $k$  and  $P_N$ .

production level  $l_j$ . In fact separate series are created for average wind power production level intervals  $\bar{x}_n \in l_j = j/m$  if  $(2j - 1)/2m < \bar{x}_n \leq (2j + 1)/2m$ , which are normalized based on the wind farm nameplate capacity  $P_N$  ( $l_j = 0.01, 0.02, \dots, 1$  p.u.). Thus, for the  $l_j$ -production level conditional range and forward differences series only those indexes  $i_{pl_j} \in [1, N - k]$  from the initial series are used for which  $l_j - 0.005 < \bar{x}_{k, i_{pl_j}} \leq l_j + 0.005$ . The filtered samples form new series,  $M_{k, i_{pl_j}}$  and  $z_{k, i_{pl_j}}$ , and the quantiles of these modified series are calculated using (4.17). The same indexes are used to obtain the filtered conditional range ramp rate series  $r_{M_{k, pl_j}}$  and forward differences ramp rate series  $r_{z_{k, pl_j}}$ . Similarly, for the  $l_j$ -production level step-changes series indexes  $j_{pl_j} \in [1, \lfloor N/k \rfloor - 1]$  are chosen for which  $l_j - 0.005 < \bar{x}_{k, j_{pl_j}} \leq l_j + 0.005$ , to create the filtered step-changes series  $y_{k, j_{pl_j}}$  and step-changes ramp rate series  $r_{y_{k, pl_j}}$ .

Figure 4.19 depicts the 95<sup>th</sup> percentile of the wind power conditional range  $Q_{M_{30}}(0.95)$ , the wind power absolute step-changes  $Q_{|y_{30}|}(0.95)$  and the wind power absolute forward differences  $Q_{|z_{30}|}(0.95)$  at the  $k = 30$ -minute time frame as a function of the wind farm nameplate capacity  $P_N$  for three interval average production levels: low ( $l_j = 0.2$  p.u.), medium ( $l_j = 0.5$  p.u.), and high ( $l_j = 0.8$  p.u.). Similarly, Fig. 4.20 depicts the 95<sup>th</sup> and Fig. 4.21 the 5<sup>th</sup> percentile of the three respective ramp rate series. From Fig. 4.19 - Fig. 4.21 it is evident that wind power variability produces wind power ramps with larger sizes and absolute ramp rates at mid-level wind power production under all three considered wind power variability metrics. As has already been stated, this is due to the large slope of the wind power vs. wind speed curve at mid-production levels, which causes even a small change in the input wind speed to have a large effect on the wind power output.

Since only a 5% of ramp rates have values lower than  $Q_{r_{M_k}}(0.05)$  and

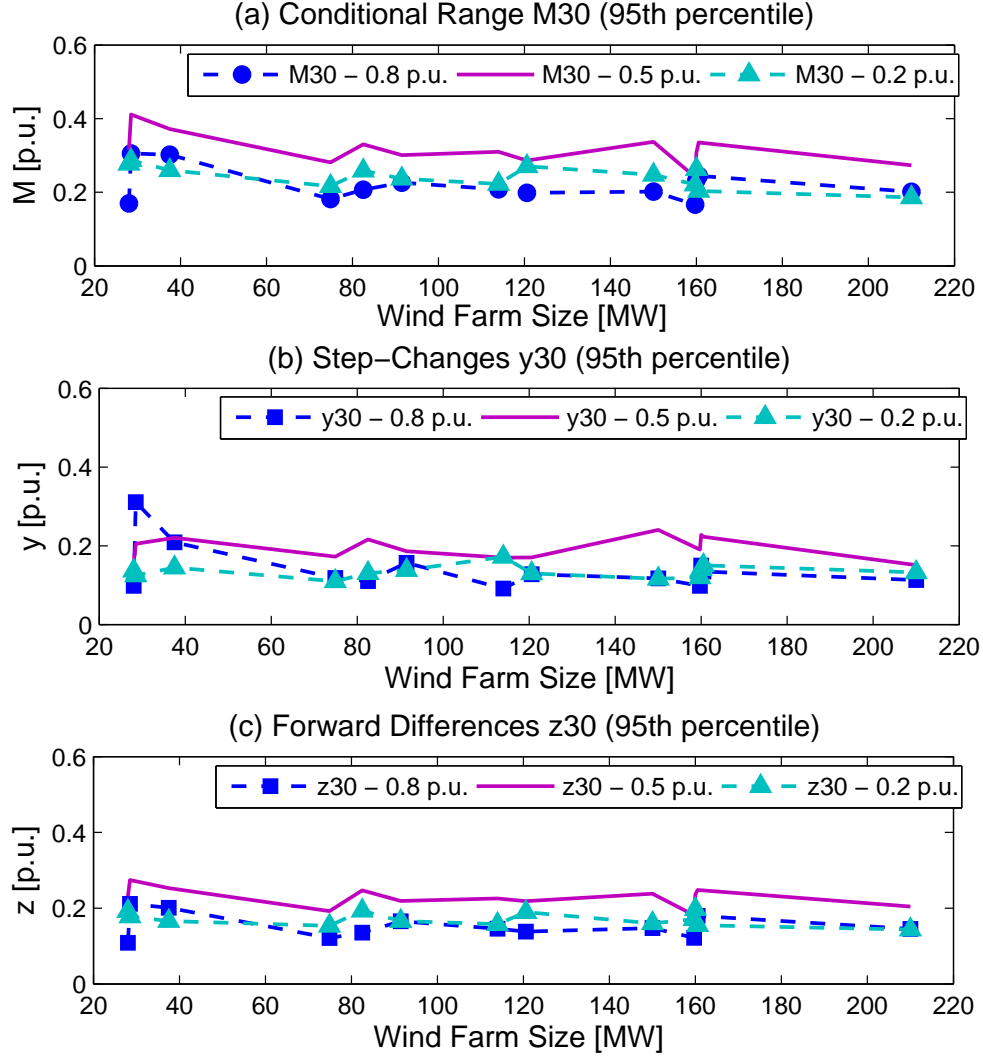


Figure 4.19: The 95<sup>th</sup> percentile of (a) the conditional range  $M_k$ , (b) the step-changes  $y_k$ , and (c) the forward differences  $z_k$  in p.u. values taken over time intervals of length 30 minutes and three different average interval production levels (low=0.2 p.u., medium=0.5 p.u., high=0.8 p.u.), as a function of the wind farm nameplate capacity  $P_N$ . Wind power ramp sizes are larger at mid-level wind power production.

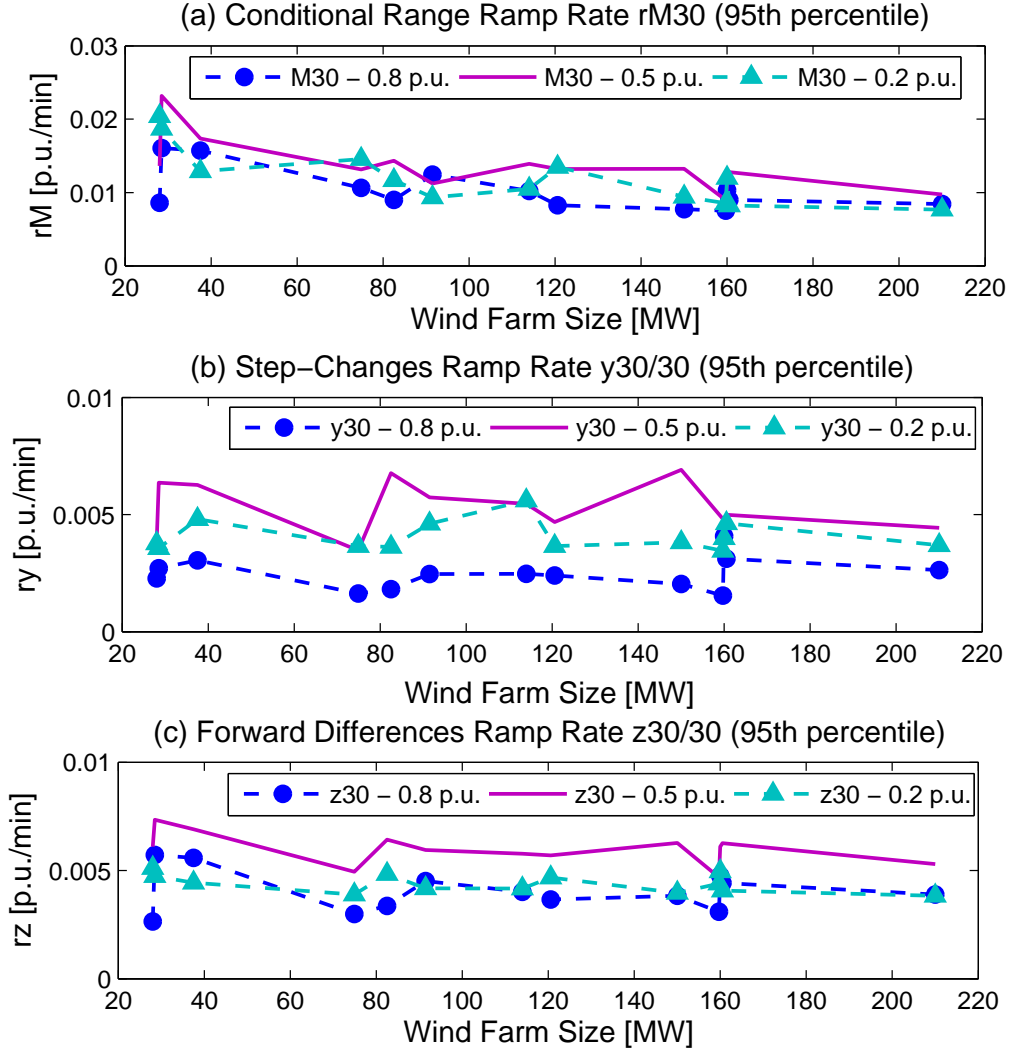


Figure 4.20: The 95<sup>th</sup> percentile of (a) the conditional range ramp rate  $r_{M_k}$ , (b) the step-changes ramp rate  $r_{y_k}$ , and (c) the forward differences ramp rate  $r_{z_k}$  in p.u./min values taken over time intervals of length 30 minutes and three different average interval production levels (low=0.2 p.u., medium=0.5 p.u., high=0.8 p.u.), as a function of the wind farm nameplate capacity  $P_N$ . Wind power ramp rates are larger at mid-level wind power production.

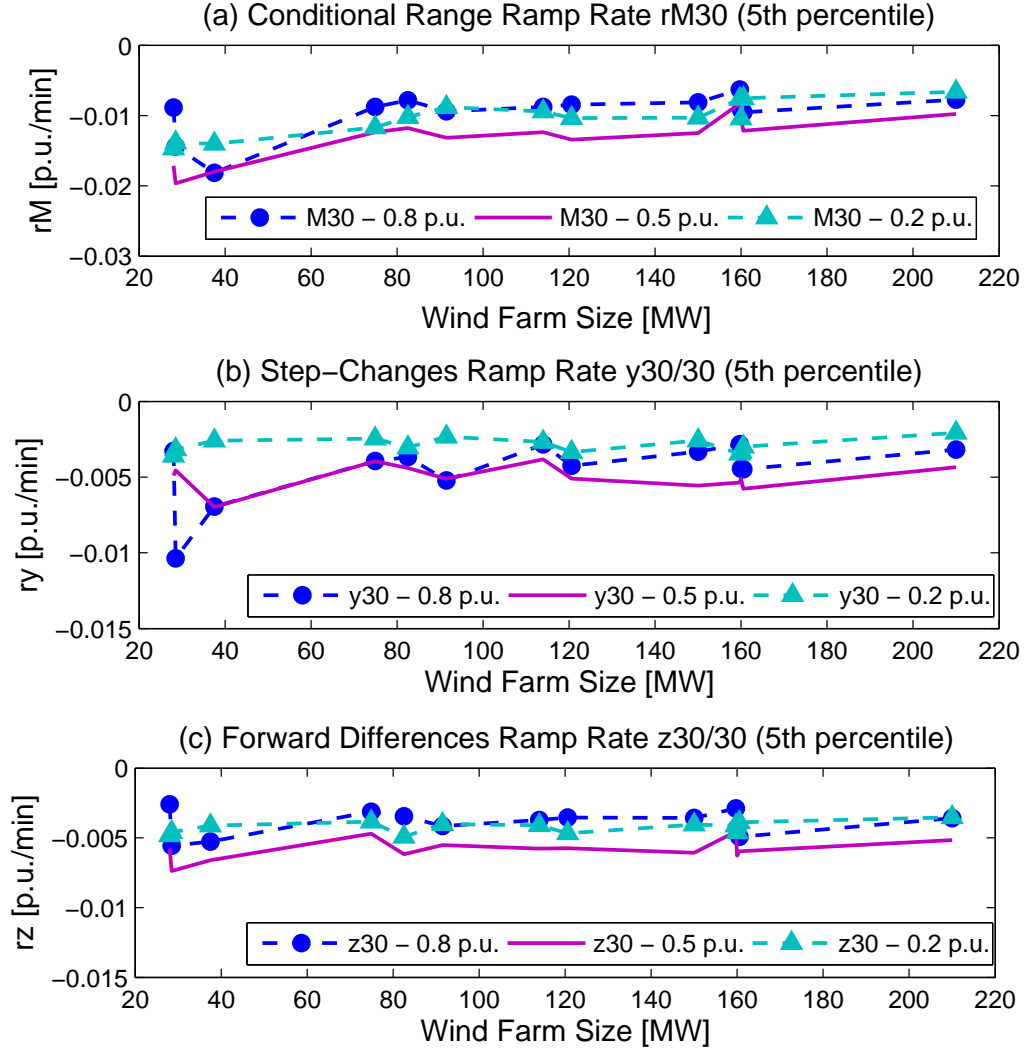


Figure 4.21: The 5<sup>th</sup> percentile of (a) the conditional range ramp rate  $r_{M_k}$ , (b) the step-changes ramp rate  $r_{y_k}$ , and (c) the forward differences ramp rate  $r_{z_k}$  in p.u./min values taken over time intervals of length 30 minutes and three different average interval production levels (low=0.2 p.u., medium=0.5 p.u., high=0.8 p.u.), as a function of the wind farm nameplate capacity  $P_N$ . Wind power ramp rates are larger at mid-level wind power production.

another 5% have ramp rate values higher than  $Q_{r_{M_k}}(0.95)$ , 90% of all ramp rates fall within the interval  $[Q_{r_{M_k}}(0.05), Q_{r_{M_k}}(0.95)]$  under the conditional range ramp rate series. Similarly, 90% of all ramp rates fall within the interval  $[Q_{r_{y_k}}(0.05), Q_{r_{y_k}}(0.95)]$  and  $[Q_{r_{z_k}}(0.05), Q_{r_{z_k}}(0.95)]$  under the step-changes and forward differences ramp rate series, respectively. The ramp rate intervals with 90% coverage probability defined previously are given in Table 4.6 for  $k = 5$ -minute time intervals and in Table 4.7 for  $k = 60$ -minute time intervals for all considered wind farms under the three ramp rate series. The values in these tables are weighted averages of the respective quantiles for all production levels  $l_j$ . For example, the given  $Q_{r_{M_5}}$  is calculated from  $[w_{l_j} \cdot Q_{r_{M_5,pl_j}}(0.05), w_{l_j} \cdot Q_{r_{M_5,pl_j}}(0.95)]$ , where the weight  $w_{l_j}$  is the probability that the 5-minute time interval has average wind power production  $l_j$ , i.e.  $w_{l_j} = P(\bar{x}_{5,j} \in l_j)$ . The respective quantiles are also calculated using a wind power series formed by the aggregated output of the 13 wind farms, denoted 'sumWF', as well as the average quantile values of the 13 wind farms, denoted 'avgWF'.

From Table 4.6 and Table 4.7 it becomes evident, that when the ramp rates are estimated based on the step-changes and forward differences they are significantly lower than the actual ramp rates over the respective time intervals. Moreover, under all ramp rate series, the positive ramp rates are larger than the negative ramp rates, which means that wind ramps up faster than it ramps down. The higher ramp rates of the 5-minute intervals compared to the ramp rates within hourly time frames, denote that high ramp rates over small time frames don't have large durations. In addition, aggregation of wind power output reduces not only the wind power ramp sizes but also the wind power ramp rates, as can be seen by the large difference between the aggregated (sumWF) and average (avgWF) quantiles.



Table 4.6: Ramp Rate Intervals with Coverage Probability 90% for 5-minute Time Intervals

Wind Farm	$Q_{r_{y_5}}$ [p.u./min]	$Q_{r_{z_5}}$ [p.u./min]	$Q_{r_{M_5}}$ [p.u./min]
WF1	[-0.0078,0.0081]	[-0.0097,0.0099]	[-0.0215,0.0225]
WF2	[-0.0061,0.0063]	[-0.007,0.0071]	[-0.012,0.0124]
WF3	[-0.007,0.0073]	[-0.0083,0.0084]	[-0.0162,0.0166]
WF4	[-0.0083,0.0081]	[-0.0102,0.0102]	[-0.0224,0.0233]
WF5	[-0.008,0.0084]	[-0.01,0.0103]	[-0.0238,0.0248]
WF6	[-0.0063,0.0066]	[-0.0073,0.0074]	[-0.0133,0.0136]
WF7	[-0.0059,0.0061]	[-0.0067,0.0069]	[-0.0115,0.0118]
WF11	[-0.0061,0.0063]	[-0.0069,0.0072]	[-0.0117,0.0122]
WF13	[-0.0064,0.0067]	[-0.0079,0.0081]	[-0.0171,0.018]
WF14	[-0.0078,0.0079]	[-0.0096,0.0097]	[-0.0226,0.0233]
WF15	[-0.0071,0.0075]	[-0.0083,0.0086]	[-0.0157,0.0164]
WF17	[-0.0058,0.0059]	[-0.0067,0.0068]	[-0.0127,0.013]
WF18	[-0.005,0.0053]	[-0.0058,0.0061]	[-0.0113,0.012]
sumWF	[-0.0002,0.0002]	[-0.0003,0.0003]	[-0.0053,0.0054]
avgWF	[-0.0067,0.007]	[-0.008,0.0082]	[-0.0163,0.0169]

Table 4.7: Ramp Rate Intervals with Coverage Probability 90% for 60-minute Time Intervals

Wind Farm	$Q_{r_{y60}}$ [p.u./min]	$Q_{r_{z60}}$ [p.u./min]	$Q_{r_{M60}}$ [p.u./min]
WF1	[-0.0025,0.0028]	[-0.003,0.0032]	[-0.0086,0.0089]
WF2	[-0.0025,0.0028]	[-0.0029,0.003]	[-0.0062,0.0068]
WF3	[-0.0024,0.0026]	[-0.0029,0.0031]	[-0.0079,0.0082]
WF4	[-0.0025,0.0027]	[-0.003,0.0033]	[-0.0074,0.0107]
WF5	[-0.0024,0.0027]	[-0.0031,0.0032]	[-0.0087,0.0102]
WF6	[-0.0024,0.0026]	[-0.0029,0.003]	[-0.0065,0.0068]
WF7	[-0.0024,0.0027]	[-0.0028,0.003]	[-0.0059,0.0064]
WF11	[-0.0023,0.0025]	[-0.0028,0.0028]	[-0.006,0.0068]
WF13	[-0.0021,0.0022]	[-0.0026,0.0026]	[-0.0068,0.0076]
WF14	[-0.0023,0.0026]	[-0.0029,0.003]	[-0.0087,0.0091]
WF15	[-0.0024,0.0027]	[-0.003,0.0031]	[-0.0071,0.0085]
WF17	[-0.0023,0.0025]	[-0.0026,0.0028]	[-0.006,0.0063]
WF18	[-0.002,0.0023]	[-0.0025,0.0026]	[-0.005,0.0058]
sumWF	[-0.0014,0.0015]	[-0.0016,0.0017]	[-0.0027,0.0029]
avgWF	[-0.0023,0.0026]	[-0.0028,0.003]	[-0.007,0.0079]

#### 4.3.4.3 Comparison Results as a Function of the Coverage Rate

Figure 4.22 depicts the comparison outcomes when the 5-minute wind power conditional range  $M_5$  and its respective ramp rate series  $r_{M_5}$  of one wind farm of capacity  $P_N=160.5$  MW (WF6) are compared to the step-changes, as a function of the conditional range coverage rate  $p \in [0, 1]$  (percentage of successfully counteracted wind power ramp sizes or ramp rates). The comparison results depicted are the ramp size difference  $dx$  in p.u. (Fig. 4.22(a)), the ramp rate difference  $dr$  in p.u./min (Fig. 4.22(b)) and the coverage rate difference  $dp$  in % (Fig. 4.22(c)), as they have been defined in Section 4.3.3. In each sub-figure of Fig. 4.22, the solid line represents results under comparison scheme A, the dashed line results under comparison scheme B and the dotted line results under comparison scheme C. For the 5-minute time frame the ramp size difference  $dx$  and coverage rate difference  $dp$  are obtained by comparing the quantiles of  $M_5$  to  $|y_5|$  under scheme A,  $M_5$  to  $|y_1|$  under scheme B, and  $M_5$  to  $5 \cdot |y_1|$  under scheme C. To obtain the ramp rate difference  $dr$  the comparison is done between the quantiles of the ramp rates  $r_{M_5}$  to  $r_{y_5}$  under scheme A,  $r_{M_5}$  to  $r_{y_1}$  under scheme B, and  $r_{M_5}$  to  $5 \cdot r_{y_1}$  under scheme C. Similarly, Fig. 4.23 depicts the comparison outcomes when the conditional range  $M$  is compared to the respective forward differences  $z$  for the 5-minute time frame.

For the 5-minute time frame, e.g. the time frame for which regulation reserves are calculated, let's assume that the necessary reserves to counteract undesired wind power ramps are set equal to  $Q_{M_5}(p)$  p.u. and that the generators providing such reserves should have a ramping capability of  $Q_{r_{M_5}}(p)$  p.u./min. Then, Fig. 4.22(a) and Fig. 4.23(a) depict the reserves  $dx$  needed, in addition to  $L \cdot Q_{|y_k|}(p)$  or  $L \cdot Q_{|z_k|}(p)$ , so as to achieve the same coverage rate as the conditional range quantile  $Q_{M_5}(p)$ , as a function of the conditional

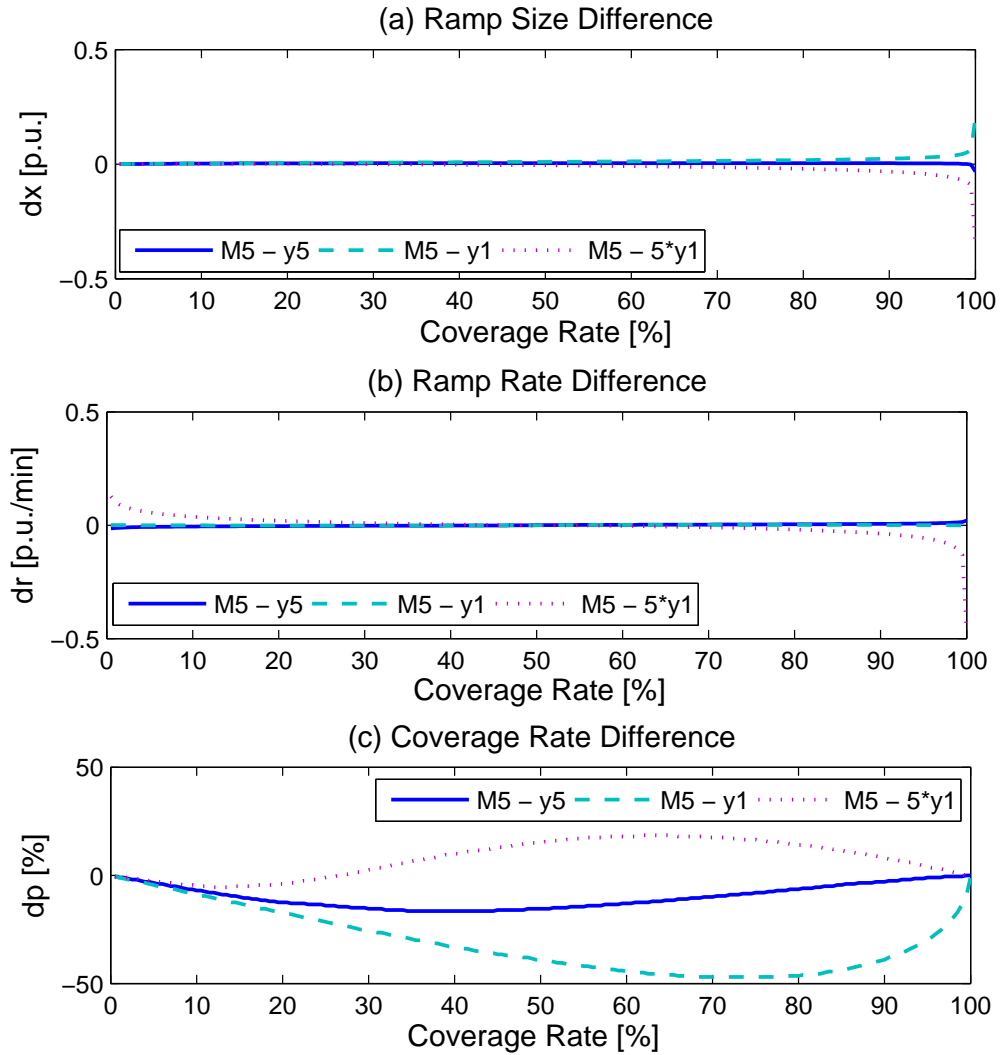


Figure 4.22: Comparison results for (a) ramp size difference  $dx$ , (b) ramp rate difference  $dr$ , and (c) coverage rate difference  $dp$  between the conditional range  $M$  and the step-changes  $y$  for the 5-minute time frame under the three comparison schemes as a function of the coverage rate  $p$ . The solid line represents comparison scheme A, the dashed line scheme B and the dotted line scheme C.

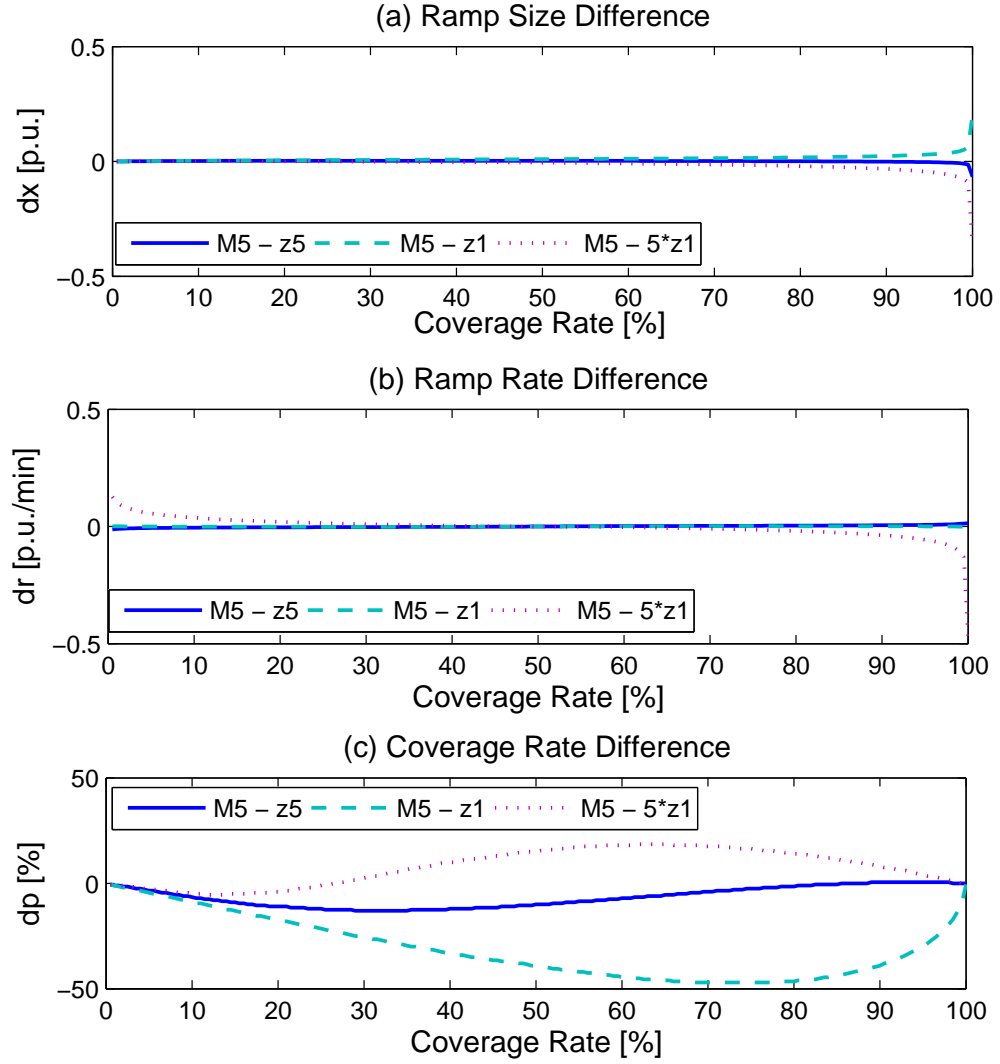


Figure 4.23: Comparison results for (a) ramp size difference  $dx$ , (b) ramp rate difference  $dr$ , and (c) coverage rate difference  $dp$  between the conditional range  $M$  and the forward differences  $z$  for the 5-minute time frame under the three comparison schemes as a function of the coverage rate  $p$ . The solid line represents comparison scheme A, the dashed line scheme B and the dotted line scheme C.

range coverage rate  $p$  given in the x-axis. The results from this comparison reveal that the absolute step-changes  $|y_1|$ , which equal the forward differences  $|z_1|$ , are inadequate to assess the size of wind power ramps over longer time intervals  $K = 5$  minutes (comparison scheme B - dashed line), since more reserves are needed to achieve the conditional range coverage rate. On the other hand, taking an exact multiplier ( $L = 5$ ) of the absolute step-changes  $|y_1|$  (comparison scheme C - dotted line) overestimates the size of the wind power ramps resulting in an overdeployment of reserves. This effect is more pronounced at high coverage rates where the ramp size difference  $dx$  can exceed absolute values of 0.2 p.u. of the wind farm nameplate capacity. Under comparison scheme A the smallest differences in ramp size are observed, which implies that using the absolute step-changes  $|y_5|$  and forward differences  $|z_5|$  quantiles to assess the size of wind power ramps in the same length 5-minute time frame results in the least error (number of not counteracted wind power ramps).

The results regarding the difference in ramping rate capabilities  $dr$  are given in Fig. 4.22(b) and Fig. 4.23(b). In these figures the ramp rates  $dr$  needed, in addition to  $L \cdot Q_{r_{y_k}}(p)$  or  $L \cdot Q_{r_{z_k}}(p)$ , so as to achieve the same coverage rate as the conditional range ramp rate quantile  $Q_{r_{M_5}}(p)$ , as a function of the conditional range ramp rate coverage probability  $p$  given in the x-axis are depicted. Under comparison scheme A, where the conditional range ramp rate  $r_{M_5}$  is compared to step-changes ramp rate  $r_{y_1}$  and the forward differences ramp rate  $r_{z_1}$ , as well as under comparison scheme B, where  $r_{M_5}$  is compared to  $r_{y_1} = r_{z_1}$ , the least differences in ramp rate capabilities are observed. However, under comparison scheme C, where the conditional range ramp rate  $r_{M_5}$  is compared to the exact multiple  $5 \cdot r_{y_1} = 5 \cdot r_{z_1}$ , positive differences  $dr$  are observed for low coverage rates and negative differences for high coverage rates  $p$ .

This means that taking exact multiples of ramp rates over smaller time frames to assess ramp rates over larger time frames results in an overestimation of the actual ramp rates, especially for high positive ramp rates, since  $dr$  is negative for high coverage rates  $p$ , and high negative ramp rates, since  $dr$  is positive for low coverage rates  $p$ .

In Fig. 4.22(c) and Fig. 4.23(c) the y-axis depicts the difference  $dp$  between the conditional range coverage rate  $p$  (nominal), given in the x-axis, and the actual step-changes or forward differences coverage rate  $p + dp$ . In these figures a negative deviation for some coverage rate  $p$  indicates that the step-changes or forward differences  $p^{th}$  quantile has much lower value than the respective conditional range  $p^{th}$  quantile. This means that assigning reserves based on a step-changes or forward differences  $p^{th}$  quantile results in an actual coverage rate of value lower than  $p$ . On the contrary, a positive deviation means that a much higher coverage rate than desired is actually achieved. From Fig. 4.22(c) and Fig. 4.23(c) it is evident that step-changes or forward differences taken over 1-minute intervals result in much lower coverage rates with respect to counteracting wind power ramp sizes in the larger 5-minute time frames (comparison scheme B), with differences reaching values of 50% (e.g. a  $p=0.75$  step-changes quantile can actually counteract only 25% of the wind power ramp sizes within the year). When the absolute step-changes  $|y_5|$  and forward differences  $|z_5|$  quantiles are compared to the same time frame  $M_5$  conditional range quantiles (comparison scheme A) the deviation from the nominal coverage rate has much lower values. This is true especially at higher coverage rates, since negative deviations are observed for low  $p$  values (at the order of 10 – 20%), with the forward differences exhibiting smaller deviations than the step-changes. Taking exact multipliers of the absolute step-changes  $|y_1|$ , which are equal to the forward differences  $|z_1|$ , to estimate the size of

wind power ramps over the longer 5-minute time frame (comparison scheme C) shows that  $5 \cdot |y_1|$  step-changes exhibit lower than the desired coverage rates at low  $p$  values and much higher than the desired coverage rates at high  $p$  values, with differences reaching 20%.

The same comparison results for the 60-minute time frame are given in Fig. 4.24 for the step-changes and Fig. 4.25 for the forward differences, as a function of the conditional range coverage rate  $p$ . Thus, in these figures step-changes and forward differences quantiles are compared to the conditional range quantiles  $Q_{M_{60}}(p)$  and  $Q_{r_{M_{60}}}(p)$ . The ramp size difference  $dx$  in p.u. is depicted in Fig. 4.24(a) and Fig. 4.25(a), the ramp rate difference  $dr$  in p.u./min is depicted in Fig. 4.24(b) and Fig. 4.25(b), and the coverage rate difference  $dp$  in % is depicted in Fig. 4.24(c) and Fig. 4.25(c). In each subfigure of Fig. 4.24 and Fig. 4.25, the solid line represents results under comparison scheme A, the dashed line results under comparison scheme B and the dotted line results under comparison scheme C.

Under comparison scheme B the conditional range  $M_{60}$  values (or ramp rates  $r_{M_{60}}$ ) are compared against the step-changes  $|y_{10}|$  (or  $r_{y_{10}}$ ) and the forward differences  $|z_{10}|$  (or  $r_{z_{10}}$ ) taken over the smaller 10-minute time frame. The dashed lines in Fig. 4.24 and Fig. 4.25 indicate that using step-changes and forward differences over a time frame to assess the size and rate of wind power ramps over longer time frames results in an underestimation of both size and rate of wind power ramps, with differences in coverage rates reaching 70%. On the other hand, under comparison scheme C, the conditional range  $M_{60}$  values (or ramp rates  $r_{M_{60}}$ ) are compared against exact multiples of the step-changes  $6 \cdot |y_{10}|$  (or  $6 \cdot r_{y_{10}}$ ) and the forward differences  $6 \cdot |z_{10}|$  (or  $6 \cdot r_{z_{10}}$ ) taken over the smaller 10-minute time frame. However, this approach results in an overestimation of the size and rate of wind power ramps, which results in



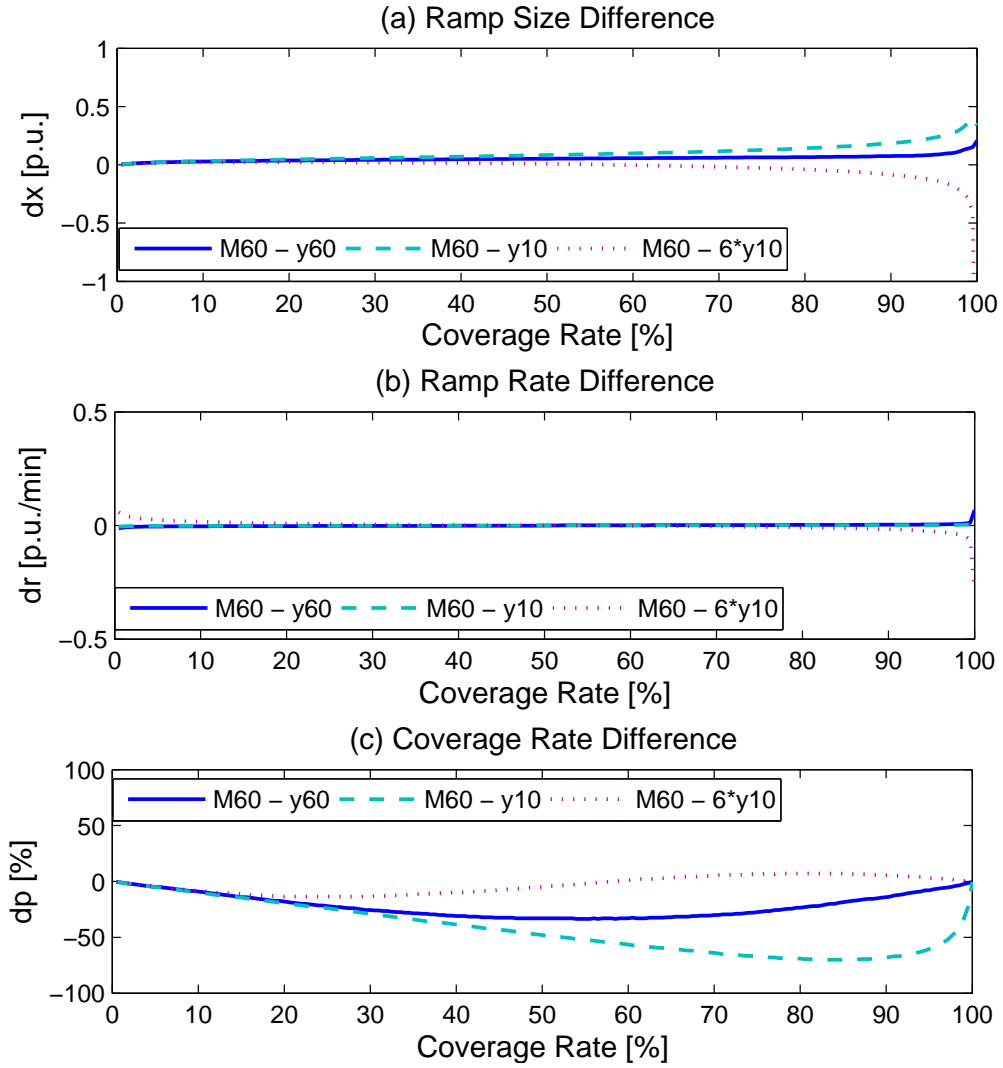


Figure 4.24: Comparison results for (a) ramp size difference  $dx$ , (b) ramp rate difference  $dr$ , and (c) coverage rate difference  $dp$  between the conditional range  $M$  and the step-changes  $y$  for the 60-minute time frame under the three comparison schemes as a function of the coverage rate  $p$ . The solid line represents comparison scheme A, the dashed line scheme B and the dotted line scheme C.

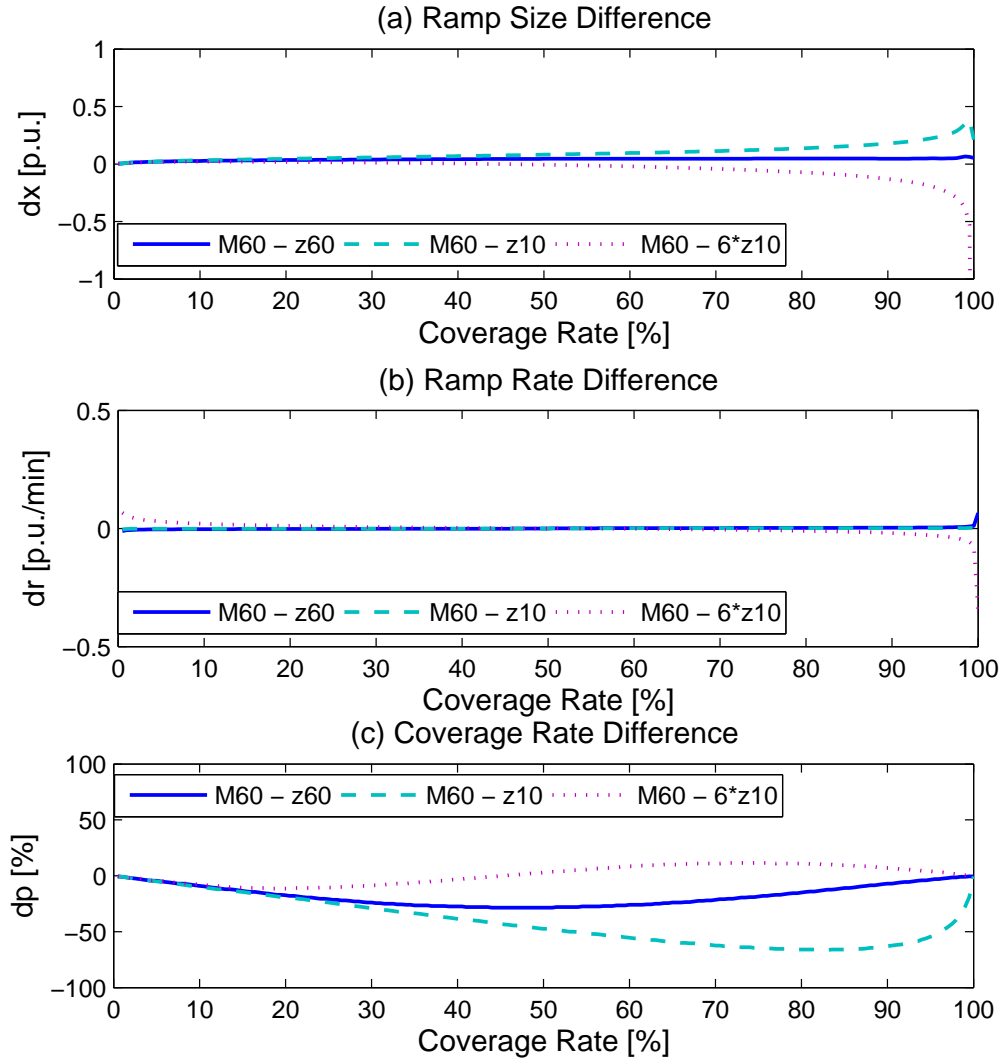


Figure 4.25: Comparison results for (a) ramp size difference  $dx$ , (b) ramp rate difference  $dr$ , and (c) coverage rate difference  $dp$  between between the conditional range  $M$  and the forward differences  $z$  for the 60-minute time frame under the three comparison schemes as a function of the coverage rate  $p$ . The solid line represents comparison scheme A, the dashed line scheme B and the dotted line scheme C.

positive coverage rate differences  $dp$  of values close to 10%. Under comparison scheme A, where the step-changes  $y_{60}$  and forward differences  $z_{60}$  (absolute values or ramp rates) are compared to the same time frame  $M_{60}$  conditional range or ramp rate values, the differences in ramp size  $dx$ , ramp rate  $dr$  and coverage rate  $dp$  exhibit the smallest values, with forward differences performing better than the step-changes. Nonetheless, the positive  $dx$  differences for high  $p$  values and the coverage rate differences reaching values of 30% reveal, that the proposed conditional range is a more effective mean in assessing the size and rate of intra-hour wind power ramps.

#### 4.3.4.4 Average Comparison Results under all Comparison Schemes

Since ramp rates differences  $dr$  depicted in Fig. 4.22 - Fig. 4.25 exhibit small values under all comparison schemes, focus is placed on ramp size differences  $dx$  and coverage rate differences  $dp$ . Figure 4.26 depicts mean ramp size differences under all comparison schemes, as a function of the time interval length  $k$ , for five different wind farms with nameplate capacities ranging from 37.5 MW to 210 MW. In every subfigure the x-value of each marker shows the time interval length  $K$ , for which the conditional range is calculated, and the y-value shows the mean  $dx$ , averaged over all coverage rates  $p$ , for each comparison scheme. In Fig. 4.26(a)-(c) the mean ramp size difference  $dx$  is given for comparison pair 1, i.e. when the conditional range quantiles  $Q_{M_K}(p)$  are compared to the absolute step-changes quantiles  $L \cdot Q_{|y_k|}(p)$ , under comparison schemes A, B, and C, respectively. Similarly, in Fig. 4.26(d)-(f) the mean ramp size difference is depicted for comparison pair 2, i.e. when the conditional range quantiles  $Q_{M_K}(p)$  are compared to the absolute forward differences quantiles  $L \cdot Q_{|z_k|}(p)$ . When several  $k$  values are used for a single  $K$  value,

e.g. 30-minute conditional range quantiles are compared against 10-minute and 15-minute step-changes under comparison scheme B, the depicted value is the average of all  $K - k$  pair differences  $dx$ . Mean coverage rate differences  $dp$  are depicted in Fig. 4.27, as a function of the time interval length  $k$ , for the same five wind farms used in Fig. 4.26. Figures 4.27(a)-(c) give the mean coverage rate difference  $dp$  for comparison pair 1 under comparison schemes A, B, and C, respectively, whereas Fig. 4.27(d)-(f) gives the mean coverage rate difference for comparison pair 2 under the three comparison schemes.

Figure 4.26 reveals that for comparison schemes A (subfigures (a) and (d)) and B (subfigures (b) and (e)), the mean ramp size difference  $dp$  is positive, indicating an underestimation of wind power ramp sizes, and increases with increasing time interval length  $K$  and decreasing wind farm size  $P_N$ . However for comparison scheme C, depicted in Fig. 4.26(c) and (e), which exhibits much lower mean ramp size differences than the other schemes, the least ramp size difference appears at the 15-minute time frame when the step-changes are used and at the 10-minute time frame when the forward differences are used, indicating a non-linear relationship between time interval length  $K$  and the ramp size difference  $dp$ . Moreover, under comparison scheme C, step-changes underestimate the size of wind power ramps (except for the 5-minute time frame), whereas forward differences overestimate the size of wind power ramps. The inconsistent results under comparison scheme C indicate that the duration of wind power ramp rates is different across different time scales and thus is not easy to estimate. Hence, just by looking at the wind power step-changes or forward differences and without an accurate estimation of the wind power ramp rate duration a reasonable assessment of the size of wind power ramps is not guaranteed. On the contrary, the proposed conditional range metric is by its definition the size of the largest wind power ramp in

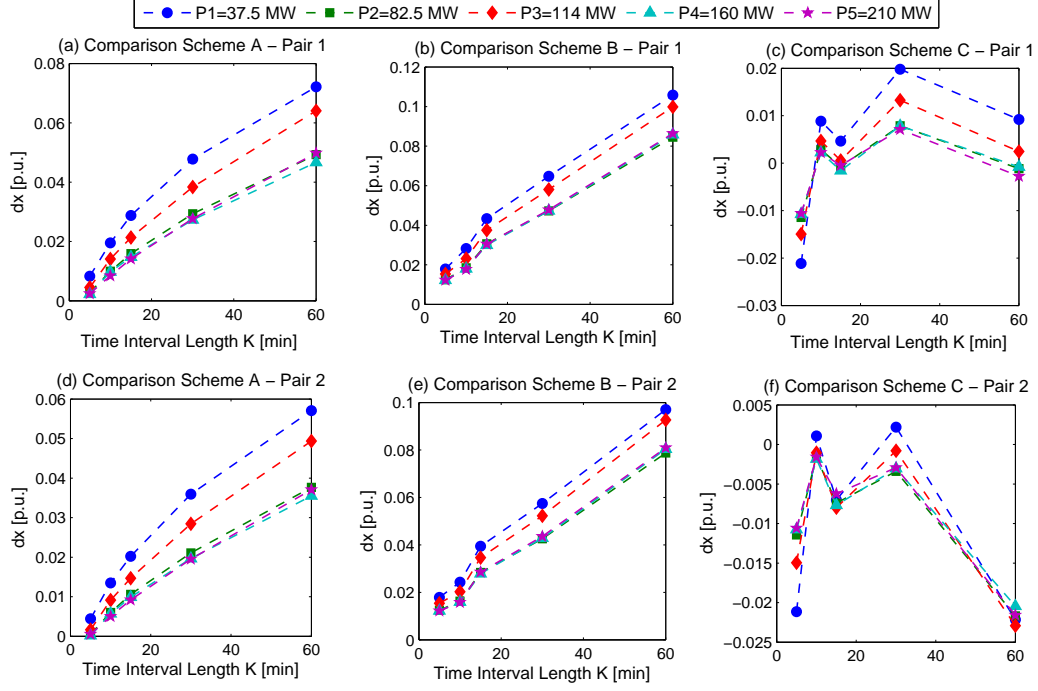


Figure 4.26: Mean ramp size difference  $dx$  as a function of the time interval length  $K$  for five wind farms of different nameplate capacities  $P_N$  when the conditional range is compared against the step-changes (pair 1) under (a) comparison scheme A, (b) comparison scheme B, (c) comparison scheme C, and when the conditional range is compared against the forward differences (pair 2) under (d) comparison scheme A, (e) comparison scheme B, (f) comparison scheme C. Ramp size differences increase in absolute numbers with decreasing wind farm capacity and increasing time interval length.

an interval, and thus its  $p^{th}$  quantile  $Q_{M_k}(p)$  gives an accurate probabilistic estimate of the size of a wind power ramp in a  $k$ -long time interval.

Most mean coverage rate differences  $dp$  depicted in Fig. 4.27 are negative, with the exception of comparing 5-minute conditional range quantiles with 1-minute absolute forward differences quantiles, which means that under all comparison schemes choosing reserves based on step-changes and forward differences quantiles results in a smaller percentage of successfully counter-

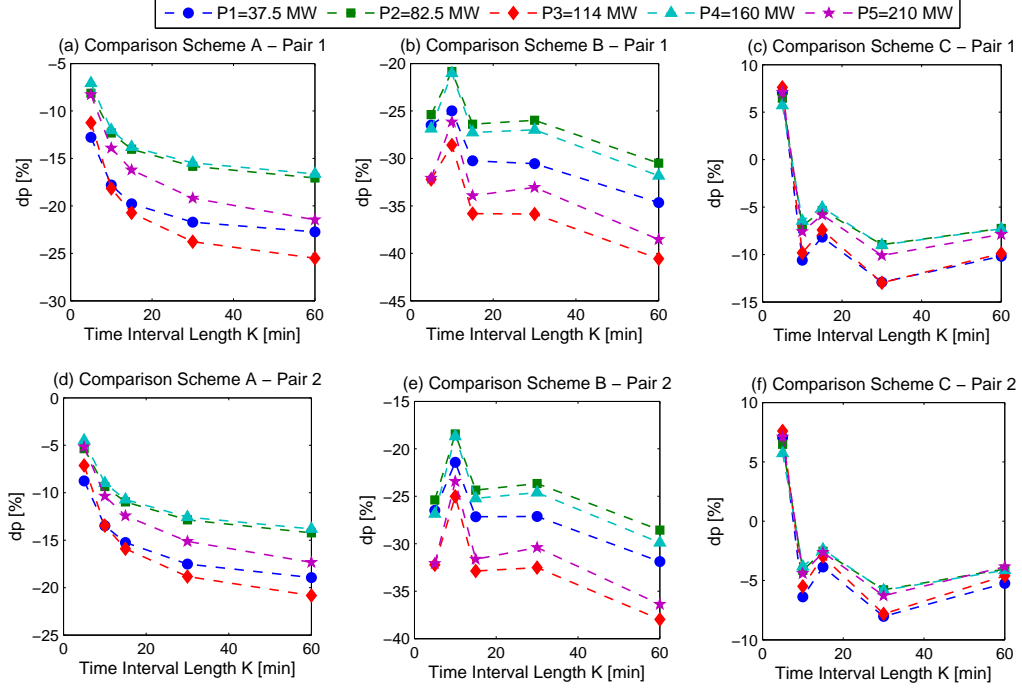


Figure 4.27: Mean coverage rate difference  $dp$  as a function of the time interval length  $K$  for five wind farms of different nameplate capacities  $P_N$  when the conditional range is compared against the step-changes (pair 1) under (a) comparison scheme A, (b) comparison scheme B, (c) comparison scheme C, and when the conditional range is compared against the forward differences (pair 2) under (d) comparison scheme A, (e) comparison scheme B, (f) comparison scheme C. Coverage rate differences increase in absolute numbers with increasing time interval length.

acted wind power ramps than the desired coverage rate  $p$ . Similarly to the ramp size, coverage rate differences  $dp$  increase in absolute numbers with increasing time interval length  $K$ . However, the effect of wind farm size  $P_N$  on coverage rate differences  $dp$  is not clear from Fig. 4.27. Nonetheless, under all time interval lengths  $K$  and wind farm sizes  $P_N$  the coverage rate differences  $dp$  are highest under comparison scheme B and lowest under comparison scheme C.

Table 4.8: Mean Absolute Deviations from the Nominal Coverage Rate ( $|dp|$  [%]) for Comparison Pair 1 (Conditional Range - Step-changes)

Comparison Scheme A					
$K$ [min]	5	10	15	30	60
avgWF	10.45	15.89	17.92	20.22	21.71
sumWF	8.53	13.05	14.41	15.51	16.04
Comparison Scheme B					
$K$ [min]	5	10	15	30	60
avgWF	28.63	25.11	31.44	31.36	36.04
sumWF	33.44	26.47	34.18	32.27	37.44
Comparison Scheme C					
$K$ [min]	5	10	15	30	60
avgWF	8.37	9.01	7.41	11.6	10.43
sumWF	9.85	7.76	6.83	9.41	8.45

Table 4.8 and Table 4.9 provide mean absolute deviations  $dp$  from the nominal coverage rate (calculated as averages of the absolute  $dp$  values over all coverage rates  $p$ ) similar to Fig. 4.27 for comparison pairs 1 and 2, respectively. In these tables 'sumWF' corresponds to mean absolute coverage rate difference  $dp$  when the aggregated wind power (summed wind power output of the 13 wind farms) is used, while 'avgWF' is the average of the mean absolute deviations  $dp$  of the 13 wind farms. Under comparison schemes A and C, taking the sum of the wind farms outputs seems to slightly reduce wind power variability resulting in lower deviations, due to the uncorrelated variations in wind farms outputs being canceled out by their addition. Comparison scheme B exhibits the largest mean absolute deviations, which indicates the importance of knowing the ramp rate duration in assessing the size of wind power ramps when using step-changes and forward differences. Moreover, the

Table 4.9: Mean Absolute Deviations from the Nominal Coverage Rate ( $|dp|$  [%]) for Comparison Pair 2 (Conditional Range - Forward Differences)

Comparison Scheme A					
$K$ [min]	5	10	15	30	60
avgWF	6.93	11.89	13.86	16.22	17.82
sumWF	5.82	10.06	11.49	12.81	13.44
Comparison Scheme B					
$K$ [min]	5	10	15	30	60
avgWF	28.63	21.96	28.76	28.36	33.65
sumWF	33.44	23.86	32.05	30.12	35.83
Comparison Scheme C					
$K$ [min]	5	10	15	30	60
avgWF	8.37	6.13	5.75	8.17	8.37
sumWF	9.85	5.97	5.89	7.36	7.31

large deviations under comparison scheme A, with an average value close to 15%, reveal the inability of the step-changes and the forward differences to effectively convey information about the wind power ramps within an interval.

#### 4.3.5 Concluding Remarks

The concept of the proposed conditional range  $M_k$  presented in Chapter 3 lies in quantifying the variability of a source using its range of outputs  $M$  over a given time interval length  $k$ . Using real-world wind power data from 13 wind farms, the step-changes, which are the most prevalent metric in quantifying wind power variability, and the forward differences are compared to the proposed conditional range. Under comparison scheme A it is exam-



ined whether tracking step-changes (or forward differences) and their rates over time frames  $k$  a conclusion on wind power variability within these intervals can be drawn, whereas under comparison schemes B and C it is examined whether step-changes (or forward differences) taken over time frames  $k$  are suitable for estimating the size and rate of wind power ramps over longer time frames. The comparison is done using the conditional range and the step-changes (or forward differences) quantiles, and the outcomes include the difference in ramp size  $dx$  and ramp rate  $dr$ , as well as the deviation  $dp$  from the conditional range nominal coverage rate  $p$ .

The comparison reveals that all metrics effectively recognize that wind power variability increases with increasing time interval length  $k$ , decreasing wind farm nameplate capacity  $P_N$  and is highest at mid-production wind power levels  $l_j$ . However, the comparison also exposes the two shortcomings of the step-changes (and forward differences), which are their inability to convey information about the wind power variability within a time interval and their lack to provide the duration of the wind power ramp rates. The first shortcoming is verified by the large deviations  $dp$  from nominal coverage rates under comparison scheme A, with average values close to 15%. Under comparison scheme B, using step-changes (or forward differences) over smaller time frames results in an underestimation of the wind power ramp sizes and rates within longer time frames. On the other hand, under comparison scheme C, using an exact multiple  $K/k$  of the step-changes (or forward differences) over smaller time frames  $k$  results in an overestimation of wind power ramps within longer time frames  $K$ . This reveals the second shortcoming of the step-changes, and signifies the importance of associating a duration with a ramp rate, so as to effectively estimate a wind power ramp size.

## 4.4 Summary

This chapter evaluates the proposed conditional range metric using real-world wind power data. In Section 4.1 a performance analysis of the proposed metric in wind power variability assessment is summarized. Using this analysis, the wind power variability over a time frame is found to increase with increasing time frame size and decreasing wind farm size. Moreover, wind power variability is highest at mid production wind power levels. In Section 4.2 the conditional range metric is used to quantify the effect of wind turbine technology and size on wind power variability. The results reveal that wind turbines connected through converters to the grid exhibit lower wind power variability compared to same size simple induction generators, and that wind power variability decreases slightly with increasing wind turbine size. Most importantly, wind power aggregation offers a significant reduction in wind power variability for all wind turbine technologies and sizes.

Moreover, Section 4.3 compares the performance of the conditional range metric to the step-changes and forward differences statistics in assessing the size and rate of intra-hour wind power ramps. The comparison reveals the shortcomings of the prevalent step-changes approach, which are their inability to convey information about the wind power variability within a time interval and their lack to provide the duration of the wind power ramp rates. The results show that the size of wind power ramps taken over a certain length  $k$  time interval is on average less than the  $p^{th}$  step-changes quantile only in  $p - 15\%$  of the  $k$ -long time intervals within a year. Since the conditional range is by definition the size of the largest wind power ramp within a  $k$ -long time interval, the power system reliability could benefit significantly by using the conditional range quantiles to estimate the size of wind power ramps.

## Chapter 5

### Forecasting the Conditional Range Metric

Wind is uncertain in its nature, which means that the actual value of wind power output in the future is unknown. To mitigate the effects of wind power uncertainty in power system planning and operations wind power forecasts are used. Different look ahead times and time resolutions are employed, depending on the system planning or operation procedures which use the wind power forecasts. Thus, hourly wind power forecasts for a 48-hour ahead time period can be used with respect to unit commitment, whereas 6-hour ahead wind power forecasts with a 5-minute resolution are used as input for economic dispatch. Several methods to obtain wind power forecasts have been developed in the past years, ranging from time series analysis to deployment of neural networks, and significant reduction in wind power forecast errors has been achieved. Nonetheless, with currently used wind power forecasting methods mean absolute prediction errors are in the range of 10%–20% for day-ahead forecasts and 5%–10% for hour-ahead forecasts.

The output of a wind power forecast consists of single values for each look ahead time, which correspond to the expected wind power output averaged over the time resolution of the forecast. Hence, a day-ahead hourly wind power forecast consists of 24 hourly averaged wind power values. However, the actual trajectory of wind power is not constant within the forecast time resolution interval, and existing wind power forecasts can not account for this

variability. Even when the hourly wind power forecast is perfect, wind power still varies within the hour and, if underestimated, this variability can have adverse effects on power system operations. These effects become more pronounced with increasing wind power penetration levels, since then intra-hour wind power variability becomes comparable to demand variability. Recall that for a 7.7% wind penetration level in the ERCOT service area, the largest wind power change in a 5-minute time interval within a given year was 781.42 MW versus a demand change of 892.52 MW.

Although the actual intra-hour wind power trajectory for an hour-period in the near future is unknown, intervals within which the wind power will lie over that hour-period can be estimated. These intervals form a wind power variability forecast, since they provide an upper and lower bound on the excursions the actual wind power output may take from the forecasted time interval average. Hence, a wind power variability forecast uses a wind power forecast as input, but provides supplemental information to the wind power forecast. This information allows for better management of wind power variability at the desired time scale with several applications, such as determining regulation and ramping requirements of controllable units to accommodate wind power variability, as well as sizing and control requirements of energy storage systems so as to achieve a more controllable wind power output. It should be noted that wind power variability forecasts rely on wind power forecasts but not on the way they are obtained. Thus, they provide a way of mitigating the adverse effects of wind power variability using state-of-the-art wind power forecasting methods. However, as the accuracy of wind power forecasts improves the reliability of wind power variability forecasts is expected to improve as well.

This chapter describes how wind power variability can be forecasted us-

ing the conditional range metric. A literature review of wind power forecasting technologies is given in Section 5.1. Section 5.2 presents how the conditional range metric quantiles can be used to provide wind power variability forecasts. Given an hourly wind power forecast, wind power variability is predicted by estimating the size of an interval within which the actual intra-hour wind power trajectory will lie. A probability distribution of this interval’s endpoints can be obtained by estimating future CRM quantiles. Details on quantile estimation and quantile estimates evaluation are presented in Sections 5.3.1 and 5.3.2, respectively. The conditional range metric quantiles are estimated in Sections 5.3.3–5.3.5 with three different methods, one static method (sample quantile) and two time-adaptive methods (exponentially weighted moving average, exponentially weighted stochastic approximation). The resulting quantile estimates are evaluated based on their reliability and the three methods are compared using the quantiles’ sharpness and resolution in Section 5.3.6. The results of CRM quantile estimation taking seasonality into account are given in Section 5.4. In Section 5.5 the incremental wind power variability forecast error, i.e. the wind power variability forecast error attributed to the wind power forecast error, is investigated, while Section 5.6 concludes the chapter.

## 5.1 Prior Work in Wind Power Forecasting

Numerous papers have been published in the past decades pertaining to wind speed and wind power prediction methodologies, turning the multidisciplinary area of wind power forecasting into an emerging technology. A detailed literature overview of the state-of-the-art in short-term wind power prediction can be found in [36], while more recent reviews of wind power and wind speed forecasting methods with different time horizons are given in [37]

and [38].

A wind power forecast provides the estimated available wind power output  $P(t + h)$  from a turbine, wind farm or region in the near future, with  $P(t)$  being the wind power at time  $t$ . Depending on the look ahead time  $h$  the following time classification of wind forecasts is suggested in [37]:

- very short-term forecasting (few seconds to 30 minutes ahead),
- short-term forecasting (30 minutes to 6 hours ahead),
- medium-term forecasting (6 hours to 1 day ahead),
- long-term forecasting (1 day to 1 week or more ahead).

The forecasting horizons are determined by the different applications of wind power forecasts in the various power system operations. Thus, a short-term wind power forecast could be useful in economic load dispatching, while a long-term wind power forecast could aid in unit commitment decisions.

Regarding the methods employed, wind power forecasts can be broadly divided into two categories:

- the ones employing a physical approach, and
- the ones employing a statistical approach,

though many new wind power forecasting models use a combination of both approaches. Another classification can be made based on whether the forecasting method employs a numerical weather prediction (NWP) model or not.

The simplest forecasting method is the persistence method (also called the naive predictor), for which the forecast for all times ahead is set to the

value it has now, i.e.  $P(t+h) = P(t)$ . Since this method is very accurate for very short-term and short-term forecasts, i.e.  $h < 6$  hours, it is often used as a benchmark which all other forecasting methods have to beat.

For short forecasting horizons, up to a few hours ahead, forecasting methods employing a statistical approach prove to be very accurate. These can be implemented either by direct time series analysis or with the use of artificial neural networks (ANN). The most widely used time series model is the Auto Regressive Moving Average (ARMA) and its variations, ARIMA and ARMAX. These models have been used on the wind power as well as the wind speed series and the results show that they can outperform the persistence model by 7-18% [39] for short-term and up to 30% [40] for very short-term forecasts. The range of improvements in [39] suggests that the ability of ARMA models varies with varying forecasting time periods. Many more time series models have been suggested employing diverse methods, such as Kalman filtering of the wind speed series [41] and wavelet transforms [42], or even the recently used smoothing techniques [43]. In addition the predictors employed in wind power forecasting vary from linear predictors [44, 45] up to grey models [46].

Though time series methods are improvements over the persistence method for short-term forecasts, in general they are outperformed by neural network (NN) models. Methods involving neural networks have been employed for short-term as well as medium-term wind power forecasting. There is great variety among these methods, including feed-forward [47, 48], recurrent [49] and radial basis function [50, 51] neural networks. Though these methods greatly outperform the persistence method results in [52] show that the neural network model configurations vary widely with site and error criteria, rendering that the selection of a suitable neural network model requires careful and

detailed analysis.

Prediction models using NWP forecasts also outperform time series approaches after about 6 hours look ahead time. These models use meteorological data such as wind speed and direction, pressure, temperature, humidity and terrain structure and their implementation usually involves three stages:

- downscaling, which yields a wind speed and direction for the turbine hub height,
- power conversion, in which the wind speed is converted to wind power through a wind power curve, and
- upscaling, which sums the single wind turbine results to an area total.

Due to their very high computational demands they are only run few times a day, limiting their usage to the preparation of medium and long-term wind power forecasts. The most common NWP systems include the Global Forecast System (GFS) run by the National Oceanic and Atmospheric Administration [53], the MM5 modeling system developed at Penn State and NCAR as a community mesoscale model [54], the international research program HIRLAM (High Resolution Limited Area Model) [55] and Prediktor, a commercial product developed by the Wind Power Meteorology research program at Risø National Laboratory for Sustainable Energy in Denmark [56].

However, the inability of an NWP model alone to provide sufficient downscaling for a particular wind farm at a particular site has led to the adoption of hybrid methods. A hybrid forecasting method combines different approaches, such as physical and statistical, or different models, such as short-term and medium-term. An advanced statistical forecasting method combining artificial neural networks and meteorological forecasts of wind speed and



direction is given in [57]. But even without a meteorological model, the combination of neural networks with fuzzy logic (ANFIS) and wavelet transforms presented in [58] provides very good results for short-term wind power forecasting. Other models combine neural networks with particle swarm optimization [59] or deploy entropy based training for the neural network model [60], with significant improvements in performance.

Moreover, the use of spatial correlation between the wind speed to be estimated and the wind speed from neighboring sites has been investigated in several papers. In [61] a neural network model using spatial correlation is used to estimate wind speed 3 hours ahead, while a fuzzy interfaced model in [62] is used to predict wind speed 2 hours ahead. Both methods show improvement over the persistent method by 28% and 29%, respectively.

Finally, the wind power output prediction is traditionally provided in the form of point forecasts, i.e. a single value for each look ahead time  $h$ , which corresponds to the expectation or most-likely outcome. However, such forecasts have limited value in decision making under uncertainty and for this reason probabilistic (ensemble) wind power forecasts have gained increasing attention in the last years. Wind power ensemble forecasts provide not just a point value but a whole probability density function of the wind power output. Indeed, quantile forecasts, interval forecasts and density forecasts, i.e. full predictive distributions for each look ahead time, are the most common ways to provide uncertainty estimates which are used to produce several scenarios of the future development of wind power. Scenarios are a critical input for various decision making problems with temporal or spatial interdependence, such as probabilistic power flows or optimal trading in multiple markets. Wind power ensemble forecasts can be created from wind speed ensembles [63, 64] or by extending wind power point forecasts [65, 66] with various statistical methods.

## 5.2 Forecasting Intra-hour Wind Power Variability

### 5.2.1 Approach

The output of an hourly wind power point forecast is one single wind power value for each look ahead time, which corresponds to the expected wind power hourly average. Given an hourly wind power point forecast, the intra-hour wind power variability can be predicted by estimating the endpoints of an interval  $[M_{low}, M_{up}]$  within which the actual intra-hour wind power trajectory will move.

Figure 5.1 depicts an hourly wind power forecast, i.e. forecast time resolution is one hour, for four hours ahead, i.e.  $h=1,2,3$ , and 4 hours, for a 160 MW wind farm. The hourly forecast is depicted with a solid line and the actual wind power trajectory at a 1 minute resolution is given with a dotted line. The forecast is perfect, since the actual hourly average equals the forecasted hourly average. The dashed lines depict the points  $M_{low}$  and  $M_{up}$ , the minimum and maximum instantaneous wind power within each hour, which define the desired intra-hour wind power variability interval  $[M_{low}, M_{up}]$ .

These intra-hour wind power variability intervals are the smallest intervals to envelope the actual wind power production. Indeed, for a 160 MW wind farm an obvious wind power variability interval, valid under any wind power trajectory, is the interval  $[0, 160]$  MW defined by its nameplate capacity. But from Fig. 5.1 it is evident that for wind power averages ranging from 84 MW in the first hour to 102 MW in the fourth hour, the instantaneous wind power values range from a minimum of 68 MW to a maximum of 123 MW in the third and fourth hour respectively, forming much smaller intervals than the obvious  $[0, 160]$  MW.

The points  $M_{low}$  and  $M_{up}$  given in Fig. 5.1 are in reality nothing but

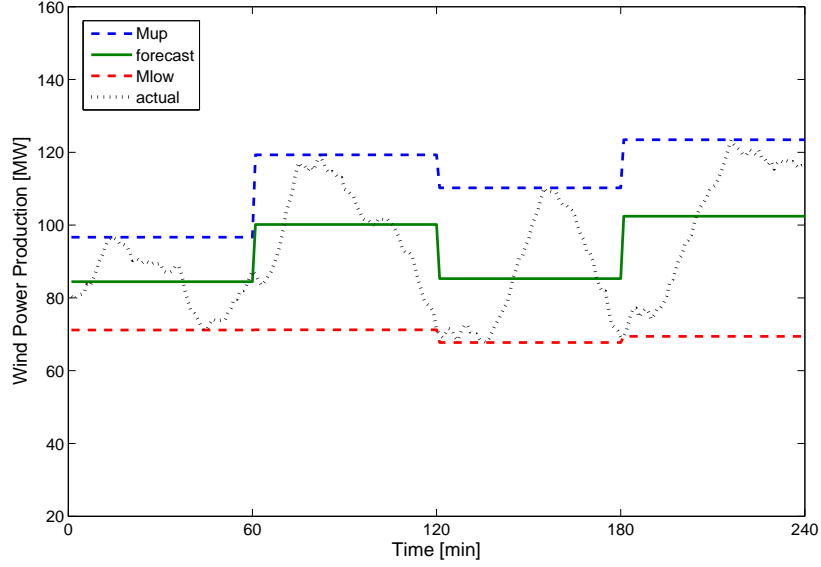


Figure 5.1: Hourly wind power forecast and intra-hour variability intervals for a 160 MW wind farm under no uncertainty. The solid line represents the perfect hourly forecast for four hours ahead, while the dotted line is the actual wind power trajectory at minute resolution. The dashed lines represent the minimum  $M_{low}$  and maximum  $M_{up}$  power output within each hour, and define the smallest intervals to envelope the actual wind power production.

the endpoints of the respective  $CRM$  intervals in these four hours. Indeed, the conditional range metric  $CRM_{i,k,l_j} = [M_{low_{i,k,l_j}}, M_{up_{i,k,l_j}}]$ , as defined with (3.4) in Section 3.2, is the interval within which the wind power output lies over a time interval starting at point  $i$ , having length  $k$  and average wind power production  $l_j$ . Thus, the dashed lines in Fig. 5.1 actually define the  $CRM$  intervals  $[M_{low_{i,k,l_j}}, M_{up_{i,k,l_j}}]$  for minutes  $i = 0, 60, 120, 180$  and  $k = 60$  minutes, e.g. for the third hour with  $i = 180$ ,  $k = 60$ , hourly average  $l_j = 102$  MW the  $CRM$  is  $[M_{low_{180,60,102}}, M_{up_{180,60,102}}] = [69, 123]$  MW.

When the actual intra-hour wind power is known, the intra-hour vari-

ability intervals are uniquely defined by the endpoints of the respective  $CRM$  intervals  $[M_{low_{i,k,l_j}}, M_{up_{i,k,l_j}}]$ . However, the actual wind power output is hardly ever known in advance and hence it is almost impossible to predict the exact wind power variability intervals. Instead, given an hourly wind power forecast a probabilistic forecast of these intervals, such as that given in Fig. 5.2, can be constructed. Figure 5.2 depicts the intra-hour wind power variability intervals for various probabilities, ranging from 5% to 95%, as differently shaded intervals around the hourly forecast. For example, with a probability of 5% the intra-hour wind power trajectory will move within the darkest shaded interval. The hourly forecast and the actual intra-hour wind power trajectory are again represented with a solid and dotted line, respectively, while the actual variability intervals are given with dashed lines. As expected, the actual wind power variability intervals are larger than the 5% and smaller than the 95% probability predicted intervals.

Thus, a wind power variability forecast is defined as a set of intervals, within which the actual wind power is expected to lie, with different probabilities assigned to them. Such a probabilistic forecast of intra-hour wind power variability intervals can be made using the  $p^{th}$  quantiles of the conditional range metric  $CRM_{k,l_j,p} = [M_{low_{k,l_j,p}}, M_{up_{k,l_j,p}}]$  as intervals. In that case, the interpretation of the wind power variability forecast is that, given a wind power forecast being  $l_j$  over a time interval of length  $k$ , the actual wind power output over the  $k$ -long time interval will fall within the  $CRM_{k,l_j,p}$  interval with probability at least  $p$ . Thus, the problem of constructing wind power variability forecasts is turned into a quantile estimation problem and the details of this problem are outline in the next section.

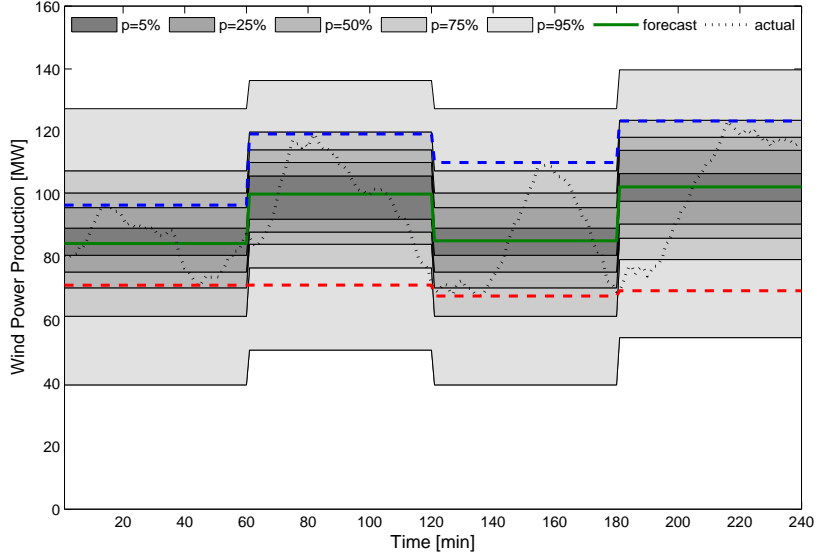


Figure 5.2: Intra-hour wind power variability intervals for various probabilities, ranging from 5% to 95%, for a 160 MW wind farm over a period of four hours. The variability intervals are depicted as differently shaded intervals around the hourly forecast. The dashed lines define the actual intervals of intra-hour wind power variability.

### 5.2.2 Problem Description

The wind power variability of a wind power point forecast for a unique future point in time  $i$ , with average wind power production  $l_j$  over a time interval  $k$ , e.g. an hourly wind power point forecast, can be forecasted by estimating the points  $[M_{low_{i,k,l_j}}, M_{up_{i,k,l_j}}]$  of the CRM interval. Estimating only one pair  $(M_{low_{i,k,l_j}}, M_{up_{i,k,l_j}})$  of future CRM endpoint values yields a single CRM estimate, denoted  $\hat{CRM}_{i,k,l_j}$ . However, estimating future CRM  $p^{th}$  quantiles, denoted  $\hat{CRM}_{k,l_j,p}$ , a probabilistic forecast of CRM can be generated. Thus, given a wind power forecast series with time resolution  $k$ , for each point of this series with value  $l_j$  a probabilistic forecast of CRM from the

quantile estimates  $\hat{CRM}_{k,l_j,p}$  is used to forecast wind power variability. Such a probabilistic forecast of CRM states that, given a forecast of the average wind power being  $l_j$  over a time interval of length  $k$ , the actual wind power over this  $k$ -long interval will fall within the  $\hat{CRM}_{k,l_j,p} = [\hat{M}_{low_{k,l_j,p}}, \hat{M}_{up_{k,l_j,p}}]$  interval with probability at least  $p$ .

The calculation of the  $p^{th}$  CRM quantile  $CRM_{k,l_j,p} = [M_{low_{k,l_j,p}}, M_{up_{k,l_j,p}}]$  from a wind power series  $x_n$ ,  $n = 1, 2, \dots, N \cdot k$ , can be done by solving the system of equations (3.7) and (3.10) with the methodology given in Section 3.3.2. The solution to this system is a unique pair of values  $(M_{low_{k,l_j,p}}, M_{up_{k,l_j,p}})$ . Averaging the wind power over non-overlapping  $k$ -long time intervals results in an  $N$ -long wind power series  $x_{k,i}$ ,  $i = 1, 2, \dots, N$ , with  $x_{k,i} = \frac{1}{k} \sum_{m=1}^k x_{k(i-1)+m}$  being the average of the  $i^{th}$  interval  $[k(i-1) + 1, k(i-1) + k]$ , denoted  $K_i$ . Let  $\tilde{x}_{k,i}$  denote a forecast of such an interval average production series  $x_{k,i}$ . Also, let  $\tilde{CRM}$  denote the CRM when the wind power range is conditioned not on the actual interval average production,  $x_{k,i} = l_j$ , but on the forecasted interval average production,  $\tilde{x}_{k,i} = l_j$ . In that case the problem of finding the  $p^{th}$  quantile of the conditional range metric  $[\tilde{M}_{low_{k,l_j}}, \tilde{M}_{up_{k,l_j}}]$  from an  $N \cdot k$ -long wind power series  $x_n$  and an  $N$ -long interval average wind power forecast series  $\tilde{x}_{k,i}$  can be mathematically formulated as follows:

Given  $k$ ,  $l_j$ , and  $p$   
Find  $\tilde{M}_{low_{k,l_j,p}}$  and  $\tilde{M}_{up_{k,l_j,p}}$

such that  $(\tilde{M}_{up_{k,l_j,p}} - \tilde{M}_{low_{k,l_j,p}})$  is minimized and such that over all  $k$ -long time intervals  $K_i$ :

$$P \left( \left\{ \inf_{n \in K_i} x_n \geq \tilde{M}_{low_{k,l_j,p}} \right\} \cap \left\{ \sup_{n \in K_i} x_n \leq \tilde{M}_{up_{k,l_j,p}} \right\} \middle| \tilde{x}_{k,i} = l_j \right) \geq p, \quad i = 1, 2, \dots, N, \quad (5.1)$$

and

$$P(\sup_{n \in K_i} \{x_n - \tilde{x}_{k,i}\} \leq \tilde{M}_{up_{k,l_j,p}} - l_j) = P(\sup_{n \in K_i} \{\tilde{x}_{k,i} - x_n\} \leq l_j - \tilde{M}_{low_{k,l_j,p}}) \quad (5.2)$$

where:

- $k$  is the time resolution of the forecast (e.g. hourly averages),
- $l_j$  is the forecasted wind power production level,
- $p$  is the desired coverage rate, and
- $K_i$  is the  $i^{th}$   $k$ -long interval  $[k(i-1)+1, k(i-1)+k]$  in the actual wind power production series  $x_n, n = 1, 2, \dots, N \cdot k$ .

When the actual wind power series  $x_n$  and the forecast series  $\tilde{x}_{k,i}$  are known, equations (5.1) and (5.2) form a system with a unique solution. The solution values  $(\tilde{M}_{low_{k,l_j,p}}, \tilde{M}_{up_{k,l_j,p}})$  define the  $p^{th}$  quantile of  $C\tilde{R}M_{k,l_j}$ , which states that, given a forecast of the average wind power being  $l_j$  over a time interval of length  $k$ , the actual wind power over this  $k$ -long interval will fall within the  $C\tilde{R}M_{k,l_j,p} = [\tilde{M}_{low_{k,l_j,p}}, \tilde{M}_{up_{k,l_j,p}}]$  interval with probability at least  $p$ .

However, trying to solve this system of equations using only the forecast series  $\tilde{x}_{k,i}$  is impossible, since with the  $N \cdot k$  actual wind power values unknown, the system is underdetermined. Thus, to forecast wind power variability an estimate of the  $p^{th}$  quantile  $C\tilde{R}M_{k,l_j,p} = [\tilde{M}_{low_{k,l_j,p}}, \tilde{M}_{up_{k,l_j,p}}]$

from historical data is used, turning wind power variability forecasting into a quantile estimation problem. The quantile estimate of  $C\tilde{R}M_{k,l_j,p}$  is denoted  $C\hat{R}M_{k,l_j,p} = [\hat{M}_{low_{k,l_j,p}}, \hat{M}_{up_{k,l_j,p}}]$ . Using these quantile estimates for various probabilities  $p$  a probabilistic forecast of wind power variability is generated.

It should be noted that for a perfect forecast, i.e.  $\tilde{x}_{k,i} = \sum_{n \in K_i} x_n$   $\forall i \in [1, N]$ , systems (3.7) and (3.10) and (5.1) and (5.2) yield the same solution,  $[M_{low_{k,l_j,p}}, M_{up_{k,l_j,p}}] = [\tilde{M}_{low_{k,l_j,p}}, \tilde{M}_{up_{k,l_j,p}}]$ . Due to lack in forecasted data for the actual wind power data at our disposal, a perfect forecast is used in all the  $C\hat{R}M$  quantile estimating methods presented in Section 5.3. In this way, the wind power variability forecasting error of each of the presented methods is evaluated ignoring the forecasting error of the wind power forecast. Section 5.5 presents an example of the wind power variability incremental error, i.e. the error in addition to the wind power forecasting error, using an artificially generated wind power forecast.

### 5.3 Estimating CRM Quantiles

This section presents a brief overview of quantile estimation techniques and evaluation criteria. Three different methods to obtain CRM quantile estimates are given and a comparison of these methods is provided. The data used in this section come from 10 wind farms (WF2, WF3, WF4, WF5, WF6, WF7, WF11, WF13, WF14, WF15 – see Appendix A.1), which are carefully chosen so that data from all regions, wind farm sizes and wind turbine technologies are represented in the analysis. The quantile estimates are calculated from the data in a training set (year 3) and evaluated on the data of a test set (year 4).



### 5.3.1 Prior Work in Quantile Estimation

As has already been stated, the  $p^{th}$  quantile  $q_X(p)$  of a random variable  $X$  with cumulative distribution function  $F_X$  is defined using the generalized inverse  $F_X^{-1}$ :

$$q_X(p) = F_X^{-1}(p) = \inf\{x : P(X \leq x) \geq p\} \quad (5.3)$$

When the distribution of  $X$  and hence the cdf  $F_X$  is unknown the quantile  $q_X(p)$  must be estimated.

The natural estimator of  $q_X(p)$  is of course its sample quantile  $Q_{X_N}(p)$ :

$$Q_{X_N}(p) = F_{X_N}^{-1}(p) \quad (5.4)$$

where  $F_{X_N}$  is the empirical cumulative distribution function defined as:

$$F_{X_N}(x) = \frac{1}{N} \sum_{i=1}^N I(X_i \leq x) \quad (5.5)$$

with  $I$  being the indicator function, i.e.  $I(X_i \leq x) = 1$ , if  $(X_i \leq x)$  and 0 otherwise. Here,  $X_1, X_2, \dots, X_N$  denote independent identically distributed replicates of the random variable  $X$ .

The sample quantile  $Q_{X_N}(p)$  can be estimated from the order statistics of the sample  $X_1, X_2, \dots, X_N$ , where the  $i^{th}$  order statistic  $X_{(i)}$  is such that  $X_{(1)} \leq X_{(2)} \leq \dots \leq X_{(N)}$ . When order statistics are used, the estimate of the  $p^{th}$  sample quantile  $\hat{Q}_{X_N}(p)$  from an  $N$ -long sample can be derived by computing a real-valued index  $h = N \cdot p + 1/2$ . When  $h$  is an integer the sample quantile estimate  $\hat{Q}_{X_N}(p)$  is given by the  $h^{th}$  order statistic:

$$\hat{Q}_{X_N}(p) = X_{(h)} \quad (5.6)$$

Otherwise one can choose from several rounding or interpolation schemes, the most simple being the inverse of the empirical cdf, where  $\hat{Q}_{X_N}(p) = X_{(\lceil h \rceil)}$ .

It should be noted that sample quantiles are biased, and the bias depends highly on the definition of the quantile and the underlying distribution of  $X$ . However, sample quantiles are asymptotically unbiased, i.e.  $\lim_{N \rightarrow \infty} E[Q_{X_N}(p)] = q_X(p)$ . Moreover, though it is relatively easy to calculate a point estimate for the  $p^{th}$  quantile  $q_X(p)$ , calculating a confidence interval for such an estimate requires special techniques like sectioning, bootstrap and Jackknife approaches [67]. Variance reduction can also be achieved using a Wilks estimator or some control variate [68].

Another way to find an estimator of  $q_X(p)$  is via quantile regression, where the sample quantile is estimated not with sorting but with optimizing. Indeed, in regression analysis estimates of the regression coefficients  $\beta$  are found with various optimization methods, e.g. least squares, to approximate the conditional mean of the response variable  $Y$  given a set of predictor variables  $X$ ,  $E[Y|X] = f(X, \beta)$ . In quantile regression it is not the conditional mean but the conditional median or other quantiles of  $Y$  that are approximated.

Let  $y_i$  denote the  $i^{th}$  observation of the response variable from an  $N$ -long sample and  $x_{i,j}$  denote the  $i^{th}$  observation of the  $j^{th}$  predictor variable, then a general linear regression model with  $k$  predictors is given by:

$$y_i = \beta_0 x_{i,0} + \beta_1 x_{i,1} + \beta_2 x_{i,2} + \dots + \beta_k x_{i,k} + \epsilon_i \quad (5.7)$$

where  $\beta_0, \beta_1, \dots, \beta_k$  are the  $k+1$  regression coefficients. The predictor  $x_{i,0}$  takes the value 1 for all observations, thus  $\beta_0$  is the intercept. For the  $i^{th}$  observation of predictor variables an estimated value of  $E[y_i|x_i]$ , denoted  $\hat{y}_i$ , is given by:

$$\hat{y}_i = \hat{\beta}_0 x_{i,0} + \hat{\beta}_1 x_{i,1} + \hat{\beta}_2 x_{i,2} + \dots + \hat{\beta}_k x_{i,k} = f(x_i, \hat{\beta}) \quad (5.8)$$

where  $\hat{\beta}_0, \hat{\beta}_1, \hat{\beta}_2, \dots, \hat{\beta}_k$  are the estimates of  $\beta_0, \beta_1, \dots, \beta_k$  and  $e_i = y_i - \hat{y}_i$  is the  $i^{th}$  residual. For the least squares method, the estimators of  $\beta_0, \beta_1, \dots, \beta_k$  are the

values which minimize the sum of the  $N$  squared residuals  $Q = \sum_{i=1}^N (y_i - \hat{y}_i)^2$ . Thus, the conditional expectation function  $E[Y|x]$  is obtained by solving the optimization problem:

$$\min_{\beta \in \mathbb{R}^{k+1}} \sum_{i=1}^N (y_i - f(x_i, \beta))^2 \quad (5.9)$$

Under the assumption that the deviations  $\epsilon_i$  are following a normal  $\mathcal{N}(0, \sigma^2)$  distribution and using matrix notation, where  $X$  is  $N \times (k+1)$ ,  $Y$  is  $N \times 1$  and  $\beta$  is  $(k+1) \times 1$ , the regression coefficient estimates are given by  $\hat{\beta} = (X^T X)^{-1} X^T Y$ . The least squares estimator  $\hat{\beta}$  has least variance among the class of unbiased estimators [69].

Acknowledging the deficiency of the least squares estimator in linear models with non-Gaussian errors a new class of statistics called regression quantiles is introduced in [70]. Using similar notation to (5.9), in quantile regression an estimate of the  $p^{th}$  conditional quantile function  $Q_{Y_N}(p)|X$  can be found by solving the optimization problem [71]:

$$\begin{aligned} \min_{\beta \in \mathbb{R}^{k+1}} \sum_{i=1}^n \rho_p(y_i - g(x_i, \beta)) = \\ \min_{\beta \in \mathbb{R}^{k+1}} \sum_{i=1}^n \rho_p(y_i - (\beta_{p,0}x_{i,0} + \beta_{p,1}x_{i,1} + \beta_{p,2}x_{i,2} + \dots + \beta_{p,k}x_{i,k})) \end{aligned} \quad (5.10)$$

where  $\rho_p(\cdot)$  is the loss function defined as:

$$\rho_p(e) = \begin{cases} pe & \text{if } e \geq 0 \\ (p-1)e & \text{if } e < 0 \end{cases} \quad (5.11)$$

and  $\beta_{p,0}, \beta_{p,1}, \beta_{p,2}, \dots, \beta_{p,k}$  are the  $k+1$  quantile regression coefficients. Thus, an estimated value of the  $p^{th}$  conditional quantile  $Q_{Y_N}(p)|x_i$ , denoted  $\hat{q}_{y_i}(p)$ , is given by:

$$\hat{q}_{y_i}(p) = \hat{\beta}_{p,0}x_{i,0} + \hat{\beta}_{p,1}x_{i,1} + \hat{\beta}_{p,2}x_{i,2} + \dots + \hat{\beta}_{p,k}x_{i,k} \quad (5.12)$$

where  $\hat{\beta}_{p,0}, \hat{\beta}_{p,1}, \hat{\beta}_{p,2}, \dots, \hat{\beta}_{p,k}$  are the regression coefficient optimizers:

$$\hat{\beta}_p = \arg \min_{\beta \in \mathbb{R}^{k+1}} \sum_{i=1}^N \rho_p(y_i - g(x_i, \beta)) \quad (5.13)$$

The loss function is quantile regression's analog of the squared-error function from standard linear regression, since in quantile regression the absolute values in (5.9) are replaced by  $\rho_p(\cdot)$  in (5.10).

A goodness-of-fit process for quantile regression analogous to the conventional  $R^2$  statistic of least squares regression, the ratio of explained to total variance in the model, is given in [72]. A linear programming formulation of the optimization problem in (5.10), which can be solved with a simplex or internal point algorithm, can be found in [73], while [74] uses a quadratic optimization problem for non-parametric quantile estimation.

Quantile regression has been used in the recent years with respect to wind power, either to produce probabilistic wind power forecasts [66, 75] or to model the uncertainty of wind energy forecasts by modeling the quantiles of wind forecast errors [76]. Moreover, a time-adaptive quantile regression algorithm, which uses a simplex method and a suitable updating procedure, can be found in [77]. When applied to wind power data, the time-adaptive model exhibits superior performance than the static quantile regression model in all the considered parameters.

The accuracy of a sample quantile estimate, both when using order statistics or quantile regression, is expected to improve as the size of the set of historical observations, i.e. the sample size  $N$ , increases. On the other hand, incremental quantile estimation refers to the case of dynamic monitoring of the quantity to be estimated, where the purpose is to estimate a quantile of the current behavior of the entity being monitored, rather than to reproduce

a number that would be obtained from the entire history of monitoring.

Incremental quantile estimation is very popular for problems involving monitoring of networked applications, since in these problems approximate quantiles from a large amount of streaming (non-static) data have to be calculated in a time-efficient manner (on-line) with devices of limited memory and computational capacity. The majority of incremental quantile estimation algorithms for network modeling assume a limited size buffer which usually holds only a subset of the observations seen so far [78, 79], while in some algorithms the buffer size is allowed to vary [80]. Accurate quantile estimates are also used in database applications and data mining to characterize the distribution of evolving data sets. In these cases the quantile estimation algorithms handle not only the insertion of new but also the deletion of old data [81].

Let  $X_{1,i}, X_{2,i}, \dots, X_{N,i}$  be the observations stored in a limited size  $N$  buffer at the  $i^{th}$  filling of the buffer from streaming data. These  $N$  observations are considered as a random sample from a distribution with cdf  $F_{X,i}$  and  $p^{th}$  quantile  $Q_{X,i}(p)$ . For  $i = 1$  the best estimate of the  $p^{th}$  quantile is the sample quantile  $\hat{Q}_{X,i}(p)$ . An incremental estimate of the  $p^{th}$  quantile  $Q_{X,i}(p)$  of the  $i^{th}$  iteration is computed knowing only the current set of  $N$  observations, the quantile estimate  $\hat{Q}_{X,(i-1)}(p)$  from the previously filled buffer, and a few tuning parameters. Methods considered for updating the quantile estimate include moving average and stochastic approximation approaches [82–84].

A simple moving average is the unweighted sample mean of the previous  $N$  points in a sample. Thus, under the moving average approach the  $p^{th}$  quantile estimate of the  $i^{th}$  iteration  $A_{X_N,i}(p)$  is updated using:

$$A_{X_N,i}(p) = (1 - i^{-1}) \cdot A_{X_N,i-1}(p) + i^{-1} \cdot \hat{Q}_{X_N,i}(p) \quad (5.14)$$

where  $\hat{Q}_{X_N,i}(p)$  is the sample quantile of the  $i^{th}$  iteration. Replacing  $i^{-1}$  in (5.14) with  $w$ , ( $0 < w < 1$ ), yields the exponentially weighted moving average estimate. For a fixed  $w$  the contribution of old observations is faded out making this method more appropriate in cases where the underlying probability distribution of the monitored entity changes over time.

Stochastic approximation approaches are based on the following algorithm, presented in [85]. Let  $M(x)$  be a non-decreasing function of  $x$  for which the equation  $M(x) = \alpha$  has a unique root  $x = \theta$ , with  $M'(\theta) > 0$ . If instead of  $M(x)$  only observations of  $N(x)$  are given, for which  $E[N(x)] = M(x)$  and  $N(x)$  is uniformly bounded, then a series  $x_n$  which converges in probability to  $\theta$  can be obtained by:

$$x_{n+1} - x_n = a_n(\alpha - N(x_n)) \quad (5.15)$$

Here  $a_1, a_2, \dots, a_n$  is a series of positive step sizes which satisfy  $\sum_{n=0}^{\infty} a_n^2 < \infty$  and  $\sum_{n=2}^{\infty} a_n / (a_1 + a_2 + \dots + a_{n-1}) = \infty$ . Sequences which satisfy these conditions are of the type  $1/n$ .

Applying the previous algorithm to quantile estimation, it is first observed that a  $p^{th}$  quantile of  $X$ ,  $q_X(p)$ , is the solution to the equation  $F(x) = p$  since  $F(q_X(p)) = p$ . Let  $z_n$  be observations for which  $P(z_n \leq x) = F(x)$  and  $y_n$  be a series defined by:

$$y_n = \begin{cases} 1 & \text{if } z_n \leq x_n \\ 0 & \text{otherwise} \end{cases} \quad (5.16)$$

Then, the series

$$x_{n+1} - x_n = a_n(p - y_n) \quad (5.17)$$

converges in  $L^2$  and hence in probability to  $q_X(p)$ . In (5.17)  $x_1$  is the best guess of  $q_X(p)$  and  $a_n$  are of the type  $1/n$ .

### 5.3.2 Evaluation of Quantile Estimates

To compare the various quantile estimation methods several performance parameters of the quantile estimates  $\hat{Q}_{X_N}(p)$  can be used. The most important performance parameters pertaining to wind power prediction are given in [76]:

- Reliability

The quantile estimate  $\hat{Q}_{X_N}(p)$  should be as close as possible to the true quantile  $q_X(p)$ . Since the true quantile is unknown, the quantile estimate is compared to the sample quantile  $Q_{X_N}(p)$ . This desired quality of the quantile estimate is termed reliability. Indeed, reliability refers to the property of a  $p^{th}$  quantile estimate  $\hat{Q}_{X_N}(p)$  having a coverage rate close to the nominal  $p$  and is defined as:

$$r_p = \hat{p}^{(p)} - p = \frac{n^{(p)}}{N} - p \quad (5.18)$$

where  $N$  is the test set length, and  $n^{(p)}$  is the number of samples where the observed  $X$  value actually lies below the estimated  $p^{th}$  quantile (number of hits).

Reliability is given in the form of reliability diagrams, either showing the observed ( $\hat{p}^{(p)}$ ) proportions or the deviation ( $\hat{p}^{(p)} - p$ ) between observed and nominal proportions of the quantile estimates, as a function of the nominal proportion  $p$ . The reliability of an estimate can be improved using recalibration methods such as general bootstrapping, smoothed bootstrapping, and adaptive resampling [86]. These approaches reduce the effect outliers in the training set can have on a quantile estimate of the test set.

- Sharpness

The sharpness of a quantile estimate can be calculated by looking at how far symmetric around 0.5 the quantile estimates are, thus how large the interval around the median is. In most cases this is done by looking at the interquartile range (*IQR*), i.e. the difference  $\hat{Q}_{X_N}(0.75) - \hat{Q}_{X_N}(0.25)$  between the 75<sup>th</sup> and the 25<sup>th</sup> percentile estimates. Given two quantile estimates with acceptable reliability the one with the smaller interval is preferred. Measures of sharpness include the mean or the median of *IQR*.

- Resolution

Resolution of a quantile estimate is its ability to distinguish between various conditions, thus to have a situation-dependent size. A quantile estimate with larger variations under the various conditions is rewarded. Measures of resolution include the standard deviation, the mean absolute deviation and the difference between the 5<sup>th</sup> and 95<sup>th</sup> percentile of *IQR*.

Other quantile estimate performance criteria for wind power forecasts include the spread/skill relationship and the skill score. The spread/skill relationship refers to the relationship between some point forecast and the actual value. On the other hand, the skill score is a numerical value used to summarize the performance of the forecast, such as the generalization of the loss function in quantile regression [87].

### 5.3.3 Sample Quantile

The simplest method to obtain a  $p^{th}$  quantile estimate  $\hat{CRM}_{k,l_j,p}$  is to use the sample quantile from the wind power data in the training set ( $x_m$ ) as



the CRM quantile estimate for the wind power data in the test set ( $y_n$ ). Let  $CRM_{\{X\}k,l_j,p} = [M_{\{X\}low_{k,l_j,p}}, M_{\{X\}up_{k,l_j,p}}]$  denote a sample quantile from the data in set  $\{X\}$ . Then, under the sample quantile estimate approach we have:

$$C\hat{R}M_{\{Y\}k,l_j,p} = [\hat{M}_{\{Y\}low_{k,l_j,p}}, \hat{M}_{\{Y\}up_{k,l_j,p}}] = [M_{\{X\}low_{k,l_j,p}}, M_{\{X\}up_{k,l_j,p}}] \quad (5.19)$$

where  $(M_{\{X\}low_{k,l_j,p}}, M_{\{X\}up_{k,l_j,p}})$  is the solution of the system of equations (3.7) and (3.10) solved in Section 3.3.2 using the  $x_m$  wind power data as input.

The reliability  $r_{k,l_j,p}$  of the  $p^{th}$  quantile estimate for a given  $k$ -long wind power production level  $l_j$  is given by:

$$r_{k,l_j,p} = \hat{p}_{k,l_j}^{(p)} - p \quad (5.20)$$

which is the deviation of the actual ( $\hat{p}_{k,l_j}^{(p)}$ ) from the nominal ( $p$ ) proportion. Here,  $\hat{p}_{k,l_j}^{(p)}$  is the number  $n_{k,l_j}^{(p)}$  of  $k$ -long time intervals in the test set with average production  $y_{k,i} = \frac{1}{k} \sum_{m=1}^k y_{k(i-1)+m} = l_j$  for which the wind power lies within the interval  $[M_{\{X\}low_{k,l_j,p}}, M_{\{X\}up_{k,l_j,p}}]$  from (5.19), divided by the total number  $N_{k,l_j}$  of  $k$ -long time intervals with average production  $l_j$ . The reliability  $r_{k,l_j,p}$  should be viewed as how well the quantile estimate performs on a wind power forecast of production  $l_j$  with forecast time resolution  $k$ , e.g. an hourly forecast of production 0.5 p.u. It should be noted that a negative reliability value means that the forecast underestimates the actual wind power variability, i.e. the actual CRM interval  $[\tilde{M}_{\{Y\}low_{k,l_j,p}}, \tilde{M}_{\{Y\}up_{k,l_j,p}}]$  is larger than the estimated interval  $[\hat{M}_{\{Y\}low_{k,l_j,p}}, \hat{M}_{\{Y\}up_{k,l_j,p}}]$ , which makes positive reliability favorable over negative reliability.

Figures 5.3 and 5.4 depict the reliability, i.e. the deviation from the nominal proportion, of various quantile estimates as a function of the wind power forecast  $l_j$ . For the deviations given in Fig. 5.3 data from a 114 MW wind farm (WF4) over  $k = 5$  minute intervals have been used, while the

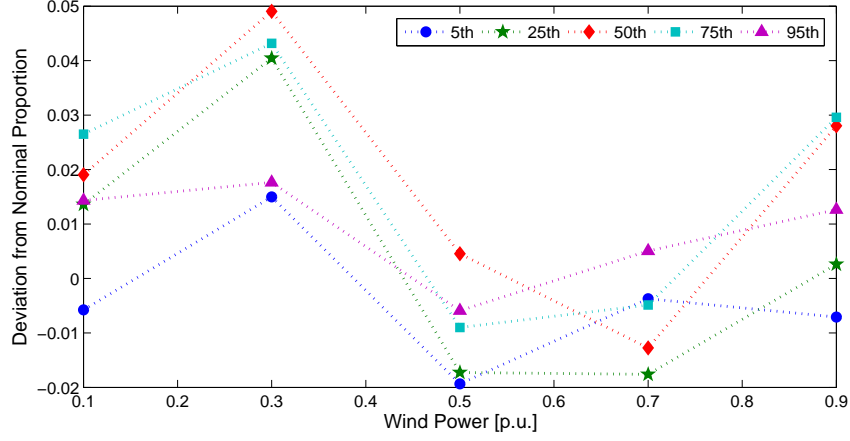


Figure 5.3: Reliability of various CRM percentile estimates as a function of the wind power forecast level  $l_j$  with forecast resolution  $k = 5$  minutes for a 114 MW wind farm (WF4). Low and high quantiles are more reliable than the median and the quartiles.

deviations given in Fig. 5.4 come from the data of a 91.5 MW wind farm (WF15) over  $k = 60$  minute intervals.

Regarding the effect of the nominal proportion  $p$  on the reliability of the CRM quantile estimates, from both Fig. 5.3 and Fig. 5.4 it is evident that high rank percentiles ( $95^{th}$ ) are more reliable than the median ( $50^{th}$ ) or the quartiles ( $25^{th}$ ,  $75^{th}$ ). This quality is highly desired, since in most cases it is the high rank quantiles, associated with low risk parameters, that are of interest. Moreover, the wider spread of the deviations in Fig. 5.4 implies that certain quantile estimates are less reliable with increasing wind power forecast resolution  $k$ . With respect to the effect of the wind power forecast level  $l_j$  on the reliability of the CRM quantile estimates no safe conclusion can be drawn from Fig. 5.3 and Fig. 5.4, since e.g. under a 5-minute forecast resolution the median appears less reliable for low wind power productions ( $l_j = 0.3$  p.u.) than for high productions ( $l_j = 0.9$  p.u.), whereas under the hourly forecasts

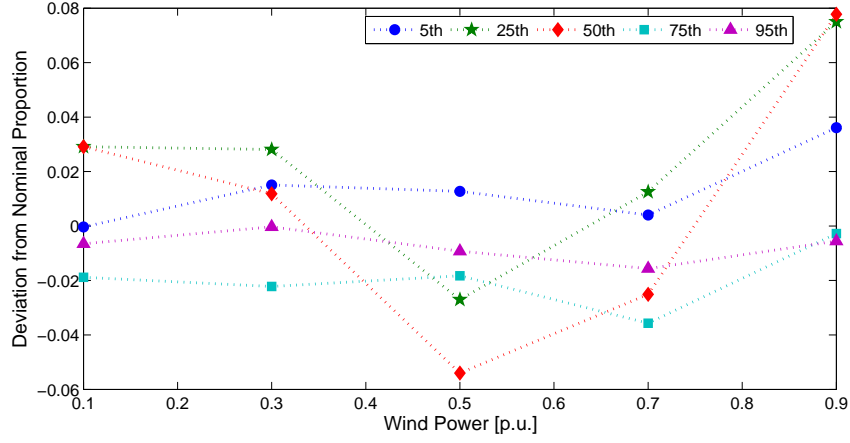


Figure 5.4: Reliability of various CRM percentile estimates as a function of the wind power forecast level  $l_j$  with forecast resolution  $k = 60$  minutes for a 91.5 MW wind farm (WF15).

this effect is reversed.

Another way to present reliability is by tabulating the nominal and actual proportions of the quantile estimates. Tables 5.1, 5.2, and 5.3 present the nominal and actual probabilities (proportions) in percent for a 160.5 MW wind farm (WF6) under various forecast time resolutions  $k$  for wind power forecast levels  $l_j = 0.1, 0.5$  and  $0.9$  p.u, respectively. The data in these tables are in agreement with the previous conclusion that higher percentile estimates perform better than lower ones. From these tables it also becomes evident that for most quantile estimates, especially low percentiles, the performance is worse for high than for medium or low wind power forecast levels, with the reliability being best at mid-production levels. This result denotes that though wind power variability is highest at wind power mid-production levels it is more predictable at these levels.

Table 5.1: Nominal and Actual Probabilities in percent for a 160.5 MW Wind Farm (WF6, Wind Power Level  $l_j = 0.1$  p.u.)

	Forecast Time Resolution k				
Nominal	5 min	10 min	15 min	30 min	60 min
5	4.98	4.29	4.80	4.11	3.74
10	10.25	9.40	9.59	8.22	8.46
15	15.57	14.75	15.77	12.73	15.35
20	20.44	19.01	21.12	16.63	20.87
25	25.91	24.29	26.28	21.74	26.18
30	30.52	30.63	31.12	27.45	30.71
35	36.18	36.22	35.71	33.07	36.02
40	40.92	41.57	41.17	37.78	41.93
45	46.12	46.24	46.07	42.99	45.87
50	51.41	50.46	51.63	50.40	52.76
55	56.75	56.15	56.48	55.31	56.69
60	62.33	60.95	61.33	60.52	60.43
65	67.26	65.93	66.43	66.93	64.76
70	72.90	70.32	71.33	70.84	68.90
75	77.41	75.33	76.89	75.85	71.46
80	81.76	80.72	81.79	80.66	75.98
85	86.48	85.14	86.22	83.37	80.51
90	91.30	89.81	90.71	87.07	85.24
95	95.68	94.34	94.95	91.28	91.54

Table 5.2: Nominal and Actual Probabilities in percent for a 160.5 MW Wind Farm (WF6, Wind Power Level  $l_j = 0.5$  p.u.)

	Forecast Time Resolution k				
Nominal	5 min	10 min	15 min	30 min	60 min
5	5.81	5.34	5.68	6.37	6.28
10	10.72	10.59	11.37	11.32	9.66
15	15.55	16.08	16.72	15.09	15.46
20	20.31	20.50	21.20	21.23	17.39
25	25.71	25.23	25.79	24.76	21.26
30	30.88	30.11	30.82	30.90	26.57
35	35.86	35.75	36.50	37.74	34.78
40	40.35	41.08	41.31	42.22	39.13
45	46.02	45.43	46.45	45.75	43.00
50	51.45	51.37	51.04	48.82	49.28
55	56.32	56.40	55.74	53.54	52.66
60	61.27	61.66	60.66	58.02	55.56
65	65.42	65.62	65.46	63.21	61.35
70	71.23	70.20	70.38	67.69	64.25
75	76.59	76.60	74.43	73.35	70.05
80	81.20	80.95	78.14	77.59	77.29
85	85.81	85.14	82.73	83.73	83.57
90	90.75	89.86	87.98	90.09	88.41
95	95.58	94.97	93.88	95.28	94.20

Table 5.3: Nominal and Actual Probabilities in percent for a 160.5 MW Wind Farm (WF6, Wind Power Level  $l_j = 0.9$  p.u.)

	Forecast Time Resolution k				
Nominal	5 min	10 min	15 min	30 min	60 min
5	8.45	9.99	10.38	10.53	10.67
10	14.92	15.79	16.17	14.57	14.22
15	20.17	20.92	22.46	21.05	19.11
20	25.81	25.25	28.54	25.10	24.89
25	31.22	30.65	33.83	30.16	28.44
30	36.06	36.44	37.43	34.82	32.44
35	41.00	43.04	40.92	40.28	37.78
40	46.64	48.03	45.11	43.72	44.00
45	51.79	52.43	48.70	48.79	48.44
50	57.06	56.63	53.99	52.83	52.44
55	61.80	60.23	59.68	58.70	56.00
60	66.51	65.42	64.07	62.96	60.89
65	71.45	69.42	67.96	69.84	64.44
70	75.53	75.08	72.75	74.49	68.89
75	80.07	78.88	78.54	79.35	76.00
80	84.27	82.54	81.94	83.60	82.22
85	88.08	87.34	86.43	86.84	85.78
90	92.39	91.47	91.62	92.31	90.67
95	95.96	96.07	95.51	96.36	95.11

However, in many cases a unique reliability value of a  $p^{th}$  CRM quantile estimate over all wind power forecast levels  $l_j$  is desired. Such a value can be obtained by taking a weighted sum of the proportions  $(\hat{p}_{k,l_j}^{(p)})$  with weights  $w_j$  equal to the probability of the  $k$ -long interval average production being  $l_j$ , i.e.  $w_j = N_{k,l_j}/N_k$  where  $N_k$  is the total number of  $k$ -long intervals. Thus, the total reliability  $r_{k,p}$  of a  $p^{th}$  CRM quantile estimate is given by:

$$r_{k,p} = \frac{\sum_j N_{k,l_j} \cdot \hat{p}_{k,l_j}^{(p)}}{\sum_j N_{k,l_j}} - p = \sum_j \frac{N_{k,l_j}}{N_k} \cdot \hat{p}_{k,l_j}^{(p)} - p \quad (5.21)$$

The total reliability penalizes deviations from the nominal proportions according to their probability of appearance. Thus, a quantile estimate can have a poor performance on some wind power level  $l_j$ , but be overall highly reliable if this level has a low probability of appearance.

A typical quantile estimate reliability diagram is given in Fig. 5.5. Such a diagram presents the total reliability of all quantile estimates, by plotting the actual  $\sum_j w_j \cdot \hat{p}_{k,l_j}^{(p)}$  against the nominal proportion  $p$  of a quantile. Figure 5.5 depicts the reliability diagrams of a 120.6 MW wind farm (WF3) for various wind power forecast resolutions  $k$ . In Fig. 5.5 the solid line represents the actual and the dotted line the nominal quantile proportion  $p$ . The almost invisible deviations of the solid from the dotted line under all forecast resolutions  $k$  indicate the high performance of all quantile estimates. Thus, to better visualize reliability the deviations from nominal proportions instead of the actual proportions are used, as they are presented in the reliability diagram of Fig. 5.6.

The results of the individual reliability diagrams in Fig. 5.6 are summarized in Fig. 5.7 to better visualize the effect of forecast resolution  $k$  on CRM quantile estimates' reliability. Figure 5.7 depicts deviations from nominal proportions for various percentiles and forecast resolutions  $k$  as a function of the

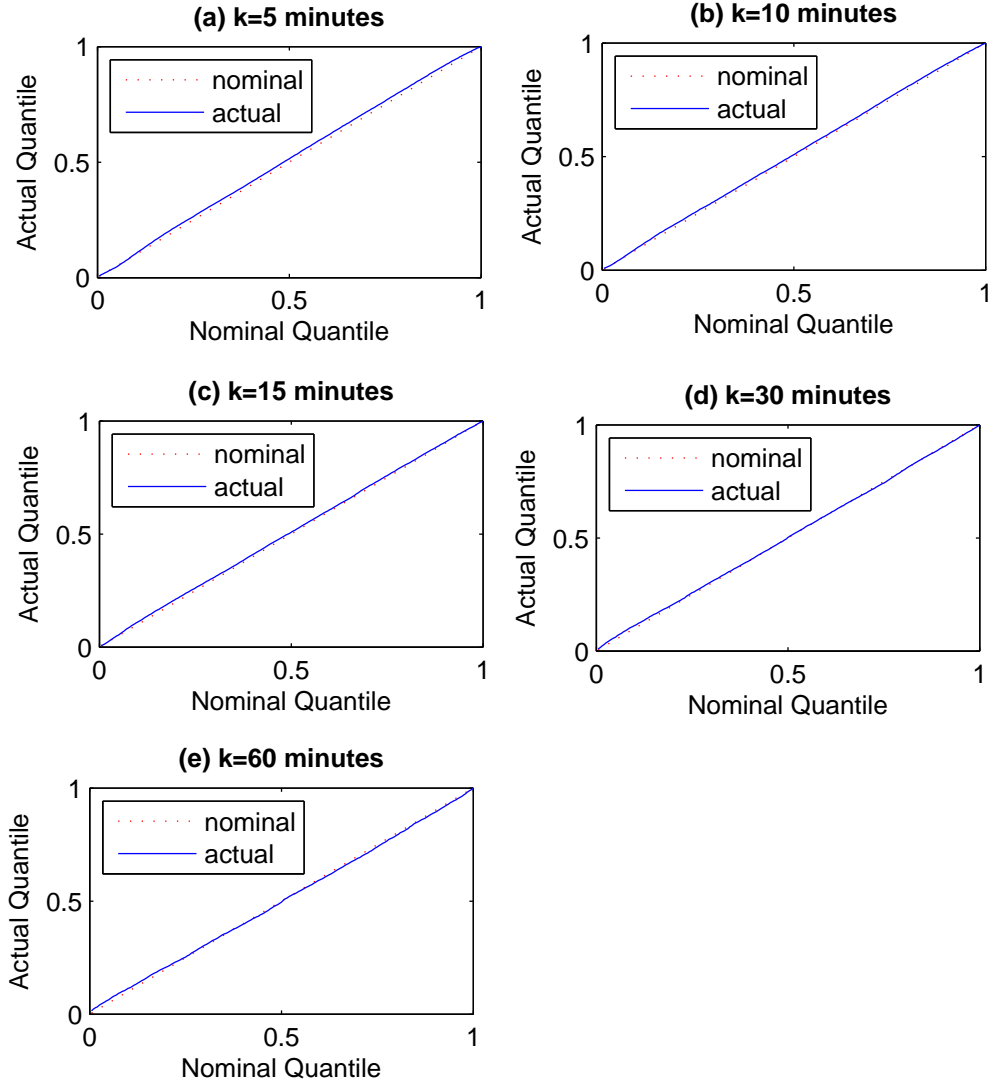


Figure 5.5: Actual proportions of the CRM quantile estimates of a 120.6 MW wind farm (WF3) for various wind power forecast resolutions  $k = 5, 10, 15, 30$  and 60 minutes. The solid line represents the actual and the dotted line the nominal proportion  $p$ .



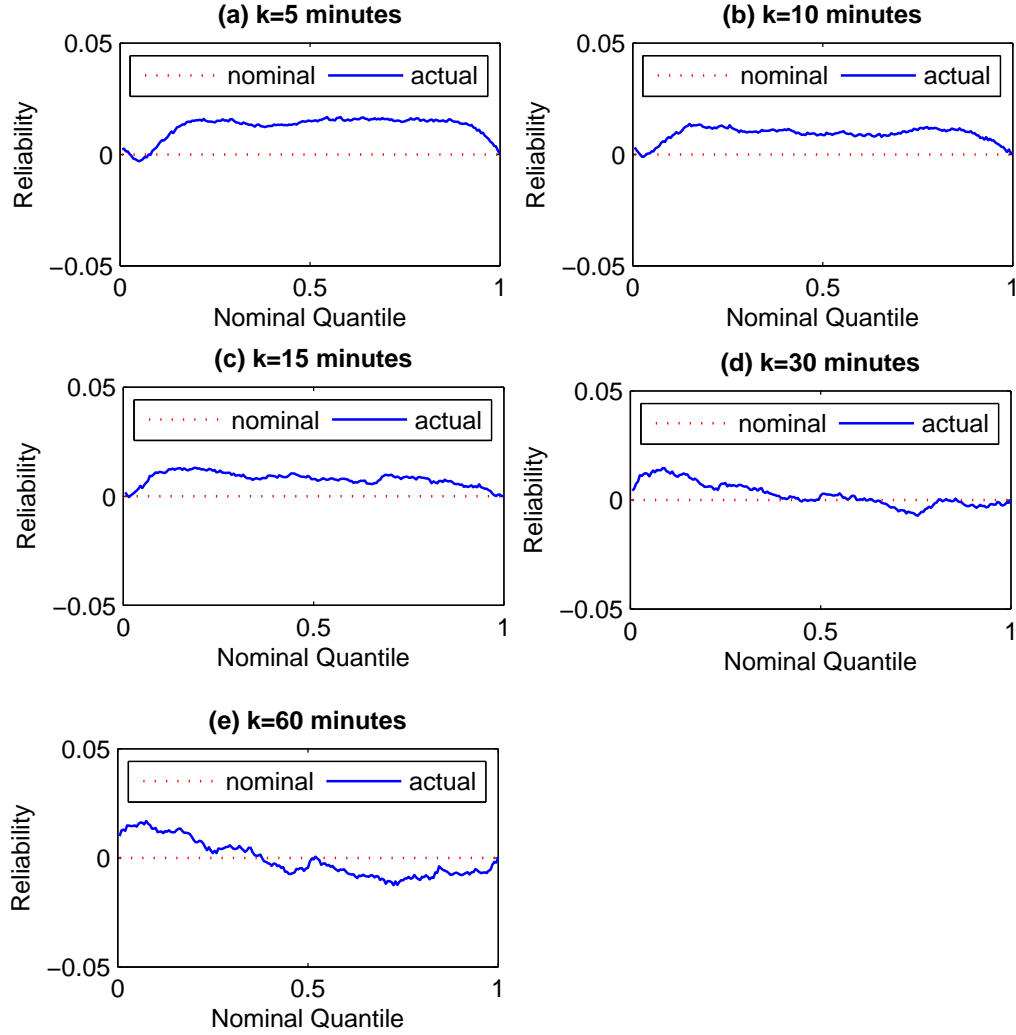


Figure 5.6: Reliability diagram of the CRM quantile estimates of a 120.6 MW wind farm (WF3) for various wind power forecast resolutions  $k = 5, 10, 15, 30$  and 60 minutes. The solid line represents the deviations from nominal of the actual and the dotted line of the nominal proportion  $p$ . The total reliability is significantly higher than the production specific reliability and improves with increasing forecast resolution.

nominal proportion  $p$ . From Fig. 5.7 and in comparison with the previous figures it becomes evident that the total reliability of each quantile estimate is significantly better than the production specific reliability, since for the total reliability deviations from nominal proportions vary between -1% and 1.5%. The reduced total reliability is attributed to the fact that performance of a quantile estimate might be low for high wind power productions, but these time intervals of high production are rare compared to low and medium wind power productions. Moreover, for quantiles above the median reliability appears to improve with decreasing forecast resolution  $k$ . This improvement is not in an absolute manner, since deviations from nominal for 5-minute averages and 60-minute averages have similar sizes, but rather because 5-minute averages have positive and 60-minute averages have negative deviations. Quantile estimates with negative deviations from the nominal are less favorable since they underestimate wind power variability.

Tables 5.4 and 5.5 provide the nominal and actual total probabilities, i.e weighted over all production levels, for all wind farms for forecast time resolutions  $k = 5$  and 60 minutes, respectively. Regarding the 95<sup>th</sup> percentile, for the majority of the wind farms the CRM quantile estimates for a 5-minute forecast resolution overestimate wind power variability, while for an hourly forecast resolution the CRM estimates underestimate wind power variability. These results indicate that the test year has more hourly intervals with higher deviations from the hourly average than the training year, whereas at the 5-minute resolution extreme deviations appear to be less frequent.

For comparison purposes the root mean square error (RMSE) of reliability is used, given by:

$$RMSE(r_k) = \sqrt{\sum_p r_{k,p}} = \sqrt{\sum_p \sum_j w_j \cdot r_{k,l_j,p}} \quad (5.22)$$

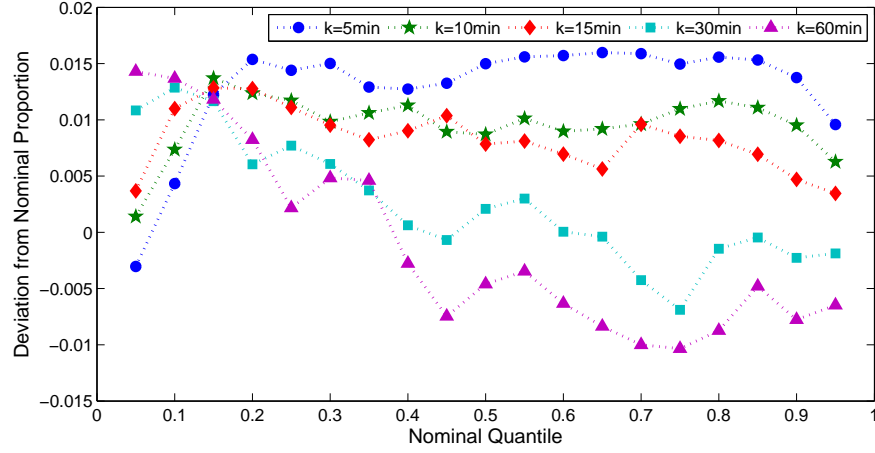


Figure 5.7: Reliability of CRM percentile estimates for various forecast resolutions  $k$  as a function of the nominal quantile  $p$  for a 120.6 MW wind farm (WF3). Deviations from nominal proportions vary between -1% and 1.5%.

The reliability RMSE summarizes the performance of all quantiles in a single value, however it does not distinguish between estimates with positive and negative deviations. Nonetheless, it is a useful means of comparing the reliability of the CRM quantile estimates among the various wind farms considered.

Figure 5.8 depicts the reliability RMSE of the CRM quantile estimates as a function of the wind farm nameplate capacity  $P_N$  for various wind power forecast resolutions  $k$ . The depicted mean deviations from nominal proportions of the CRM quantile estimates vary between 0.5% and 5.5%, while for hourly forecast resolutions deviations are less than 4%. Regarding the effect of forecast resolution  $k$ , most wind farms exhibit a small spread of reliability RMSE with varying resolution, which means that the reliability of a quantile estimate is not drastically affected by the forecast resolution. This result is also supported by the fact that there is no unique ordering of quantile estimate performance by forecast resolution, as for some wind farms the estimates

Table 5.4: Nominal and Actual Total Probabilities in percent for all Wind Farms (Forecast Time Resolution  $k = 5$  minutes)

	Wind Farm									
Nom.	2	3	4	5	6	7	11	13	14	15
5	6.4	4.7	5.1	6.9	4.8	5.3	6	5.5	8.2	4.5
10	10.7	10.4	10.2	12.9	9.7	10.5	11.2	10.5	12.5	9.8
15	15.1	16.2	15.6	18.1	14.8	16.0	16.8	15.5	16.1	15.2
20	19.6	21.5	21.2	23.0	19.8	21.3	22.4	20.7	19.6	20.8
25	24.2	26.4	26.3	27.9	24.9	26.8	28.0	25.8	23.3	26.3
30	28.9	31.5	31.7	32.9	29.8	32.1	33.8	30.7	27.1	31.6
35	33.8	36.3	36.8	38.0	34.8	37.1	38.8	35.8	31.3	36.9
40	38.8	41.3	42.1	43.1	39.9	42.5	43.6	41.0	35.7	42.2
45	44.1	46.3	47.1	48.0	45.1	47.6	48.3	46.2	40.3	47.6
50	49.2	51.5	52.2	52.9	50.3	52.7	52.8	51.4	45.1	52.7
55	54.7	56.6	57.1	58.0	55.5	57.8	57.5	56.6	50.2	57.7
60	60.0	61.6	62.0	63.0	60.9	62.7	62.2	61.9	55.3	62.7
65	65.4	66.6	67.2	68.0	66.0	67.8	66.9	67.1	60.4	67.7
70	70.8	71.6	72.1	72.7	71.2	72.8	71.7	72.3	65.5	72.6
75	76.1	76.5	77.2	77.5	76.3	77.6	76.5	77.5	70.6	77.5
80	81.4	81.6	82.2	82.2	81.3	82.6	81.4	82.4	76.0	82.3
85	86.4	86.5	87.0	86.9	86.3	87.3	86.2	87.4	81.6	87.1
90	91.4	91.4	91.7	91.3	91.1	91.6	90.9	92.1	87.5	91.8
95	96.0	96.0	96.1	95.9	95.7	95.9	95.5	96.4	94.3	96.1

Table 5.5: Nominal and Actual Total Probabilities in percent for all Wind Farms (Forecast Time Resolution  $k = 60$  minutes)

	Wind Farm									
Nom.	2	3	4	5	6	7	11	13	14	15
5	5.1	6.4	5.9	7.2	4.4	6.4	7.6	5.4	3.9	6.6
10	9.6	11.4	11.6	12.4	9.2	11.8	14	10.6	7.7	12.3
15	14.6	16.2	17.3	17.5	14.1	17.3	20.6	15.5	11.9	17.5
20	19.0	20.8	22.4	22.9	19.4	22.9	26.7	20.6	16.4	23.1
25	24.1	25.2	27.9	27.9	24.7	28.4	32.3	26.0	21.1	28.0
30	29.2	30.5	33.1	32.9	30.2	33.3	36.7	31.1	25.8	33.1
35	34.4	35.5	37.9	37.6	35.5	38.5	41.1	36.2	29.9	38.0
40	39.0	39.7	42.9	43.0	40.5	42.6	45.2	41.0	34.1	42.7
45	44.1	44.3	47.5	48.2	45.4	47.2	49.2	46.0	39.7	47.3
50	49.4	49.5	52.2	53.0	50.3	52.0	53.3	51.1	44.7	51.7
55	55.2	54.7	56.7	57.9	55.2	56.5	57.5	56.0	49.2	56.3
60	60.0	59.4	61.5	63.3	59.8	61.1	62.0	61.3	54.3	60.7
65	65.0	64.2	66.1	68.8	64.5	66.0	66.2	66.4	60.5	65.2
70	69.9	69.0	70.9	73.7	69.3	70.4	70.4	71.2	66.6	69.8
75	74.6	74.0	74.9	78.3	73.6	74.8	74.9	75.6	71.6	74.3
80	79.3	79.1	79.9	83.2	78.5	79.3	79.4	80.4	76.7	79.3
85	84.0	84.5	84.6	87.7	83.5	84.0	84.2	84.8	82.7	84.0
90	89.6	89.2	89.5	92.1	88.5	88.9	89.0	89.6	88.4	89.3
95	95.2	94.4	94.5	96.3	94.0	94.6	93.8	94.3	93.8	94.5

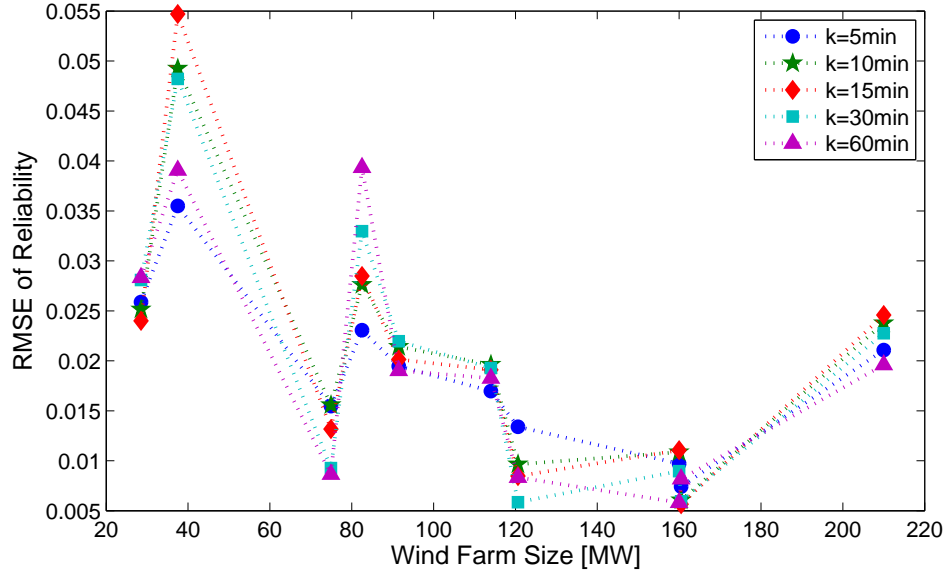


Figure 5.8: RMSE of CRM quantile estimates' reliability for various wind power forecast resolutions  $k$  as a function of wind farm nameplate capacity.

perform better for hourly forecasts, while for others the best performance is for 5-minute averaged forecasts. On the other hand, for wind farms within the same region deviations from nominal tend to decrease with increasing wind farm nameplate capacity and increasing wind turbine size.

For the remainder of this chapter focus will be placed on the total  $r_{k,p}$  and not the production specific  $r_{k,l_j,p}$  reliability of the CRM quantile estimates and their root mean squared error of reliability  $\text{RMSE}(r_k)$ . Specifically, for the time adaptive quantile estimation methods presented next, the tuning parameters are chosen with respect to minimization of the  $\text{RMSE}(r_k)$ .

### 5.3.4 Exponentially Weighted Moving Average

In Section 5.3.3 a static method to obtain CRM quantile estimates is provided, in which the  $p^{th}$  quantile estimate  $\hat{CRM}_{k,l_j,p}$  does not change over time. In this section a time adaptive method to estimate CRM quantiles is described, using an exponentially weighted moving average (EWMA) approach to update the quantile estimates following an equation similar to (5.14).

Under this method, a limited size buffer holds the last  $N_{b,k}$  observed wind power values  $x_n$ ,  $n = 1, 2, \dots, N_{b,k}$ . Let the sample quantile of the values contained in the buffer at its  $i^{th}$  filling be denoted as  $CRM_{\{I\}k,l_j,p} = [M_{low\{I\}k,l_j,p}, M_{up\{I\}k,l_j,p}]$ . The pair  $(M_{low\{I\}k,l_j,p}, M_{up\{I\}k,l_j,p})$  is the solution of the system of equations (3.7) and (3.10) solved in Section 3.3.2 using the  $N_{b,k}$  wind power data stored in the  $i^{th}$  filling of the buffer as input. Also, let  $CRM_{\{I\}k,l_j,p}^*$  denote the  $p^{th}$  CRM quantile estimate for the wind power values stored in the  $i^{th}$  filling of the buffer. An exponentially weighted moving average estimate of the  $p^{th}$  CRM quantile  $CRM_{\{I\}k,l_j,p}^*$  of the  $i^{th}$  iteration is computed as follows:

$$CRM_{\{I\}k,l_j,p}^* = (1 - w_{b,k}) \cdot CRM_{\{I-1\}k,l_j,p}^* + w_{b,k} \cdot CRM_{\{I\}k,l_j,p} \quad (5.23)$$

where  $CRM_{\{I-1\}k,l_j,p}^*$  is the estimate of the  $p^{th}$  CRM quantile obtained from the previously filled buffer,  $CRM_{\{I\}k,l_j,p}$  is the sample quantile of the  $i^{th}$  iteration and  $w_{b,k}$  is the weight. For  $i = 1$  the best estimate of the  $p^{th}$  CRM quantile is the sample quantile. i.e.  $CRM_{\{1\}k,l_j,p}^* = CRM_{\{1\}k,l_j,p}$  and  $CRM_{\{0\}k,l_j,p}^* = 0$ . After each evaluation of (5.23) the obtained quantile  $CRM_{\{I\}k,l_j,p}^*$  is used as an estimate for the wind power data of the  $(i+1)^{th}$  filling of the buffer. Thus, for the wind power data in the  $(i+1)^{th}$  iteration  $\hat{CRM}_{\{I+1\}k,l_j,p}$  is used as a  $p^{th}$  quantile estimate, where

$$\hat{CRM}_{\{I+1\}k,l_j,p} = CRM_{\{I\}k,l_j,p}^* \quad i = 1, 2, \dots \quad (5.24)$$

For  $i = 1$  the last  $N_{b,k}$  wind power points of the training set (year 3) are used to fill the buffer. Then the buffer fills from the data in the test set (year 4). For each of the considered  $N_{b,k}$ -long subsets the exponentially weighted moving average estimate of the  $p^{th}$  CRM quantile  $CRM_{k,l_j,p}^*$  is calculated from (5.23). Then, each of the calculated quantiles is used as an estimate on the wind power data of the next  $N_{b,k}$ -long set, according to (5.24).

The values of the buffer size  $N_{b,k}$  and weight  $w_{b,k}$  used to obtain the quantile estimates for each wind farm and forecast time resolution  $k$  are given in Table 5.6. These values are the outcome of iterative calculations with the goal of minimizing the  $RMSE(r_k)$  for each forecast time resolution. For most wind farms a buffer size corresponding to  $N_{b,k} = 2$  weeks of wind power data is used for forecast time resolutions  $k = 5, 10$  and 15 minutes, while  $N_{b,k} = 4$  weeks is used for forecast time resolutions  $k = 30$  and 60 minutes. For two of the wind farms  $N_{b,k} = 8$  weeks produces the most optimal results under the method considered. The choice of the buffer size  $N_{b,k}$  is significant, because it affects the sample quantile  $CRM_{\{I\},k,l_j,p}$  at each iteration  $i$ , thus a small buffer size may produce a very inaccurate sample quantile. Regarding the weights  $w_{b,k}$ , small weights indicate that older quantile estimates are taken more into account than the current sample quantile. A weight of  $w_{b,k} = 0$  corresponds to using the sample quantile of a subset of the training set as the quantile estimate for the entire test set. On the other hand, large weights indicate that the sample quantile of the previous filled buffer performs better than older quantile estimate values. The  $w_{b,k}$  values in Table 5.6 vary from zero to one, with optimal  $w_{b,k}$  values being small for half of the considered wind farms.

The  $p^{th}$  CRM quantile estimates  $\hat{CRM}_{\{I\},k,l_j,p}$ ,  $i \geq 2$ , are evaluated using their total reliability from (5.21). Fig.5.9 depicts the reliability diagrams, i.e. deviations from nominal proportions, of the CRM quantile estimates of a



Table 5.6: Buffer Size  $N_{b,k}$  in Weeks and Weights  $w_{b,k}$  for all Wind Farms and Forecast Time Resolutions  $k$  (Exponentially Weighted Moving Average)

		Forecast Time Resolution k				
		5 min	10 min	15 min	30 min	60 min
WF2	$w_{b,k}$	0.6	0.2	0.2	0.3	0.14
	$N_{b,k}$	2	2	2	4	4
WF3	$w_{b,k}$	0.8	0.8	0.9	0.9	1
	$N_{b,k}$	8	8	8	8	8
WF4	$w_{b,k}$	0.7	0.7	0.7	1	1
	$N_{b,k}$	2	2	2	4	4
WF5	$w_{b,k}$	0.3	0.4	0.5	0.6	0.5
	$N_{b,k}$	2	2	2	4	4
WF6	$w_{b,k}$	0.1	0.06	0.05	0.2	0.1
	$N_{b,k}$	2	2	2	4	4
WF7	$w_{b,k}$	0.7	0.7	0.7	1	1
	$N_{b,k}$	2	2	2	4	4
WF11	$w_{b,k}$	0	0	0	0.2	0.1
	$N_{b,k}$	2	2	2	4	4
WF13	$w_{b,k}$	0.8	0.7	0.7	0.56	0.5
	$N_{b,k}$	8	8	8	8	8
WF14	$w_{b,k}$	1	1	0.9	1	1
	$N_{b,k}$	2	2	2	4	4
WF15	$w_{b,k}$	0.5	0.6	0.6	0.3	0.2
	$N_{b,k}$	2	2	2	4	4

210 MW wind farm (WF7) for various wind power forecast resolutions  $k = 5, 10, 15, 30$  and 60 minutes. In these diagrams, the dotted line represents deviations from nominal of the nominal proportions  $p$ , i.e. zero deviations. The dashed line represents deviations from nominal proportions using the sample quantile from data in the training set (year 3) as a CRM quantile estimate on the wind power data in the test set (year 4), as described in Section 5.3.3. The solid line depicts deviations from nominal proportions when the exponentially weighted moving average quantile is used as an estimate on the test set (year 4).

Figure 5.9 reveals that when the quantile estimate is updated periodically using an exponentially weighted moving average approach its reliability shows improvement for small forecast time resolutions and high rank quantiles. To compare the performance of the exponentially weighted moving average approach on the considered wind farms and forecast resolutions the reliability RMSE from (5.22) is used, which summarizes the performance of all CRM quantile estimates. The reliability RMSE values are depicted in Fig. 5.10 as a function of the wind farm nameplate capacity for various forecast time resolutions. Under the exponentially weighted moving average approach reliability RMSE values range from 0.5% to 4%, a range reduced compared to the respective Fig. 5.8 of the sample quantile estimate approach.

Indeed, Fig. 5.11 depicts the reliability RMSE difference between the exponentially weighted moving average and the sample quantile estimate approach as a function of the wind farm nameplate capacity for various wind power forecast resolutions. A negative difference indicates that the exponentially weighted moving average is more reliable than the sample quantile estimate. The reliability RMSE of the time adaptive estimate is higher than that of the static sample quantile estimate by no more than 0.67%, while the

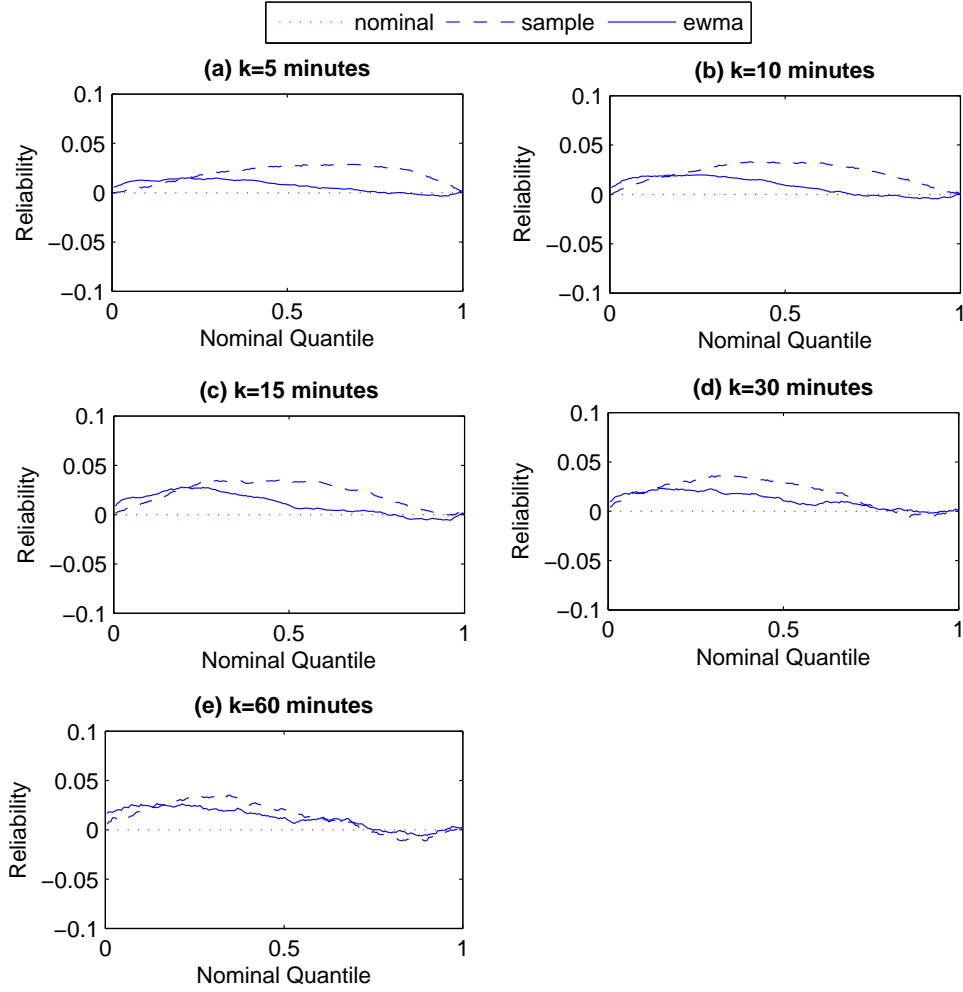


Figure 5.9: Reliability diagram of the CRM quantile estimates of a 210 MW wind farm (WF7) for various wind power forecast resolutions  $k = 5, 10, 15, 30$  and  $60$  minutes under the exponentially weighted moving average quantile estimate approach. The solid line represents the deviations from nominal proportions using an exponentially weighted moving average (ewma) quantile estimate, while the dashed line represents deviations from nominal using a sample quantile estimate. Updating the quantile estimate at each iteration improves the quantile estimate reliability, especially for small forecast time resolutions and high rank quantiles.

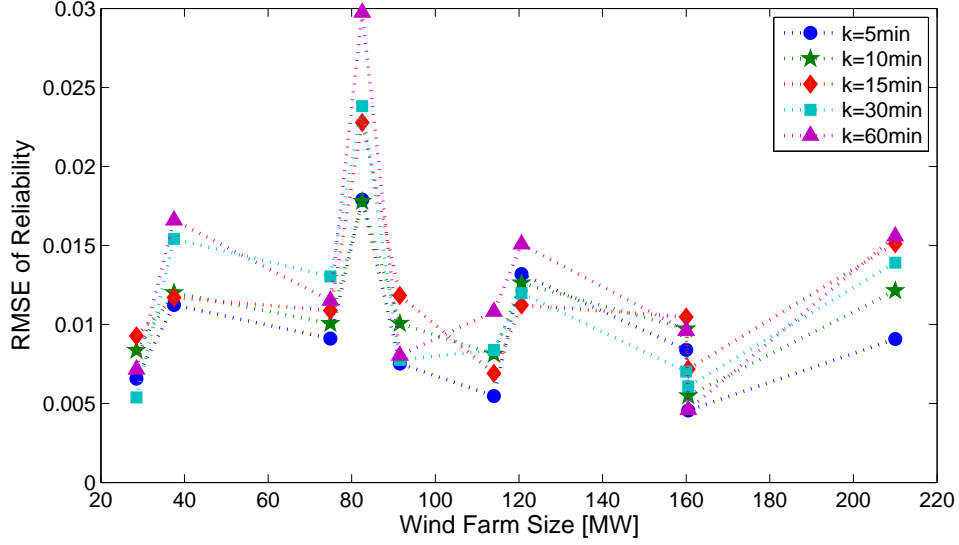


Figure 5.10: RMSE of CRM quantile estimates' reliability under the exponentially weighted moving average quantile estimate approach for various wind power forecast resolutions  $k$  as a function of wind farm nameplate capacity.

maximum reduction reaches 4.3%. Average reliability RMSE reduction for all wind farms considered is 1% under all forecast resolutions.

Comparing Fig.5.10 and Fig.5.11, it is observed that in all the cases where the sample quantile estimate has reliability RMSE more than 1% a reduction in RMSE is observed with the exponentially weighted moving average quantile estimate. However, in some cases with sample quantile estimate reliability RMSE less than 1% a slight increase in reliability is observed, which is not of high significance since an RMSE of 1% already indicates a quantile estimate of adequate reliability. Thus, the exponentially weighted moving average quantile estimate performs better than the sample quantile for the wind farms and forecast resolutions considered, however finding the optimal buffer size  $N_{b,k}$  and weight  $w_{b,k}$  can be cumbersome. Consequently, though time adaptive

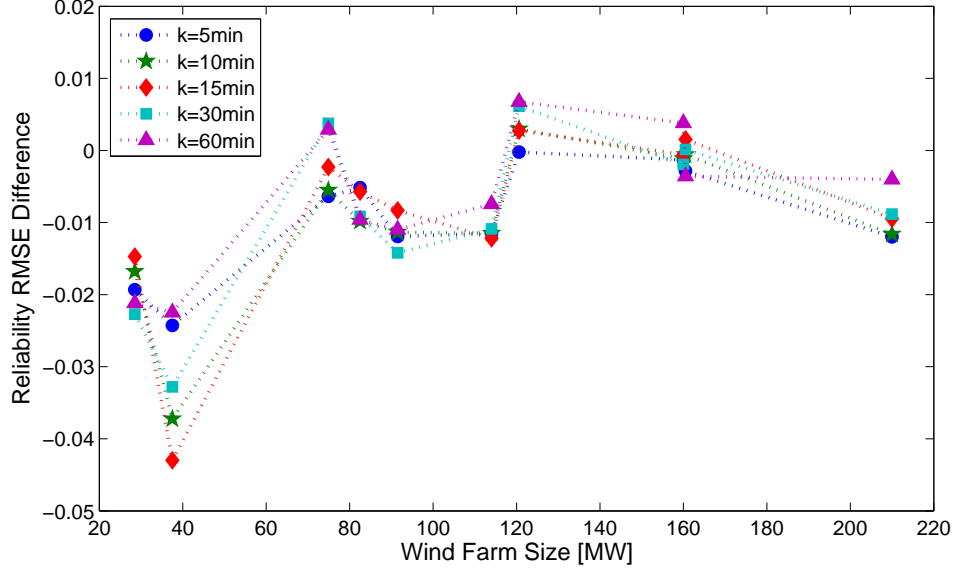


Figure 5.11: CRM quantile reliability RMSE difference between the exponentially weighted moving average and the sample quantile estimate approach as a function of wind farm nameplate capacity for various wind power forecast resolutions. The time adaptive exponentially weighted moving average quantile estimate is in most cases at least as reliable as the static sample quantile estimate.

methods seem to better capture the variable nature of wind power resulting in more reliable  $p^{th}$  CRM quantile estimates, their computational aspects should also be taken into account.

### 5.3.5 Exponentially Weighted Stochastic Approximation

In this section an exponentially weighted stochastic approximation approach is considered for obtaining a CRM quantile estimate. Expanding on (5.17) for a random variable  $X$  and an  $N$ -long buffer the following update equation is proposed in [83] for the  $p^{th}$  quantile estimate of the  $i^{th}$  iteration

$S_{X_N,i}(p)$ :

$$S_{X_N,i}(p) = S_{X_N,i-1}(p) + \hat{f}_{X_N,i}(p)^{-1} \cdot w_i \cdot \left( p - \frac{\sum_{i=1}^N I(X_{N,i} \leq S_{X_N,i-1}(p))}{N} \right) \quad (5.25)$$

where  $I(\cdot)$  is the indicator function,  $w_i$  is the weight, and  $\hat{f}_{X_N,i}(p)$  is the incremental density estimate at the  $i^{th}$  iteration. The weights  $w_i$  can be of the form  $1/n$  for stationary data or constant for non-stationary data. In reality, the stochastic approximation quantile estimate is essentially derived from a local linear approximation of the true cdf  $F_{X,i}$  at the true quantile  $q_{X,i}(p)$ , since  $f_{X,i}(p) = F'_{X,i}(q_{X,i}(p))$  is the density of  $F_{X,i}$  at  $q_{X,i}(p)$ . The complexity of the stochastic approximation approach stems from using this density of the underlying distribution, which is in general unknown and has to be estimated from the data. Definitions of the  $f_{X,i}$  estimates and methods to update them can be found in [83, 84].

For the CRM quantile estimates the algorithm presented in [84] is adopted. In this algorithm the weights are constant, thus this quantile estimation method is an exponentially weighted stochastic approximation approach. As before, a limited size buffer holds the last  $N_{b,k}$  observed wind power values  $y_n$ ,  $n = 1, 2, \dots, N_{b,k}$  of the data in the test set  $Y$ . Let the sample quantile from the wind power values in the training set  $X$  be denoted as  $CRM_{\{X\}k,l_j,p} = [M_{low\{X\}k,l_j,p}, M_{up\{X\}k,l_j,p}]$ , and let  $CRM_{\{I\}k,l_j,p}^* = [M_{low\{I\}k,l_j,p}^*, M_{up\{I\}k,l_j,p}^*]$  denote the  $p^{th}$  CRM quantile estimate for the wind power values stored in the  $i^{th}$  filling of the buffer.

The initialization of the algorithm is done by calculating  $CRM_{\{0\}k,l_j,p}^*$  and  $f_{\{0\}k,l_j,p}^*$ :

1. Set  $CRM_{\{0\}k,l_j,p}^*$  to be the sample quantile of the wind power values in

the training set  $X$ , i.e.

$$CRM_{\{0\}k,l_j,p}^* = CRM_{\{X\}k,l_j,p} = [M_{low\{X\}k,l_j,p}, M_{up\{X\}k,l_j,p}] \quad (5.26)$$

2. Estimate the scale of  $f_{\{0\}k,l_j,p}^*$  using the interquartile range  $r_{\{0\}k,l_j}^*$ . Take

$$c_{up\{0\}k,l_j}^* = r_{up\{0\}k,l_j}^* \sum_{i=1}^{M_{k,l_j}} \frac{i^{-1/2}}{M_{k,l_j}} = (M_{up\{X\}k,l_j,0.75} - M_{up\{X\}k,l_j,0.25}) \sum_{i=1}^{M_{k,l_j}} \frac{i^{-1/2}}{M_{k,l_j}} \quad (5.27)$$

$$c_{low\{0\}k,l_j}^* = r_{low\{0\}k,l_j}^* \sum_{i=1}^{M_{k,l_j}} \frac{i^{-1/2}}{M_{k,l_j}} = (M_{low\{X\}k,l_j,0.25} - M_{up\{X\}k,l_j,0.75}) \sum_{i=1}^{M_{k,l_j}} \frac{i^{-1/2}}{M_{k,l_j}} \quad (5.28)$$

where  $M_{k,l_j}$  is the length of the subset of the test set with  $k$ -long average wind power being  $l_j$ .

3. Take the initial density estimate  $f_{\{0\}k,l_j,p}^*$  to be:

$$f_{\{0\}k,l_j,p}^* = (2c_{\{0\}k,l_j}^* M_{k,l_j})^{-1} \max\left\{\sum_{i=1}^{M_{k,l_j}} A_{\{0\}i,k,l_i,p}, 1\right\} \quad (5.29)$$

where

$$A_{\{0\}i,k,l_j,p} = I(|M_{up i,k,l_j} - M_{up\{X\}k,l_j,p}| \leq c_{up\{0\}k,l_j}^*) \cdot I(|M_{low i,k,l_j} - M_{low\{X\}k,l_j,p}| \geq c_{low\{0\}k,l_j}^*) \quad (5.30)$$

and  $c_{\{0\}k,l_j}^* = (c_{up\{0\}k,l_j}^* + c_{low\{0\}k,l_j}^*)/2$ . This is the density of observations in a neighborhood of size  $2c_{\{0\}k,l_j}^*$  of  $CRM_{\{0\}k,l_j,p}^*$ , unless the fraction of observations in the neighborhood is zero.

When the  $N_{b,k}$  wind power values of the  $i^{th}$  filling of the buffer from the test data become available, the quantile  $CRM_{\{I\}k,l_j,p}^*$  and the density  $f_{\{I\}k,l_j,p}^*$  estimates are updated as follows:

1. The quantile estimate  $CRM_{\{I\}k,l_j,p}^*$  is given by:

$$CRM_{\{I\}k,l_j,p}^* = CRM_{\{I-1\}k,l_j,p}^* + \frac{w_{b,k}}{f_{\{I-1\}k,l_j,p}^*} \left( p - \frac{B_{\{I\}k,l_j,p}}{N_{b,k,l_j}} \right) \quad (5.31)$$

where

$$B_{\{I\}k,l_j,p} = \sum_{i=1}^{N_{b,k,l_j}} I(M_{up_{i,k,l_j}} \leq M_{up\{I-1\}k,l_j,p}^*) \cdot I(M_{low_{i,k,l_j}} \geq M_{low\{I-1\}k,l_j,p}^*) \quad (5.32)$$

with  $N_{b,k,l_j}$  being the length of a subset of the data in the buffer with  $k$ -long average wind power being  $l_j$ .

2. The density estimate  $f_{\{I\}k,l_j,p}^*$  is given by:

$$f_{\{I\}k,l_j,p}^* = (1 - w_{b,k})f_{\{I-1\}k,l_j,p}^* + \frac{w_{b,k}}{2c_{\{I-1\}k,l_j}^* N_{b,k}} \max\left\{\sum_{i=1}^{N_{b,k}} A_{\{I\}i,k,l_j,p}, 1\right\} \quad (5.33)$$

where

$$A_{\{I\}i,k,l_j,p} = I(|M_{up_{i,k,l_j}} - M_{up\{I-1\}k,l_j,p}^*| \leq c_{up\{I-1\}k,l_j}^*) \cdot I(|M_{low_{i,k,l_j}} - M_{low\{I-1\}k,l_j,p}^*| \geq c_{low\{I-1\}k,l_j}^*) \quad (5.34)$$

3. The neighborhood size of the next updating  $c_{\{I\}k,l_j}^*$  is defined using the interquartile range of the current quantile estimate:

$$c_{up\{I\}k,l_j}^* = r_{up\{I\}k,l_j}^* \cdot c(I, k, l_j) = (M_{up\{I\}k,l_j,0.75} - M_{up\{I\}k,l_j,0.25}) \cdot c(I, k, l_j) \quad (5.35)$$

$$c_{low\{I\}k,l_j}^* = r_{low\{I\}k,l_j}^* \cdot c(I, k, l_j) = (M_{low\{I\}k,l_j,0.25} - M_{up\{I\}k,l_j,0.75}) \cdot c(I, k, l_j) \quad (5.36)$$

where  $c(I, k, l_j) = \sum_{i=1+(I-1) \cdot N_{b,k,l_j}}^{I \cdot N_{b,k,l_j}} i^{-1/2} / N_{b,k,l_j}$  is the average updating weight the stochastic approximation estimator would assign to the  $N_{b,k,l_j}$  values of the  $i^{th}$  filling of the buffer and  $c_{\{I\}k,l_j}^* = (c_{up\{I\}k,l_j}^* + c_{low\{I\}k,l_j}^*) / 2$ .



After each evaluation of (5.31) the obtained quantile  $CRM_{\{I\}k,l_j,p}^*$  is used as an estimate for the wind power data of the  $(i+1)^{th}$  filling of the buffer. Thus, for the wind power data in the  $(i+1)^{th}$  iteration  $C\hat{R}M_{\{I+1\}k,l_j,p}$  is used as a  $p^{th}$  quantile estimate, where

$$C\hat{R}M_{\{I+1\}k,l_j,p} = CRM_{\{I\}k,l_j,p}^* \quad i = 0, 1, \dots \quad (5.37)$$

For  $i = 0$  the initial quantile and density estimated are obtained from all the data in the training set (year 3) and not an  $N_{b,k}$ -long subset of it. Then the buffer fills from the data in the test set (year 4). For each of the considered  $N_{b,k}$ -long subsets the stochastic approximation estimate of the  $p^{th}$  CRM quantile  $CRM_{k,l_j,p}^*$  is calculated from (5.31). Then, each of the calculated quantiles is used as an estimate on the wind power data of the next  $N_{b,k}$ -long set, according to (5.37).

The reason for choosing a large training set to obtain initial estimates is because under the exponentially weighted stochastic approximation method initial estimates are crucial for the convergence of the method, since poor estimates of  $CRM_{\{0\}k,l_j,p}^*$  and  $f_{\{0\}k,l_j,p}^*$  will lead to estimates further along in the process being no better than the sample quantile estimate. Moreover, since a large number of iterations is necessary so as to reach convergence, a fairly small buffer size  $N_{b,k}$  of one week is considered for all forecast time resolutions and wind farms. The values of the weight  $w_{b,k}$  used to obtain the quantile estimates for each wind farm and forecast time resolution  $k$  are given in Table 5.7. These values are the outcome of iterative calculations with the goal of minimizing the  $RMSE(r_k)$  for each forecast time resolution. As is the case for the exponentially weighted moving average, small weights  $w_{b,k}$  put more weight on the initial quantile estimates with  $w_{b,k} = 0$  corresponding to using the sample quantile of the training set as the quantile estimate for the entire

Table 5.7: Weights  $w_{b,k}$  for all Wind Farms and Forecast Time Resolutions  $k$  (Stochastic Approximation)

	Forecast Time Resolution k				
	5 min	10 min	15 min	30 min	60 min
WF2	0.24	0.62	0.46	0.26	0.18
WF3	0.56	0.44	0.44	0.24	0.2
WF4	0.76	0.7	0.84	0.48	0.38
WF5	0.76	0.68	0.62	0.56	0.36
WF6	0.46	0.08	0.06	0	0.22
WF7	0.66	0.64	0.62	0.56	0.46
WF11	0.7	0.72	0.66	0.46	0.36
WF13	0.7	0.54	0.5	0.18	0.26
WF14	0.34	0	0.02	0.02	0
WF15	0.68	0.64	0.5	0.44	0.34

test set. On the other hand, large weights indicate that the initial quantile estimate needs heavier adjustment. The  $w_{b,k}$  values in Table 5.7 vary from zero to 0.84, with optimal  $w_{b,k}$  taking mid-range values ([0.4-0.7]) for half of the considered wind farms. Comparing the values in Tables 5.6 and 5.7, the optimal  $w_{b,k}$  values have similar levels under both methods for most of the considered wind farms.

The  $p^{th}$  CRM quantile estimates  $C\hat{R}M_{\{I\}k,l_j,p}$ ,  $i \geq 2$ , are evaluated using their total reliability from (5.21). Fig.5.12 depicts the reliability diagrams, i.e. deviations from nominal proportions, of the CRM quantile estimates of a 210 MW wind farm (WF7) for various wind power forecast resolutions  $k = 5, 10, 15, 30$  and 60 minutes. In these diagrams, the dotted line represents de-

viations from nominal of the nominal proportions  $p$ , i.e. zero deviations. The dashed line represents deviations from nominal proportions using the sample quantile from data in the training set (year 3) as a CRM quantile estimate on the wind power data in the test set (year 4), as described in Section 5.3.3. The solid line depicts deviations from nominal proportions when exponentially weighted stochastic approximation is used to obtain a quantile estimate on the test set (year 4).

Figure 5.12 reveals that when the quantile estimate is updated periodically using an exponentially weighted stochastic approximation approach its reliability shows improvement, especially for small forecast time resolutions, for all rank quantiles. For large forecast time resolutions high rank quantiles under the exponentially weighted stochastic approximation approach have positive reliability, which is favored over the negative reliability of the sample quantiles. To compare the performance of the exponentially weighted stochastic approximation approach on the considered wind farms and forecast resolutions the reliability RMSE from (5.22) is used, which summarizes the performance of all CRM quantile estimates. The reliability RMSE values are depicted in Fig. 5.13 as a function of the wind farm nameplate capacity for various forecast time resolutions. Using an exponentially weighted stochastic approximation approach the reliability RMSE values of the CRM quantile estimates are less than 1% for all but two wind farms.

Indeed, Fig. 5.14 depicts the reliability RMSE difference between the stochastic approximation and the sample quantile estimate approach as a function of the wind farm nameplate capacity for various wind power forecast resolutions. The reliability RMSE of the exponentially weighted stochastic approximation estimate is at least as good as the sample quantile's for all forecast time resolutions and wind farms considered, since all differences are

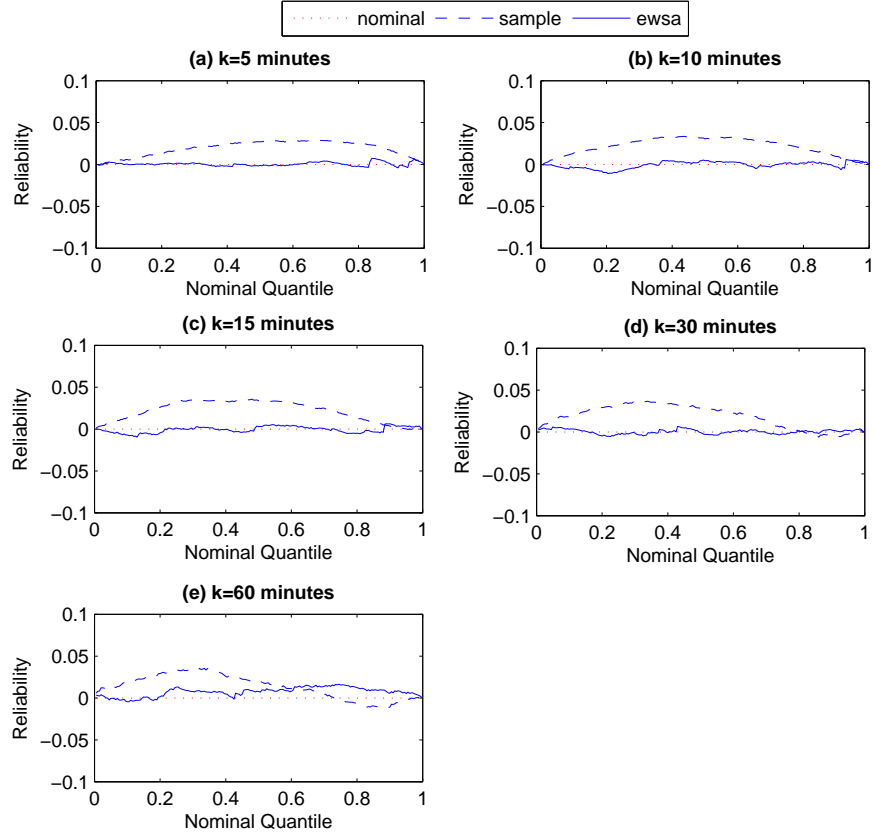


Figure 5.12: Reliability diagram of the CRM quantile estimates of a 210 MW wind farm (WF7) for various wind power forecast resolutions  $k = 5, 10, 15, 30$  and 60 minutes under the exponentially weighted stochastic approximation quantile estimate approach. The solid line represents the deviations from nominal proportions using exponentially weighted stochastic approximation (ewsa) quantile estimate, while the dashed line represents deviations from nominal using a sample quantile estimate. The reliability of the CRM quantiles under the exponentially weighted stochastic approximation approach is very close to the nominal one, especially for small forecast time resolutions, for all rank quantiles. For large forecast time resolutions high rank quantiles under the exponentially weighted stochastic approximation approach have positive reliability, which is favored over the negative reliability of the sample quantiles.

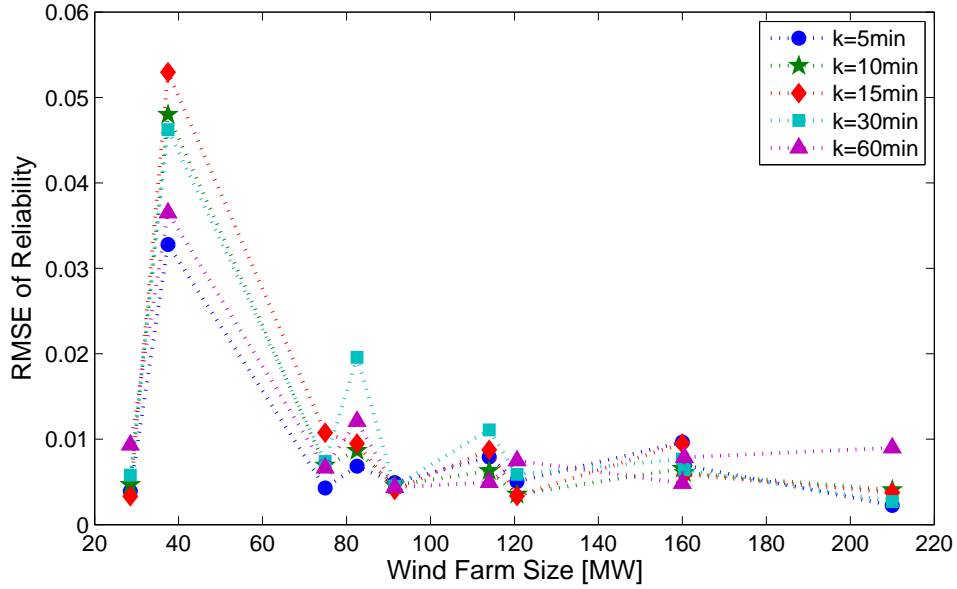


Figure 5.13: RMSE of CRM quantile estimates' reliability under the exponentially weighted stochastic approximation quantile estimate approach for various wind power forecast resolutions  $k$  as a function of wind farm nameplate capacity.

either zero or negative. For the majority of the wind farms reliability is significantly improved with deviations reaching 3% and average reliability RMSE reduction for all wind farms considered is close to 1% under all forecast time resolutions  $k$ .

However, for a 37.5 MW wind farm (WF14) quantile estimates under a sample and an exponentially weighted stochastic approximation approach are almost identical since in both cases reliability RMSE values are similar and in the range of 4%. In this case the optimal weights under the exponentially weighted stochastic approximation approach are close to zero and lead to a quantile estimate as good as the initial guess. On the other hand, for the same wind farm under the exponentially weighted moving average with weights close

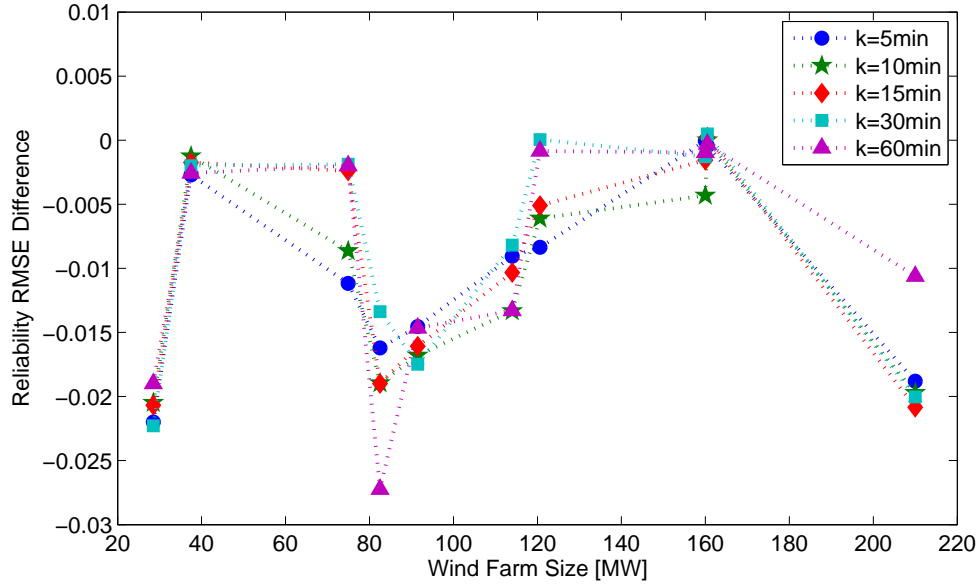


Figure 5.14: CRM quantile reliability RMSE difference between the exponentially weighted stochastic approximation and the sample quantile estimate approach as a function of wind farm nameplate capacity for various wind power forecast resolutions. The exponentially weighted stochastic approximation quantile estimate is in all cases at least as reliable as the sample quantile estimate.

to 1, a significantly reduced RMSE compared to that of the sample quantile estimate is reached. This means that for the specific wind farm the training set's sample quantile is a bad initial estimate. But although the exponentially weighted moving average can recover from this bad initial estimate in the period of a year, the exponentially weighted stochastic approximation would need more time to do so. Thus, though the exponentially weighted stochastic approximation approach leads to more reliable CRM quantile estimates, the choice of initial estimates and iterations, i.e. length and number of filled buffers, significantly affects the convergence of the method.

### 5.3.6 Method Evaluation and Comparison

In this section the three considered CRM quantile estimation methodologies are compared using the reliability RMSE, the sharpness and the resolution of the resulting quantile estimates. Let  $y_m$ ,  $m = 1, 2, \dots, M$ , denote the actual wind power data in the test set and the  $k$ -averaged wind power data of the test set  $y_{k,i} = \sum_{m=(i-1)k+1}^{ik} y_m$ ,  $i = 1, 2, \dots, \lfloor M/k \rfloor$  denote a perfect wind power forecast series with forecast time resolution  $k$ . For each point  $y_{k,i}$  of the wind power forecast series a wind power variability forecast consisting of  $CRM_{k,l_j=y_{k,i},p}$  quantile estimates for various probabilities  $p$  is generated with one of the three considered approaches: static sample (Sample), exponentially weighted moving average (EWMA) and exponentially weighted stochastic approximation (EWSA).

The reliability of the quantile estimates for each method and forecast time resolution is calculated from (5.21) and the reliability RMSE from (5.22). The sharpness of the quantile estimates is evaluated using the sample mean of the interquartile range series, while for the resolution the sample standard deviation of the interquartile range series is used. The interquartile range series  $IQR_{k,i}$  is calculated from the 75<sup>th</sup> and 25<sup>th</sup> quantile estimates of each point in the wind power forecast series  $y_{k,i}$ . Two positive interquartile range series are generated for the upper  $M_{up}$  and lower  $M_{low}$  interval endpoints of the conditional range interval, i.e:

$$IQR_{up_{k,i}} = M_{up_{k,l_j=y_{k,i},0.75}} - M_{up_{k,l_j=y_{k,i},0.25}} \quad i = 1, 2, \dots, \lfloor M/k \rfloor \quad (5.38)$$

and

$$IQR_{low_{k,i}} = M_{low_{k,l_j=y_{k,i},0.25}} - M_{low_{k,l_j=y_{k,i},0.75}} \quad i = 1, 2, \dots, \lfloor M/k \rfloor \quad (5.39)$$

Thus, for each quantile estimation methodology two sharpness values:

$$s_{k,up} = \sum_i \frac{IQR_{up_{k,i}}}{[M/k]} \quad (5.40)$$

and

$$s_{k,low} = \sum_i \frac{IQR_{low_{k,i}}}{[M/k]} \quad (5.41)$$

along with two resolution values

$$RES_{k,up} = \sqrt{\frac{1}{[M/k] - 1} \sum_{i=1}^{[M/k]} (IQR_{up_{k,i}} - s_{k,up})^2} \quad (5.42)$$

and

$$RES_{k,low} = \sqrt{\frac{1}{[M/k] - 1} \sum_{i=1}^{[M/k]} (IQR_{low_{k,i}} - s_{k,low})^2} \quad (5.43)$$

are calculated.

The reliability RMSE, sharpness (up and low) and resolution (up and low) values under the three considered approaches (sample, ewma and ewsa) are given in Tables 5.8, 5.9, 5.10, 5.11, and 5.12, respectively, for all wind farms considered and for wind power forecast time resolutions  $k= 5, 10, 15, 30$  and  $60$  minutes. In these tables for each wind farm and forecast time resolution the performance of the best quantile estimate is highlighted in bold. It is reminded that the lowest reliability RMSE, the lowest sharpness and the highest resolution are rewarded.

The reliability RMSE of the quantile estimates under the three different approaches has already been analyzed in Sections 5.3.3–5.3.5. As is verified by Table 5.8 adapting the quantile estimate using an exponentially weighted moving average or stochastic approximation approach leads in more reliable quantile estimates than the static sample quantile approach, with the exponentially weighted stochastic approximation achieving on average lower deviations



Table 5.8: RMSE of Reliability ( $RMSE(r_k)$ ) in percent for all Wind Farms using three Quantile Estimate Approaches (Sample, EWMA, EWSA)

k = 5 minutes										
	Wind Farm									
Estimate	2	3	4	5	6	7	11	13	14	15
Sample	0.97	1.34	1.7	2.59	0.74	2.11	2.31	1.55	3.55	1.95
EWMA	<b>0.84</b>	1.32	<b>0.55</b>	0.66	<b>0.46</b>	0.91	1.79	0.91	<b>1.12</b>	0.75
EWSA	0.97	<b>0.63</b>	0.99	<b>0.46</b>	0.7	<b>0.23</b>	<b>1.22</b>	<b>0.43</b>	3.48	<b>0.61</b>
k = 10 minutes										
	Wind Farm									
Estimate	2	3	4	5	6	7	11	13	14	15
Sample	1.09	0.96	1.96	2.52	0.61	2.38	2.76	1.56	4.92	2.14
EWMA	0.97	1.26	0.81	0.84	<b>0.55</b>	1.21	1.78	1.01	<b>1.2</b>	1.01
EWSA	<b>0.84</b>	<b>0.56</b>	<b>0.63</b>	<b>0.54</b>	0.61	<b>0.54</b>	<b>1.1</b>	<b>0.71</b>	4.8	<b>0.51</b>
k = 15 minutes										
	Wind Farm									
Estimate	2	3	4	5	6	7	11	13	14	15
Sample	1.11	0.85	1.91	2.4	<b>0.56</b>	2.46	2.85	1.32	5.47	2.01
EWMA	1.05	1.12	<b>0.69</b>	0.93	0.72	1.51	2.28	1.09	<b>1.17</b>	1.18
EWSA	<b>0.98</b>	<b>0.42</b>	0.95	<b>0.35</b>	0.59	<b>0.86</b>	<b>1.48</b>	<b>1.08</b>	5.3	<b>0.41</b>
k = 30 minutes										
	Wind Farm									
Estimate	2	3	4	5	6	7	11	13	14	15
Sample	0.9	<b>0.59</b>	1.93	2.81	<b>0.59</b>	2.28	3.3	0.93	4.82	2.2
EWMA	<b>0.7</b>	1.2	<b>0.84</b>	<b>0.54</b>	0.61	1.39	<b>2.38</b>	1.3	<b>1.54</b>	0.78
EWSA	0.8	0.62	1.16	0.68	0.64	<b>0.46</b>	3.24	<b>0.75</b>	4.62	<b>0.51</b>
k = 60 minutes										
	Wind Farm									
Estimate	2	3	4	5	6	7	11	13	14	15
Sample	0.58	0.83	1.82	2.83	0.82	1.96	3.93	0.86	3.91	1.9
EWMA	0.96	1.51	1.08	<b>0.72</b>	<b>0.46</b>	1.56	2.97	1.15	<b>1.66</b>	<b>0.8</b>
EWSA	<b>0.52</b>	<b>0.75</b>	<b>0.72</b>	1.48	0.8	<b>0.95</b>	<b>2.36</b>	<b>0.73</b>	3.65	1.07

Table 5.9: Sharpness of  $M_{up}(s_{k,up})$  in percent for all Wind Farms using three Quantile Estimate Approaches (Sample, EWMA, EWSA)

k = 5 minutes										
	Wind Farm									
Estimate	2	3	4	5	6	7	11	13	14	15
Sample	<b>1.28</b>	<b>1.43</b>	1	<b>0.8</b>	<b>0.91</b>	<b>0.96</b>	<b>1.01</b>	0.87	<b>0.85</b>	0.72
EWMA	1.44	1.56	<b>0.96</b>	0.91	0.97	0.99	1.03	<b>0.87</b>	0.88	0.77
EWSA	1.72	1.66	1.61	1.02	1	1.21	1.09	0.98	0.93	<b>0.72</b>
k = 10 minutes										
	Wind Farm									
Estimate	2	3	4	5	6	7	11	13	14	15
Sample	<b>2.07</b>	<b>2.27</b>	1.67	<b>1.46</b>	<b>1.52</b>	<b>1.58</b>	<b>1.7</b>	1.55	<b>1.47</b>	<b>1.26</b>
EWMA	2.26	2.37	<b>1.51</b>	1.66	1.62	1.65	1.74	<b>1.5</b>	1.53	1.36
EWSA	2.42	2.61	2.01	1.94	1.61	1.79	1.84	1.72	1.61	2.21
k = 15 minutes										
	Wind Farm									
Estimate	2	3	4	5	6	7	11	13	14	15
Sample	<b>2.7</b>	<b>2.83</b>	2.16	<b>1.99</b>	<b>1.99</b>	2.06	<b>2.22</b>	2.07	<b>1.96</b>	<b>1.69</b>
EWMA	2.8	3.01	<b>1.89</b>	2.27	2.12	2.16	2.3	<b>2.03</b>	2.09	1.87
EWSA	3.14	3.21	2.19	2.49	2.22	<b>1.14</b>	2.41	2.29	2.13	1.85
k = 30 minutes										
	Wind Farm									
Estimate	2	3	4	5	6	7	11	13	14	15
Sample	4.16	<b>3.97</b>	3.16	<b>3.22</b>	<b>3.06</b>	<b>3.1</b>	<b>3.37</b>	<b>3.29</b>	<b>3.11</b>	<b>2.72</b>
EWMA	<b>4.12</b>	4.14	2.76	3.39	3.3	3.28	3.58	3.38	3.36	3
EWSA	4.65	4.4	<b>3.13</b>	3.64	3.34	3.4	3.65	3.58	3.37	2.75
k = 60 minutes										
	Wind Farm									
Estimate	2	3	4	5	6	7	11	13	14	15
Sample	6.27	<b>5.57</b>	4.49	<b>5.1</b>	<b>4.62</b>	<b>4.59</b>	<b>5.14</b>	<b>5.29</b>	<b>4.84</b>	<b>4.32</b>
EWMA	<b>5.95</b>	5.82	<b>3.89</b>	5.15	5.03	4.92	5.43	5.48	5.23	4.69
EWSA	6.82	5.97	4.33	5.5	4.99	4.93	5.47	5.63	5.16	4.52

Table 5.10: Sharpness of  $M_{low}$  ( $s_{k,low}$ ) in percent for all Wind Farms using three Quantile Estimate Approaches (Sample, EWMA, EWSA)

k = 5 minutes										
	Wind Farm									
Estimate	2	3	4	5	6	7	11	13	14	15
Sample	1.27	<b>1.42</b>	1.01	<b>0.81</b>	<b>0.91</b>	0.96	<b>1.01</b>	<b>0.87</b>	<b>0.86</b>	<b>0.73</b>
EWMA	<b>0.89</b>	1.58	0.97	0.92	0.99	1	1.05	0.89	0.89	0.78
EWSA	1.66	1.68	<b>0.55</b>	0.89	1.05	<b>0.94</b>	1.17	1	0.94	0.9
k = 10 minutes										
	Wind Farm									
Estimate	2	3	4	5	6	7	11	13	14	15
Sample	2	<b>2.24</b>	1.67	1.45	<b>1.52</b>	<b>1.57</b>	<b>1.7</b>	1.55	<b>1.47</b>	1.25
EWMA	<b>1.58</b>	2.43	1.64	1.67	1.66	1.69	1.79	<b>1.54</b>	1.58	1.4
EWSA	2.75	2.64	<b>1.59</b>	<b>1.44</b>	1.84	1.78	1.96	1.79	1.63	<b>0.58</b>
k = 15 minutes										
	Wind Farm									
Estimate	2	3	4	5	6	7	11	13	14	15
Sample	2.55	<b>2.76</b>	2.13	<b>1.95</b>	<b>1.99</b>	<b>2.05</b>	<b>2.21</b>	2.07	<b>1.94</b>	<b>1.67</b>
EWMA	<b>2.2</b>	3.04	<b>1.98</b>	2.35	2.18	2.22	2.37	<b>2.07</b>	2.2	1.92
EWSA	3.42	3.25	2.28	2.03	2.23	3.46	2.55	2.38	2.17	1.98
k = 30 minutes										
	Wind Farm									
Estimate	2	3	4	5	6	7	11	13	14	15
Sample	3.74	<b>3.81</b>	3.05	<b>3.08</b>	<b>2.98</b>	<b>3.02</b>	<b>3.29</b>	<b>3.28</b>	<b>3.06</b>	<b>2.64</b>
EWMA	<b>3.47</b>	4.19	<b>2.8</b>	3.53	3.35	3.32	3.65	3.48	3.47	3.08
EWSA	4.99	4.48	3.22	3.43	3.44	3.44	3.75	3.75	3.45	3.21
k = 60 minutes										
	Wind Farm									
Estimate	2	3	4	5	6	7	11	13	14	15
Sample	<b>5.29</b>	<b>5.17</b>	4.26	<b>4.83</b>	<b>4.34</b>	<b>4.35</b>	<b>4.88</b>	<b>5.04</b>	<b>4.68</b>	<b>4.06</b>
EWMA	5.68	5.95	<b>4</b>	5.42	5.09	5	5.58	5.7	5.68	4.89
EWSA	6.93	6.07	4.41	5.52	4.93	4.89	5.57	5.78	5.31	4.49

Table 5.11: Resolution of  $M_{up}$  ( $RES_{k,up}$ ) in percent for all Wind Farms using three Quantile Estimate Approaches (Sample, EWMA, EWSA)

k = 5 minutes										
	Wind Farm									
Estimate	2	3	4	5	6	7	11	13	14	15
Sample	0.59	0.61	0.35	0.35	0.32	0.33	0.37	<b>0.34</b>	0.29	0.25
EWMA	0.54	<b>0.61</b>	0.37	<b>0.51</b>	<b>0.4</b>	0.41	0.42	0.32	0.29	0.31
EWSA	<b>1.4</b>	0.55	<b>3.01</b>	0.38	0.38	<b>0.79</b>	<b>0.49</b>	0.32	<b>0.3</b>	<b>0.68</b>
k = 10 minutes										
	Wind Farm									
Estimate	2	3	4	5	6	7	11	13	14	15
Sample	0.84	0.88	0.57	0.6	0.57	0.61	0.62	<b>0.58</b>	0.54	0.46
EWMA	0.93	<b>1.01</b>	0.54	0.93	0.71	<b>0.76</b>	0.71	0.54	0.48	0.61
EWSA	<b>1.17</b>	0.83	<b>1.8</b>	<b>1.08</b>	<b>0.98</b>	0.6	<b>0.74</b>	0.57	<b>0.56</b>	<b>5.58</b>
k = 15 minutes										
	Wind Farm									
Estimate	2	3	4	5	6	7	11	13	14	15
Sample	1.05	1.04	0.71	0.78	0.75	0.79	0.82	0.76	0.74	0.62
EWMA	<b>1.23</b>	<b>1.32</b>	0.76	<b>1.26</b>	<b>0.97</b>	1	<b>0.97</b>	0.76	0.69	<b>0.88</b>
EWSA	1.17	1.02	<b>0.79</b>	1.04	0.8	<b>7.12</b>	0.95	<b>0.76</b>	<b>0.77</b>	0.69
k = 30 minutes										
	Wind Farm									
Estimate	2	3	4	5	6	7	11	13	14	15
Sample	1.52	1.37	1.01	1.16	1.14	1.22	1.2	1.11	1.2	1
EWMA	1.67	<b>1.79</b>	1.19	<b>1.72</b>	<b>1.41</b>	<b>1.59</b>	<b>1.55</b>	<b>1.29</b>	1.22	1.49
EWSA	<b>1.87</b>	1.45	<b>1.23</b>	1.39	1.36	1.33	1.35	1.2	<b>1.29</b>	<b>2.26</b>
k = 60 minutes										
	Wind Farm									
Estimate	2	3	4	5	6	7	11	13	14	15
Sample	2.15	1.85	1.4	1.77	1.76	1.91	1.81	1.79	1.91	1.61
EWMA	<b>2.57</b>	<b>2.8</b>	1.85	<b>2.83</b>	<b>2.22</b>	<b>2.57</b>	<b>2.51</b>	<b>2.29</b>	1.87	<b>2.54</b>
EWSA	2.41	2.12	<b>1.86</b>	2.45	2.02	2.21	2.1	2.02	<b>2.1</b>	1.83

Table 5.12: Resolution of  $M_{low}$  ( $RES_{k,low}$ ) in percent for all Wind Farms using three Quantile Estimate Approaches (Sample, EWMA, EWSA)

k = 5 minutes										
	Wind Farm									
Estimate	2	3	4	5	6	7	11	13	14	15
Sample	0.61	0.61	0.37	0.35	0.33	0.33	0.38	<b>0.35</b>	0.29	0.26
EWMA	0.29	<b>0.61</b>	0.35	0.51	<b>0.4</b>	0.41	<b>0.42</b>	0.33	0.29	0.31
EWSA	<b>1.49</b>	0.54	<b>3.03</b>	<b>0.57</b>	0.27	<b>0.97</b>	0.4	0.32	<b>0.29</b>	<b>0.54</b>
k = 10 minutes										
	Wind Farm									
Estimate	2	3	4	5	6	7	11	13	14	15
Sample	0.88	0.92	0.6	0.62	0.58	0.6	0.64	0.61	<b>0.54</b>	0.48
EWMA	0.49	<b>1.04</b>	0.69	0.92	<b>0.72</b>	<b>0.75</b>	<b>0.71</b>	0.53	0.49	0.61
EWSA	<b>1.02</b>	0.82	<b>1.74</b>	<b>1.55</b>	0.64	0.54	0.6	<b>0.58</b>	0.53	<b>5.86</b>
k = 15 minutes										
	Wind Farm									
Estimate	2	3	4	5	6	7	11	13	14	15
Sample	<b>1.12</b>	<b>1.12</b>	<b>0.76</b>	0.82	0.78	0.78	0.85	<b>0.8</b>	0.75	0.66
EWMA	0.76	1.31	0.74	<b>1.26</b>	0.99	0.99	<b>0.95</b>	0.7	<b>0.76</b>	0.86
EWSA	1	1.02	0.73	<b>1.53</b>	0.89	<b>6.55</b>	0.78	0.77	0.73	<b>1.05</b>
k = 30 minutes										
	Wind Farm									
Estimate	2	3	4	5	6	7	11	13	14	15
Sample	1.64	<b>1.49</b>	1.1	1.27	1.2	1.21	1.28	<b>1.24</b>	<b>1.25</b>	1.09
EWMA	1.22	1.74	<b>1.19</b>	1.66	<b>1.43</b>	<b>1.57</b>	<b>1.46</b>	1.23	1.22	1.43
EWSA	<b>1.65</b>	1.36	1.17	<b>1.67</b>	1.05	1.16	1.23	1.19	1.24	<b>1.82</b>
k = 60 minutes										
	Wind Farm									
Estimate	2	3	4	5	6	7	11	13	14	15
Sample	<b>2.34</b>	2.05	1.67	2.09	1.87	1.9	2.01	1.95	2.05	1.75
EWMA	2.16	<b>2.63</b>	1.9	<b>2.73</b>	<b>2.12</b>	<b>2.48</b>	<b>2.42</b>	<b>2.18</b>	<b>2.16</b>	<b>2.51</b>
EWSA	1.89	1.85	<b>1.91</b>	2.17	1.88	2	2.04	1.86	2.02	1.8

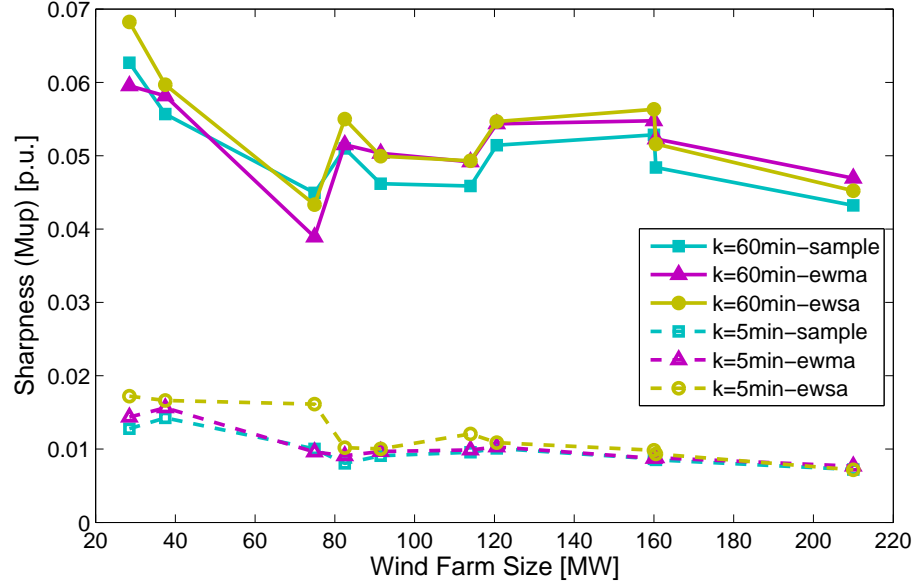


Figure 5.15: Sharpness of CRM upper endpoint estimate  $M_{up}$  as a function of the wind farm nameplate capacity under the three quantile estimation methods (sample, ewma, ewsa) for forecast time resolutions  $k = 5$  minutes (dashed lines) and 60 minutes (solid lines). Sharpness increases with increasing forecast time resolution, has similar values under the three methods and is lowest under the sample quantile approach.

from nominal proportions.

Figure 5.15 depicts the sharpness of the upper CRM endpoint estimate  $M_{up}$  as a function of the wind farm nameplate capacity for forecast time resolutions  $k = 5$  and 60 minutes under the three considered quantile estimation methods (sample, ewma, ewsa). In this figure dashed lines refer to 5-minute resolution and solid lines to 60-minute resolution. As expected, from Fig. 5.15 it is evident that sharpness increases with increasing forecast time resolution  $k$  for all methods considered, since wind power is more variable over longer periods of time. Moreover, the quantile estimate's sharpness is similar under all methods, but is in general lower under the sample quantile estimate approach.

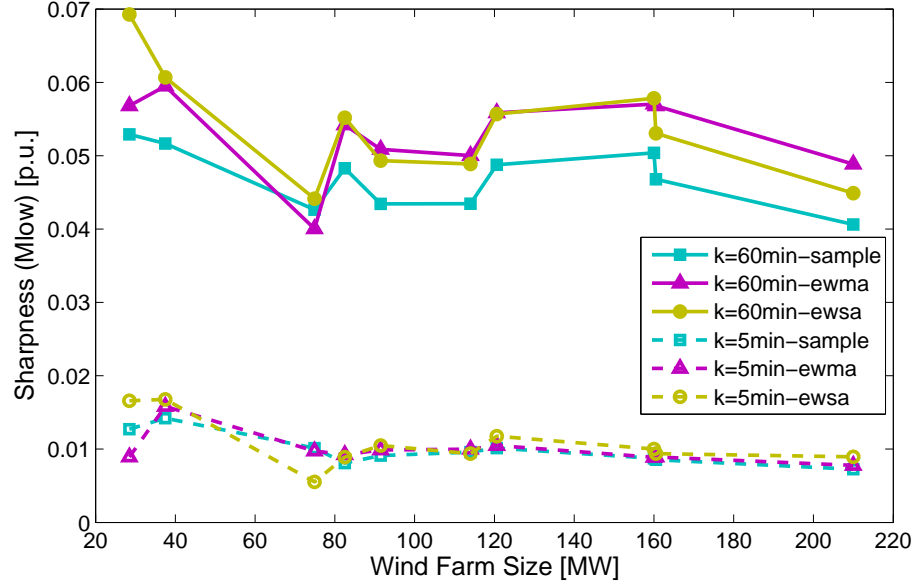


Figure 5.16: Sharpness of the CRM lower endpoint estimate  $M_{low}$  as a function of the wind farm nameplate capacity under the three quantile estimation methods (sample, ewma, ewsa) for forecast time resolutions  $k = 5$  minutes (dashed lines) and 60 minutes (solid lines). The difference in sharpness of  $M_{low}$  estimates between the three methods is more pronounced than in the case of the sharpness of  $M_{up}$ .

Thus, the sample quantiles result in the smallest intra-hour wind power variability intervals, but not in the most reliable ones. Similarly, Fig. 5.16 depicts the sharpness of the lower CRM endpoint estimate  $M_{low}$  as a function of the wind farm nameplate capacity for forecast time resolutions  $k = 5$  and 60 minutes under the three considered quantile estimation methods (sample, ewma, ewsa). The conclusions are analogous with more pronounced differences between the three methods, especially for larger forecast time resolutions.

The resolution of the upper and lower CRM endpoints  $M_{up}$  and  $M_{low}$  is given in Fig. 5.17 and Fig. 5.18, respectively, as a function of the wind farm nameplate capacity for forecast time resolutions  $k = 5$  minutes (dashed

lines) and 60 minutes (solid lines). Again, the resolution of the estimates presumes similar values under the three considered quantile estimation methods and increases with increasing forecast time resolution  $k$ . For small forecast time resolutions the exponentially weighted stochastic approximation quantile has larger resolution, whereas for large forecast time resolutions the exponentially weighted moving average estimate produces the largest resolution. An increased resolution reveals that the time-adaptive methods can better distinguish between situations of different wind power variability, making them more appealing for wind power variability forecasts. However, the computational burden to obtain these estimates should also be considered.

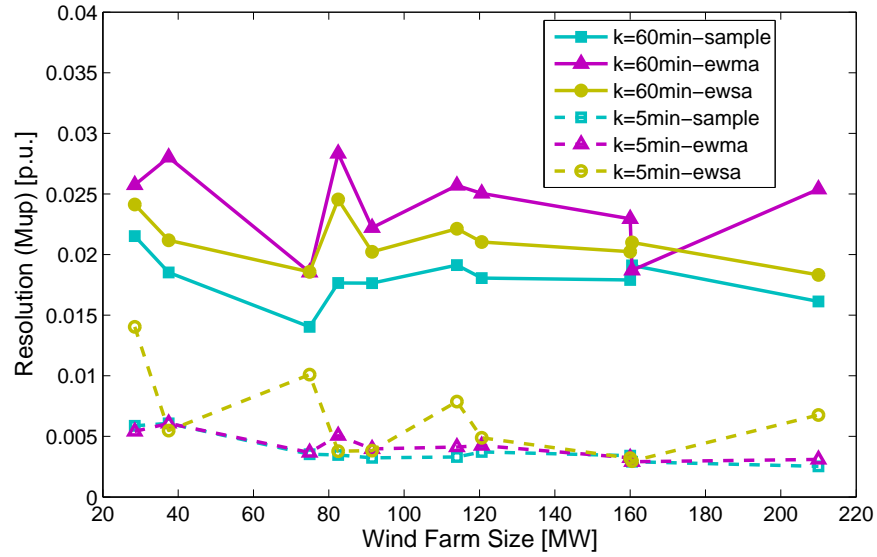


Figure 5.17: Resolution of the CRM upper endpoint  $M_{up}$  as a function of the wind farm nameplate capacity under the three quantile estimation methods (sample, ewma, ewsa) for forecast time resolutions  $k = 5$  minutes (dashed lines) and 60 minutes (solid lines). For 5-minute forecasts quantile resolution is higher under the exponentially weighted stochastic approximation approach, whereas for 60-minute forecasts the exponentially weighted moving average estimate is more situation-dependent.



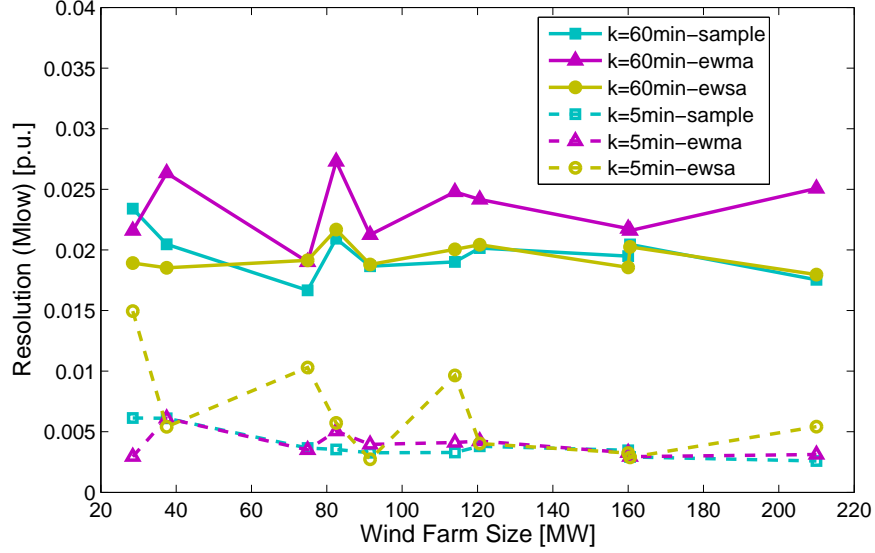


Figure 5.18: Resolution of the CRM lower endpoint  $M_{low}$  as a function of the wind farm nameplate capacity under the three quantile estimation methods (sample, ewma, ewsa) for forecast time resolutions  $k = 5$  minutes (dashed lines) and 60 minutes (solid lines).

## 5.4 CRM Sample Quantiles with Seasonal Considerations

Since sample quantiles have acceptable levels of reliability, sharpness and resolution, and are the easiest to calculate, a sample quantile estimate approach with seasonal considerations has also been examined, using data from wind farms WF1, WF2, WF5, WF6, WF11, WF13, WF17, and WF18 (see Appendix A.1). The training set includes the data spanning from December of year 1 to November of year 2, while the test set includes the data spanning from December of year 2 to November of year 3. Under this approach, for a wind power forecast time resolution  $k$ , the  $p^{th}$  CRM quantile estimate of each wind power forecast level  $l_j$ , of a specific month and season in the test set, is

set equal to the  $p^{th}$  CRM sample quantile of a subset of the training set.

Let  $l_{j,m,s}$  denote a wind power forecast of average production  $l_j$  at month  $m$  and season  $s$ . Also, let  $CRM_{\{X\}k,l_j,p}$  denote a sample quantile from the data in set  $\{X\}$ . Then considering seasonal effects, for a wind power forecast time resolution  $k$  the  $p^{th}$  CRM quantile estimate of each wind power forecast level  $l_j$  at month  $m$  and season  $s$  can be calculated from:

$$\hat{CRM}_{k,l_{j,m,s},p} = CRM_{\{X\}k,l_j,p} \quad (5.44)$$

where  $\{X\}$  is a subset of the training set.

Three subsets  $\{X\}$  of the training set are used to determine the CRM quantile estimate:

- $\{X\} = \text{year}$   
which includes all the data in the test set (year = December of year 1 – November of year 2) ,
- $\{X\} = \text{season}$   
which includes the data in the test set from season  $s$  ( $s = \text{winter (December of year 1 – February of year 2), spring (March – May of year 2), summer (June – August of year 2), fall (September – November of year 2)}$ )),
- $\{X\} = \text{month}$   
which includes the data in the test set from month  $m$  ( $m = \text{December of year 1 and each month of year 2}$ ).

Thus, when seasonality is taken into account the CRM quantile estimate in the test set is set equal to the same production level and forecast time resolution sample quantile of the entire training set (year) or the respective seasonal

(season) or monthly (month) subset of the training set.

Figure 5.19 depicts the overall reliability diagrams of the CRM quantile estimates of a 160.5 MW wind farm (WF6) using yearly, seasonal and monthly sample quantiles as estimates. The reliability diagrams depict the deviation from nominal proportions (reliability) of the CRM quantiles as a function of the nominal proportions  $p$  for various wind power forecast time resolutions  $k=5, 10, 15, 30$  and 60 minutes. In these diagrams the dotted line represents the reliability of the nominal proportions (zero deviations) and the solid lines the reliability of the actual quantile estimates, according to the three subsets used to determine the sample quantile (year, season, month).

From Fig. 5.19 it is evident that the three sample quantiles (yearly, seasonal, monthly) exhibit similar reliability values, with differences increasing slightly with increasing wind power forecast time resolutions. From the reliability diagrams of the specific wind farm given in Fig. 5.19 the monthly sample quantile seems to perform better than the seasonal and yearly sample quantiles. However, this is true only for low rank quantiles, since for higher ranks it is the yearly sample quantile that exhibits the lowest deviations from nominal proportions. Moreover, this result is not universal, since for other wind farms the seasonal sample quantile presents a slightly better performance than the monthly and the yearly sample quantile, but again not for all quantiles.

To compare the performance of the yearly, seasonal and monthly sample quantiles their reliability RMSE from (5.22) is used. The reliability RMSE of the three estimates is given in Table 5.13 for all wind farms considered and for various wind power forecast time resolutions. For each wind farm and forecast time resolution the performance of the best quantile estimate is highlighted in bold.

The results in Table 5.13 are in agreement with the previous conclu-

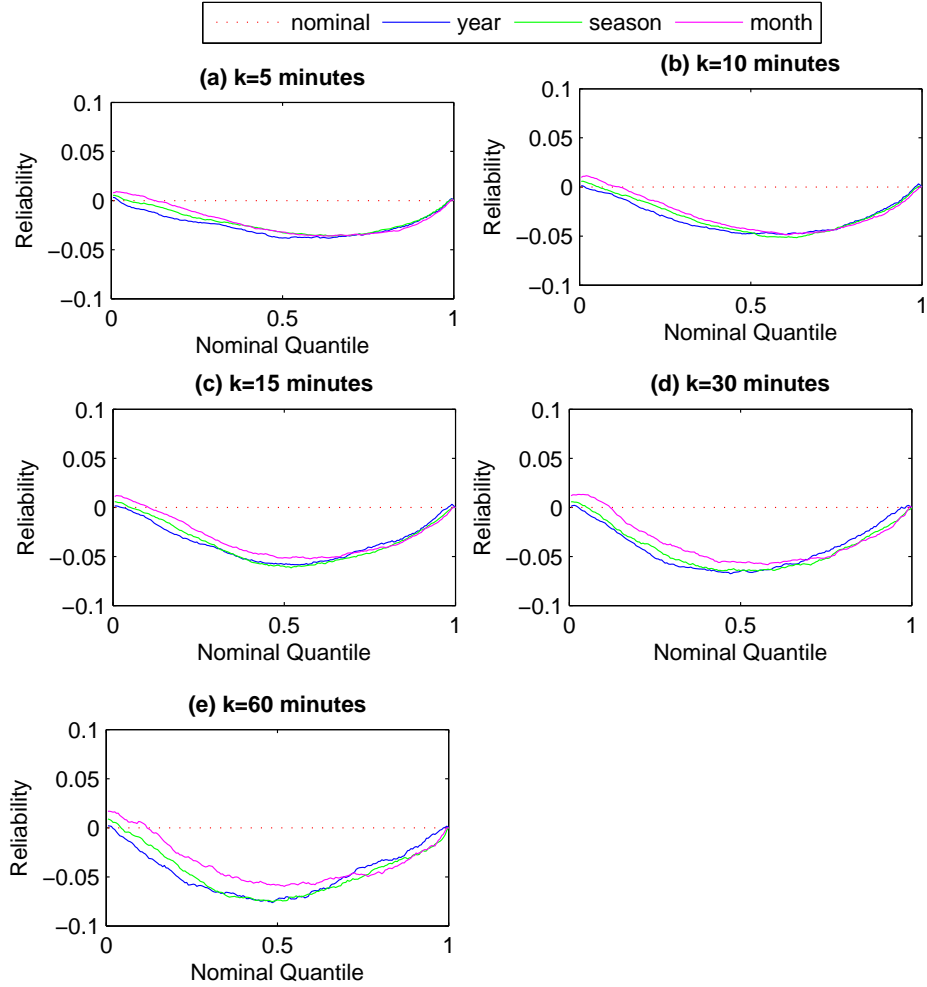


Figure 5.19: Reliability diagrams of the CRM quantile estimates of a 160.5 MW wind farm (WF6) for various wind power forecast resolutions  $k = 5, 10, 15, 30$  and  $60$  minutes. Yearly, seasonal and monthly quantiles are used as quantile estimates. The solid lines represent the deviations from nominal of the actual and the dotted line of the nominal proportion  $p$ . Yearly, seasonal and monthly sample quantiles exhibit similar reliability values, with the monthly sample quantile outperforming the others for small rank quantiles, and the yearly sample quantile performing best for high rank quantiles.

Table 5.13: RMSE of Reliability in percent for all Wind Farms using three Sample Quantiles (Year, Season, Month)

k = 5 minutes								
	Wind Farm							
Sample	1	2	5	6	11	13	17	18
Year	0.65	3.72	<b>0.82</b>	2.49	1.34	3.09	1.63	1.06
Season	<b>0.36</b>	3.68	1.00	<b>2.17</b>	1.41	2.91	<b>0.44</b>	<b>0.81</b>
Month	0.88	<b>2.92</b>	1.10	2.17	<b>0.32</b>	<b>1.94</b>	2.26	1.80
k = 10 minutes								
	Wind Farm							
Sample	1	2	5	6	11	13	17	18
Year	0.83	4.16	1.20	3.11	1.66	3.17	2.03	1.20
Season	<b>0.53</b>	4.37	<b>0.77</b>	2.99	1.96	3.05	<b>0.41</b>	<b>0.95</b>
Month	1.14	<b>3.41</b>	1.45	<b>2.84</b>	<b>0.52</b>	<b>1.73</b>	2.59	2.06
k = 15 minutes								
	Wind Farm							
Sample	1	2	5	6	11	13	17	18
Year	1.00	4.34	1.33	3.56	1.94	3.28	2.29	1.24
Season	<b>0.58</b>	4.72	<b>0.71</b>	3.59	2.19	2.97	<b>0.50</b>	<b>0.83</b>
Month	1.26	<b>3.65</b>	1.58	<b>3.18</b>	<b>0.56</b>	<b>1.83</b>	2.75	2.13
k = 30 minutes								
	Wind Farm							
Sample	1	2	5	6	11	13	17	18
Year	1.24	4.32	1.42	4.12	2.43	3.23	2.38	1.22
Season	<b>0.43</b>	4.79	<b>0.61</b>	4.14	2.73	3.05	<b>0.59</b>	<b>0.80</b>
Month	1.51	<b>3.56</b>	1.81	<b>3.64</b>	<b>0.64</b>	<b>1.86</b>	2.96	2.27
k = 60 minutes								
	Wind Farm							
Sample	1	2	5	6	11	13	17	18
Year	1.46	4.57	1.26	4.51	2.41	3.22	2.58	1.32
Season	<b>0.40</b>	5.05	<b>0.74</b>	4.52	2.99	3.60	<b>0.95</b>	<b>0.75</b>
Month	1.74	<b>3.60</b>	2.04	<b>3.69</b>	<b>0.49</b>	<b>1.96</b>	3.21	2.36

sion, that no sample quantile performs best for all wind farms, as for half of the wind farms the seasonal quantile performs best, while for the rest the monthly quantile has lower reliability RMSE, with deviations approaching 2%. But even when each wind farm is considered individually, the best sample quantile varies by wind forecast time resolution  $k$ , e.g. for WF3 and  $k = 5$  minutes the yearly sample quantile outperforms the other quantiles, while for all other forecast resolutions the seasonal sample quantile performs best.

Moreover, the results in this table verify again that even when seasonality is considered, the performance of the sample quantiles does not necessarily present a monotonic relation to wind power forecast time resolution  $k$ . Indeed, only for WF6 reliability RMSE of the yearly, seasonal and monthly sample quantiles increases with increasing  $k$ , while for all other wind farms reliability RMSE presents a non-monotonic relationship with  $k$ . Nonetheless, monotonicity is more frequent for monthly sample quantiles, than for yearly or seasonal.

Figure 5.20 depicts the reliability RMSE of the three CRM quantile estimates as a function of the wind farm nameplate capacity  $P_N$  for wind power forecast resolutions equal to 5 and 60 minutes. Blue markers indicate reliability RMSE for 5-minute and pink markers for 60-minute wind forecast resolution. The filled markers represent reliability RMSE of monthly and seasonal sample quantiles. The results in this figure verify that no unique sample quantile performs best for all wind farms, however for most wind farms reliability RMSE of the yearly quantile falls between reliability RMSE of the seasonal and monthly quantiles. Regarding the effect of wind farm nameplate capacity on reliability RMSE no safe conclusion can be drawn, indicating that the performance of quantile estimates is affected more by the estimation method used and less by other factors.

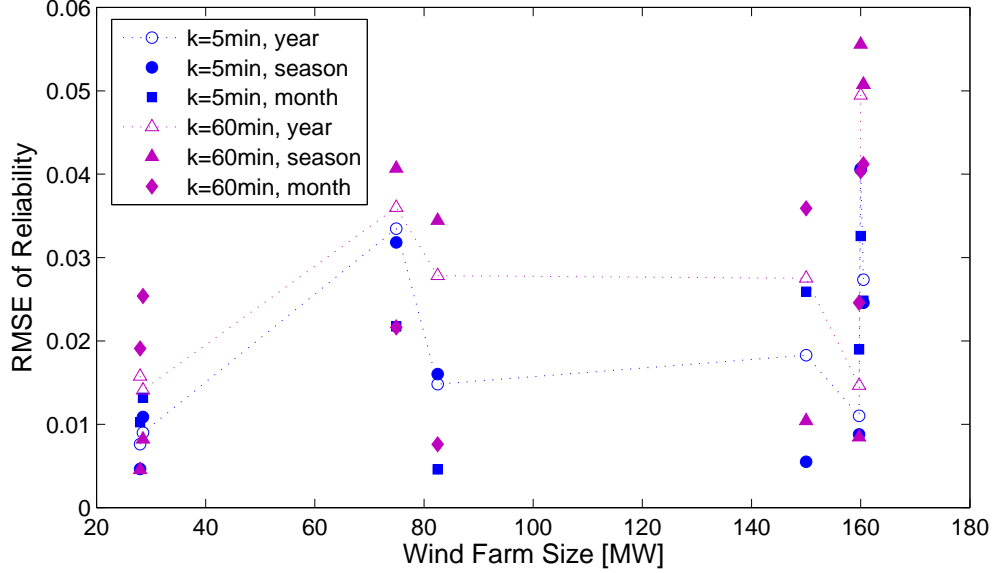


Figure 5.20: Reliability RMSE of the three CRM quantile estimates (yearly, seasonal, monthly) for wind power forecast resolutions  $k = 5$  and 60 minutes as a function of wind farm nameplate capacity. For most wind farms reliability RMSE of the yearly sample quantile falls between reliability RMSE of the monthly and seasonal sample quantiles.

## 5.5 Wind Power Variability Incremental Forecast Error

In Sections 5.3.3 – 5.3.6 methods to obtain  $p^{th}$  CRM quantile estimates  $\hat{CRM}_{k,l_j,p}$  are presented and compared. Due to lack in forecasted data these methods are all evaluated on perfectly forecasted  $k$ -averaged wind power productions. Since wind power variability is present even under perfect forecasts, the need to provide reliable wind power variability forecasting methods is essential and in this sense the results from the previous sections indicate the reliability levels the presented methods can reach as wind power forecasting technologies improve.

In this section a wind power forecast of the test set is generated artifi-

cially by making certain assumptions on wind power forecast errors and their distribution. The sample quantiles of the training set are used as CRM quantile estimates for the forecasted wind power series and the reliability RMSE of these estimates is calculated. Comparing the results between a perfect and the generated forecast the incremental forecast error, i.e. the wind power variability forecast error attributed to the wind power forecast error, is investigated.

### 5.5.1 Wind Power Forecast Series Formation

Given a  $k$ -averaged wind power series  $y_{k,i}$ ,  $i = 1, 2, \dots, N$ , and the respective forecasted series  $\tilde{y}_{k,i}$  the forecast error series  $\epsilon_{k,i}$  is defined by the difference between the actual and the forecasted value:

$$\epsilon_{k,i} = y_{k,i} - \tilde{y}_{k,i} \quad (5.45)$$

To make true inferences about a forecast error distribution an actual forecasted wind power series is necessary, and more specifically the forecasted wind power series pertaining to the actual wind power series at our disposal. In the absence of such a forecast series, certain assumptions have been made about the forecast error distribution, which enable the generation of a wind power forecast series from an actual wind power series.

If the actual and forecasted wind power series of a wind farm are normalized based on the wind farm nameplate capacity, then the forecast error in (5.45) is the normalized forecast error and the normalized mean absolute error (NMAE) is defined by:

$$\text{NMAE}_k = \frac{1}{N} \sum_{i=1}^N |\epsilon_{k,i}| \quad (5.46)$$

In the absence of any other information, the forecast errors  $\epsilon_k$  are assumed to follow a Normal distribution as in [88], with mean  $\mu_{\epsilon_k}$  and variance  $\sigma_{\epsilon_k}^2$  such



that:

$$\int_{-\infty}^{\infty} |\epsilon_k| \cdot \frac{1}{\sigma_{\epsilon_k} \sqrt{2\pi}} e^{\frac{-(\epsilon_k - \mu_{\epsilon_k})^2}{2\sigma_{\epsilon_k}^2}} d\epsilon_k = \text{NMAE}_k \quad (5.47)$$

In (5.45), negative forecast errors  $\epsilon_{k,i}$  overestimate the actual wind power, while positive forecast errors indicate underestimation of the actual wind power. The frequencies of over- and underestimation forecasting errors provide useful information about the forecast error distribution. However, when only the NMAE is known, equal chances of overestimation and underestimation can be assumed. In this case:

$$\int_{-\infty}^0 \frac{1}{\sigma_{\epsilon_k} \sqrt{2\pi}} e^{\frac{-(\epsilon_k - \mu_{\epsilon_k})^2}{2\sigma_{\epsilon_k}^2}} d\epsilon_k = 0.5 \quad (5.48)$$

The solution of the system of equations (5.47) and (5.48) yields:

$$\mu_{\epsilon_k} = 0 \quad (5.49)$$

and

$$\sigma_{\epsilon_k} = \frac{\text{NMAE}_k}{2} \cdot \sqrt{2\pi} \quad (5.50)$$

The NMAE is a value which, most of the times, forecast providers make available to their end-users. In [89] normalized wind power forecast errors for various central wind power forecasting programs in the United States and Canada are given, while [90] summarizes results from various European wind power forecasting models. Based on the values given in [90] NMAE for hour-ahead forecasts lies between 5% and 10%, while for day ahead forecasts the range of NMAE is between 10% and 15%. The values of  $\text{NMAE}_k$  used for the various wind power forecast resolutions  $k$  are given in Table 5.14. The reasoning behind these values is that forecasts with smaller time resolution values  $k$  are updated more frequently and thus an hour ahead forecast error is

Table 5.14: NMAE<sub>k</sub> for various Forecast Resolutions  $k$

$k$ [min]	NMAE <sub>k</sub>
5	8%
10	8%
15	8%
30	15%
60	15%

assumed, while for forecasts with larger time resolutions a day-ahead forecast error is considered more suitable.

Assuming Gaussianity, a normalized forecast series  $\tilde{y}_k = y_k - \epsilon_k$  can be generated from an actual normalized wind power series  $y_k$  by sampling the forecast errors  $\epsilon_k$  randomly from a normal distribution  $\mathcal{N}(\mu_{\epsilon_k}, \sigma_{\epsilon_k}^2)$ . However, each normalized wind power forecast point  $\tilde{y}_{k,i}$  is bounded below by zero and above by one:

$$\begin{aligned} 0 \leq \tilde{y}_{k,i} \leq 1 &\Rightarrow 0 \leq y_{k,i} - \epsilon_{k,i} \leq 1 \\ &\Rightarrow y_{k,i} - 1 \leq \epsilon_{k,i} \leq y_{k,i} \end{aligned} \quad (5.51)$$

Thus, for each actual wind power  $y_{k,i}$  the forecast error  $\epsilon_{k,i}$  has to be sampled randomly from a truncated normal distribution  $\mathcal{TN}_a^b(\mu, \sigma^2)$  with mean  $\mu = \mu_{\epsilon_k} = 0$ , standard deviation  $\sigma = \sigma_{\epsilon_k} = \frac{\text{NMAE}_k}{2} \cdot \sqrt{2\pi}$ , lower bound  $a = a_{k,i} = y_{k,i} - 1$  and upper bound  $b = b_{k,i} = y_{k,i}$ .

The probability density function  $f_X(x)$  of a variable  $X$  following a truncated normal distribution  $X \sim \mathcal{TN}_a^b(\mu, \sigma^2)$  is defined by:

$$f_X(x) = \begin{cases} \frac{\frac{1}{\sigma\sqrt{2\pi}} e^{-\frac{(x-\mu)^2}{2\sigma^2}}}{\Phi(\frac{b-\mu}{\sigma}) - \Phi(\frac{a-\mu}{\sigma})} & \text{for } a \leq x \leq b \\ 0 & \text{otherwise} \end{cases} \quad (5.52)$$

where  $\Phi(\cdot)$  is the cumulative distribution function of the standard normal  $\mathcal{N}(0, 1)$  distribution. Figure 5.21 depicts the density of normalized forecast errors  $\epsilon_k$  following a normal  $\mathcal{N}(0, \sigma_{\epsilon_k}^2)$  and a truncated normal  $\mathcal{TN}_{y_k-1}^{y_k}(0, \sigma_{\epsilon_k}^2)$  distribution with  $\sigma_{\epsilon_k}^2 = \pi \cdot \text{NMAE}_k^2/2$ . For Fig. 5.21 the actual wind power value is set to  $y_k = 0.7$  p.u. and the normalized mean absolute error is taken to be  $\text{NMAE}=0.25$ . As expected, the truncated normal acquires more density within the bounds  $[-0.3, 0.7]$  than the normal distribution.

To generate a random sample from a truncated normal distribution it is first noted that if  $X \sim \mathcal{TN}_a^b(\mu, \sigma^2)$ , then:

$$z \equiv \frac{x - \mu}{\sigma} \sim \mathcal{TN}_{a_z}^{b_z}(0, 1) \quad (5.53)$$

follows a truncated standard normal distribution with bounds:

$$a_z = \frac{a - \mu}{\sigma} \quad (5.54)$$

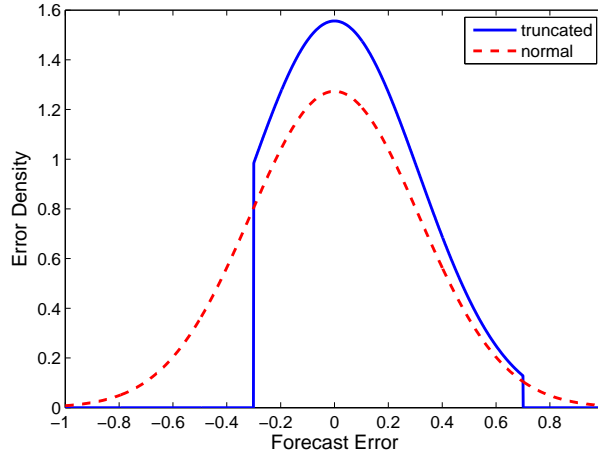


Figure 5.21: Density of normalized forecast errors  $\epsilon_k$  under a normal  $\mathcal{N}(0, \pi \cdot \text{NMAE}_k^2/2)$  and a truncated normal  $\mathcal{TN}_{y_k-1}^{y_k}(0, \pi \cdot \text{NMAE}_k^2/2)$  distribution with  $y_k = 0.7$  and  $\text{NMAE}=0.25$ .

and

$$b_z = \frac{b - \mu}{\sigma} \quad (5.55)$$

To generate standard normal random numbers the inverse cumulative distribution function method is used. The cdf of the random variable  $Z$  is:

$$F_Z(z) = \frac{\Phi(z) - \Phi(a_z)}{\Phi(b_z) - \Phi(a_z)} \quad (5.56)$$

Then, for a uniform random variable  $U \sim \mathcal{U}(0, 1)$  we have:

$$u = F_Z(z) \Rightarrow u(\Phi(b_z) - \Phi(a_z)) + \Phi(a_z) = \Phi(z) \quad (5.57)$$

thus,

$$z = F_Z^{-1}(u) = \Phi^{-1}(\Phi(a_z) + u(\Phi(b_z) - \Phi(a_z))) \quad (5.58)$$

where  $\Phi^{-1}(\cdot)$  is the inverse of the standard normal cdf, termed probit function, and is defined for  $p \in (0, 1)$  using the inverse of the error function  $\text{erf}(v) = \frac{2}{\sqrt{\pi}} \int_0^v e^{-t^2} dt$ :

$$\Phi^{-1}(p) = \sqrt{2} \text{erf}^{-1}(2p - 1) \quad (5.59)$$

Thus the algorithm used for producing the forecast series  $\tilde{y}_{k,i}$  is summarized as follows. For each actual wind power  $y_{k,i}$ :

1. Generate a uniform random number  $u_{k,i} \sim \mathcal{U}(0, 1)$ .
2. Calculate  $z_{k,i}$  from (5.58) using  $a_z = 2(y_{k,i} - 1)/(\sqrt{2\pi}\text{NMAE}_k)$  and  $b_z = 2y_{k,i}/(\sqrt{2\pi}\text{NMAE}_k)$ .
3. Get the forecasted wind power  $\tilde{y}_{k,i} = y_{k,i} - z_{k,i}\sqrt{2\pi}\text{NMAE}_k/2$ .

For each forecast time resolution  $k$  the values of the normalized mean absolute errors  $\text{NMAE}_k$  are taken from Table 5.14. The algorithm is implemented in MATLAB which has a ready to use inverse error function  $\text{erf}^{-1}$  and a random uniform number generator.

### 5.5.2 Evaluation of the CRM Quantile Estimates from the Forecast on the Actual Wind Power Data

The sample quantile estimate approach is used to evaluate the CRM quantile estimate on the forecasted wind power series. Under this approach, the sample quantile from the wind power data in the training set is used as the CRM quantile estimate for the data in the test set according to (5.19). Let  $y_m$ ,  $m = 1, 2, \dots, M$ , denote the actual wind power data in the test set and  $y_{k,i}$ ,  $i = 1, 2, \dots, \lfloor M/k \rfloor$  the  $k$ -averaged wind power data of the test set. Also, let  $\tilde{y}_{k,i}$  be a forecast wind power series calculated from  $y_{k,i}$  using the algorithm described in Section 5.5.1. Then, for each point  $\tilde{y}_{k,i} = l_j$  in the forecast series the  $p^{th}$  CRM quantile estimate  $C\hat{R}M_{k,l_j,p} = [\hat{M}_{low_{k,l_j,p}}, \hat{M}_{up_{k,l_j,p}}]$  is set equal to the sample quantile of the training set, conditioned on the  $k$ -averaged wind power  $\bar{x}_k$  of the training set being  $\bar{x}_k = l_j$ .

$$C\hat{R}M_{\{Y\}k,l_j=\tilde{y}_{k,i},p} = [\hat{M}_{\{Y\}low_{k,l_j=\tilde{y}_{k,i},p}}, \hat{M}_{\{Y\}up_{k,l_j=\tilde{y}_{k,i},p}}] = [M_{low_{k,\bar{x}_k=l_j,p}}, M_{up_{k,\bar{x}_k=l_j,p}}] \quad (5.60)$$

where  $(M_{low_{k,l_j,p}}, M_{up_{k,l_j,p}})$  is the solution of the system of equations (3.7) and (3.10) solved in Section 3.3.2 using the  $x_n$  wind power data as input. It should be noted that in (5.60) the wind power level  $l_j$  refers to the forecasted wind power series. Thus, for each forecasted wind power level  $l_j$  the respective CRM sample quantile of the training set is used as an estimate on the test set.

However, the quantile estimates are then evaluated on the actual and not the forecasted wind power data of the test set. Indeed, the  $p^{th}$  CRM quantile estimate should be such, that:

$$P \left( \left\{ \inf_{m \in K_i} y_m \geq \hat{M}_{low_{k,l_j,p}} \right\} \cap \left\{ \sup_{m \in K_i} y_m \leq \hat{M}_{up_{k,l_j,p}} \right\} \middle| \tilde{y}_{k,i} = l_j \right) \geq p, \quad i = 1, 2, \dots, \lfloor M/k \rfloor \quad (5.61)$$

where  $K_i$  is the  $i^{th}$   $k$ -long interval  $[k(i-1)+1, ki]$  in the actual wind power series  $y_m$ ,  $m = 1, 2, \dots, M$ , of the test set.

The wind farms considered for wind power variability analysis using sample quantile as estimates and artificially generated wind power forecasts are WF2, WF3, WF4, WF5, WF6, WF7, WF11, WF13, WF14, and WF15 (see Appendix A.1). The training set from which the sample quantiles come includes the data from year 3, while the test set from which the actual and perfect wind power forecast series are generated includes the data from year 4. The resulting quantile estimates are evaluated using their reliability and RMSE of reliability.

The total reliability  $r_{k,p}$  of a  $p^{th}$  CRM quantile estimate is again given by:

$$r_{k,p} = \sum_j \frac{N_{k,l_j}}{N_k} \cdot \hat{p}_{k,l_j}^{(p)} - p \quad (5.62)$$

where  $N_k$  is the length of the forecasted wind power series  $\tilde{y}_{k,i}$  of the test set and  $N_{k,l_j}$  is the length of the subset of these data with  $\tilde{y}_{k,i} = l_j$ . Here  $\hat{p}_{k,l_j}^{(p)}$  is the proportion of the  $k$ -long intervals in the test set with forecasted production  $\tilde{y}_{k,i} = l_j$  for which the actual wind power  $y_m$  lies within the interval  $[\hat{M}_{low_{k,l_j,p}}, \hat{M}_{up_{k,l_j,p}}]$  from (5.60).

The reliability diagrams, i.e. deviations from nominal proportions, of the CRM quantile estimates of a 120.6 MW wind farm (WF3) for various wind power forecast time resolutions  $k = 5, 10, 15, 30$  and 60 minutes are given in Fig. 5.22. In these diagrams, the dotted line represents deviations from nominal of the nominal proportions  $p$ , i.e. zero deviations. The dashed line represents deviations from nominal of the actual proportions using a CRM quantile estimate on a perfect wind power forecast and the solid line deviations when an actual (artificial) wind power forecast is used.

As expected, deviations from nominal proportions are higher in the case of an actual forecast and increase with increasing wind power forecast time resolution  $k$ . However, for higher rank quantiles differences between the perfect and actual forecast quantile estimates are smaller. Table 5.15 presents the reliability RMSE in percent for all wind farms under various wind power forecast resolutions, using a perfect and an actual wind power forecast.

From Fig. 5.22 it becomes evident that the reliability of each quantile estimate when an actual wind power forecast is used is much less than the  $\text{NMAE}_k$  of the wind power forecast for each wind power forecast time resolution  $k$ . For example, though the  $\text{NMAE}_k$  for  $k=60$  minutes is 15% (taken from Table 5.14), the reliability of all quantile estimates is less than 11%. Thus the uncertainty of the wind power variability forecast is less than the uncertainty of the wind power forecast used as input. This is true for all wind farms considered, as can be seen from Table 5.15. However, the reliability RMSE and the NMAE should not be confused. An NMAE of 15% means that the average absolute wind power forecast error is 0.15 p.u. (based on the wind farm's nameplate capacity). Thus, NMAE refers to deviations of a forecast from an actual wind power production and is measured in power units. On the other hand, reliability RMSE refers to the ability to produce quantile estimates with proportions close to the nominal. Thus, reliability of RMSE refers to deviation from proportions and is a unitless number. A reliability RMSE of 10% means e.g. that the CRM 75<sup>th</sup> percentile estimate using an artificial forecast corresponds on average to an actual 85<sup>th</sup> or 65<sup>th</sup> percentile.

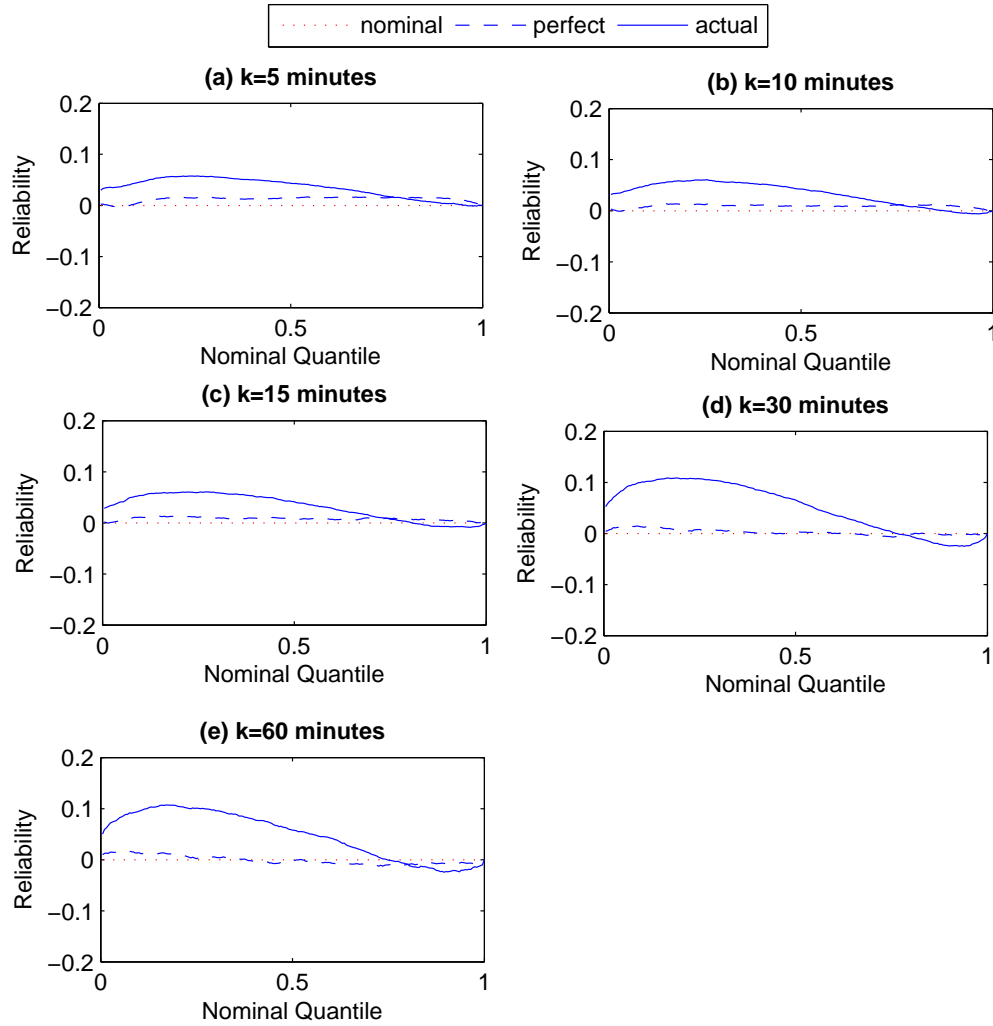


Figure 5.22: Reliability diagram of the CRM quantile estimates of a 120.6 MW wind farm (WF3) for various wind power forecast resolutions  $k = 5, 10, 15, 30$  and  $60$  minutes under the sample quantile estimate approach using an artificial wind power forecast. The solid line represents the deviations from nominal of the actual proportion using an actual forecast, while the dashed line represents deviations from nominal of the actual proportions using a perfect forecast. Uncertainty in the wind power forecast increases deviations from nominal proportions.



Table 5.15: RMSE of Reliability in percent for all Wind Farms using Sample Quantiles on Actual and Perfect Wind Power Forecasts

k = 5 minutes										
	Wind Farm									
Forecast	2	3	4	5	6	7	11	13	14	15
Perfect	0.97	1.34	1.70	2.59	0.74	2.11	2.31	1.55	3.55	1.95
Actual	3.45	3.92	3.29	6.45	2.06	3.77	6.62	3.58	2.78	3.79
k = 10 minutes										
	Wind Farm									
Forecast	2	3	4	5	6	7	11	13	14	15
Perfect	1.09	0.96	1.96	2.52	0.61	2.38	2.76	1.56	4.92	2.14
Actual	3.78	3.95	4.09	6.54	2.29	4.45	7.05	3.71	1.68	4.38
k = 15 minutes										
	Wind Farm									
Forecast	2	3	4	5	6	7	11	13	14	15
Perfect	1.11	0.85	1.91	2.40	0.56	2.46	2.85	1.32	5.47	2.01
Actual	3.91	3.97	4.37	6.66	2.41	4.59	7.28	3.67	1.61	4.37
k = 30 minutes										
	Wind Farm									
Forecast	2	3	4	5	6	7	11	13	14	15
Perfect	0.90	0.59	1.93	2.81	0.59	2.28	3.30	0.93	4.82	2.20
Actual	7.75	6.94	7.89	11.34	5.59	7.29	11.90	6.84	5.72	7.96
k = 60 minutes										
	Wind Farm									
Forecast	2	3	4	5	6	7	11	13	14	15
Perfect	0.58	0.83	1.82	2.83	0.82	1.96	3.93	0.86	3.91	1.90
Actual	8.26	6.62	9.36	11.64	6.35	7.69	12.69	6.67	7.44	8.56

### 5.5.3 Comparison of the CRM Sample Quantiles between a Perfect and an Actual Wind Power Forecast

Figure 5.23 depicts the reliability RMSE increment when the actual (artificial) instead of the perfect wind power forecast is used as a function of the wind farm nameplate capacity for various wind power forecast time resolutions  $k$ . The reliability RMSE increment is on average 2% for wind power forecast resolutions  $k=5, 10$  and  $15$  minutes and 6% for wind power forecast resolutions  $k=30$  and  $60$  minutes and does not vary much by wind farm size. It is reminded that the respective wind power forecast mean absolute errors are  $\text{NMAE}_k=8\%$  for  $k=5, 10$  and  $15$  minutes and  $\text{NMAE}_k=15\%$  for  $k=30$  and  $60$  minutes.

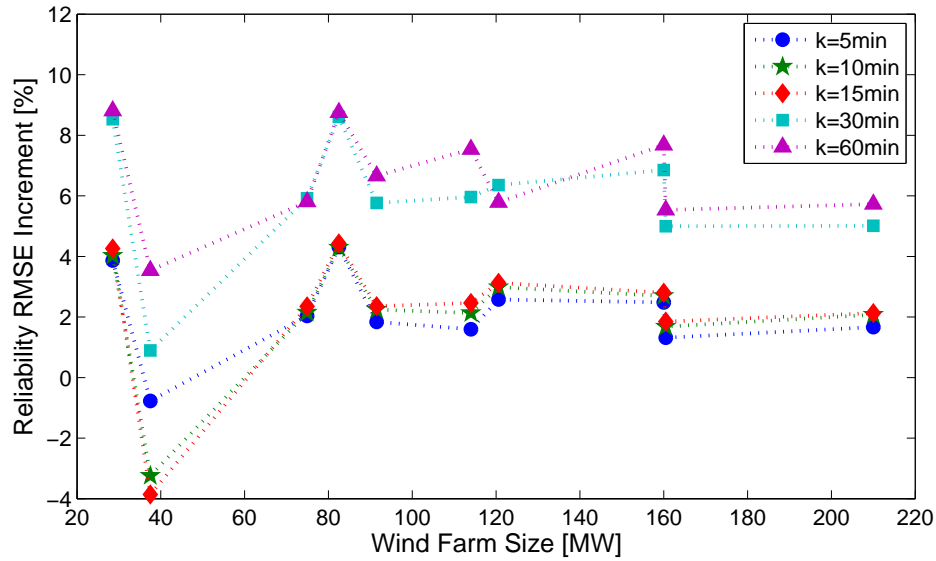


Figure 5.23: CRM quantile reliability RMSE increment when an actual (artificial) instead of a perfect wind power forecast is used as a function of wind farm nameplate capacity for various wind power forecast time resolutions. The reliability RMSE increment is similar for same NMAE values, regardless of wind farm size.

To better understand the effect of the wind power forecast NMAE on the CRM quantile estimates the expected size  $\hat{C}R_k$  of the estimated CRM interval will be used, as defined in (3.21):

$$\hat{C}R_k = \frac{\sum_p \hat{C}R_{k,p}}{q} = \frac{\sum_p \sum_j \hat{C}R_{k,l_j,p} \cdot P(\tilde{y}_{k,i} = l_j)}{q} \quad (5.63)$$

where  $q$  is the quantile resolution,  $w_j = P(\tilde{y}_{k,i} = l_j)$  are the frequencies of appearance of the various forecasted wind power production levels, and  $\hat{C}R_{k,l_j,p} = \hat{M}_{up,k,l_j,p} - \hat{M}_{low,k,l_j,p}$  is the size of the respective estimate CRM interval. When the sample quantile of the training set is used the estimate  $\hat{C}R_{k,l_j,p}$  takes the same values, regardless of whether a perfect or an actual forecast is used. Then, the mean absolute difference in the expected interval size when an actual instead of a perfect forecast is used is given by:

$$MAD_{CR} = \frac{\sum_p \sum_j \hat{C}R_{k,l_j,p} \cdot |P(\tilde{y}_{k,i} = l_j) - P(y_{k,i} = l_j)|}{q} \quad (5.64)$$

Thus, the reason why CRM quantile estimate size and reliability RMSE change with varying wind power forecast NMAE is that the weights  $w_j$  change between a perfect and an actual forecast.

Figure 5.24 depicts the CRM expected size difference when an actual instead of a perfect wind power forecast is used as a function of wind farm nameplate capacity for various wind power forecast time resolutions. For wind power forecast resolutions  $k=5, 10$  and  $15$  minutes the wind power forecast NMAE is  $0.08$  p.u. while the difference in expected CRM interval size is less than  $0.002$  p.u. (normalized on the wind farm size). Respectively, for wind power forecast resolutions  $k=30$  and  $60$  minutes the wind power forecast NMAE is  $0.15$  p.u. while the difference in expected CRM interval size is less than  $0.015$  p.u.

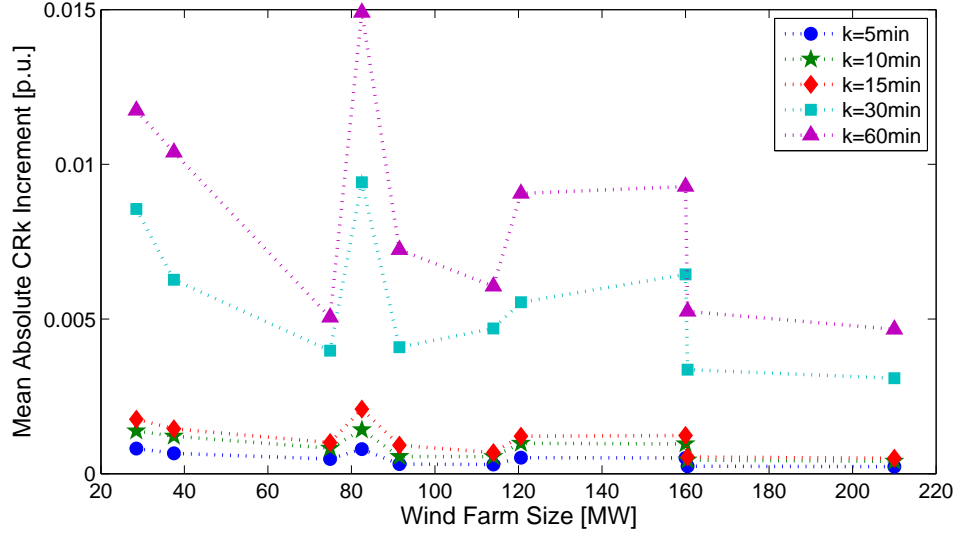


Figure 5.24: CRM expected size difference when an actual (artificial) instead of a perfect wind power forecast is used as a function of wind farm nameplate capacity for various wind power forecast time resolutions. The difference in CRM size is much smaller than the respective wind power forecast NMAE.

The CRM quantile estimate reliability RMSE of all wind farms as a function of the wind power forecast NMAE is depicted in Fig. 5.25 for wind power forecast resolution  $k=5$  minutes and in Fig. 5.26 for wind power forecast resolution  $k=60$  minutes. Similarly, Fig. 5.27 and 5.28 depict the expected increase in CRM interval size of all wind farms as a function of NMAE. In these figures the solid lines refer to smaller wind farms with capacities less than 100 MW and the dashed lines to wind farms with capacities greater than 100 MW.

From Fig. 5.25 and Fig. 5.26 it is evident that the reliability RMSE of the CRM quantile estimates increases with increasing wind power forecast error NMAE, and in fact this increase is higher for smaller than for larger wind farms, especially for smaller forecast time resolutions. However, the relative

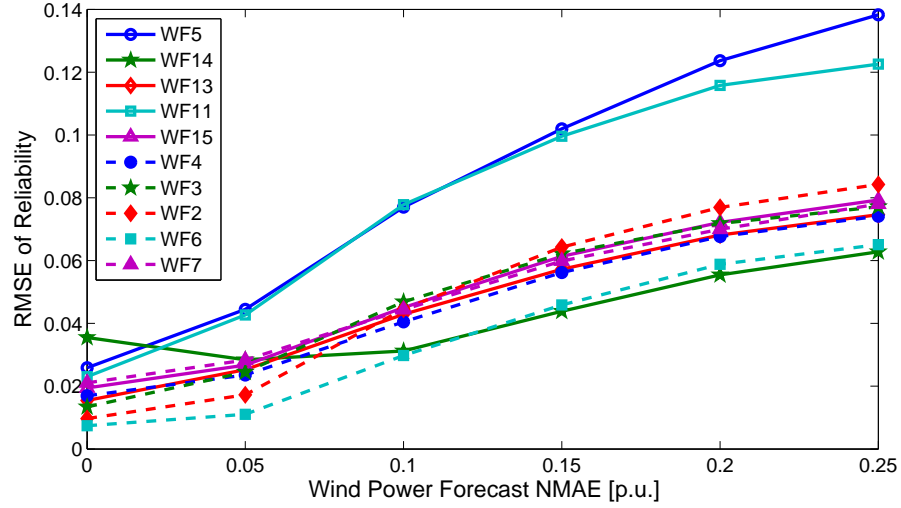


Figure 5.25: CRM quantile estimate reliability RMSE as a function of the wind power forecast NMAE for wind power forecast resolution  $k=5$  minutes.

increase in reliability RMSE is decreasing as the wind power forecast errors increase.

Regarding the CRM interval size, it also increases with increasing forecast error, and in fact in an almost linear relationship as can be seen from Fig. 5.27 and Fig. 5.28. The mean absolute CRM interval size increment is less than 0.005 p.u. regardless of NMAE for  $k=5$  minutes, and for  $k=60$  minutes the highest CRM increment is almost ten times lower as the respective NMAE. Thus, with increasing uncertainty in the average wind power production the expected CRM interval size increases as well, but at a much slower rate.

It should be noted that the results obtained in this section regarding the effect of wind power forecast uncertainty on wind power variability forecast uncertainty are based on certain assumptions on the forecast error sizes and their distribution. More accurate results and conclusions require the use of a large set of forecasted data paired with actual data.

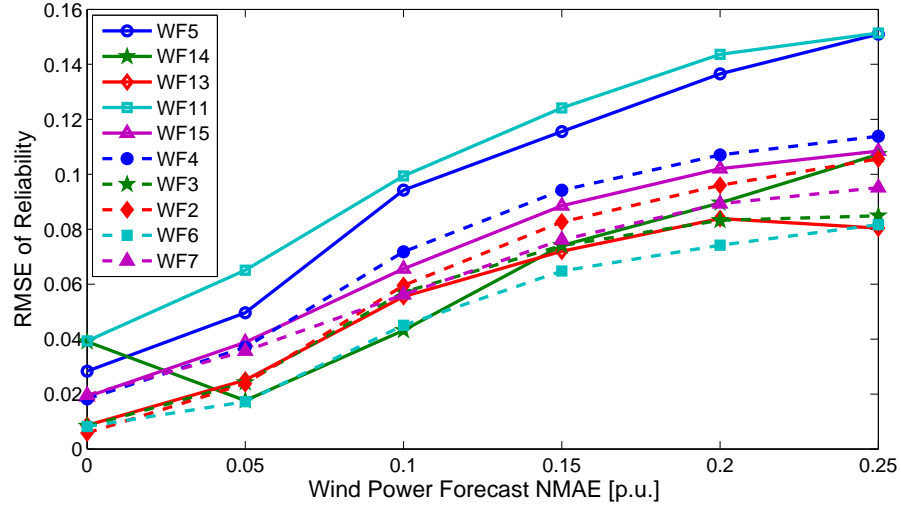


Figure 5.26: CRM quantile estimate reliability RMSE as a function of the wind power forecast NMAE for wind power forecast resolution  $k=60$  minutes. Reliability RMSE increases with increasing wind power forecast error by a higher rate for smaller (solid lines) than for larger (dashed lines) wind farms.

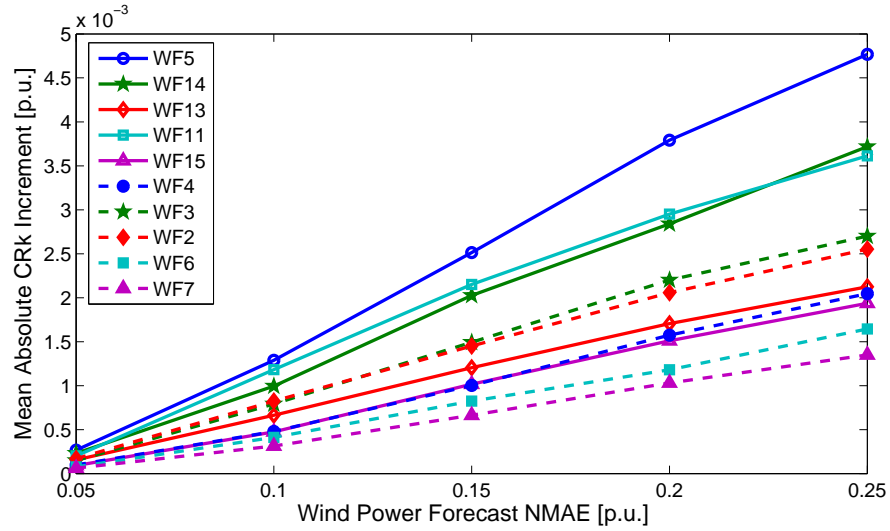


Figure 5.27: CRM expected size difference when an actual instead of a perfect wind power forecast is used as a function of the wind power forecast NMAE for  $k=5$  minutes.

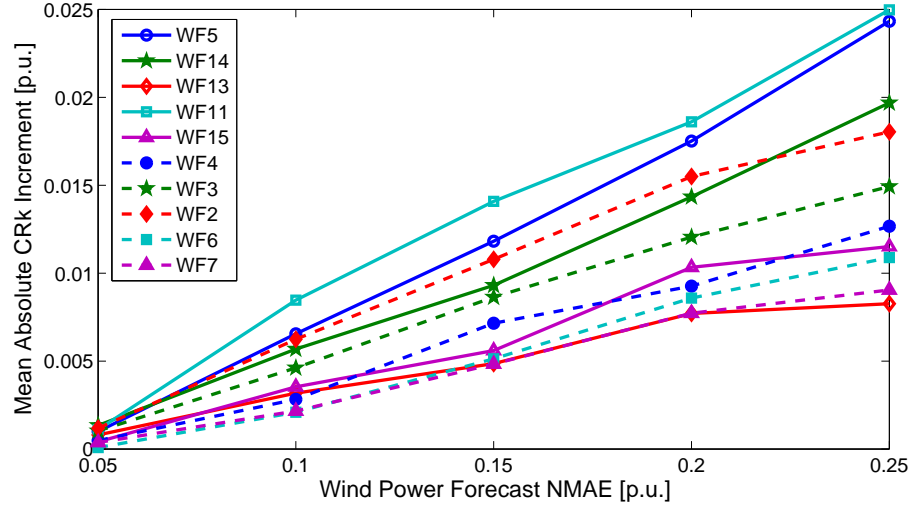


Figure 5.28: CRM expected size difference when an actual instead of a perfect wind power forecast is used as a function of the wind power forecast NMAE for  $k=60$  minutes. With increasing uncertainty in average wind power its variability increases too, but by a much smaller increment.

## 5.6 Concluding Remarks

Wind power is inherently variable and uncertain. The effects of wind power uncertainty on power system planning, operations and costs are mitigated using wind power forecasts, which are generated from an increasing number of methods with significant reduction in forecast errors, as is summarized in Section 5.1. Realizing that intra-hour wind power variability exists even under perfect hourly forecasts and becomes comparable to demand variability as wind power penetration levels increase, makes the call for intra-hour wind power variability forecasts natural.

The proposed wind power variability forecasts consist of intervals within which the wind power output will lie with a certain probability as is described in Section 5.2. To obtain these probabilistic intervals the conditional

range metric quantiles are estimated with one static (sample quantile) and two time-adaptive methods (exponentially weighted moving average, exponentially weighted stochastic approximation) presented in Section 5.3. The resulting quantile estimates from the three methods are compared using their reliability, sharpness and resolution. Reliability refers to the method’s ability to produce quantiles with proportions close to the nominal ones, whereas sharpness indicates consistence in quantile estimates and resolution signifies the ability to produce situation-dependent quantile estimates.

Under all considered methods, reliability tends to be better at mid-production levels, denoting that though wind power variability is highest at mid-production levels it is more predictable at these levels. Moreover, the total reliability of each quantile estimate is significantly better than the production specific reliability. Average expected deviations from nominal proportions are close to 1% under all methods, whereas maximum expected deviations don’t exceed 5% and minimum expected deviations are lower than 0.5%. Regarding the effect of the nominal proportion, high rank quantiles tend to be more reliable than lower rank quantiles for all methods, a quality highly desired since it is the high rank quantiles associated with low risk parameters that are of interest. While reliability appears to be unaffected by wind power forecast time resolution, it tends to improve with increasing wind farm nameplate capacity and increasing wind turbine size.

Both time-adaptive quantile estimation approaches considered produce more reliable estimates than the static sample quantile method, since they can effectively improve upon the reliability of a bad initial sample quantile estimate. Evolving quantiles are also more appropriate for distinguishing between different wind power variability situations, however the computational aspects of time-adaptive methods need to be factored in. In addition, as can be seen



from the results in Section 5.4, seasonal analysis of historical data can lead to better initial estimates for the time-adaptive methods.

Finally, the analysis using an artificial wind power forecast presented in Section 5.5 reveals that the reliability of the quantile estimates deteriorates with increasing wind power forecast error levels. In fact, the increase in deviation from nominal proportions is higher for smaller sized wind farms and larger wind power forecast time resolutions. Nonetheless, the increase in the expected wind power variability interval size is not proportional, revealing that intra-hour wind power variability increases with increasing hourly wind power uncertainty, but at a much slower rate.

## Chapter 6

### Example Application of the Conditional Range Metric: Energy Storage System Size Estimation

Wind power is very variable and unpredictable and these characteristics of wind power pose significant risk to both system planners and operators, as well as wind farm owners and investors. The effects of wind power variability on system planning and operations, which appear in the form of increased ramp rates, increased time periods with minimum generation, and increased operating reserve requirements, have been examined in the various wind integration studies presented in Section 2.2. Regarding wind farm owners and investors, wind power variability has been considered as one of the largest inhibiting factors in participating in day-ahead and hour-ahead markets. Deviations from wind generation schedules beyond a certain tolerance band would incur significant penalties [91, 92].

The proposed conditional range metric and the resulting wind power variability forecasts provide system operators and wind farm owners with useful information about past, present and future wind power variability. This information can be summarized in sets of wind power inequalities of the form:

$$M_{low_{k,l_j,p}} \leq x_n \leq M_{up_{k,l_j,p}} \quad \text{with probability } p \quad (6.1)$$

for various probabilities  $p$ . When  $x_n$  refers to historical wind power time series data with average production level of  $l_j$  over  $k$ -long time intervals,

the endpoints of the inequality in (6.1) are obtained using the methodology presented in Section 3.3. When  $x_n$  refers to future wind power data, (6.1) forces wind power production with  $k$ -long forecast  $\tilde{x}_k = l_j$  to lie within  $[\hat{M}_{low_{k,l_j,p}}, \hat{M}_{low_{k,l_j,p}}]$ , which are the quantile estimates of  $CRM$  calculated with one of the methodologies presented in Section 5.3.

Probabilistic wind power inequalities in the form of (6.1) using historical data can be useful in assessing wind power variability, as has already been pointed out in Chapter 4. Through these inequalities influential variables on wind power variability, such as the wind farm nameplate capacity or the wind turbine generator size, can be identified. The quantification of wind power variability under various conditions is useful in determining critical periods with increased wind power variability or large wind power ramps, and allows for better management of wind power variability in general. Moreover, the exploration of the characteristics of wind power variability can assist in deciding the flexibility requirements of future generation portfolios so as to accommodate the increasing wind power penetration.

Indeed, acknowledging that the effects of wind power variability become more adverse as wind power penetration levels increase, deems the development of wind power management strategies necessary. Wind power variability forecasts in the form of the inequalities of (6.1) can be used as input in new wind power management tools or be integrated in existing power system key management functions. Such inequalities can then be applied to decision support tools which use stochastic analysis and optimization, such as probabilistic power flow problems, optimal generation scheduling algorithms (e.g. stochastic economic dispatch), or even transmission congestion management tools. Furthermore, the use of short-term wind power variability forecasts can aid in the establishment of new reserve estimation algorithms and reserve allocation

procedures. On the other hand, and perhaps more from a wind farm owner's perspective, wind power variability forecasts are a significant tool to hedge against wind power uncertainty through the coordination between wind power plants and pumping storage plants.

This chapter provides an example application of how wind power variability forecasts can be used to mitigate the effects of intra-hour wind power variability, by providing a methodology to estimate the size (power and energy capacities) of an energy storage system with the goal of minimizing deviations from the forecasted hourly average wind power production. The coupling of wind farms with energy storage units so as to reduce the effects of wind power variability and uncertainty has been the subject of numerous papers within the past years [93–99]. A simple probabilistic method to predict the ability of energy storage in increasing the penetration of intermittent renewable generation in weak electricity grids is presented in [93]. The application of storage-based standing reserves in managing wind power fluctuations and uncertainty in wind generation forecasts is investigated in [94]. In [95] authors use dynamic programming for computing the optimal energy storage - wind farm coordination so as to minimize the wind generation schedule deviation. Similarly, in [96] authors model a co-located power generation and energy storage block, which contains wind generation, a gas turbine and a fast-ramping energy storage unit. The system is designed to produce near-constant power at a reasonable cost, while still delivering a fraction of that power from wind. In [97] a battery energy storage system is sized to obtain an optimal dispatched power level from a wind farm. Dynamic sizing of energy storage capacity is proposed for different delivery periods in [98], essentially using energy storage as a risk hedging means against penalties for deviations from the agreed wind generation schedule.

While some of these papers contain methodologies for simulating different forecast errors, e.g. Gaussianity is proposed in [94] and an exponentially weighted moving average approach is given in [99], most of these papers are based on given wind power profiles, and in others wind power is erroneously represented with an average wind power value over a time interval (ranging from 5 minutes to one hour). In the proposed energy storage size estimation methodology, a probabilistic forecast of the hourly average wind power production and the inverse of the joint cumulative distribution of the maximum and minimum deviations from the hourly average are used to generate hour-long wind power production scenarios, following an approach similar to that described in [100].

In Section 6.1 the methodology to generate the hour-long wind power production scenarios is presented and Section 6.2 describes how the energy storage system characteristics and their statistics are determined. The proposed methodology is then applied on real-world wind power production data and the evaluation of the results is given in Section 6.3, while Section 6.4 concludes the chapter.

- **Publication:** Part of the work presented in this chapter has been published in [5]:
  - T. Boutsika and S. Santoso, “Sizing an energy storage system to minimize wind power imbalances from the hourly average,” in *Power and Energy Society General Meeting, 2012 IEEE*, July 2011, pp. 1-8.

## 6.1 Generation of Hour-long Wind Power Production Scenarios

When an energy storage system is used to minimize power imbalances, it essentially operates as an integrator of the respective energy imbalances. Thus, its capacity is determined not only by the magnitude but also by the sequence of the power imbalances, making a wind power time series a necessary input for the energy storage system sizing methodology. This section describes the methodology to generate wind power production scenarios with qualities similar to an actual wind power profile. Generating scenarios instead of using a real-world wind power time series allows for a larger number of realistic cases to be explored and improves the performance of the resulting statistics.

The proposed methodology to generate hour-long wind power production scenarios with a one-minute resolution requires a probabilistic forecast  $f_L$  of the hourly average wind power production  $l_j$ , and the inverse of the joint cumulative distribution  $F_{(A,B),l_j}^{-1}$  of the minimum  $a$  and maximum  $b$  deviations from the hourly average  $l_j$ .

For the wind power production time series  $x_n$  with a one-minute resolution the probabilistic forecast of the hourly average  $l_j$  is defined as its probability mass function:

$$f_L(l_j) = P(\bar{x}_n \in l_j), \quad (6.2)$$

where  $\bar{x}_n$  refers to average wind power production:

$$\bar{x}_n = \frac{1}{60} \sum_{n=k}^{k+59} x_n, \quad k = (i-1) \cdot 60 + 1, i \in \mathbb{N} \quad (6.3)$$

Here  $\bar{x}_n \in l_j = j/m$  refers to the normalized average wind power production interval  $(2j-1)/2m < \bar{x}_n \leq (2j+1)/2m$ , where  $1/m$  is the production resolution and  $j = 1, 2, \dots, m$ . The desired one-minute resolution stems from the

typical resolution of real-world wind power data used to evaluate the proposed methodology. However (6.2) and (6.3) can be adapted to match any desired time series or average production level resolution. The cumulative probability mass function of  $\bar{x}_n$  is then given by:

$$F_L(l_j) = P(\bar{x}_n \leq l_j) = \sum_{i \leq j} f_L(l_i). \quad (6.4)$$

Figures 6.1 and 6.2 depict the probability and the cumulative probability mass function, respectively, for a production resolution of  $1/m=0.05$  p.u., using data from a 160.5 MW wind farm over one year (WF6, year 4 - see Appendix A.1).

The joint cumulative probability distribution function  $F_{(A,B),l_j}$  of the minimum  $a$  and maximum  $b$  deviations from the hourly average  $l_j$  is defined as:

$$F_{(A,B),l_j}(a, b) = P((A \leq a) \cap (B \leq b)) \quad (6.5)$$

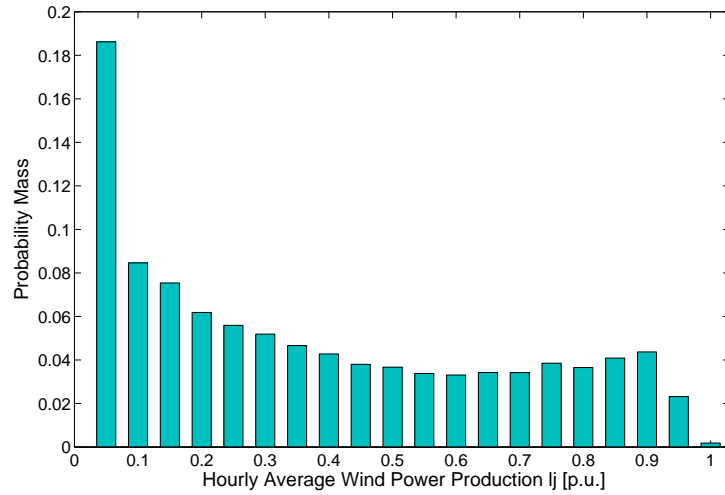


Figure 6.1: Probability mass function of the hourly averages over a year for a 160.5 MW wind farm (WF6, year 4). Most mass is concentrated at low production levels.

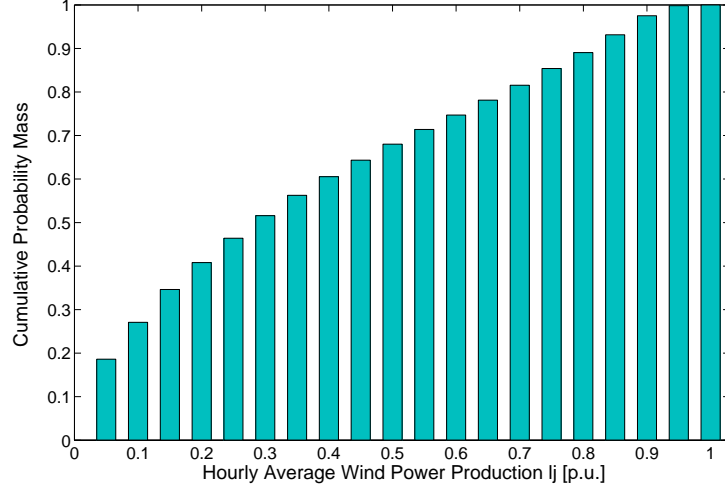


Figure 6.2: Cumulative probability mass function of the hourly averages over a year for a 160.5 MW wind farm (WF6, year 4).

which states that the wind power production  $x_n$  stays within the interval  $[l_j - a, l_j + b]$  for all points within the hour,  $n \in [k, k + 59]$ ,  $k = (i - 1) \cdot 60 + 1$ ,  $i \in \mathbb{N}$ , with probability at least  $p$ . The respective inverse of the joint cumulative distribution function, also known as the quantile function  $Q_{(A,B),l_j}(p)$ , is then defined as:

$$\begin{aligned} F_{(A,B),l_j}^{-1}(p) &= Q_{(A,B),l_j}(p) \\ &= \{(a, b) : F_{(A,B),l_j}(a, b) = p\} \end{aligned} \quad (6.6)$$

Thus, for any  $l_j$  hourly average wind power production and any given  $p \in (0, 1)$  the previously defined quantile function essentially provides the values  $a = l_j - M_{low_k, l_j, p}$  and  $b = l_j + M_{up_k, l_j, p}$ . To obtain a finite subset of the target set of the quantile function in (6.6) from an  $N$ -long wind power time series  $x_n$ , the system of equations (3.7) and (3.10) from Section 3.3 is repeatedly solved for various discrete probabilities  $p$  over its support  $p \in (0, 1)$ . Figure 6.3 de-



picts the quantile function for  $l_j=0.5$  p.u.,  $m = 20$  and  $p = 0.1, 0.2, \dots, 0.9$ , using data from a 160.5 MW wind farm over one year (WF6, year 4). For example, Fig. 6.3 shows that with a 70% probability the largest minimum deviation from the hourly average is less than  $a = 0.122$  p.u., whereas the largest maximum deviation is less than  $b = 0.126$  p.u.

To generate one hour-long wind power production scenario  $x_n$ , with  $n \in [1, 60]$ , first an hourly average production level  $\bar{x}_n = l_j = j/m$  has to be decided. For this, a production level  $l_j$  is randomly chosen so as to follow the probability distribution of hourly average production levels  $f_L$ . To generate the random variable  $L$  from a uniform random variable  $\mathcal{U}(0, 1)$  it needs to be passed through the inverse of the cumulative probability mass function  $F_L$  ( $L \sim F_L^{-1}(\mathcal{U})$ ), with  $F_L$  taken from (6.4). It should be noted that since the probability distribution of the hourly average  $f_L(l_j)$  is discrete rather than

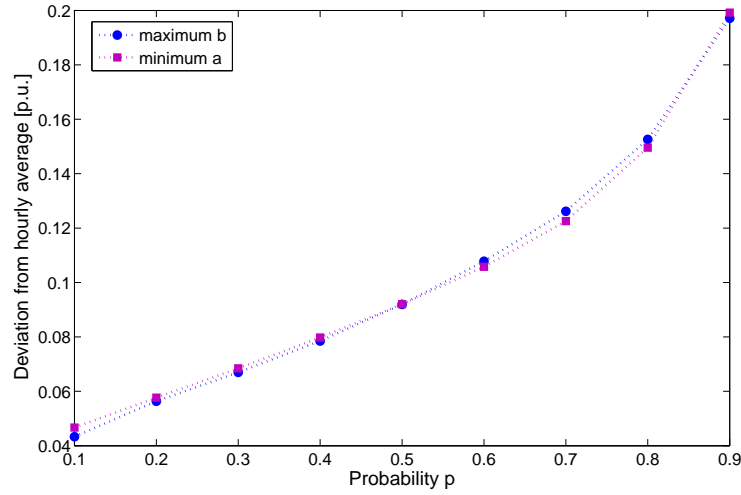


Figure 6.3: Quantile function of the minimum  $a$  and maximum  $b$  deviations from the hourly average  $l_j = 0.5$  p.u. over a year for a 160.5 MW wind farm (WF6, year 4).

continuous, there may be gaps between values in the domain of its cumulative distribution function  $F_L(l_j)$ , which means that the randomly chosen hourly averages may not exactly follow  $f_L(l_j)$ .

After deciding the hourly average  $l_j$  the minimum  $a$  and maximum  $b$  deviations from the hourly average are chosen randomly. Again, to generate the random variable pair  $(A, B)$  from a uniform random variable  $\mathcal{U}(0, 1)$  it needs to be passed through the inverse of the cumulative joint probability distribution function  $F_{(A,B)}$  ( $(A, B) \sim F_{(A,B)}^{-1}(\mathcal{U})$ ) from (6.6). Thus, sampling a random number  $p$  uniformly from  $(0, 1)$  and passing it through the quantile function  $Q_{(A,B),l_j}$  in (6.6) returns a unique pair of minimum  $a$  and maximum  $b$  deviations from the hourly average  $l_j$ . In this way two points of the hour-long wind power production scenario are defined, the minimum production  $x_1 = l_j - a$  and the maximum production  $x_2 = l_j + b$ .

Next, the remaining 58 points from the hour-long wind power production scenario  $x_n$ ,  $n = 3, \dots, 60$ , need to be chosen. Disregarding any other possibly obtained information on the parametric wind power production intra-hour distribution, the points are chosen from a common probability distribution. A first choice for a common distribution is the normal distribution  $\mathcal{N}(\mu, \sigma^2)$ , with parameters mean  $\mu = l_j$  and standard deviation  $\sigma = (b + a)/4 = (x_2 - x_1)/4$ . The reasoning for choosing the above mean is that the randomly chosen wind power production points will have an average close to  $l_j$ . The choice of the standard deviation stems from the fact that 95% of the values from a normal distribution lie within two standard deviations from the mean, thus 95% of the randomly chosen wind power production points will lie within  $[l_j - (b + a)/2, l_j + (b + a)/2]$ . Alternatively, the remaining 58 points from the hour-long wind power production scenario can be sampled randomly from a uniform distribution  $\mathcal{U}(l_j - a, l_j + b)$ , which however will provide satisfactorily

results only if  $a$  and  $b$  are almost equal.

In general, the deviations  $a$  and  $b$  are not centered around the hourly average  $l_j$ , thus  $b - a \neq 0$ . In this case, choosing the wind power production points uniformly from  $\mathcal{U}(l_j - a, l_j + b)$  results in the average of the generated hour-long production differing from the desired average  $l_j$  by  $(b - a)/2$ . If the wind power production points are chosen from a normal distribution  $\mathcal{N}(\mu, \sigma^2) = \mathcal{N}(l_j, (b + a)^2/16)$  the desired average  $l_j$  is preserved, but probably more than 5% of the generated wind power production points will lie outside  $[l_j - a, l_j + b]$ , which alters the desired maximum and minimum wind power production points in the scenario. To overcome this issue, the wind power production points can be sampled randomly from a truncated normal distribution with parameters  $\mu = l_j$ ,  $\sigma = (b + a)/4$ , minimum value  $l_j - a$  and maximum value  $l_j + b$ . For the truncated normal the desired minimum  $a$  and maximum  $b$  deviations are preserved, while, according to [101], the average of the generated hour-long production will differ from the desired average  $l_j$  only by:

$$\frac{\frac{1}{\sqrt{2\pi}} \left[ e^{-\frac{1}{2} \frac{16a^2}{(a+b)^2}} - e^{-\frac{1}{2} \frac{16b^2}{(a+b)^2}} \right]}{\Phi\left(\frac{4b}{a+b}\right) - \Phi\left(-\frac{4a}{a+b}\right)} \sigma \quad (6.7)$$

where  $\Phi(\cdot)$  is the standard normal cumulative distribution function. Since the inverse of the joint cumulative probability distribution  $F_{(A,B),l_j}^{-1}$  of the minimum  $a$  and maximum  $b$  deviations from the hourly average  $l_j$  is conditioned on  $l_j$  a distribution which produces an hourly average closer to  $l_j$  is preferable, and thus the remaining 58 points from the hour-long wind power production scenario are chosen from the truncated normal distribution  $\mathcal{TN}_{l_j-a}^{l_j+b}(l_j, (b+a)^2/16)$  using the algorithm described in Section 5.5.1.

Finally, since the size of the energy storage needed to minimize the

deviations  $x_n - \bar{x}_n$  from the hourly average  $\bar{x}_n$  is dependent not only on the magnitude but also on the sequence of the deviations, the sequence of the 60 generated wind power production points  $x_n$ ,  $n = 1, 2, \dots, 60$  is randomized by rearranging their order, either ascending or descending with equal probabilities. The reason behind this simplistic arrangement is that over longer time frames the changes in the output of a wind farm appear less as noise and rather follow a distinct trend, increasing or decreasing, which is dictated by weather related changes in the wind speed.

Thus the algorithm used for producing one hour-long wind power production scenario  $x_n$ , with  $n \in [1, 60]$ , is summarized as follows:

1. Generate a uniform random number  $u \sim \mathcal{U}(0, 1)$  and pass it through the inverse of (6.4) to obtain an hourly average  $l_j$ .
2. Generate a uniform random number  $p \sim \mathcal{U}(0, 1)$  and pass it through (6.6) to obtain minimum  $a$  and maximum  $b$  deviations from the hourly average  $l_j$ .
3. Take two points to be the minimum  $x_1 = l_j - a$  and the maximum production  $x_2 = l_j + b$  in the scenario.
4. Obtain the remaining 58 points by sampling randomly from a truncated normal  $\mathcal{TN}_{l_j-a}^{l_j+b}(l_j, (b+a)^2/16)$ .
5. Perform a Bernoulli trial with  $p = 0.5$ . If the result is 0 order the  $x_n$  generated wind power points in ascending order, else order them in descending order.

Figure 6.4 shows five hour-long wind power production scenarios having the same average  $l_j = 0.3$  p.u., maximum  $l_j + b = 0.382$  p.u., and minimum

$l_j - a = 0.186$  p.u., generated using the described methodology. The dashed line corresponds to an actual wind power production series of a 160.5 MW wind farm (WF6), from which the hourly average probability distribution and the inverse of the joint cumulative probability distribution function of the minimum and maximum deviations from the hourly average have been taken using the data in one year (year 4). The dashed line in Fig. 6.4 clearly contradicts the ordering (ascending or descending) of the minute wind power values assumption, however the evaluation of the proposed ESS sizing methodology on real-world wind power data will quantify the effect of the invalidity of this simplistic assumption.

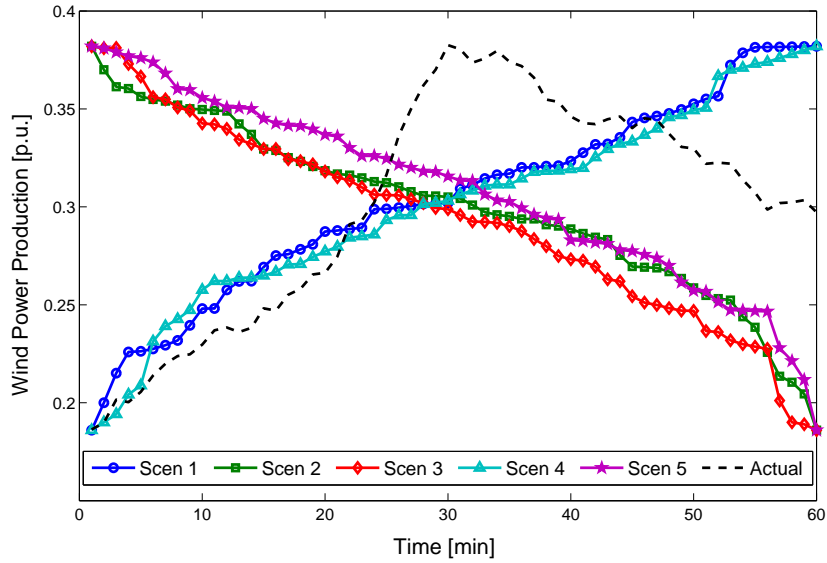


Figure 6.4: Five 60-minute wind production scenarios having the same hourly average, maximum and minimum production. The dashed line corresponds to an actual hourly wind power production of a 160.5 MW wind farm (WF6). The required storage size to compensate for wind power imbalances from the hourly average is different for each scenario, since it is determined by both the exact magnitude and sequence of the imbalances.

## 6.2 Statistical Calculation of the ESS Capacities

In this section the methodology to calculate the statistics of the capacities (power and energy) of the energy storage system (ESS) used to minimize power imbalances from a desired production level is presented. For each hour-long wind power production scenario  $m$  generated using the methodology presented in Section 6.1 the following time series are defined with a one-minute resolution,  $i = 1, 2, \dots, 60$ :

- Wind power production  $P_{w,m}(i)$ ,
- ESS power  $P_{b,m}(i)$ ,
- ESS energy  $E_{b,m}(i)$ .

For each minute  $i = 1, 2, \dots, 60$  the ESS power  $P_{b,m}(i)$  is defined as the difference between the desired power production  $P_d$  and the wind power production  $P_{w,m}(i)$ :

$$P_{b,m}(i) = P_d - P_{w,m}(i) \quad (6.8)$$

Similarly, the ESS energy  $E_{b,m}(i)$  is defined as the difference between the energy in the previous time-step  $E_{b,m}(i-1)$  and the energy charged into the battery or discharged from the battery in the current cycle  $P_{b,m}(i)$  (actually  $P_{b,m}(i) \cdot \Delta t$ , where  $\Delta t$  refers to one step in the time series, i.e. 1 minute). When the ESS power output is positive  $P_{b,m}(i) \geq 0$  there is a wind power deficiency and the ESS is discharged:

$$E_{b,m}(i) = E_{b,m}(i-1) - P_{b,m}(i) \cdot \sqrt{\eta} \quad (6.9)$$

while a negative ESS power output  $P_{b,m}(i) < 0$  signifies a wind power surplus and the charging of the ESS:

$$E_{b,m}(i) = E_{b,m}(i-1) - P_{b,m}(i)/\sqrt{\eta} \quad (6.10)$$

In (6.9) and (6.10)  $\eta$  refers to the roundtrip efficiency of the storage system, defined as the ratio of the energy used for charging to the energy used for discharging the storage system:

$$\eta = \frac{E_{charging}}{E_{discharging}} \quad (6.11)$$

The losses are then divided geometrically between the charging and discharging portions of the ESS cycle as in [96]. The described methodology is generic and sets no limit to the technology used in the ESS, which could be implemented using batteries, flywheels, supercapacitors or even ancillary services. However, it should be noted that the choice of technology heavily affects the resulting roundtrip efficiency, which can range from 70% for batteries and supercapacitors to 90% for flywheels.

For each wind power production scenario  $m$  the following ESS characteristics are then defined:

- Minimum ESS power

$$P_{min,m} = \min_i P_{b,m}(i) \quad (6.12)$$

- Maximum ESS power

$$P_{max,m} = \max_i P_{b,m}(i) \quad (6.13)$$

- ESS power capacity

$$P_{size,m} = \max_i |P_{b,m}(i)| \quad (6.14)$$

- Minimum ESS energy

$$E_{min,m} = \min_i E_{b,m}(i) \quad (6.15)$$

- Maximum ESS energy

$$E_{max,m} = \max_i E_{b,m}(i) \quad (6.16)$$

- ESS energy capacity

$$E_{size} = E_{max} - E_{min} \quad (6.17)$$

In (6.9) and (6.10) the ESS is considered to be initially discharged,  $E_b(0) = 0$ , and the energy of the ESS is assumed to take negative values. This assumption simplifies the calculation of the ideal initial energy in the ESS, which for each scenario is the resulting minimum ESS energy  $E_{min}$ , i.e.  $E_b(0)_{ideal} = |E_{min}|$ . Moreover, if the desired production  $P_d$  is taken as the hourly average, then  $P_b$  will assume both positive and negative values forcing  $P_{min}$  to be negative.

For  $M$  hour-long wind power production scenarios, generated using the methodology described in Section 6.1, the ESS characteristics form  $M$ -long data samples from which their statistics, such as the sample mean, the sample standard deviation and the sample quantiles, can be estimated. The reason for choosing to calculate the sample quantiles of the ESS characteristics is that they can easily be linked to a desired risk parameter  $\alpha = 1 - p$ . Choosing an ESS with energy capacity  $E_{size} = Q_{E_{size}}(p)$ , where  $Q_{E_{size}}(p)$  is the  $(p)^{th}$  sample quantile of the  $E_{size}$  characteristic, means that there is a risk of  $(1 - p)\%$  of not covering potential wind power imbalances from the hourly average with the specific ESS. Since  $p$  is the probability that the ESS can actually cover potential wind power imbalances from the hourly average,  $p$  is often referred to as the coverage rate.

In the work presented in this application the desired production is set at the forecasted hourly average wind power production,  $P_d = l_j$ , since the goal is to estimate the size of an ESS so as to minimize wind power imbalances



from the hourly average. All power imbalances have to be absorbed, thus wind curtailment is not considered as an option. It is worthwhile to point out that the purpose of the proposed method is to minimize deviations from the generation schedule, which is set at the forecasted hourly average, and thus allow wind farm owners to fully participate in electricity markets and avoid deviation penalties. The proposed method is not intended to result in profit maximization.

Alternatively, in [97] the optimal desired production  $P_d$  for each wind power production scenario is estimated so as to maximize the benefit  $W$  of producing  $P_d$ . The benefit is considered the income from selling the produced energy at the unit price of the wind energy  $c_{price}$ , deducted by the amortized capital costs of the ESS power capacity  $c_{power}$  (in  $\$/MW$ ) and the ESS energy capacity  $c_{energy}$  (in  $\$/MWh$ ):

$$W = c_{price} \cdot P_d - c_{power} \cdot P_{size} - c_{energy} \cdot E_{size} \quad (6.18)$$

To find the optimal  $P_d^*$  the benefit in (6.18) is calculated in an iterative manner for values of  $P_d = 0.01, 0.02, \dots, 1$  p.u. It should be noted that (6.18) does not take into account operating costs of the ESS and deviation costs incurred from deviating from the desired production  $P_d$ .

Estimating the optimal desired production requires prior knowledge of energy market prices and deviation costs, which can vary by region, season and time of day. In addition, operating and capital costs of an ESS depend heavily on the storage technology used (e.g. batteries, flywheels, supercapacitors) and these costs are even harder to estimate if the wind power imbalances are compensated using other generators (ancillary services). Indeed, the investment in an ESS should be the result of a detailed feasibility study which goes beyond the scope of this example application. The proposed methodology deals only

with a first step in this process which is to estimate the size of the ESS based on a wind power production forecast. Depending on the resulting size, the most profitable can then be chosen from the available storage technologies.

### **6.3 Application of the ESS Size Estimation Methodology to Real-world Wind Power Data**

The proposed methodology to estimate the capacities of an ESS so as to minimize the deviations from the wind power production hourly average is evaluated using real-world wind power production data. The data come from 10 wind farms in the ERCOT system, with nameplate capacities ranging from 28.5 MW to 210 MW (WF2 - WF7, WF11, WF13, WF14, WF15 - see Appendix A.1). They include wind power production data with a 1-minute resolution spanning a period of two years. One year is used as a training year for the proposed methodology and the other one as a test year (years 3 and 4, respectively - see Appendix A.1). The evaluation process involves evaluation of the validity of the generated scenarios as well as of the ESS size estimation methodology. The estimated ESS characteristics for a specific wind farm are presented in detail and the performance of the estimated ESS characteristics quantiles using the data in the training year is evaluated on the data of the test year, for all the considered wind farms.

#### **6.3.1 Evaluation of the Generated Scenarios**

The evaluation of the validity of the generated scenarios is done by comparing the probability distributions of the actual data and the data from the generated scenarios. The probability distributions are compared by measuring their statistical distance [102]. The total variation distance of two probability

measures  $f$  and  $\hat{f}$  with an event space comprising of a finite set of discrete events  $x$  is given by:

$$\delta(f, \hat{f}) = \sum_x |f(x) - \hat{f}(x)| \quad (6.19)$$

Alternatively, the statistical distance of two distributions can be measured using their Kullback-Leibler divergence:

$$D_{KL}(f||\hat{f}) = \sum_x f(x) \log \frac{f(x)}{\hat{f}(x)} \quad (6.20)$$

which is the expected number of extra bits required to code samples from  $f$  when using a code based on  $\hat{f}$ , rather than using a code based on  $f$ .

To evaluate the validity of the generated scenarios the probability distribution  $f_L$  of the hourly average wind power production  $l_j$ , as well as the inverse of the joint cumulative distribution  $F_{(A,B),l_j}^{-1}$  of the minimum  $a$  and maximum  $b$  deviations from the hourly average  $l_j$  from wind power production data of a 160.5 MW wind farm (WF6) from the training year (year 3) are used. Using the methodology described in Section 6.1 50,000 hour-long wind power production scenarios are generated, a number large enough to guarantee an adequate number of scenarios for each hourly average wind power production level.

Figure 6.5 depicts the probability mass functions of the hourly average wind power production of the actual data  $f_L$  and the generated scenarios data  $\hat{f}_L$ . The two distributions are very similar and their statistical distance using (6.19) is found to be  $\delta(f_L, \hat{f}_L) = 0.02$ . Since the probability distributions of the hourly average wind power production exhibit such a small statistical distance the joint probability mass functions of the minimum  $a$  and maximum  $b$  deviations from the hourly average productions are compared using deviations over all the hourly averages  $f_{(A,B)} = P(A = a \cap B = b)$ , calculated

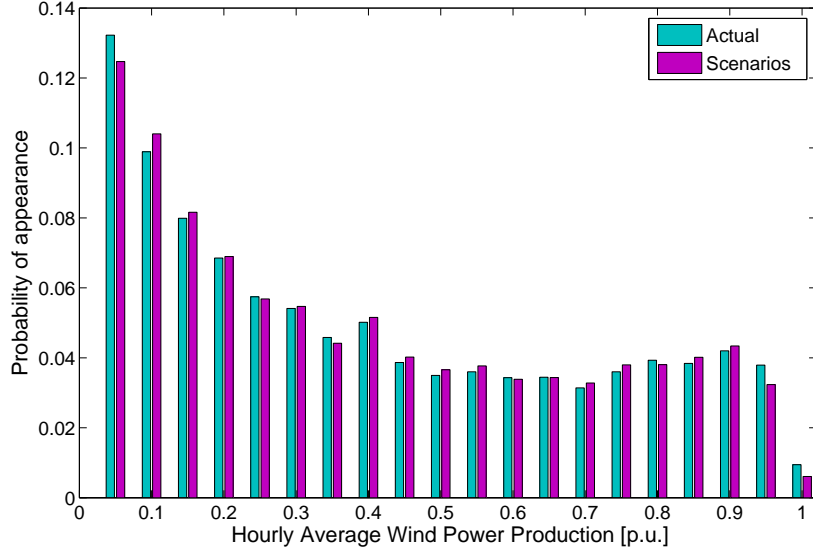


Figure 6.5: The probability mass functions of the hourly average wind power production using the actual data (year 3) and the data from the generated scenarios for a 160.5 MW wind farm (WF6). The two distributions have a small statistical distance (total variation distance = 0.02)

from all the points in the deviation pairs series  $(a_i, b_i)$  defined in (3.8) and (3.9) of Section 3.3, rather than using deviations by individual hourly average  $f_{(A,B),l_j} = P(A = a \cap B = b | \bar{x}_n = l_j)$ . The difference between the joint probability mass functions of the maximum and minimum deviations from the hourly average wind power production using the actual data  $f_{(A,B)}$  and the data from the generated scenarios  $\hat{f}_{(A,B)}$  for the 160.5 MW wind farm is presented in Fig. 6.6. The Kullback-Leibler divergence of the two joint distributions using (6.20) is found to be  $D_{KL}(f_{(A,B)} || \hat{f}_{(A,B)}) = 1.4612$ , which is considered acceptable, although the biggest differences occur for small deviations which are the deviations with most mass.

The results in Fig. 6.5 and Fig. 6.6 reveal that the generated sce-

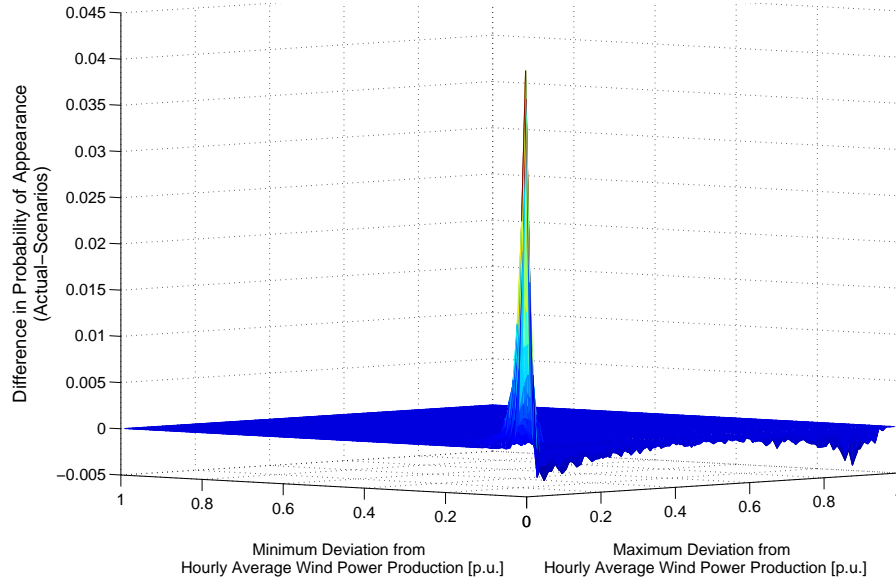


Figure 6.6: The difference (actual - scenarios) between the joint probability mass functions of the maximum and minimum deviations from the hourly average wind power production using the actual data (year 3) and the data from the generated scenarios for a 160.5 MW wind farm (WF6).

narios are probabilistically correct, since they respect the hourly wind power production distribution and the joint probability distribution of the deviations from the hourly average. Figure 6.7 depicts the probability mass functions of the wind power production using all the wind power production points from the actual data in the training year (year 3) and the data from the generated scenarios for the 160.5 MW wind farm. The probability mass function of the wind power production is defined as:

$$f_W(w) = P(x_n = w), \quad (6.21)$$

where  $x_n$  is the whole wind power production series formed from the minute-points in all the available hours. The comparison of the distributions  $f_W$  from the original data and  $\hat{f}_W$  from the generated data is used to evaluate

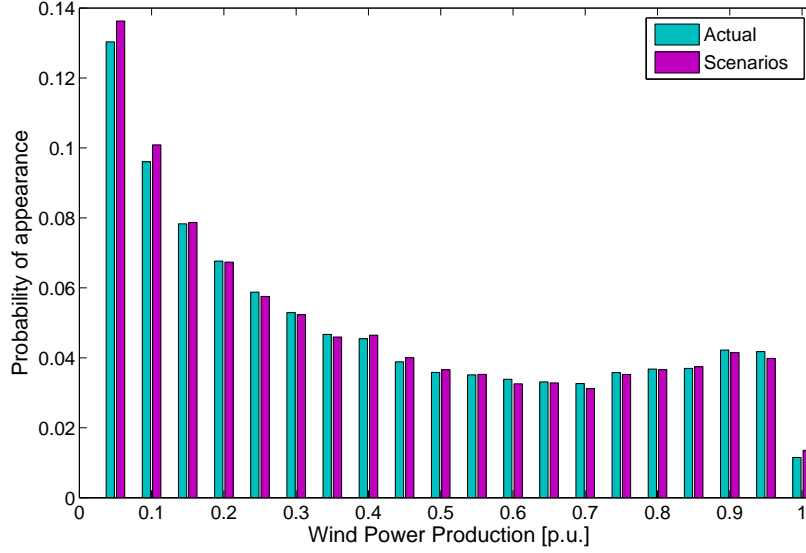


Figure 6.7: The probability mass functions of the wind power production using the actual data (year 3) and the data from the generated scenarios for a 160.5 MW wind farm (WF6). The two distributions have a small statistical distance (total variation distance = 0.01)

the assumption made in Section 6.1 that the wind power production points in an hour are normally distributed between the minimum and maximum. The small statistical distance of the two distributions which is found to be  $\delta(f_W, \hat{f}_W) = 0.01$  using (6.19) justifies this assumption.

### 6.3.2 Statistics of the ESS Characteristics

With the methodology described in Section 6.1,  $M = 50,000$  hour-long wind power production scenarios are generated using the data of a 160.5 MW wind farm (WF6) from the training year (year 3). For each of the 50,000 generated hours for the 160.5 MW wind farm the characteristics of the ESS, as defined in Section 6.2, are calculated from the ESS power  $P_{b,m}(i)$  and energy

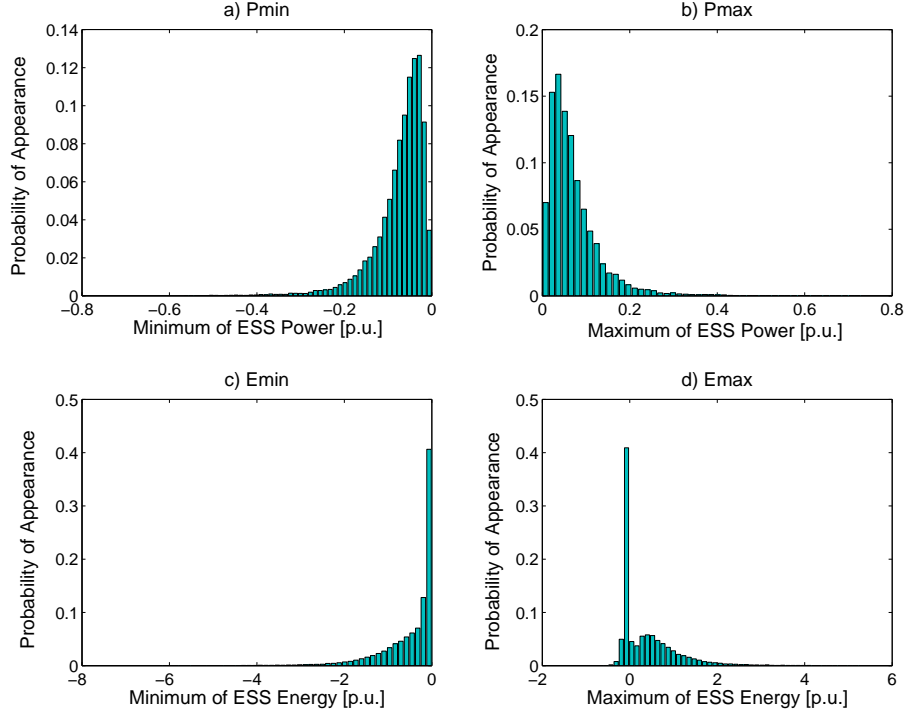


Figure 6.8: The probability mass functions of the a) minimum power  $P_{min}$ , b) maximum power  $P_{max}$ , c) minimum energy  $E_{min}$ , and d) maximum energy  $E_{max}$  of the ESS for a 160.5 MW wind farm (WF6) calculated from 50,000 hour-long generated scenarios using the data in the training year (year 3). Most mass is concentrated on small absolute values.

$E_{b,m}(i)$  series,  $m = 1, 2, \dots, M$ , using a roundtrip efficiency of  $\eta = 0.9$ .

Figure 6.8 depicts the probability mass functions of the ESS characteristics (minimum and maximum ESS power  $P_{min,m}$  and  $P_{max,m}$ , minimum and maximum ESS energy  $E_{min,m}$  and  $E_{max,m}$ ) of the respective 50,000-long time series. The minimum and maximum ESS power  $P_{min,m}$  and  $P_{max,m}$  are calculated from (6.12) and (6.13), respectively, while the minimum and maximum ESS energy  $E_{min,m}$  and  $E_{max,m}$  are calculated from (6.15) and (6.16),

respectively, for  $m = 1, 2, \dots, M$ . Most probability mass is concentrated on small absolute values for all ESS characteristics ( $0 - 0.2$  p.u.<sub>*P*</sub> for ESS power and  $0 - 2$  p.u.<sub>*E*</sub> for ESS energy). It should be noted that the ESS power is per-unitized based on the wind farm nameplate capacity,  $1 \text{ p.u.}_P = 160.5 \text{ MW}$ , while the ESS energy is per-unitized based on the wind farm nameplate capacity times the time step unit which is 1 minute, thus  $1 \text{ p.u.}_E = 160.5 \text{ MW}\cdot\text{min}$ . It is reminded that, according to (6.8), in each scenario  $m$ , the minimum ESS power  $P_{min,m}$  appears at the minute  $i$  when the wind power production has the largest positive deviation from the hourly average for which  $P_{b,i} = P_d - P_{w,i} \leq 0$  and thus  $P_{min,m}$  assumes negative values. Similarly, since the ESS is considered initially discharged the minimum ESS energy  $E_{min,m}$  in each scenario  $m$  assumes non-positive values.

The percentiles  $Q(p\%)$  of the ESS power capacity  $P_{size,m}$  and the ESS energy capacity  $E_{size,m}$  calculated from the respective  $M = 50,000$ -long data samples,  $m = 1, 2, \dots, M$ , are given in Fig. 6.9 as a function of the percentile rank  $p$ . Figure 6.10 depicts the same informations as Fig. 6.9, but only for ranks within  $[85, 100]$ .

From Fig. 6.10 it can be observed that a risk parameter of  $\alpha = 0\%$ , representing a completely risk averse operator, results in a necessary ESS size of  $Q_{Psize}(100\%) = 0.72 \text{ p.u.}_P = 116.6 \text{ MW}$  and  $Q_{Esize}(100\%) = 5.95 \text{ p.u.}_E = 15.9 \text{ MWh}$  to cover for all wind power imbalances from the hourly average wind power production. Such an ESS size is significantly larger than the respective size for a risk parameter of  $\alpha = 5\%$  with  $Q_{Psize}(95\%) = 0.21 \text{ p.u.}_P = 32.9 \text{ MW}$  and  $Q_{Esize}(95\%) = 2.29 \text{ p.u.}_E = 6.1 \text{ MWh}$ . Thus, as expected, lower risk parameters signify lower penalties due to deviations from the generation schedules but higher investment costs.

Figure 6.11 depicts the 95<sup>th</sup> percentile of the ESS power ( $Q_{Psize}(95\%)$ )



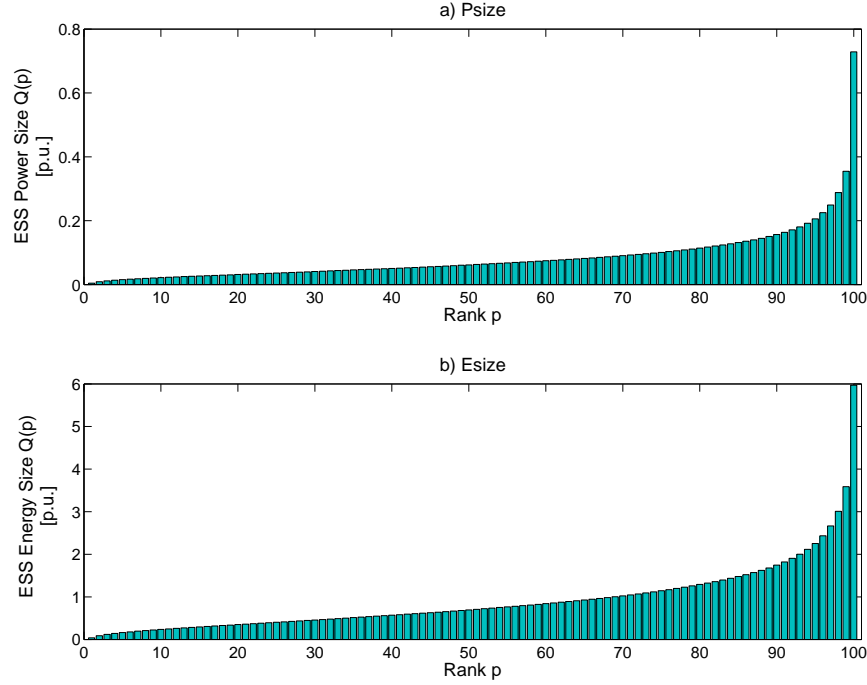


Figure 6.9: The quantile  $Q(p)$  of the a) power size  $P_{size}$  b) energy size  $E_{size}$  of the ESS as a function of the quantile rank  $p$  for a 160.5 MW wind farm (WF6) calculated from 50,000 hour-long generated scenarios using the data in the training year (year 3).

and energy ( $Q_{Esize}(95\%)$ ) capacities as a function of the hourly average wind power production level  $l_j$  for the same 160.5 MW wind farm (WF6). To obtain this graph  $M = 50,000$  scenarios are generated for each hourly average wind power production level  $l_j = 0.01, 0.02, \dots, 1$  p.u. Essentially, this means that for each hourly average production level  $l_j$  the algorithm described in Section 6.1 is repeated 50,000 times omitting step 1 and using the quantile function of (6.6) calculated from the data in the training year (year 3). Then, for each hourly average production  $l_j$  the ESS power  $P_{size,m}$  and energy  $E_{size,m}$  for each sce-

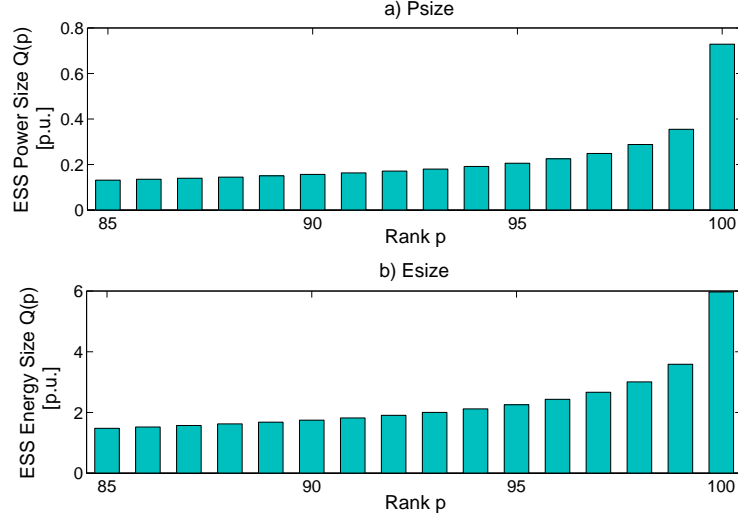


Figure 6.10: The 85<sup>th</sup> to 100<sup>th</sup> percentiles  $Q(p)$  of the a) power size  $P_{size}$  b) energy size  $E_{size}$  of the ESS as a function of the quantile rank  $p$  for a 160.5 MW wind farm (WF6) calculated from 50,000 hour-long generated scenarios using the data in the training year (year 3).

nario are calculated from (6.14) and (6.17), respectively, for  $m = 1, 2, \dots, M$  and the respective 95<sup>th</sup> percentiles are obtained by sorting the series. Thus, an ESS with the power and energy capacities depicted in Fig. 6.11 fails to capture the imbalances from the respective hourly average  $l_j$  in at most  $0.05 \cdot 50,000 = 2,500$  of the 50,000 generated hours. From Fig. 6.11 it is observed that the ESS power capacities for mid-level hourly average wind power productions ( $0.3 \leq l_j \leq 0.7$  p.u.) are in the range of 0.3 p.u.<sub>P</sub>, which are almost tripple in size compared to the ESS capacities for low ( $0 \leq l_j \leq 0.1$  p.u. p.u.) and high ( $0.9 \leq l_j \leq 1$  p.u.) wind power productions. This is also true for the ESS energy capacities which are close to 3 p.u.<sub>E</sub> for mid-level, compared to values less than 1 p.u.<sub>E</sub> for low and high hourly average wind power productions. This indicates a higher variability for mid-level wind power productions, attributed

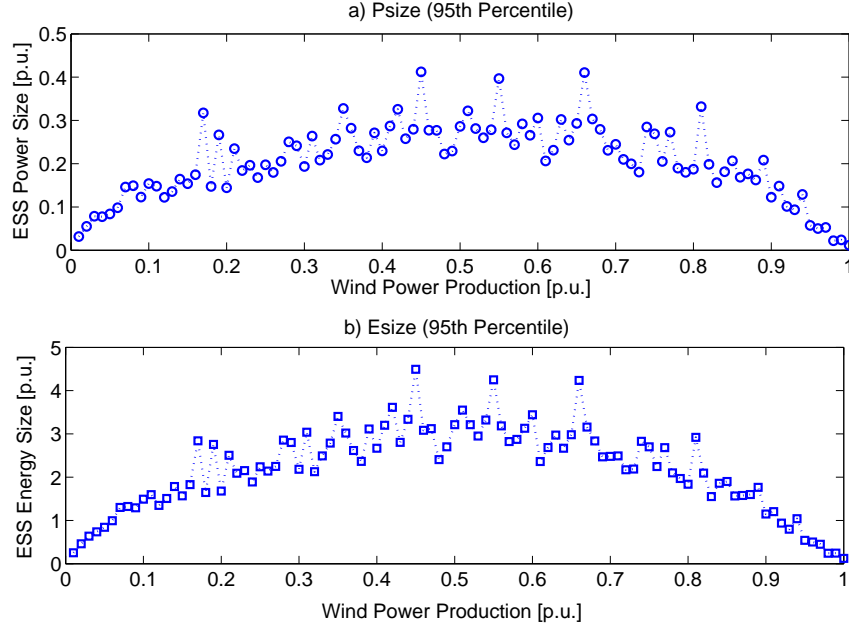


Figure 6.11: The 95<sup>th</sup> percentile of the a) power size  $P_{size}$  and b) energy size  $E_{size}$  of the ESS for a 160.5 MW wind farm (WF6) as a function of the hourly average wind power production  $l_j$  calculated from 50,000 hour-long generated scenarios for each  $l_j$  using the data in the training year (year 3). ESS capacities are higher at mid-level wind power production.

to the large slope of the wind power versus wind speed curve at mid-level production, which causes even a small change in the input wind speed to have a large effect on the wind power output.

### 6.3.3 Evaluation of ESS Characteristics Coverage Rates

To evaluate the proposed ESS size estimation methodology the real-world wind power data from 10 wind farms in the ERCOT system are used (WF2, WF3, WF4, WF5, WF6, WF7, WF11, WF13, WF14, and WF15 - see Appendix A.1). Using the methodology described in Section 6.1 50,000 hour-long wind power production scenarios with a one-minute resolution are

generated for each wind farm. To generate the scenarios the inverse of the joint cumulative distribution  $F_{(A,B),l_j}^{-1}$  of the minimum  $a$  and maximum  $b$  deviations from the hourly average  $l_j$  from the data in the training year (year 3) and the probability mass function  $f_L$  of the hourly average wind power production  $l_j$  from the data in the test year (year 4) are used. The percentiles ( $p\%$ ) of the ESS characteristics from all the scenarios are then calculated for each wind farm.

The 95<sup>th</sup> percentile of the minimum and maximum ESS power  $P_{min}$  and  $P_{max}$ , as well as the minimum and maximum ESS energy  $E_{min}$  and  $E_{max}$  for each wind farm is given in Table 6.1. For example, from Table 6.1 it can be seen that for a 160.5 MW wind farm, in 47,500 out of the 50,000 generated hours, the largest positive deviation from the hourly average is less than  $|P_{min}|=31.8$  MW, whereas in 47,500 hours (not necessarily the same as before)

Table 6.1: 95<sup>th</sup> Percentile of the ESS Characteristics

WF Size [MW]	$P_{min}$ [MW]	$P_{max}$ [MW]	$E_{min}$ [MWh]	$E_{max}$ [MWh]
28.5	-5.5142	4.9915	-0.909	0.8135
37.5	-8.1898	7.7907	-1.3668	1.2198
74.9	-13.7183	12.875	-2.2277	1.9901
82.5	-16.1886	15.7229	-2.6351	2.3571
91.5	-19.0653	17.5752	-3.0218	2.7593
114	-21.3965	20.3066	-3.5357	3.1578
120.6	-22.0853	20.5871	-3.5893	3.2011
160	-29.6718	28.8935	-4.8991	4.3494
160.5	-31.7706	30.1854	-4.9307	4.5259
210	-36.0137	33.9795	-5.7061	5.1079

the largest negative deviation from the hourly average is less than  $P_{max}=30.2$  MW. Similarly, in 47,500 hours the largest amount of energy charged into the ESS is less than  $E_{max}=4.5$  MWh, whereas in some other 47,500 hours the largest amount of energy discharged from the ESS is less than  $|E_{min}|=4.9$  MWh.

Figure 6.12 depicts the 95<sup>th</sup> percentile of the ESS power capacity  $P_{size}$  and the ESS energy capacity  $E_{size}$  as a function of the wind farm nameplate capacity. Though the ESS characteristics increase with wind farm size in absolute numbers, the decreasing trend in Fig. 6.12 indicates that wind power variability decreases with increasing wind farm size. This decrease is attributed to the fact that a higher number of wind turbines with a wider geographical spread in a large wind farm has a more pronounced effect on the variability cancellations in their output.

Using Fig. 6.12 it can be seen that for a 160.5 MW wind farm in 47,500 out of the 50,000 generated hours an ESS with size  $P_{size}=0.2141$  p.u. $_P=33.7$  MW and  $E_{size}=2.33$  p.u. $_E=6.23$  MWh is sufficient to accommodate imbalances from the hourly average. From the analyzed 95<sup>th</sup> percentiles of the 160.5 MW wind farm it becomes evident that  $Q_{E_{size}}(0.95) \leq Q_{E_{max}}(0.95) - Q_{E_{min}}(0.95)$ , since a largest amount of charged energy equal to  $Q_{E_{max}}(0.95)$  hardly ever coincides with a largest amount of discharged energy of  $Q_{E_{max}}(0.95)$  in the same hour. Similarly,  $Q_{P_{size}}(0.95) \geq \max\{|Q_{P_{min}}(0.95)|, |Q_{P_{max}}(0.95)|\}$ , since the ESS power capacity  $P_{size}$  time series is calculated using the maximum of either the largest positive or largest negative deviation from the hourly average, and thus assumes values that are larger than the respective  $P_{max}$  and  $P_{min}$  ESS time series.

To estimate the ESS capacities the generated scenarios use the inverse of the joint cumulative distribution  $F_{(A,B),l_j}^{-1}$  of the minimum  $a$  and maximum

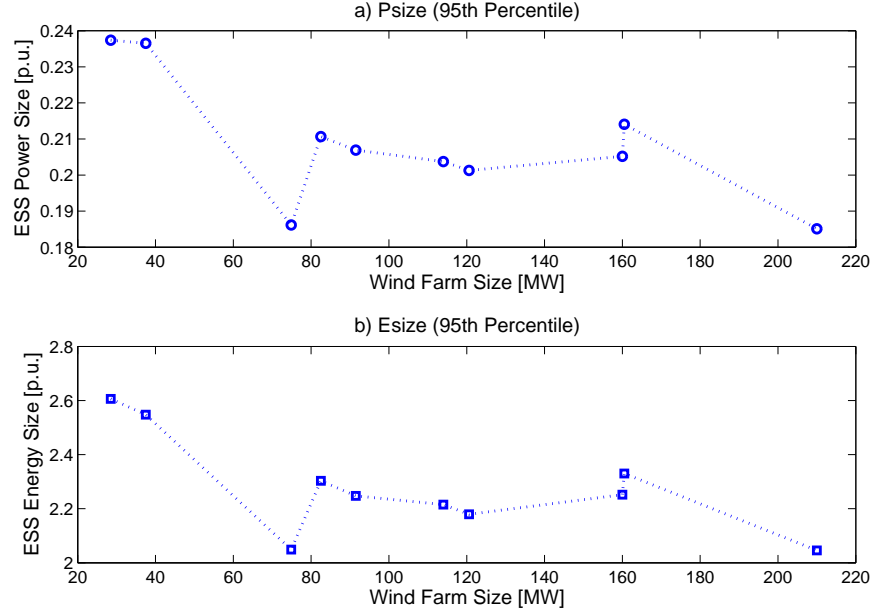


Figure 6.12: The 95<sup>th</sup> percentile of the a) power size  $P_{size}$  and b) energy size  $E_{size}$  of the ESS as a function of the wind farm nameplate capacity. The decreasing trend indicates that wind power variability decreases with increasing wind farm size.

$b$  deviations from the hourly average  $l_j$  from one year's data (year 3) and the probability mass function  $f_L$  of the hourly average wind power production  $l_j$  from the next year's data (year 4). This corresponds to the case where a wind farm owner (or the system operator) generates scenarios to estimate the necessary ESS capacities so as to firm its future production having some knowledge only on past wind power variability and a forecast of future wind power production. The probability mass function  $f_L$  can be considered a probabilistic forecast for one specific hour for which the wind farm owner has to cover potential imbalances with a certain coverage rate  $p$ . When the wind farm owner has a perfect forecast of the hourly average  $l_j$ , the necessary ESS size can be estimated by creating a graph similar to that presented in Fig. 6.11 for the

desired coverage rate  $p$ .

However, for the specific evaluation methodology considered, the wind farm owner's goal is to estimate the size of an ESS so as to be able to cover deviations from the hourly average not for just one hour but for at least  $1 - a\%$  of the hours in the test year. Here  $a\%$  could be the maximum allowable percentage of hours in a year, where wind power imbalances from the hourly average are not covered, for which no penalty is applied. An application of such a criterion for applying penalties is probable, since such criteria are already used for power system reliability performance [9]. To estimate this ESS size the wind farm owner uses historical data for wind power variability, i.e. the quantile function of the minimum  $a$  and maximum  $b$  deviations from the hourly average  $l_j$  of the data in the training year. Moreover, it is assumed that the wind farm owner has perfect knowledge of the probability mass function  $f_L$  of the hourly averages in the test year. This assumption may not seem realistic, but in general there is bigger uncertainty with respect to the near-future wind power production than the average wind power output over the long run.

At this point it should be noted, that the proposed ESS size estimation methodology provides the ESS power and energy capacities to minimize imbalances from the hourly average assuming that a same size ESS is available at the beginning of each hour. Thus, the estimated ESS size can be thought of as the storage size to be rented at each hour from a hypothetical energy storage market. The storage power and energy capacities of the market should be such, that in each hour the wind farm owner can use up all the rented power and energy in either direction (charging or discharging). When the problem is viewed from a power system operator perspective, the generators providing ancillary services form such a market. Obtaining the ESS size which optimizes the wind farm performance over the whole test year would need the application

of dynamic programming and the generation of year-long scenarios to account for relations between successive hours.

To evaluate the estimated ESS size the wind farm owner can compare it against the size he would choose if he had knowledge about actual wind power variability over the hours in the test year. Indeed, since the goal of the proposed methodology is to estimate the size of an ESS, its evaluation is done by comparing the resulting estimated ESS capacities ( $Q_{scen}$ ) for a certain risk parameter  $\alpha$  to the same risk parameter ESS capacities of the actual data ( $Q_{actual}$ ). That is the estimated ESS size quantiles,  $Q_{Psize,scen}(1 - \alpha\%)$  and  $Q_{Esize,scen}(1 - \alpha\%)$ , from the generated scenarios are compared to the actual ones,  $Q_{Psize,actual}(1 - \alpha\%)$  and  $Q_{Esize,actual}(1 - \alpha\%)$ . The estimated quantiles are calculated from the generated scenarios using minimum and maximum deviations from the data in the training year and the probability mass function of the hourly average wind power production from the data in the test year. The actual quantiles are calculated from the data in the test year. Using the ESS power  $P_b(i)$  and energy  $E_b(i)$  series,  $i = 1, 2, \dots, 60$ , from each hour in the test year the ESS characteristics of each hour are calculated from (6.12) - (6.17) and the resulting quantiles of the ESS characteristics time series are termed the actual quantiles ( $Q_{actual}$ ). The results of this comparison for the ESS power and energy sizes under a risk parameter  $\alpha = 5\%$  are given in Table 6.2.

The results in Table 6.2 reveal that the estimated from the actual ESS sizes have small differences for all the wind farms, with the absolute difference being on average 10%. Regarding the ESS power capacity, the wind farm owner could achieve capturing wind power imbalances from the hourly average for 95% of the hours in the test year with a smaller sized ESS than the estimated one. On the other hand, the smaller estimated than the actual ESS



Table 6.2: 95<sup>th</sup> Percentile of the ESS Characteristics Using the Generated Scenarios and the Actual Data

WF Size	$P_{size}$ (scenarios)	$E_{size}$ (scenarios)	$P_{size}$ (actual)	$E_{size}$ (actual)
[MW]	[MW]	[MWh]	[MW]	[MWh]
28.5	5.9348	1.0858	5.1302	1.0608
37.5	8.9881	1.6135	8.4138	1.8148
74.9	14.8934	2.7317	13.4663	2.9368
82.5	17.9075	3.2631	17.4627	3.8228
91.5	20.6926	3.7457	19.1748	4.2814
114	23.6331	4.2822	22.4251	4.9283
120.6	24.1547	4.359	22.8293	5.0801
160	32.8279	6.0053	31.2786	6.9753
160.5	34.5712	6.2714	30.4	6.8147
210	38.8704	7.1603	35.4976	8.0049

energy capacity values indicate that the wind farm owner would eventually not be able to capture wind power imbalances for less than 5% of the hours in the test year, which would result in wind power imbalances penalties being applied.

The ESS sizing methodology essentially provides ESS characteristics quantile estimates, thus the reliability of the quantile estimates is used for their evaluation. It is reminded that reliability refers to the difference between the actual from the nominal proportions (coverage rates), and ideally the wind farm owner would like these differences to be zero. That is, when the wind farm owner estimates the ESS characteristics for certain risk parameter  $\alpha = 1 - p$  he would like the estimated ESS characteristics to be able to cover wind power imbalances from the hourly average with a coverage rate  $\hat{p}$

as close as possible to the nominal coverage rate  $p$ . The actual coverage rate  $\hat{p}$  is defined as the value for which  $Q_{scen}(\hat{p}) = Q_{actual}(p)$  and it corresponds to the ratio of hours in the test year for which the estimated ESS can cover wind power imbalances from the hourly average to the total number of hours in the test year. If  $\hat{p} > p$  (positive reliability) the ESS covers imbalances but is more expensive, whereas for  $\hat{p} < p$  (negative reliability) wind power imbalances are not covered and penalties may apply. From this perspective, positive reliability is favored over negative reliability. If the penalty considered is  $c_{dev}$  \$/MWh of not firmed wind power energy, that is wind power energy imbalances not covered by the ESS, then the quantity  $c_{dev}(Q_{actual}(p) - Q_{scen}(p))(\hat{p} - p) \cdot (\text{hours in a year})$  provides an upper bound on the deviation penalties.

Figure 6.13 depicts the actual coverage rate of the estimated 95<sup>th</sup> percentile for all the ESS characteristics on the actual data as a function of the wind farm size. The dashed line in Fig. 6.13 corresponds to the nominal coverage rate  $p = 0.95$ . The small deviations of the actual from the nominal coverage rates indicate that the estimated ESS characteristics are very close to the actual ones with absolute deviations from the actual coverage rates not exceeding 2.4% and a mean absolute deviation of 1.2%. Figures 6.13(a)-(c) reveal that the ESS estimated power characteristics have positive reliability, which means that from a power perspective the estimated ESS can capture wind power imbalances for more than 95% hours in the test year (close to 96%). However, in terms of energy, the estimated ESS manages to cover wind power imbalances from the hourly average only for 93.5% of the hours in the test year, as can be seen from Fig. 6.13(f). Moreover, similar ESS characteristics for similar-sized wind farms in Table 6.2 imply that in the absence of historical wind power variability data, the proposed methodology can be applied using respective data of similar-sized wind farms with analogous results.

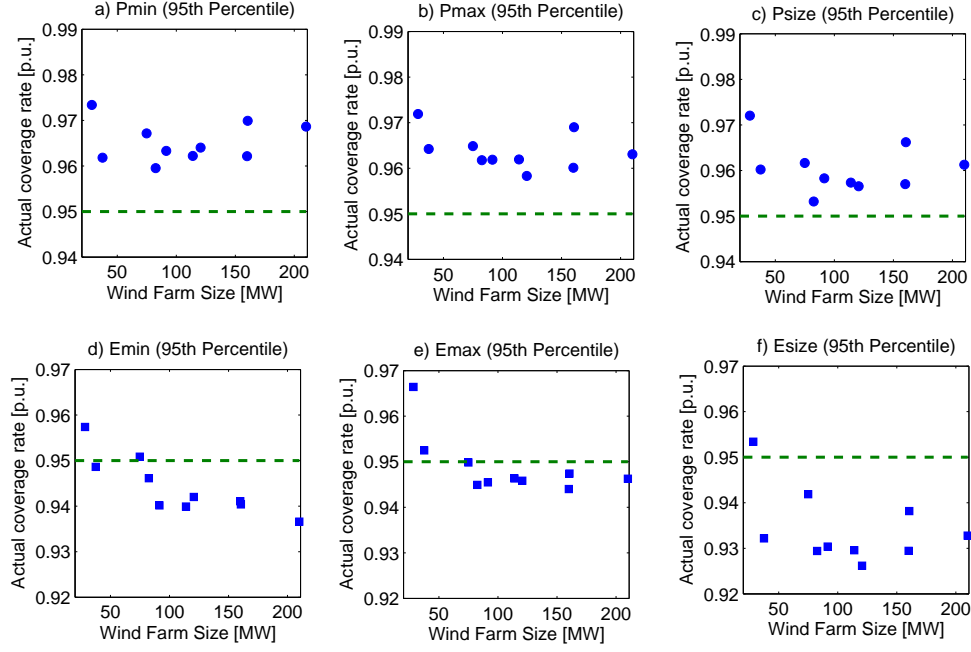


Figure 6.13: Actual coverage rate of the estimated 95<sup>th</sup> percentile of the a) minimum power  $P_{min}$ , b) maximum power  $P_{max}$ , c) power size  $P_{size}$ , d) minimum energy  $E_{min}$ , e) maximum energy  $E_{max}$ , and f) energy size  $E_{size}$  of the ESS, as a function of the wind farm nameplate capacity. The dashed line represents the nominal coverage rate  $p = 0.95$ . The mean absolute deviation from the actual coverage rate is less than 1.5%.

Several factors account for the deviations in the ESS capacities in Table 6.2, or similarly the deviations of the actual from the nominal proportions in Fig. 6.13, which means that there might be room for further minimization of the already small deviations. One factor contributing to the deviations between the actual and the estimated quantities stems from the inability to properly invert the cumulative probability mass function of the hourly averages given in (6.4), which results in differences between the probability mass function of the hourly averages in the actual data and the generated scenarios.

As is pointed out in Section 5.5.3 a change in the probabilities (weights) of the hourly averages can significantly affect the resulting ESS estimates. In addition, the deviations in ESS power are also attributed to using the wind power deviations from the hourly averages of the data in a past year, which signifies that a better knowledge of future wind power variability, such as using an exponentially weighted stochastic approximation to periodically update the quantile function in (6.6) as described in Section 5.3.5, can furthermore improve the results. On the other hand, the deviations in ESS energy are heavily affected by the way the intermediate points in a scenario are picked (normality and ordering assumption), thus they could benefit from using more realistic intra-hour wind power scenarios, for example by taking into account the quantile functions for intra-hour time resolutions.

## 6.4 Concluding Remarks

Variability is an inherent characteristic of wind power and the coupling of wind farms with energy storage units is considered a promising approach in reducing the effects of wind power variability and uncertainty on power system operations, and in allowing wind farm owners a higher participation in day-ahead and hour-ahead energy markets. The example application of the CRM presented in this chapter provides a methodology to estimate the size (power and energy capacities) of an energy storage system with the goal of minimizing deviations from the hourly average wind power production. Using only a probabilistic forecast of the hourly average wind power production and the inverse of the joint cumulative distribution of the maximum and minimum deviations from the hourly average, hour-long wind power production scenarios are generated from the algorithm described in Section 6.1. The statistics

of the energy storage system's characteristics, given in Section 6.2, are then estimated from these scenarios as a function of the desired risk parameter.

The evaluation of the proposed methodology using real-world wind power data presented in Section 6.3 reveals that the data from the generated scenarios have probability distributions which exhibit a small statistical distance to those of the actual data. Moreover, when the estimated ESS capacities, calculated having some knowledge on past wind power variability and knowledge of a forecast of future wind power production, are compared to the ESS capacities of the actual data, they exhibit coverage rates which are very close to the nominal ones, with an average absolute deviation less than 1.5%. Thus, the proposed methodology can be used by wind farm owners so as to estimate the size of an ESS which can firm the produced output and allow for participation in energy markets. Alternatively, since the proposed methodology poses no restrictions on the technology used to implement the ESS, it can be used by power system operators so as to estimate the power and energy to be provided from ancillary services.

## Chapter 7

### Conclusion and Future Work

Variability is an inherent characteristic of wind power, which, along with uncertainty, poses significant risk to power system planners and operators, as well as wind farm owners and investors. The adverse effects of wind power variability and uncertainty on system-wide reliability, operations, ancillary services, and costs are examined in wind integration studies performed all over the world in the recent years.

Realizing that wind power variability will be present even when all uncertainty is removed with perfect wind power forecasts, makes the ability to effectively measure wind power variability of critical importance, because it allows engineers to quantify and therefore manage wind power variability at the desired time scale. With nowadays wind power penetration levels, intra-hour variation of wind power (in MW) becomes comparable to that of load variation, hence the need for a metric to quantify intra-hour wind power variability is more prominent. However, current variability metrics presented in Section 2.2 fail to effectively capture intra-hour variations deeming a novel intra-hour wind power variability metric necessary.

This chapter summarizes the most important results from the research contributions of the work presented herein and identifies future research objectives.

- *Development of the conditional range metric to quantify intra-hour wind power variability*

The main objective of the work presented herein is the development of an intra-hour wind power variability metric and it is met with the work described in Chapter 3, which provides a formal definition of the proposed conditional range metric (CRM) to quantify intra-hour wind power variability. With the conditional range metric the variability of wind power is characterized by the size of the interval  $[M_{low_{k,l_j}}, M_{up_{k,l_j}}]$  within which a wind power output with average  $l_j$  lies over a given time frame of length  $k$  (the larger the size of this interval the higher the wind power variability). Using  $p^{th}$  sample quantiles of the CRM, denoted  $CRM_{k,l_j,p} = [M_{low_{k,l_j,p}}, M_{up_{k,l_j,p}}]$ , the proposed metric becomes a probabilistic intra-hour wind power variability metric, which allows power system operators and wind farm owners to make decisions based on their willingness to accept a certain level of risk.

- *Assessment of intra-hour wind power variability*

The performance analysis of the proposed metric in wind power variability assessment given in Sections 4.1 and 4.2 reveals that intra-hour wind power variability is larger at mid-level wind power production  $l_j$  and increases with increasing time interval length  $k$  and increasing coverage probability  $p$ . The higher variability at mid-level wind power productions is attributed to the large slope of the wind power curve at mid-level productions. Moreover, wind power variability appears to decrease with increasing wind turbine and wind farm size, since a large number of wind turbines allows for more positive changes being canceled out by negative changes in their wind power outputs, and is lower when wind turbines

are connected to the grid through converters.

*Future Work:* The efficacy of the proposed metric in quantifying wind power variability should also be demonstrated using different sets of real-world wind power data, such as data with higher resolutions, e.g. seconds, or data from off-shore wind farms. In addition, the ability of the proposed metric to effectively characterize wind power variation and estimate the size of wind power ramps over time frames exceeding the hour should be investigated. Most importantly, since wind power aggregation is found to offer a significant reduction in wind power variability for all wind turbine technologies and sizes, the study of methodologies to reliably estimate this reduction under more general conditions should be explored. Thus, a future research contribution should be directed towards providing a conditional range metric updating procedure when the output of a new wind farm or turbine is added to an existing aggregated output, using spatio-temporal correlation between the additional and the existing wind power output.

- *Evaluation of the conditional range metric against existing metrics*

The comparison of the conditional range metric to the step-changes and forward differences statistics in assessing the size and rate of intra-hour wind power ramps presented in Section 4.3 reveals the shortcomings of the prevalent step-changes approach, which are their inability to convey information about the wind power variability within a time interval and their lack to provide the duration of the wind power ramp rates. The results show that reserves based on the conditional range metric manage to accommodate intra-hour wind power variations for an additional 15% of hours within a given year, with significant benefits for power system



reliability.

*Future Work:* For the comparison purposes a ramp rate associated with the conditional range is provided, but further analysis is deemed necessary to determine whether the inclusion of ramp rates in the conditional range metric is of significant benefit to power system operators. Another aspect to be investigated is the addition of a sign to the conditional range metric, indicating a positive or negative largest change in wind power output over a time interval.

- *Development of methods to forecast wind power variability*

The proposed wind power variability forecasts described in Chapter 5 use  $p^{th}$  CRM quantiles to construct probabilistic intervals within which wind power output will lie. One static (sample quantile) and two time-adaptive methods (exponentially weighted moving average, exponentially weighted stochastic approximation) are given for estimating CRM quantiles and the resulting quantile estimates are compared using their reliability, sharpness and resolution. Reliability tends to be better at mid-production levels, denoting that though wind power variability is highest at mid-production levels it is more predictable at these levels. Moreover, reliability appears to be unaffected by wind power forecast time resolution, but it tends to improve with increasing wind farm nameplate capacity and increasing wind turbine size. Under all considered methods, high rank quantiles tend to be more reliable than lower rank quantiles, with average expected deviations from nominal proportions close to 1% and maximum expected deviations less than 5%. Using time-adaptive quantile estimation approaches results in more reliable estimates and more effective differentiation between various wind

power variability situations, however the computational aspects of time-adaptive methods need to be factored in. In addition, the analysis using an artificial wind power forecast reveals that intra-hour wind power variability increases with increasing hourly wind power uncertainty, but at a much slower rate.

*Future Work:* Though the proposed quantile estimation methods produce reliable CRM quantiles, the performance of additional methods based on optimization techniques, such as quantile regression and time adaptive regression, should also be investigated. Regarding the artificial wind power forecast results, a verification using real-world wind power forecasts coupled with the respective actual wind power data is necessary. Moreover, the methods to obtain the proposed wind power variability forecasts are based on point wind power forecasts, but the increasing popularity of ensemble wind power forecasts in the past decade calls for an adaptation of these methods to produce reliable wind power variability forecasts from probabilistic wind power forecasts.

- *Demonstration of the utility of the conditional range metric*

The provision of algorithms to construct wind power inequalities of the form  $\{M_{lowk,l_j,p} \leq x_n \leq M_{upk,l_j,p} \text{ with probability } p\}$ , which bound the wind power output  $x_n$  over a time interval of length  $k$  and average wind power production  $l_j$ , using either historical wind power data or future CRM  $p^{th}$  quantile estimates, opens the door to numerous applications. Such an example application of the CRM, given in Chapter 6, presents a methodology to estimate the size (power and energy capacities) of an energy storage system with the goal of minimizing deviations from the hourly average wind power production. The evaluation of the proposed

methodology using real-world wind power data reveals that when the estimated ESS capacities, calculated having some knowledge on past wind power variability and knowledge of future wind power production through a forecast, are compared to the ESS capacities of the actual data, they exhibit coverage rates which are very close to the nominal ones, with an average absolute deviation less than 1.5%.

*Future Work:* The proposed methodology can be enhanced using correlation analysis between intra-hour variations over different length time intervals, which will result in more representative hourly wind power output scenarios. The generation of reliable scenarios is considered the most important base product in wind power and other renewable energy forecasting methods. Using such scenarios, a sizing methodology which provides the optimal ESS to counteract intra-hour variations over a longer period, e.g. a 24-hour period, should also be considered by applying dynamic programming techniques.

## Appendices

# Appendix A

## Wind Power Data

### A.1 Data Description

The real-world wind power data used in this dissertation come from the Electric Reliability Council of Texas (ERCOT), one of the Independent System Operators in North America. The ERCOT region occupies the entire Texas Interconnection, which covers nearly all of the state of Texas in the United States. The data come from a total of 18 wind farms, with nameplate capacities ranging from 28 MW to 226.5 MW, from three different regions in the ERCOT system. They include wind power production data with a 1-minute resolution spanning a period from one up to four years. Table A.1 gives a detailed description of the wind farms capacities and turbines, while Table A.2 presents the data timespan for each wind farm.

Table A.1: Wind Farm Data

Wind Farm Name	Capacity [MW]	Number of Turbines	Turbine Manufacturer	Region
WF1	28.0	42	Vestas	2
WF2	160.0	160	Mitsubishi	2
WF3	120.6	67	Vestas	1
WF4	114.0	76	GE	1
WF5	28.5	38	Zond	3
WF6	160.5	107	Enron	3
WF7	210.0	140	GE	1
WF8	184.0	80	Siemens	1
WF9	226.5	151	GE	1
WF10	115.0	50	Siemens	1
WF11	82.5	125	Vestas	3
WF12	84.0	56	GE	2
WF13	74.9	107	NegMicon	3
WF14	37.5	25	GE	1
WF15	91.5	61	GE	1
WF16	135.0	90	GE	1
WF17	150.0	100	Enron	1
WF18	159.7	242	Vestas	3

Table A.2: Timespan of Wind Power Data

Name	Year 1	Year 2	Year 3	Year 4
WF1	Jan-Dec	Jan-Dec	Jan-Dec	—
WF2	Jan-Dec	Jan-Dec	Jan-Dec	Jan-Dec
WF3	—	—	Jan-Dec	Jan-Dec
WF4	—	—	Jan-Dec	Jan-Dec
WF5	Jan-Dec	Jan-Dec	Jan-Dec	Jan-Dec
WF6	Jan-Dec	Jan-Dec	Jan-Dec	Jan-Dec
WF7	—	—	Jan-Dec	Jan-Dec
WF8	—	—	—	Jan-Dec
WF9	—	—	—	Jan-Dec
WF10	—	—	—	Jan-Dec
WF11	Jan-Dec	Jan-Dec	Jan-Dec	Jan-Dec
WF12	—	—	—	Jan-Dec
WF13	Jan-Dec	Jan-Dec	Jan-Dec	Jan-Dec
WF14	—	—	Jan-Dec	Jan-Dec
WF15	—	—	Jan-Dec	Jan-Dec
WF16	—	—	—	Jan-Dec
WF17	Jan-Dec	Jan-Dec	Jan-Dec	Jan-Oct
WF18	Jan-Dec	Jan-Dec	Jan-Dec	Jan-Oct

## A.2 Data Pre-processing

The available wind power data were pre-processed to eliminate bad data, occurring either in the form of flat data or data spikes. Flat data segments, which are periods for which the accurate wind power measurement is missing, having a length up to and including 5 minutes were filled in with linear interpolation between the closest points, while flat data segments longer than 5 minutes were excluded from the data set. Data spikes also represent lost communication between the wind farm and the monitoring system which is restored minutes later, and were recognized in the form of an unusual large step-change of a negative sign followed by a step-change of almost equal magnitude but opposite sign. Data segments between data spikes were treated in the same manner as flat data, i.e. they were either excluded or replaced with linear interpolation. Data pre-processing resulted in less than 10% of the initial data being excluded or replaced. It should be noted that when the wind speed rises above the cut-off speed the wind power output experiences a sudden drop and the wind farm becomes unavailable. This situation also appears as a large step-change of negative sign in the data, but it cannot be considered a data spike, since it is due to the physical limitations of the wind turbines and not because of a malfunction in the monitoring system. However, these incidents are rare and none was present in our data.



## Appendix B

### Wind Speed Data and Wind Power Curves

#### B.1 Wind Speed Data

The wind speed time series used in this dissertation are real-world wind speed data with a 1-minute resolution spanning a period of 30 weeks. The data are measured at a height of 65 m and come from measurements at two wind farms in Iowa. The first wind speed series (WS1) has mean  $\mu_1 = 7.874$  m/sec and standard deviation  $\sigma_1 = 3.578$  m/sec, while the second series (WS2) presents slightly less variability with  $\mu_2 = 7.167$  m/sec and  $\sigma_2 = 3.325$  m/sec. The histogram of the two wind speed series is given in Fig. B.1.

#### B.2 Wind Power Curves

The available wind power curves correspond to six different wind power turbines. The turbines are classified according to their generator type [34] and their size.

The generator types are:

1. Type I: Fixed Speed Induction Generator
2. Type II: Variable Slip Induction Generator
3. Type III: Double-fed Induction Generator (DFIG)
4. Type IV: Synchronous Generator with IGBT Converter (Full Converter).

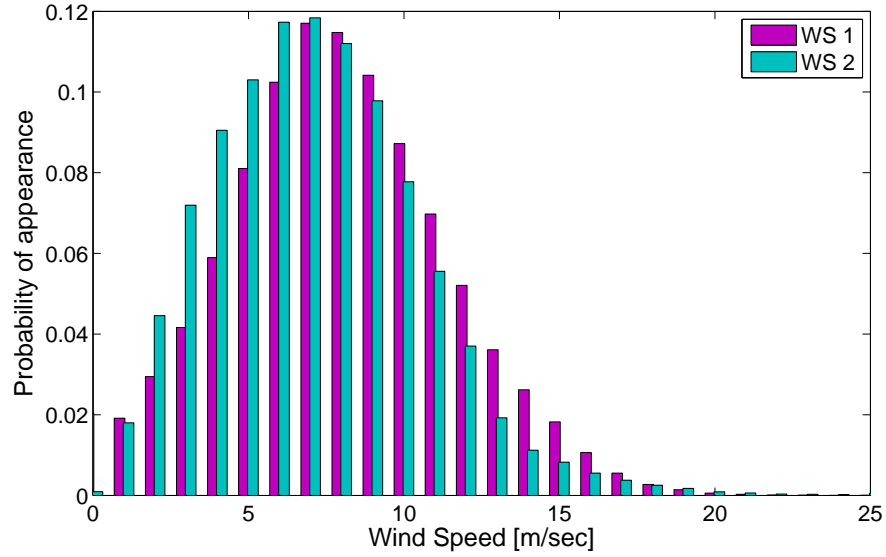


Figure B.1: Probability mass function of the wind speed series. The second wind speed series (WS2) exhibits a lower mean and standard deviation than the first series (WS1).

The considered turbines include four 1500 kW turbines (Type I, Type II, Type III, Type IV), and two variable slip induction generator turbines with sizes 660 kW (Size A) and 1650 kW (Size B). The wind turbine data are summarized in Table B.1 and the respective wind power curves are depicted in Fig. B.2. All the data come from the manufacturers' technical specifications.

Table B.1: Wind Turbine Data

Curve Name	Power [kW]	Diameter [m]	Hubheight [m]	Manufacturer	Model
Type I	1500	72	62	Neg-Micon	NM 72C
Type II	1500	63	64	Vestas	V 63
Type III	1500	77	65	GE	GE 1.5
Type IV	1500	65	65	Vensys	VS 70
Size A	660	47	65	Vestas	V 47
Size B	1650	66	65	Vestas	V 66

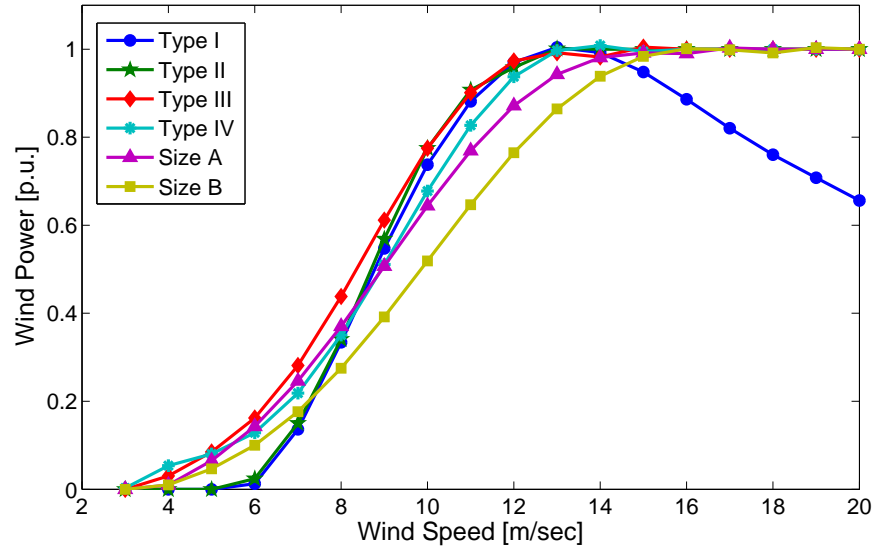


Figure B.2: Wind power curves.

## Bibliography

- [1] “Global Wind Energy Council.” [Online]. Available: <http://www.gwec.net/>
- [2] T. Boutsika and S. Santos, “Quantifying short-term wind power variability using the conditional range metric,” *Sustainable Energy, IEEE Transactions on*, vol. 3, no. 3, pp. 369–378, July 2012.
- [3] —, “Quantifying the effect of wind turbine size and technology on wind power variability,” in *Power and Energy Society General Meeting, 2013 IEEE*, July 2013, pp. 1–5.
- [4] —, “Quantifying short-term wind power variability,” in *Power and Energy Society General Meeting, 2011 IEEE*, July 2011, pp. 1–7.
- [5] —, “Sizing an energy storage system to minimize wind power imbalances from the hourly average,” in *Power and Energy Society General Meeting, 2012 IEEE*, July 2012, pp. 1–8.
- [6] D. Anderson, D. Sweeney, and T. Williams, *Essentials of Statistics for Business and Economics*. Southwestern Educational Publishing, 2008.
- [7] B. Parson, et.al., “Grid impacts of wind power variability: recent assessments from a variety of utilities in the United States,” in *European Wind Energy Conference, 2006*.
- [8] E. Ela, B. Kirby, E. Lannoye, M. Milligan, D. Flynn, B. Zavadil, and M. O’Malley, “Evolution of operating reserve determination in wind

power integration studies,” in *Power and Energy Society General Meeting, 2010 f*, July 2010, pp. 1–8.

- [9] “Reliability standards for the bulk electric systems of North America,” North American Electric Reliability Corporation, June 2009. [Online]. Available: <http://www.nerc.com>
- [10] “Xcel Energy and the Minnesota Department of Commerce: Wind Integration Study,” EnerNex Corporation, Wind Logics, Inc., Technical report, September 2004. [Online]. Available: <http://www.uwig.org>
- [11] “2006 Minnesota Wind Integration Study,” EnerNex Corporation, Technical report, November 2006. [Online]. Available: <http://www.uwig.org>
- [12] “The New York State Energy Research and Development Authority: The effects of integrating wind power on transmission system planning, reliability, and operations,” GE Energy Consulting, Technical report, March 2005. [Online]. Available: <http://www.nyserda.org/>
- [13] “Analysis of wind generation impact on the Electric Reliability Council of Texas ancillary services requirements,” GE Energy, Technical report, March 2008. [Online]. Available: <http://www.uwig.org>
- [14] “Growing Wind: Final Report of the NYISO 2010 Wind Generation Study,” New York Independent System Operator, Technical report, September 2010. [Online]. Available: <http://www.uwig.org/>
- [15] “Northwestern Energy Montana Wind Integration Study,” GENIVAR, Technical report, June 2011. [Online]. Available: <http://www.uwig.org>

- [16] “Nebraska Statewide Wind Integration Study,” Enernex Corporation, Vertyx, Nebraska Power Association, Technical report, March 2010. [Online]. Available: <http://www.nrel.gov>
- [17] “Western Wind and Solar Integration Study,” GE Energy, Technical report, May 2010. [Online]. Available: <http://www.uwig.org>
- [18] “SPP WITF Wind Integration Study,” Charles River Associates, Technical report, September 2011. [Online]. Available: <http://www.uwig.org>
- [19] H. Louie, “Characterizing and modeling aggregate wind plant power output in large systems,” in *Power and Energy Society General Meeting, 2010 IEEE*, 2010, pp. 1–8.
- [20] —, “Evaluation of probabilistic models of wind plant power output characteristics,” in *Probabilistic Methods Applied to Power Systems (PMAPS), 2010 IEEE 11th International Conference on*, 2010, pp. 442–447.
- [21] “Arizona Public Service Wind Integration Cost Impact Study,” Northern Arizona University, Technical report, September 2007. [Online]. Available: <http://www.uwig.org>
- [22] “New England Wind Integration Study,” GE Energy Applications and System Engineering, Enernex Corporation, AWS Truepower, Technical report, December 2010. [Online]. Available: <http://www.uwig.org>
- [23] “PGE Wind Integration Study Phase II,” Portland General Electric, Enernex Corporation, Technical report, September 2011. [Online]. Available: <http://www.uwig.org>

- [24] “Avista Corporation Wind Integration Study,” EnerNex Corporation, Technical report, March 2007. [Online]. Available: <http://www.uwig.org>
- [25] “Eastern Wind Integration and Transmission Study (EWITS),” EnerNex Corporation, Technical report, January 2010. [Online]. Available: <http://www.nrel.gov/>
- [26] “CAISO Integration of Renewable Resources - Transmission and operating issues and recommendations for integrating renewable resources on the California ISO-controlled grid,” California ISO, Technical report, November 2007. [Online]. Available: <http://www.caiso.com>
- [27] J. Apt, “The spectrum of power from wind turbines,” *Journal of Power Sources*, vol. 169, no. 2, pp. 369–374, 2007.
- [28] W. Katzenstein, E. Fertig, and J. Apt, “The variability of interconnected wind plants,” *Energy Policy*, vol. 38, no. 8, pp. 4400–4410, 2010.
- [29] P. Doody and S. Santoso, “A comparative metric to quantify the variability of wind power,” in *Power Energy Society General Meeting, 2009. PES '09. IEEE*, 2009, pp. 1–6.
- [30] V. Madisetti and D. Williams, *Digital Signal Processing Handbook: Cr-cnetbase 1999*. CRC Press, 1999.
- [31] “Flexibility requirements and potential metrics for variable generation: Implications for system planning studies,” North American Electric Reliability Corporation, August 2010. [Online]. Available: <http://www.nerc.com>

- [32] R. Serfling, “Quantile functions for multivariate analysis: approaches and applications,” *Statistica Neerlandica*, vol. 56, no. 2, pp. 214–232, 2002.
- [33] Y. Zuo and J. Serfling, “General notions of statistical depth function,” *Annals of Statistics*, vol. 28, no. 2, pp. 461–482, 2000.
- [34] E. Muljadi and A. Ellis, “Validation of wind power plant models,” in *Power and Energy Society General Meeting - Conversion and Delivery of Electrical Energy in the 21st Century, 2008 IEEE*, July 2008, pp. 1–7.
- [35] J. Manwell, J. McGowan, and A. Rogers, *Wind Energy Explained: Theory, Design and Application*. Wiley, 2010.
- [36] G. Giebel, G. Kariniotakis, and R. Brownsword, “The State of the Art in Short-term Prediction of Wind Power.” Deliverable report of the EU project ANEMOS, Technical report, August 2003. [Online]. Available: <http://anemos.cma.fr/>
- [37] S. Soman, H. Zareipour, O. Malik, and P. Mandal, “A review of wind power and wind speed forecasting methods with different time horizons,” in *North American Power Symposium (NAPS), 2010*, Sept. 2010, pp. 1–8.
- [38] C. Monteiro, H. Keko, R. Bessa, V. Miranda, A. Botterud, J. Wang, and G. Conzelmann, “A Quick Guide to Wind Power Forecasting: State of the Art 2009.” Argonne, National Laboratory, Technical report, November 2009. [Online]. Available: <http://www.dis.anl.gov/pubs/65614.pdf>



- [39] M. Milligan, M. Schwartz, and Y. Wan, "Statistical wind power forecasting models: Results for U.S. wind farms," in *Windpower, Austin, TX*, May 18-21, 2003.
- [40] C. Tantareanu, *Wind Prediction in Short Term: A First Step for a Better Wind Turbine Control*. Nordvestjysk Folkecenter for Vedvarende Energi, 1992.
- [41] E. Bossanyi, "Short-term wind prediction using kalman filters," *Wind Engineering*, vol. 9, no. 1, pp. 1–8, 1985.
- [42] K. Hunt and G. Nason, "Wind speed modelling and short-term prediction using wavelets," *Wind Engineering*, vol. 25, no. 1, pp. 55–61, 2001.
- [43] M. Lobo and I. Sanchez, "Regional wind power forecasting based on smoothing techniques, with application to the spanish peninsular system," *Power Systems, IEEE Transactions on*, vol. 27, no. 4, pp. 1990–1997, Nov. 2012.
- [44] G. Kariniotakis, E. Nogaret, and G. Stavrakis, "Advanced short-term forecasting of wind power production," in *European Wind Energy Conference, Dublin, Ireland*, October 1997.
- [45] G. Ryahi and M. Abedi, "Short term wind speed forecasting for wind turbine applications using linear prediction method," *Renewable Energy*, vol. 33, no. 1, pp. 35–41, January 2008.
- [46] T. El-Fouly, "Improved grey predictor rolling models for wind power prediction," *IET Generation, Transmission and Distribution*, vol. 1, pp. 928–937(9), November 2007.

- [47] A. Sfetsos, “A novel approach for the forecasting of mean hourly wind speed time series,” *Renewable Energy*, vol. 27, no. 1, pp. 163–174, January 2001.
- [48] K. Bhaskar and S. Singh, “Awnn-assisted wind power forecasting using feed-forward neural network,” *Sustainable Energy, IEEE Transactions on*, vol. 3, no. 2, pp. 306–315, April 2012.
- [49] G. Venayagamoorthy, K. Rohrig, and I. Erlich, “One step ahead: Short-term wind power forecasting and intelligent predictive control based on data analytics,” *Power and Energy Magazine, IEEE*, vol. 10, no. 5, pp. 70–78, Sept. 2012.
- [50] G. Sideratos and N. Hatziargyriou, “Probabilistic wind power forecasting using radial basis function neural networks,” *Power Systems, IEEE Transactions on*, vol. 27, no. 4, pp. 1788–1796, Nov. 2012.
- [51] A. Togelou, G. Sideratos, and N. Hatziargyriou, “Wind power forecasting in the absence of historical data,” *Sustainable Energy, IEEE Transactions on*, vol. 3, no. 3, pp. 416–421, July 2012.
- [52] G. Li and J. Shi, “On comparing three artificial neural networks for wind speed forecasting,” *Applied Energy*, vol. 87, no. 7, pp. 2313–2320, 2010.
- [53] “Global Forecast System.” [Online]. Available: <http://www.emc.ncep.noaa.gov/>
- [54] “MM5.” [Online]. Available: <http://www.mmm.ucar.edu/mm5/>
- [55] “High Resolution Limited Area Model (hirlam).” [Online]. Available: <http://hirlam.org/>

- [56] “Prediktor.” [Online]. Available: <http://www.prediktor.dk/>
- [57] G. Sideratos and N. Hatzigiargyriou, “An advanced statistical method for wind power forecasting,” *Power Systems, IEEE Transactions on*, vol. 22, no. 1, pp. 258–265, Feb. 2007.
- [58] J. Catalão, H. Pousinho, and V. Mendes, “Hybrid wavelet-pso-anfis approach for short-term wind power forecasting in Portugal,” *Sustainable Energy, IEEE Transactions on*, vol. 2, no. 1, pp. 50–59, Jan. 2011.
- [59] N. Amjady, F. Keynia, and H. Zareipour, “Wind power prediction by a new forecast engine composed of modified hybrid neural network and enhanced particle swarm optimization,” *Sustainable Energy, IEEE Transactions on*, vol. 2, no. 3, pp. 265–276, July 2011.
- [60] R. Bessa, V. Miranda, and J. Gama, “Entropy and correntropy against minimum square error in offline and online three-day ahead wind power forecasting,” *Power Systems, IEEE Transactions on*, vol. 24, no. 4, pp. 1657–1666, Nov. 2009.
- [61] M. Alexiadis, P. Dokopoulos, and H. Sahsamanoglou, “Wind speed and power forecasting based on spatial correlation models,” *Energy Conversion, IEEE Transactions on*, vol. 14, no. 3, pp. 836–842, Sep. 1999.
- [62] I. Damousis, M. Alexiadis, J. Theocharis, and P. Dokopoulos, “A fuzzy model for wind speed prediction and power generation in wind parks using spatial correlation,” *Energy Conversion, IEEE Transactions on*, vol. 19, no. 2, pp. 352–361, June 2004.

- [63] H. Nielsen, T. Nielsen, H. Madsen, G. Giebel, J. Badger, L. Landbergt, K. Sattler, L. Voulund, and J. Tofting, “From wind ensembles to probabilistic information about future wind power production – results from an actual application,” in *Probabilistic Methods Applied to Power Systems, 2006. PMAPS 2006. International Conference on*, June 2006, pp. 1–8.
- [64] J. Taylor, P. McSharry, and R. Buizza, “Wind power density forecasting using ensemble predictions and time series models,” *Energy Conversion, IEEE Transactions on*, vol. 24, no. 3, pp. 775–782, Sept. 2009.
- [65] J. Juban, N. Siebert, and G. Kariniotakis, “Probabilistic short-term wind power forecasting for the optimal management of wind generation,” in *Power Tech, 2007 IEEE Lausanne*, July 2007, pp. 683–688.
- [66] H. A. Nielsen, H. Madsen, and T. S. Nielsen, “Using quantile regression to extend an existing wind power forecasting system with probabilistic forecasts,” *Wind Energy*, vol. 9, no. 1-2, pp. 95–108, 2006.
- [67] P. Hall and A. Rieck, “Improving coverage accuracy of nonparametric prediction intervals,” *Journal of the Royal Statistical Society: Series B (Statistical Methodology)*, vol. 63, no. 4, pp. 717–725, 2001.
- [68] C. Cannamela and J. Garnier, “Controlled stratification for quantile estimation,” *Annals of Applied Statistics*, vol. 2, no. 4, pp. 1554–1580, 2008.
- [69] M. Kutner, C. Nachtsheim, and J. Neter, *Applied Linear Regression Models*, ser. McGraw-Hill/Irwin series Operations and decision sciences. McGraw-Hill, 2004.

- [70] R. Koenker and G. Basset, “Quantile regression,” *Econometrica*, vol. 46, no. 1, pp. 33–50, January 1978.
- [71] R. Koenker and K. H. Hallock, “Quantile regression,” in *Journal of Economic Perspectives*, vol. 15, no. 4, Fall 2001, pp. 143–156.
- [72] R. Koenker and J. A. F. Machado, “Goodness of fit and related inference processes for quantile regression,” *Journal of the American Statistical Association*, vol. 94, no. 448, pp. 1296–1310, 1999.
- [73] R. Koenker, *Quantile Regression*, ser. Econometric Society Monographs. Cambridge University Press, 2005.
- [74] I. Takeuchi, Q. Le, T. Sears, and A. Smola, “Nonparametric quantile estimation,” *Journal of Machine Learning Research*, vol. 6, pp. 1231–1264, 2006.
- [75] J. B. Bremnes, “Probabilistic wind power forecasts using local quantile regression,” *Wind Energy*, vol. 7, no. 1, pp. 47–54, 2004.
- [76] J. K. Møller, “Modeling of uncertainty in wind energy forecast,” Master’s thesis, Technical University of Denmark, Department of Informatics and Mathematical Modelling, 2006.
- [77] J. K. Møller, H. A. Nielsen, and H. Madsen, “Time-adaptive quantile regression,” *Computational Statistics and Data Analysis*, vol. 52, no. 3, pp. 1292–1303, 2008.
- [78] M. Greenwald and S. Khanna, “Space-efficient online computation of quantile summaries,” *SIGMOD Rec.*, vol. 30, no. 2, pp. 58–66, May 2001.

- [79] K. Tschumitschew and F. Klawonn, “Incremental quantile estimation,” *Evolving Systems*, vol. 1, pp. 253–264, 2010.
- [80] E. Chen and W. Kelton, “Simulation-based estimation of quantiles,” in *Simulation Conference Proceedings, 1999 Winter*, vol. 1, 1999, pp. 428–434.
- [81] A. C. Gilbert, Y. Kotidis, S. Muthukrishnan, and M. J. Strauss, “How to summarize the universe: dynamic maintenance of quantiles,” in *Proceedings of the 28th international conference on Very Large Data Bases*, ser. VLDB ’02, 2002, pp. 454–465.
- [82] L. Tierney, “A space-efficient recursive procedure for estimating a quantile of an unknown distribution,” *Journal of Scientific and Statistical Computing*, vol. 4, pp. 706–711, 1983.
- [83] J. Cao, L. Li, A. Chen, and T. Bu, “Tracking quantiles of network data streams with dynamic operations,” in *INFOCOM, 2010 Proceedings IEEE*, March 2010, pp. 1–5.
- [84] F. Chen, D. Lambert, and J. C. Pinheiro, “Incremental quantile estimation for massive tracking,” in *Proceedings of the sixth ACM SIGKDD international conference on Knowledge discovery and data mining*, ser. KDD ’00. New York, NY, USA: ACM, 2000, pp. 516–522.
- [85] H. Robbins and S. Monro, “A stochastic approximation method,” *Annals of Mathematical Statistics*, vol. 23, no. 3, pp. 400–407, 1951.
- [86] P. Pinson and G. Kariniotakis, “On-line assessment of prediction risk for wind power production forecasts,” *Wind Energy*, vol. 7, no. 2, pp. 119–132, 2004.

- [87] T. Gneiting and A. E. Raftery, "Strictly proper scoring rules, prediction and estimation," Department of Statistics, University of Washington, Technical report, September 2005.
- [88] A. G. Tsikalakis, N. D. Hatziargyriou, Y. A. Katsigiannis, and P. S. Georgilakis, "Impact of wind power forecasting error bias on the economic operation of autonomous power systems," *Wind Energy*, vol. 12, no. 4, pp. 315–331, 2009.
- [89] K. Porter and J. Rogers, "Status of centralized wind power forecasting in north america," NREL, Technical report, April 2010.
- [90] G. N. Kariniotakis, I. Marti, T. S. Nielsen, G. Giebel, J. Tambke, I. Waldl, J. Usaola, R. Brownsword, G. Kallos, U. Focken, I. Sanchez, N. Hatziargyriou, and A. M. Palomares, "Advanced short-term forecasting of wind generation - anemos," *Power Systems, IEEE Transactions on*, vol. 22, no. 1, pp. 1–9, Feb. 2007.
- [91] E. DeMeo, K. Porter, and C. Smith, "Wind Power and Electricity Markets," Utility Wind Integration Group, Technical report, October 2011. [Online]. Available: <http://www.uwig.org/windinmarketstableOct2011.pdf>
- [92] D. Hedberg, M. Emnett, G. Sodeberg, N. McIntire, R. Gramlich, and R. Kondziolka, "FERC Order 890: What Does it Mean for the West?" National Association of Regulatory Utility Commissioners (NARUC), National Wind Coordinating Collaborative (NWCC), and the Western Governors' Association, Technical report, 2007. [Online]. Available: <http://www.nationalwind.org/assets/publications/ferc890.pdf>

- [93] J. Barton and D. Infield, “Energy storage and its use with intermittent renewable energy,” *Energy Conversion, IEEE Transactions on*, vol. 19, no. 2, pp. 441–448, June 2004.
- [94] M. Black and G. Strbac, “Value of bulk energy storage for managing wind power fluctuations,” *Energy Conversion, IEEE Transactions on*, vol. 22, no. 1, pp. 197–205, March 2007.
- [95] S. Dutta and T. Overbye, “Optimal storage coordination for minimal wind generation schedule deviation,” in *North American Power Symposium (NAPS), 2010*, Sept. 2010, pp. 1–7.
- [96] E. Hittinger, J. Whitacre, and J. Apt, “Compensating for wind variability using co-located natural gas generation and energy storage,” *Energy Systems*, vol. 1, pp. 417–439, 2010.
- [97] X. Wang, D. Mahinda Vilathgamuwa, and S. Choi, “Determination of battery storage capacity in energy buffer for wind farm,” *Energy Conversion, IEEE Transactions on*, vol. 23, no. 3, pp. 868–878, Sept. 2008.
- [98] P. Pinson, G. Papaefthymiou, B. Kloeckl, and J. Verboomen, “Dynamic sizing of energy storage for hedging wind power forecast uncertainty,” in *Power Energy Society General Meeting, 2009. PES '09. IEEE*, July 2009, pp. 1–8.
- [99] G. Koeppel and M. Korps, “Improving the network infeed accuracy of non-dispatchable generators with energy storage devices,” *Electric Power Systems Research*, vol. 78, no. 12, pp. 2024–2036, 2008.



- [100] P. Pinson, H. Madsen, H. A. Nielsen, G. Papaefthymiou, and B. Kloeckl, “From probabilistic forecasts to statistical scenarios of short-term wind power production,” *Wind Energy*, vol. 12, no. 1, pp. 51–62, 2009.
- [101] N. Johnson, S. Kotz, and N. Balakrishnan, *Continuous univariate distributions*, ser. Wiley Series in Probability and Mathematical Statistics: Applied Probability and Statistics. Wiley & Sons, 1994, vol. 1.
- [102] C. Bishop, *Pattern recognition and machine learning*. Springer, 2009.

## Vita

Thekla Boutsika was born in Greece in 1979. She received the Diploma in Electrical and Computer Engineering from the Aristotle University of Thessaloniki, Greece and the Postgraduate Specialization Diploma in Energy Production and Management from the National Technical University of Athens, Greece in 2002 and 2004, respectively. In 2003 she joined the Distribution Division of the Public Power Corporation of Greece, where she was engaged in studying the technical requirements imposed on the interconnection of distributed generation, and in the evaluation of power quality technical guidelines and grid codes. She enrolled in the Ph.D. program in Electrical Engineering at the University of Texas at Austin in 2007, after receiving a scholarship from the Fulbright Foundation in Greece. Her research interests include wind energy, wind integration, wind power forecasting, stochastic processes and stochastic optimization. She is a member of the Technical Chamber of Greece.

Permanent address: 12 Kallipoleos Str.  
Thessaloniki, GR 55134  
Greece

This dissertation was typeset with L<sup>A</sup>T<sub>E</sub>X<sup>†</sup> by the author.

---

<sup>†</sup>L<sup>A</sup>T<sub>E</sub>X is a document preparation system developed by Leslie Lamport as a special version of Donald Knuth's T<sub>E</sub>X Program.